Distribution Agreement

In presenting this thesis or dissertation as a partial fulfillment of the requirements for an advanced degree from Emory University, I hereby grant to Emory University and its agents the non-exclusive license to archive, make accessible, and display my thesis or dissertation in whole or in part in all forms of media, now or hereafter known, including display on the world wide web. I understand that I may select some access restrictions as part of the online submission of this thesis or dissertation. I retain all ownership rights to the copyright of the thesis or dissertation. I also retain the right to use in future works (such as articles or books) all or part of this thesis or dissertation.

Signature:

_____   _____

Savannah J. Post   Date

A Three-Pronged Approach to Combatting Antibiotic Resistance

By

Savannah J. Post

Doctor of Philosophy

Chemistry

_____
William, M. Wuest, Ph.D.
Advisor

_____
Simon B. Blakey, Ph.D.
Committee Member

_____
Dennis C. Liotta, Ph.D.
Committee Member

Accepted:

_____
Kimberly Jacob Arriola, Ph.D, MPH
Dean of the James T. Laney School of Graduate Studies

_____
Date

A Three-Pronged Approach to Combatting Antibiotic Resistance

By

Savannah J. Post

B.S., Berry College, 2017

Advisor: William M. Wuest, Ph.D.

An abstract of

A dissertation submitted to the Faculty of the

James T. Laney School of Graduate Studies of Emory University

in partial fulfillment of the requirements for the degree of

Doctor of Philosophy in Chemistry

2022

Abstract

A Three-Pronged Approach to Combatting Antibiotic Resistance
By Savannah J. Post

Widespread use of antibiotics and the decline of pharmaceutical investment has led to the proliferation of antibiotic resistance in many important diseases. Herein I discuss three different strategies that utilize small molecules to combat this growing problem: species-selective inhibition, combination therapies, and anti-virulence. Many currently utilized antibiotics are broad-spectrum, meaning that they target both Gram-positive and Gram-negative species. An alternative strategy is to take a more targeted approach wherein compounds selectively target a specific pathogen or group of pathogens, to protect the human microbiome. Promysalin is a natural product that exhibits species-selective inhibition against *Pseudomonas aeruginosa*, which has developed widespread clinical resistance. My research has elaborated on previous work in our group, and I have strategically developed several panels of analogs based on computational modeling, in search of more potent derivatives. I have also explored promysalin in combination with various antibiotics and other small molecules as a second strategy for combatting bacterial resistance. The final approach I explored to circumvent resistance emergence is the use of anti-virulence strategies. Virulence aids in bacterial pathogenicity but is not required for growth. By targeting these pathways instead of killing the bacteria, we are minimizing the selective pressure to mutate and develop resistance. The cahuitamycins are a group of natural products that inhibit biofilm formation in *Acinetobacter baumannii*, a known virulence behavior. My work has focused on the first total synthesis and analog development of these natural products. These findings have set the stage for future work in our lab investigating the mechanism of action of these new antimicrobial compounds.

A Three-Pronged Approach to Combatting Antibiotic Resistance

By

Savannah J. Post

B.S., Berry College, 2017

Advisor: William M. Wuest, Ph.D.

A dissertation submitted to the Faculty of the

James T. Laney School of Graduate Studies of Emory University

in partial fulfillment of the requirements for the degree of

Doctor of Philosophy in Chemistry

2022

Table of Contents

FDAA - 1-fluoro-2,4-dinitrobenzene-5-alanine amide

HMBC - Heteronuclear Multiple Bond Correlation

HOBt - Hydroxybenzotriazole

HPLC - high-performance liquid chromatography

HRESIMS - high-resolution time-of-flight electrospray ionization mass spectrometry

HRMS - high resolution mass spectrometry

IR - infrared

LLS - longest linear sequence

MDR - multi-drug resistant

MIC - minimum inhibitory concentration

mRNA - messenger RNA

NMR - Nuclear magnetic resonance

NRPS - nonribosomal peptide synthetase

OD600 - optical density at 600 nm

PABA - para aminobenzoic acid

QS - quorum sensing

RNA - Ribonucleic Acid

RT - room temperature

RND - resistance-nodulation-cell division

Sdh - succinate dehydrogenase

SEM - standard error of mean

SMX - sulfamethoxazole

TFA - trifluoroacetic acid

THF - tetrahydrofuran

TMP - trimethoprim

TLC - thin layer chromatography

TOCSY - Total Correlation Spectroscopy

tRNA - transfer RNA

Chapter 1. Introduction

1.1   Antibiotics and Resistance

1.1.1   Traditional Mechanisms of Action

There was a time when bacterial infections were an automatic death sentence, but the rise of antibiotics revolutionized healthcare, beginning with use of sulfonamides, the first broad-spectrum antibiotics used clinically.[1] Around that same time, the initial discovery of penicillin in 1928[2] sparked the "Golden Age" of antibiotic discovery. Between 1940 and 1970, nearly 30 new classes of antibiotics were discovered, comprising great structural diversity, and spanning five distinct mechanisms of action.[1] Namely, all known antibiotics at the time acted via inhibition of cell wall synthesis, nucleic acid synthesis, protein synthesis, folate synthesis, or membrane disruption. These mechanisms will be briefly described herein, with representative examples for each.

1.1.1.1 Cell Wall Synthesis

One of the most common antibiotic mechanisms of action is inhibition of cell wall synthesis. The cell wall is vital for the survival of bacteria, as it provides rigidity to the cell.[3] Furthermore, since mammalian cells do not possess a cell wall, this is an attractive antibiotic target due to the inherent selectivity for bacterial over human cells.[4] Biosynthetically, a critical step in the formation of cells walls is crosslinking, wherein the linear peptidoglycan chains are linked

together by transpeptidase enzymes.[5] While many antibiotics target other steps in cell wall synthesis, inhibition of crosslinking is the most common mechanism, being employed by both beta-lactams and glycopeptides, among others. Beta-lactams function by covalently bonding with a specific class of transpeptidases, penicillin binding proteins, at their active site, rendering them unable to interact with peptidoglycan chains.[6] Conversely, glycopeptides bind directly to peptidoglycan chains, creating steric encumbrance that prevents their crosslinking.[7] Together these two classes serve to inhibit separate parts of the same process, resulting in the same overall effect of a weakened cell wall.

1.1.1.2 Nucleic Acid Synthesis

Another important mechanism of action is the inhibition of nucleic acid synthesis, both DNA and RNA, which are both required for cell replication and division. When DNA is not being replicated, it organizes into supercoiled double-stranded structure to remain stable and inaccessible until it is needed. As such, when DNA replication is initiated, the first step is to uncoil and unzip the two strands, which is carried out by topoisomerases and helicases, respectively.[8] Quinolones are the most common class of DNA synthesis inhibitors, and act by inhibiting topoisomerases. Over the years, there have been several generations of quinolones, which vary in both their activity and mechanism. They vary in which topoisomerase enzyme they target, whether they function by interacting directly with the active site or with the enzyme-DNA complex, and whether they act broadly against all bacteria or more specifically target certain classes of bacteria.

Equally important for cell replication is transcription, the process of converting DNA to messenger RNA (mRNA). Inhibition of this process is much less common than DNA synthesis, with the rifamycins being one of the only classes of antibiotics to shut down mRNA synthesis. The

2

main enzyme required for this process is RNA polymerase, which is directly responsible for creating the growing mRNA strand. Rifamycins act by binding to the active site of RNA polymerase, prohibiting the growing mRNA strand from moving through the active site during elongation.[8] Of note, eukaryotic RNA polymerase has significant structural differences from the bacterial enzyme, making the rifamycins highly selective with little toxicity.

1.1.1.3 Protein Synthesis

Following transcription, mRNA is converted into proteins during a process called translation. During this process, the ribosome, a large complex of proteins, reads the mRNA strand and builds on corresponding amino acids to form the growing peptide chain. The ribosome, which is comprised of two major subunits, 50S and 30S, is one of the most common antibiotic targets, with over 10 distinct classes of antibiotics disrupting some aspect of its function.[9] Namely, aminoglycosides and tetracyclines, among others, target the 30S subunit specifically. Most antibiotics that inhibit protein synthesis are bacteriostatic, meaning they inhibit further growth, essentially stalling bacterial replication. However, aminoglycosides are unique in that they are bactericidal, meaning that they actually kill bacterial cells they come in contact with.[8] The reason for this is complex, but is believed to be due to a combination of multiple mechanisms through which these antibiotics can act.[10] That said, this bactericidal activity has made aminoglycosides one of the most widely utilized protein-targeting antibiotic classes. On the other hand, tetracyclines like most other protein inhibitors, are bacteriostatic. They function by blocking transfer RNA (tRNA) from binding to the ribosome.[8] tRNA is responsible for bringing the appropriate amino acid to the ribosome, so, as mentioned, disrupting this process stalls protein synthesis and in turn

cell growth. Although tetracyclines can also bind to eukaryotic ribosomes, they are poorly transported into eukaryotic cells, rendering them selective for bacterial inhibition.

Many other classes of antibiotics target the 50S subunit of ribosomes, including macrolides and chloramphenicol, among others. Although chloramphenicol binds to the 50S unit on the other side of the tRNA active site, it still serves to block binding of tRNA, resulting in the same outcome of tetracyclines. Furthermore, chloramphenicol binds reversibly, making its mechanism bacteriostatic. While chloramphenicol does not bind to most eukaryotic ribosomes, it can bind to mitochondrial ribosomes, resulting in adverse side effects that have limited its clinical use. On the other hand, macrolides, especially erythromycin, have been widely used in the clinic. This class binds to a slightly different position on the 50S subunit, instead prohibiting the exit of the growing peptide chain. Similar to others, they bind reversibly, making them bacteriostatic. Finally, they do not bind eukaryotic ribosomes, making them completely selective for bacterial cells.

1.1.1.4 Folate Synthesis

Folate is essential for cell growth in both bacteria and humans, as it is an important coenzyme for many biological pathways.[11] However, humans do not possess the necessary machinery to produce this metabolite, so we must obtain it through our diet. As such, folate synthesis represents an attractive antibiotic target since this pathway is only present in bacterial cells. Consequently, many classes of antibiotics have been identified that inhibit folate synthesis and derivatization including sulfonamides and trimethoprim, among others. Sulfonamides share structural similarity to para aminobenzoic acid (PABA), the first precursor in the folate synthesis pathway.[8] As such, sulfonamides compete with PABA for binding in the active site of the first enzyme, dihydropteroate synthase (DHPS). On the other hand, 2,4-diaminopyrimidines inhibit a

later step, in which folate is derivatized to tetrahydrofolate by the enzyme dihydrofolate reductase (DHFR). Unlike DHPS, DHFR is present in human cells, making selectivity a concern in this case. Consequently, many synthetic 2,4-diaminopyrimidine analogs were tested against bacterial and human DHFR until trimethoprim was identified, which is 1000-fold more active against the bacterial enzyme than the human.

1.1.1.5 Membrane Disruption

Cellular membranes serve many important functions in cells. In addition to providing a protective barrier that can selectively import or export specific molecules, membranes also house proteins that act as receptors to recognize external cell to cell signals and initiate an internal cellular response. Membranes also serve as the main structural feature distinguishing between the two main classifications of bacteria, Gram-negative and Gram-positive. Gram-positive species contain a single cellular membrane, housed inside the cell wall, while Gram-negative species possess two cell membranes, one inside and one outside the cell wall. This is an important distinction, as the outer membrane serves as an extra barrier for antibiotics, making Gram-negative bacteria generally more difficult to target. That said, disinfectants have been widely successful and primarily work through disruption of the cell membrane. Additionally, a small number of antibiotics have been utilized that function through this mechanism, primarily antimicrobial peptides (AMPs). Most of these compounds (disinfectants and AMPs) are amphiphilic in nature, in that they contain both hydrophobic and hydrophilic portions. They are often positively charged, which creates an attraction to the negatively charged phosphate groups on membranes, causing the initial binding of these molecules. After initial interaction, the hydrophobic portion of the molecule can interact with the lipids in membrane, causing disruption of the structure and rigidity of the membrane

through various mechanisms.[8] Although eukaryotic membranes have similar composition, they are overall less negatively charged than bacterial cells, leading to some level of selectivity for bacterial cells. Nevertheless, human toxicity can be a problem with these types of compounds, which owes to the relatively widespread use in disinfectants that are used externally compared to antibiotics that are taken internally.

1.1.2   Resistance Mechanisms

Many of these antibiotics and others have made a significant impact in the healthcare[12] and agriculture[13] industries. As such, they have often been overused and misused, accelerating the spread of bacterial resistance[14–16] and reducing their effectiveness. Furthermore, in the 50+ years since the golden age of antibiotic discovery, only about 10 new classes of antibiotics have been introduced to the clinic.[1] Of those, only one functions through a novel mechanism outside of the five described above.[17] These factors together have contributed to the rapid rise in antibiotic resistant infections. According to the Centers for Disease Control and Prevention (CDC), 2.8 million people in the United States alone contract antibiotic-resistant infections each year, resulting in 35,000 deaths.[18] In order to combat this growing problem, it is important to understand the mechanisms through which bacteria commonly evade antibiotic treatment. Herein, three of the most common resistance mechanisms will be discussed: efflux, target modification, and drug inactivation.

1.1.2.1 Decreased Drug Uptake

Most antibiotic targets are inside the cell, so by nature they must enter, and remain inside, the cell to be effective. As such, bacteria have evolved to prevent this by either limiting uptake of

the drug or forcing it back out if it does get in. The source of limited drug uptake is most commonly the outer membrane. This means that Gram-positive species are inherently less capable of preventing drug uptake than Gram-negative species. In addition to the innate barrier that the outer membrane of Gram-negative bacteria provides, many have evolved additional mechanisms to further restrict uptake. Most drugs gain access into Gram-negative strains through porins in the outer membranes. As such, modifications to these porins can affect the ability of drugs to enter the cell. This is commonly achieved through two main mechanisms: (1) decrease in the number of porins present; (2) structural modifications to the porins that change the type of molecules that can be transported through them.[19] These mechanisms have been observed in many different strains and confer resistance to multiple classes of antibiotics.[20–23]

1.1.2.2 Efflux

Efflux pumps are protein channels that transport small molecules out of the cell. There are five main classes of efflux pumps, which differ in the driving force they use to transport the compounds. Some use ATP as an active energy source, while most use passive transport coupled to ion gradients like Na^+ or H^+.[24] Most are single-component pumps bound in the inner membrane, but one class, the resistance-nodulation-cell division (RND) family, are multi-component pumps that span the inner and outer membrane of Gram-negative cells.[25] Many efflux pumps are intrinsically expressed in order to extrude toxins or compounds in their native environment. However, in the presence of antibiotics, bacteria often modify these pumps to transport the antibiotic or overexpress existing pumps to increase drug efflux efficiency.[24] Furthermore, there has been increased incidence of multi-drug efflux pumps, which can accommodate a wide range of structural features and thus efflux many different antibiotic classes.

1.1.2.3 Target Modification

Another common mechanism of drug resistance is target modification, wherein mutations are made to the drug's target enzyme such that the drug has decreased or no binding affinity for the altered target.[26,27] This resistance mechanism is common for beta-lactams and quinolones, where penicillin binding proteins and topoisomerases are structurally altered, decreasing binding affinity of their respective drugs and conferring resistance.[28,29] This mechanism has also been observed in folate synthesis inhibitors, where mutations in DHPS and DHFR confer resistance to sulfonamides and trimethoprim, respectively.[30,31] In general, these types of mutations can also hinder binding of the native substrate, so bacteria have evolved highly specific structural modifications that decrease drug binding with little to no effect on binding of the native substrate.

1.1.2.4 Drug Inactivation

Finally, bacteria often alter the drug itself in some way to render it inactive. Perhaps the most well-known example of this is beta-lactamases, which hydrolyze the lactam rings, abolishing the binding of beta-lactams to penicillin binding proteins.[24] These enzymes have been widely identified in many different bacterial species, both Gram-negative and Gram-positive.[32–34] Since this has become such a widespread source of resistance, much work has been done toward finding effective inhibitors for beta-lactamases, and these compounds are commonly co-administered with beta-lactams.[35–37] Another common mechanism of drug inactivation is acetylation, in which enzymes transfer an acetyl group directly to the drug, rendering them ineffective. This has been detected for aminoglycosides, chloramphenicol, and quinolones, among others.[38–41]

1.1.3   ESKAPE Pathogens

These various resistance mechanisms have become widespread, and of particular concern are the ESKAPE pathogens (*Enterococcus faecium*, *Staphylococcus aureus, Klebsiella pneumoniae*, *Acinetobacter baumannii*, *Pseudomonas aeruginosa*, and *Enterobacter* species), cleverly named as they often "escape" the activity of many antibiotics.[42] Together, these species represent the most common cause of nosocomial infections and are especially prevalent in immunocompromised patients.[43,44] These organisms have a high incidence of multidrug resistant (MDR) strains[44–49] and utilize virulence behaviors such as the formation of biofilms[50–52] and the expression of nutrient acquisition systems,[53–55] and have thus been the focus of a growing body of research.[56]

Due to the growing concern surrounding these pathogens and others, there is rising impetus to identify new antimicrobials, especially those that act through novel mechanisms to avoid the common resistance mechanisms described above. A selection of novel strategies is described in the following section including species-selective inhibition, combination therapies, and anti-virulence strategies. Each of these has been investigated to some extent through the work described herein, and so the following section provides a brief background for each. Furthermore, the work described herein has particular relevance to two of the ESKAPE pathogens, *P. aeruginosa* and *A. baummannii*, which will be discussed in greater detail in their respective chapters.

1.2   Alternative Approaches to Bacterial Inhibition

Despite the growing incidence of bacterial resistance, more and more pharmaceutical companies are shutting down their antibiotic development divisions due to the high cost and low success rate of bringing a drug to market.[57] This has resulted in fewer resources devoted to research

on novel therapeutics, while bacterial resistance continues to rise at an alarming rate.[58] This has caused speculation of a post-antibiotic era,[59] in which the ability to treat bacterial infections would mirror that of the pre-antibiotic era when a bacterial infection was often a death sentence.[12] This would negate decades of progress in modern medicine, which has inspired the search for new strategies to treat infection that are less prone to resistance development.

Owing to their structural diversity and complexity, natural products often have very specific and selective mechanisms of action, opposed to more ubiquitous broad-acting killing. As such, they represent an attractive starting point for the identification of novel antimicrobials. Historically, they have been the inspiration for many existing drugs, and between 1981-2019, only 33% of newly approved small-molecule drugs were in no way related to, inspired by, or derived from natural products.[60] Several factors likely contribute to this fact. First, they have several characteristics that are important features of drug molecules including high levels of hydrogen-bonding, saturation, hydrophilicity, and rigidity.[61–64] Furthermore, they have been evolved by nature for a specific protective purpose in a highly diverse natural ecosystem.[65] As such, they often exhibit very specific and targeted activity. The benefit of this particular attribute will be discussed in the following section.

1.2.1   Species-Selective Inhibition

Most FDA-approved antibiotics are broad-spectrum, meaning that they target both Gram-negative and Gram-positive species. This results in non-specific killing of most or all bacterial species present. This may seem advantageous, but over 10,000 bacterial species have been identified within the human body, and most of them are commensal, or beneficial, species. These strains are vital to the overall human microbiome which is implicated in many facets of human

health.[66–73] Additionally, a healthy and diverse microbiome comprised of various commensal strains can aid in fending off pathogenic species. At best, even narrow-spectrum antibiotics, which target either Gram-negative or Gram-positive species, still affect many species their respective classification, without differentiating between pathogenic and commensal strains. In so doing, they cause other long-lasting consequences that could be mitigated through the development of more specific antimicrobials that target only the pathogenic species.

Additionally, common mechanisms of action among existing antibiotics contribute to the growing problem of bacterial resistance. Because they generally function through one of five common mechanisms, resistance to one antibiotic often confers resistance to many other antibiotics and even other classes. This results in multi-drug resistant strains, which are very difficult to treat and are responsible for many deaths worldwide. As such, antimicrobials with novel mechanisms that evade existing resistance mechanisms are vital to the future success of antibiotics.

Overall, compounds that selectively inhibit pathogenic species in a novel way have the potential to kill existing resistant bacterial strains while also preserving the fragile human microbiome. Natural products have the potential to address both of these shortcomings. As they evolved in a complex ecosystem rich with diverse microbial species, they are often very targeted and selective. Furthermore, they have the potential to function through unique, undiscovered mechanisms of action due to their structural diversity from existing antibiotics. One example of a species-selective natural product which exhibits a novel mechanism of action, promysalin, will be discussed in Chapter 2.

1.2.2   Combination Therapies

Combination therapies entail the use of multiple drugs in the treatment of a specific ailment. This strategy has shown great success in cancer treatment[74,75] and antivirals,[76–78] among others, and has become the standard treatment regime for such diseases.[79] However, this strategy has been less utilized in antibiotics and its effectiveness in this context has been contradictory.[80–84] However, one very effective antibiotic combination used in the clinic is sulfamethoxazole and trimethoprim, which will be discussed further in Chapter 3. While effective combination therapies in antibiotics have been limited to date, the success of sulfamethoxazole/trimethoprim as well as success in other diseases provides a basis for further investigation into this strategy.

In many situations, combination therapies are comprised of multiple, previously known FDA-approved drugs. By repurposing existing drugs, immense cost and time is saved by not pursuing the development and approval of a new drug.[85] One concern with combination therapies is negative drug-drug interactions, potentially mitigating the effectiveness of one drug or causing unforeseen side effects. However, the right drug pair has the potential for many significant advantages. Drug combinations can be either antagonistic, where one drug reduces the effectiveness of the other, additive, wherein they have little to no effect on one another, or synergistic, in which one drug increases the potency of the other drug. Even in an additive combination there are benefits. For instance, the same level of activity can be achieved with a lower dose of each drug when in combination, potentially decreasing any adverse side effects caused by either one.[86,87] A synergistic combination further enhances this effect, making this the gold standard for combination therapies. Perhaps the greatest advantage to combination therapy is the potential to overcome existing resistance and mitigate its development. By utilizing two drugs that function through unrelated mechanisms, upon emergence of a single resistance mechanism,

the other drug would remain effective. Therefore, the bacteria would have to evolve two distinct resistance genes in order to overcome the combination therapy. This is highly unlikely, as resistance genes often come at the price of high fitness costs for the bacteria, meaning they become less healthy and viable overall.[88] As such, the cost of two disparate resistance genes is often too high a price and the bacteria are unable to survive such in such states. In all, combination therapies have the potential to revive antibiotics that have succumbed to widespread resistance, potentially improve upon their prior activity, and reduce the development of additional antibiotic resistance.

1.2.3   Anti-virulence

Another strategy to circumvent resistance is to target bacterial virulence behaviors, which refer to an organism's ability to establish infection. This strategy does not target vital life processes of the bacteria, which results in less selective pressure for resistant mutations.[89] Additionally, this would cause less damage to the host commensal microbiome, as it does not actually kill or inhibit growth of any species. Bacteria possess many mechanisms for virulence or pathogenicity. Of particular relevance to this work is iron acquisition. Iron is a necessity for nearly all living systems, and iron limitation has been shown to reduce acute infection in numerous bacterial species.[90,91] In aerobic conditions, iron primarily exists as Fe^{3+}, which is poorly soluble in aqueous environments. Additionally, animals have evolved systems to sequester iron away from bacteria, providing a form of innate immunity to infection. To gain a competitive advantage, pathogens have evolved methods for obtaining this micronutrient in iron-deficient conditions. One of the most crucial strategies is the production of siderophores, a diverse array of iron-binding small molecules (270 structurally characterized)[92] produced by bacteria,[93] plants,[94] and fungi.[95] Siderophores are biosynthesized in the bacterial cell, excreted into the extracellular space, and form high affinity iron (III) chelate

complexes. These complexes are recognized by receptors on the bacterial surface and actively transported into the cell where the iron is extracted (either by reduction from Fe^{3+} to Fe^{2+} or chemical degradation of the siderophore) to be used or stored (Figure 1.1A). Beyond their iron-affinity, alternative roles for siderophore-like molecules include cell signaling, detoxification, oxidative-stress response, and antibacterial activity.[93] Due to the imminent and growing threat of MDR pathogens, the antibiotic potential of this class of molecules is of immediate and broad impact.
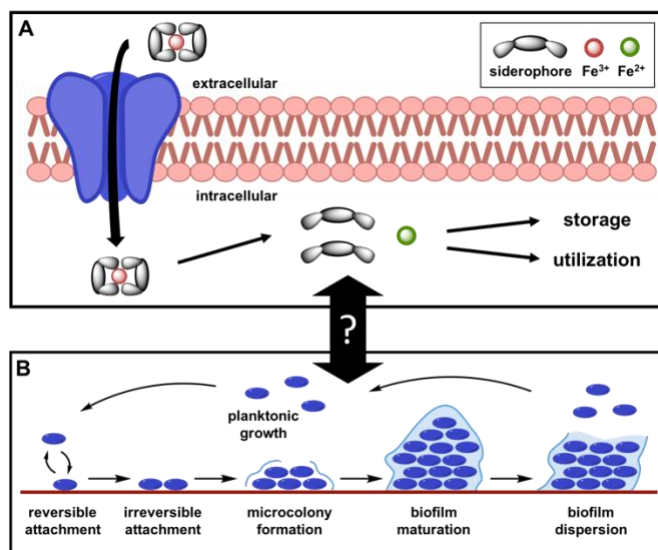
Figure 1.1. *(A) Overview of iron acquisition by siderophores. (B) Steps in biofilm formation.*

Through investigations into siderophores and other iron-chelating molecules, additional effects on biofilms have been observed. The formation of biofilms is a virulence behavior in which an extracellular polymeric matrix is excreted by the bacteria to form a three-dimensional microbial community (Figure 1.1B). Biofilm cells enter a lower metabolic state[96] and adhere to surfaces to form protective barriers. Together, these mechanisms make antibiotics and host immune defenses less effective,[51] and are thus a major contributor to resistance. As such, investigations of anti-biofilm compounds have garnered wide interest. The evidence supporting a link between iron

acquisition and biofilm formation has been rudimentary, and the exact details of this connection are unclear. In some pathogens it is well-documented, but in many cases the literature is sparse and contradictory. Herein we highlight some of the major findings that explore the relationship between iron depletion and biofilm formation in the ESKAPE pathogens and define the areas that require further investigation.

One strategy for the manipulation of bacterial iron homeostasis is the use of exogenous iron chelators. These have been studied as therapeutics for many many years,[97–100] but experiments looking at the effect of iron depravation on biofilm formation did not begin until the early 2000s. This effect has been most studied in *P. aeruginosa*, where several iron chelators including ethylenediaminetetraacetic acid (EDTA), diethylenetriaminepentaacetic acid (DTPA), desferoxamine (DFO), and deferasirox (DFS) have been shown to reduce biofilm formation.[101–103] Furthermore, combination of DFO or DFS with antibiotics like tobramycin were able to disrupt existing biofilms.[102] However, investigations into these effects in other ESKAPE pathogens has been less common and more inconclusive.[104] Moreover, An innate limitation of using exogenous iron chelators to disrupt bacterial functions is that different species are able to sequester iron from different sources. Some studies have shown secondary infections after treatment with iron chelators, resulting from a new species that is able to utilize iron from this complex gaining a competitive advantage over the initial pathogen.[105] As such, choice of a chelator with activity against multiple pathogens is critical. Alternatively, multiple iron chelators that are structurally diverse could be co-administered, in an effort to mitigate the effects of a broad range of species. Overall, initial results show some promise as a strategy for combatting MDR infections, and the repurposing of previously approved drugs provides a streamlined approach to obtaining a viable therapeutic, although further investigation is required.

An alternative to iron chelators is the use of gallium as a redox-stable iron mimic. Gallium (III) can compete with iron (III) in many binding interactions due to its similar atomic radius and valence.[106] However, because the gallium (II) oxidation state has never been observed, it does not have the redox properties required for the biological activity of iron and can thus inhibit iron-dependent enzymes. For example, an iron (III) reductase responsible for extraction of the metal from a siderophore-chelate would be ineffective on a gallium-bound complex (Figure 1.2). Furthermore, iron-dependent enzymes in critical life-sustaining processes such as respiration require the redox-cycling between iron (II) and iron (III) and are thus potentially susceptible to gallium inhibition (Figure 1.2). However, investigations into antibacterial properties of gallium-based therapies have been more widespread in planktonic cells,[107,108] with only limited studies in biofilms.[109–112] These preliminary studies, combined with others showing synergy between gallium and known antibiotics[108] make this an attractive strategy. Additionally, the use of gallium is less likely to develop resistance, because any change resulting in decreased binding or uptake of gallium would also reduce uptake of iron that is crucial to the survival of the bacteria.[113,114] However, one challenge that has been observed with gallium therapies is cytotoxicity,[115] as iron is crucial for many human processes in addition to bacterial. Furthermore, gallium salts are not very soluble in the gut, reducing their bioavailability.[116] The use of siderophore-gallium "Trojan-
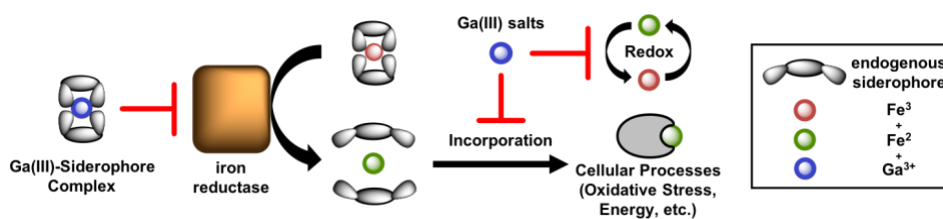

Figure 1.2. *Effect of gallium treatments on iron utilization. Gallium-siderophore complexes inhibit iron-reductase. Gallium salts inhibit other iron-dependent redox processes. (B) Structures of relevant gallium and iron complexes. Chelating atoms are highlighted in red.*

horse" strategies has been one approach to overcome this limitation and deliver the gallium into cells. All in all, these therapies hold promise but still require much more investigation.

Rather than targeting iron directly through chelators or gallium supplementation, an alternative approach is to inhibit bacterial methods of iron acquisition or utilization. Potential sites for inhibition that have been studied in various bacteria include siderophore biosynthesis,[117] outer membrane receptors,[118] iron release enzymes,[119] and signaling receptors[120] (Figure 1.3A). Compared to the use of exogenous iron chelators and gallium complexes, targeting siderophore-mediated processes directly has been less studied. The data presented herein are more preliminary and very few compounds are known to target these processes directly. However, these results demonstrate the potential for future investigations using small molecule inhibitors.

Siderophore biosynthesis is perhaps the most studied step in this process. Brown and coworkers performed transcriptomic analysis and unsurprisingly found that three *A. baumannii* siderophore biosynthesis gene clusters were significantly upregulated under iron-poor conditions.[121] However, many additional genes involved in motility were down-regulated, and this decrease in motility was confirmed through phenotypic assays. Of particular interest among the down-regulated genes were those that encode for type I and type IV pili. Homologous structures have been associated with motility and biofilm formation in other species, including *E. coli* and *P. aeruginosa*.[122–124] These results hint that both siderophore production and motility-related biofilm formation in *A. baumannii* are mediated by iron levels, but the details of this connection and how it translates to a phenotypic relationship between iron and biofilm formation necessitates further study.

A more recent study conducted proteomic analysis of both *S. aureus* planktonic and biofilm cells.[125] The results indicate that biofilms contain a decreased amount of iron-uptake proteins and
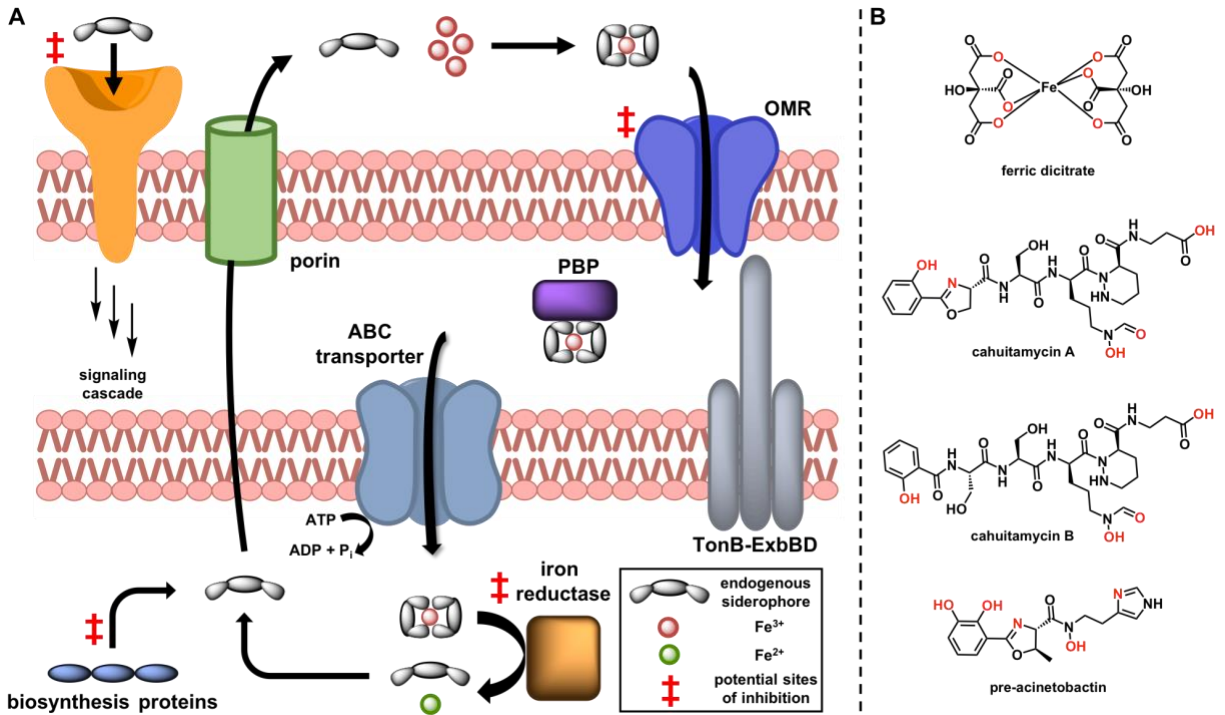
Figure 1.3. *(A) Overview of siderophore-mediated iron acquisition. Following biosynthesis, siderophores are exported through porins. They bind iron in the extracellular space and these complexes are taken into the periplasm through outer membrane receptors (OMRs). Periplasmic binding proteins (PBPs) transfer the complex to ATP-binding cassette (ABC) transporters, which bring them into the cytoplasm. Iron reductase catalyses the reduction of iron (III) to iron (II), which induces release by the siderophore. (B) Structures of siderophores and siderophore mimics. Chelating atoms are highlighted in red.*

an increased amount of the iron-storage protein FtnA, which suggests that biofilms may require lower levels of iron. This is not surprising, as iron is required for many cellular processes involved in replication and growth,[126] and biofilm cells often down-regulate metabolism. This gives further support to the transcriptomic results in *A. baumannii*, suggesting that low iron levels may trigger the cells to form biofilms and enter this lower metabolic state. In a highly virulent strain of Gram-positive *S. aureus*, iron-poor conditions induce biofilm formation.[127] Subsequently, two virulence determinants for this strain were identified, which allow the formation of biofilms in iron-poor conditions.[128] These findings suggests that iron-regulated biofilm formation may be highly strain-dependent. Additional studies looking at the formation of *S. aureus* biofilms found that they form

more readily in plasma with normal iron levels, compared to plasma that is iron-deficient or rich in iron.[129] This may suggest a "goldilocks" relationship between iron and biofilms, in which too much iron does not signal for biofilm formation, too little iron does not allow cell growth, but at just the right iron concentration biofilm formation is stimulated.

In *P. aeruginosa*, the link between iron utilization systems and biofilm formation has been studied more directly, with a minireview on the topic published in 2018.[130] Meyer and coworkers confirmed that pyoverdine, the endogenous siderophore in *P. aeruginosa*, is a virulence factor.[131] These results were observed *in vitro* and *in vivo* and have been validated by *in vivo* follow-up studies.[132,133] All of these data matched previous reports that pyoverdine, but not pyochelin (another *P. aeruginosa* siderophore), is required for growth in human serum.[134] Building on this foundation, Banin and coworkers found that a genetic mutant unable to produce pyoverdine, while exhibiting planktonic growth similar to that of the parent, formed only thin, uniform biofilms under iron-poor conditions, in contrast to the mushroom-like shape that is typical of *P. aeruginosa* biofilms grown under flow conditions.[135] Furthermore, supplementation of DFO or ferric dicitrate (Figure 1.3B) restores the mushroom-like shape of biofilms, indicating the bacteria was able to utilize iron from these complexes. Subsequently, they identified three possible gene clusters that may be responsible for the cellular uptake of these exogenous iron-chelators. Finally, they provided preliminary data showing that the ferric uptake regulator (Fur) protein plays a role in biofilm formation, but additional work is required to elucidate the mechanism and validate the results *in vivo*.

Another key process involved in virulence and biofilm formation in which siderophores have been implicated is intercellular signaling. Lamont et. al. showed that pyoverdine regulates its own production, as well as the production of exotoxin A and PrpL protease, all of which are virulence

factors in *P. aeruginosa*.[136] Subsequent identification of pyoverdine outer-membrane receptors in *P. aeruginosa*,[137] followed by the discovery of a bacteriocin that kills *P. aeruginosa* by selectively targeting these receptors,[138,139] provide a basis for future investigation of novel small molecules that target this uptake. In a recent high-throughput screen for pyoverdine biosynthesis genes, Kang and Kirienko report that early biofilm formation is required for complete pyoverdine biosynthesis.[140] This suggests that siderophore production may signal biofilm formation. Further investigation is necessary to determine if one of these virulence traits has a direct, causative effect on the other.

Only preliminary results have been reported on the relationship between siderophores and virulence in the other ESKAPE pathogens. Yersiniabactin, an endogenous siderophore of *K. pneumoniae*, was confirmed as a virulence factor in vivo.[141] Additionally, a hypervirulent strain of *K. pneumoniae* produced more siderophores than the wild type.[142] Another group screened 55 *E. faecium* and *E. faecalis* strains for antimicrobial resistance and siderophore production.[143] They found a direct correlation between siderophore production and fluoroquinolone resistance, and found that siderophores were present in large quantities in ciprofloxacin- and norfloxacin-resistant strains. Thus, their results provided initial evidence that siderophore production may contribute to virulence in *Enterococcus* species and aid in their resistance to various antibiotics. Additional studies should be executed to investigate whether this virulence is directly related to biofilm formation. Overall, targeting the synthesis siderophores will have a number of effects on the pathogenicity of the bacteria, and represents a viable strategy to disarm them.

A recent report disclosed a group of newly discovered natural products called the cahuitamycins (Figure 1.3B), which show promise as biofilm inhibitors.[144] Sherman and coworkers show quantitative and qualitative inhibition of *A. baumannii* biofilm formation when

grown in the presence of these molecules, without any inhibition of planktonic growth. Furthermore, these molecules show moderate to strong iron chelation and possess canonical hydroxamate and phenolate-oxazoline moieties typically found in siderophores. The exception is cahuitamycin B (Figure 1.3B), which contains no oxazoline and does not inhibit biofilm growth. However, when biofilms were grown in the presence of DFO no inhibition was observed. Together, these results suggest that the mechanism of these molecules is more complex than merely sequestering iron. Pre-acinetobactin (Figure 1.3B), an endogenous siderophore of *A. baumannii*, also possesses a phenolate-oxazoline moiety. It is thus plausible that the cahuitamycins are recognized by acinetobactin uptake proteins. However, it remains unclear why the bacteria would be unable to utilize the iron once the complex is brought inside the cell. Nevertheless, these molecules are a launching point to probe the relationship between iron chelation and biofilm formation in *A. baumannii* and provide rationale for using small molecules to disrupt these virulence pathways.

Targeting siderophore pathways has enormous potential as a therapeutic due to the substantial evidence that they play a role in biofilm formation. However, to date there are very few small molecules that are known to target a specific protein in this pathway. One possible explanation is that some species may have redundancy in this area. For example, *P. aeruginosa* has over 30 genes that encode for iron receptors, although there is homology between many of them.[145] Thus, if this strategy is to be utilized, it is vital that the approach be broad enough to target multiple receptors to avoid simple upregulation of alternative iron import pathways. The use of small molecules that mimic endogenous siderophores has shown potential in this area, as they utilize the innate machinery of the bacteria to gain entrance into the cell. Overall, these results provide evidence that

inhibition of siderophore pathways may be a viable strategy to inhibit biofilm formation as an

alternative to traditional therapeutic strategies.

1.3　References

(1)　Hutchings, M.; Truman, A.; Wilkinson, B. Antibiotics: Past, Present and Future. *Curr. Opin. Microbiol.* **2019**, *51*, 72–80. https://doi.org/10.1016/J.MIB.2019.10.008.

(2)　Sengupta, S.; Chattopadhyay, M. K.; Grossart, H. The Multifaceted Roles of Antibiotics and Antibiotic Resistance in Nature. *Front. Microbiol.* **2013**, *4* (47), 1–13. https://doi.org/10.3389/fmicb.2013.00047.

(3)　Glycobiology, J. H.-; 2001, undefined. Formation of the Glycan Chains in the Synthesis of Bacterial Peptidoglycan. *academic.oup.com* **2001**, *11* (3), 25–36.

(4)　Barreteau, H.; Kovač, A.; … A. B.-F. microbiology; 2008, undefined. Cytoplasmic Steps of Peptidoglycan Biosynthesis. *academic.oup.com*.

(5)　Sarkar, P.; Yarlagadda, V.; Ghosh, C.; Haldar, J. MedChemComm A Review on Cell Wall Synthesis Inhibitors with an Emphasis on Glycopeptide Antibiotics †. *Cite this Med. Chem. Commun* **2017**, *8*, 516. https://doi.org/10.1039/c6md00585c.

(6)　Kohanski, M. A.; Dwyer, D. J.; Collins, J. J. How Antibiotics Kill Bacteria: From Targets to Networks. **2010**. https://doi.org/10.1038/nrmicro2333.

(7)　Kahne, D.; Leimkuhler, C.; Lu, W.; Walsh, C. Glycopeptide and Lipoglycopeptide Antibiotics. **2005**. https://doi.org/10.1021/cr030103a.

(8)　Bhattacharjee, M. Chemistry of Antibiotics and Related Drugs.

(9)　Poehlsgaard, J.; Douthwaite, S. The Bacterial Ribosome as a Target for Antibiotics. *Nat. Rev. Microbiol.* **2005**, *3* (11), 870–881. https://doi.org/10.1038/NRMICRO1265.

(10)　Davis, B. D. Mechanism of Bactericidal Action of Aminoglycosides. **1987**.

(11)　Folate (Folic Acid) – Vitamin B9 | The Nutrition Source | Harvard T.H. Chan School of Public Health https://www.hsph.harvard.edu/nutritionsource/folic-acid/ (accessed Apr 7, 2022).

(12)　Aminov, R. I. A Brief History of the Antibiotic Era: Lessons Learned and Challenges for the Future. *Front. Microbiol.* **2010**, *1* (134), 1–7.

(13)　Michael, C. A.; Dominey-howes, D.; Labbate, M.; Maria, C.; Elisabeth, J. The Antimicrobial Resistance Crisis: Causes, Consequences, and Management. *Front. Public Heal.* **2014**, *2* (145), 1–8. https://doi.org/10.3389/fpubh.2014.00145.

(14)　Wright, G. D. Antibiotic Resistance in the Environment: A Link to the Clinic? *Curr. Opin. Microbiol.* **2010**, *13* (5), 589–594. https://doi.org/10.1016/j.mib.2010.08.005.

(15)　Nesme, J.; Cecillon, S.; Delmont, T. O.; Monier, J.; Vogel, T. M.; Simonet, P. Large-Scale Metagenomic-Based Study of Antibiotic Resistance in the Environment. *Curr. Biol.* **2014**, *24*, 1096–1100. https://doi.org/10.1016/j.cub.2014.03.036.

(16)　Lipsitch, M.; Samore, M. H. Antimicrobial Use and Antimicrobial Resistance: A Population Perspective. *Emerg. Infect. Dis.* **2002**, *8* (4), 347–354.

(17)　Diacon, A. H.; Pym, A.; Grobusch, M.; Patientia, R.; Rustomjee, R.; Page-Shipp, L.; Pistorius, C.; Krause, R.; Bogoshi, M.; Churchyard, G.; Venter, A.; Allen, J.; Palomino, J. C.; De Marez, T.; van Heeswijk, R. P. G.; Lounis, N.; Meyvisch, P.; Verbeeck, J.; Parys,

W.; de Beule, K.; Andries, K.; Neeley, D. F. M. The Diarylquinoline TMC207 for Multidrug-Resistant Tuberculosis. *N. Engl. J. Med.* **2009**, *360* (23), 2397–2405. https://doi.org/10.1056/NEJMoa0808427.

(18)   Centers for Disease Control and Prevention. Antibiotic Resistance Threats in the United States. **2019**. https://doi.org/CS239559-B.

(19)   Kumar, A.; reviews, H. S.-A. drug delivery; 2005, undefined. Bacterial Resistance to Antibiotics: Active Efflux and Reduced Uptake. *Elsevier*.

(20)   Gill, M. J.; Simjee, S.; Al-Hattawi, K.; Robertson, B. D.; Easmon, C. S. F.; Ison, C. A. Gonococcal Resistance to β-Lactams and Tetracycline Involves Mutation in Loop 3 of the Porin Encoded at the PenB Locus. *Antimicrob. Agents Chemother.* **1998**, *42* (11), 2799–2803. https://doi.org/10.1128/AAC.42.11.2799.

(21)   Cornaglia, G.; Mazzariol, A.; Fontana, R.; Satta, G. Diffusion of Carbapenems through the Outer Membrane of Enterobacteriaceae and Correlation of Their Activities with Their Periplasmic Concentrations. *Microb. Drug Resist.* **1996**, *2* (2), 273–276. https://doi.org/10.1089/MDR.1996.2.273.

(22)   Chow, J.; Chemotherapy, D. S.-J. of A.; 1991, undefined. Imipenem Resistance Associated with the Loss of a 40 KDa Outer Membrane Protein in Enterobacter Aerogenes. *academic.oup.com* **1991**, *28*, 499–504.

(23)   Thiolas, A.; Bornet, C.; Davin-Régli, A.; … J. P.-B. and; 2004, undefined. Resistance to Imipenem, Cefepime, and Cefpirome Associated with Mutation in Omp36 Osmoporin of Enterobacter Aerogenes. *Elsevier*.

(24)   Reygaert, W. C. An Overview of the Antimicrobial Resistance Mechanisms of Bacteria. *AIMS Microbiol.* **1900**, *4* (3), 482–501. https://doi.org/10.3934/microbiol.2018.3.482.

(25)   Blair, J. M. A.; Richmond, G. E.; Piddock, L. J. V. Multidrug Efflux Pumps in Gram-Negative Bacteria and Their Role in Antibiotic Resistance. *Future Microbiol.* **2014**, *9* (10), 1165–1177. https://doi.org/10.2217/FMB.14.66.

(26)   Science, W. R.-C. L.; 2009, undefined. Methicillin-Resistant Staphylococcus Aureus (MRSA): Molecular Aspects of Antimicrobial Resistance and Virulence. *clsjournal.ascls.org* **2009**, *22*.

(27)   Beceiro, A.; Tomás, M.; Bou, G. Antimicrobial Resistance and Virulence: A Successful or Deleterious Association in the Bacterial World? *Clin. Microbiol. Rev.* **2013**, *26* (2), 185–230. https://doi.org/10.1128/CMR.00059-12.

(28)   Chemotherapy, P. H.-J. of A.; 2003, undefined. Mechanisms of Quinolone Action and Microbial Response. *academic.oup.com* **2003**, *51*, 29–35. https://doi.org/10.1093/jac/dkg207.

(29)   Redgrave, L.; Sutton, S.; microbiology, M. W.-T. in; 2014, undefined. Fluoroquinolone Resistance: Mechanisms, Impact on Bacteria, and Role in Evolutionary Success. *Elsevier*.

(30)   Huovinen, P.; Sundstro¨m, L.; Sundstro¨m, S.; Go¨, G.; Swedberg, G.; Sko¨ld, O.; Sko¨ld, S. Trimethoprim and Sulfonamide Resistance. *Antimicrob. Agents Chemother.* **1995**, *39* (2), 279–289. https://doi.org/10.1128/AAC.39.2.279.

(31)   Vedantam, G.; Guay, G. G.; Austria, N. E.; Doktor, S. Z.; Nichols, B. P. Characterization of Mutations Contributing to Sulfathiazole Resistance in Escherichia Coli. *Antimicrob. Agents Chemother.* **1998**, *42* (1), 88–93. https://doi.org/10.1128/AAC.42.1.88.

(32)   Schultsz, C.; Geerlings, S. Plasmid-Mediated Resistance in Enterobacteriaceae: Changing Landscape and Implications for Therapy. *Drugs* **2012**, *72* (1), 1–16. https://doi.org/10.2165/11597960-000000000-00000.

(33) Chancey, S. T.; Zähner, D.; Stephens, D. S. Acquired Inducible Antimicrobial Resistance in Gram-Positive Bacteria. *Future Microbiol.* **2012**, *7* (8), 959–978. https://doi.org/10.2217/FMB.12.63.

(34) Pfeifer, Y.; Cullik, A.; microbiology, W. W.-I. journal of medical; 2010, undefined. Resistance to Cephalosporins and Carbapenems in Gram-Negative Bacterial Pathogens. *Elsevier* **2010**. https://doi.org/10.1016/j.ijmm.2010.04.005.

(35) Thomson, K. S. Extended-Spectrum-β-Lactamase, AmpC, and Carbapenemase Issues. *J. Clin. Microbiol.* **2010**, *48* (4), 1019–1025. https://doi.org/10.1128/JCM.00219-10.

(36) Bush, K. Proliferation and Significance of Clinically Relevant β-Lactamases. *Ann. N. Y. Acad. Sci.* **2013**, *1277* (1), 84–90. https://doi.org/10.1111/NYAS.12023.

(37) Jacoby, G. A. AmpC B-Lactamases. *Clin. Microbiol. Rev.* **2009**, *22* (1), 161–182. https://doi.org/10.1128/CMR.00036-08.

(38) Schwarz, S.; Kehrenberg, C.; … B. D.-F. microbiology; 2004, undefined. Molecular Basis of Bacterial Resistance to Chloramphenicol and Florfenicol. *academic.oup.com*.

(39) Robicsek, A.; Strahilevitz, J.; Jacoby, G.; medicine, M. M.-N.; 2006, undefined. Fluoroquinolone-Modifying Enzyme: A New Adaptation of a Common Aminoglycoside Acetyltransferase. *nature.com*.

(40) Ramirez, M.; updates, M. T.-D. resistance; 2010, undefined. Aminoglycoside Modifying Enzymes. *Elsevier*.

(41) Blair, J.; Webber, M.; Baylay, A.; … D. O.-N. reviews; 2015, undefined. Molecular Mechanisms of Antibiotic Resistance. *nature.com*.

(42) Navidinia, M. The Clinical Importance of Emerging ESKAPE Pathogens in Nosocomial Infections. *J. Paramed. Sci.* **2016**, *7*.

(43) Fick, R. B. *Pseudomonas Aeruginosa, the Opportunist : Pathogenesis and Disease*; 1993.

(44) Rice, L. B. Progress and Challenges in Implementing the Research on ESKAPE Pathogens. *Infect. Control Hosp. Epidemiol.* **2010**, *31* (1), 7–10. https://doi.org/10.1086/655995.

(45) Moskowitz, S. M.; Emerson, J. C.; McNamara, S.; Shell, R. D.; Orenstein, D. M.; Rosenbluth, D.; Katz, M. F.; Ahrens, R.; Hornick, D.; Joseph, P. M.; Gibson, R. L.; Aitken, M. L.; Benton, W. W.; Burns, J. L. Randomized Trial of Biofilm Testing to Select Antibiotics for Cystic Fibrosis Airway Infection. *Pediatr. Pulmonol.* **2011**, *46* (2), 184–192. https://doi.org/10.1002/ppul.21350.

(46) Moskowitz, S. M.; Foster, J. M.; Emerson, J. C.; Gibson, R. L.; Burns, J. L. Use of Pseudomonas Biofilm Susceptibilities to Assign Simulated Antibiotic Regimens for Cystic Fibrosis Airway Infection. *J. Antimicrob. Chemother.* **2005**, *56* (5), 879–886. https://doi.org/10.1093/jac/dki338.

(47) Lewis, K. Multidrug Tolerance of Biofilms and Persister Cells. *Curr. Top. Microbiol. Immunol.* **2008**, *322*, 107–131. https://doi.org/10.1007/978-3-540-75418-3_6.

(48) Gould, I. M. Treatment of Bacteraemia: Meticillin-Resistant Staphylococcus Aureus (MRSA) to Vancomycin-Resistant S. Aureus (VRSA). *Int. J. Antimicrob. Agents* **2013**, *42*, 17–21. https://doi.org/10.1016/j.ijantimicag.2013.04.006.

(49) Gardete, S.; Tomasz, A. Mechanisms of Vancomycin Resistance in Staphylococcus Aureus. *J. Clin. Invest.* **2014**, *124*, 2836–2840. https://doi.org/10.1172/JCI68834.

(50) Dijkshoorn, L.; Nemec, A.; Seifert, H. An Increasing Threat in Hospitals: Multidrug-Resistant Acinetobacter Baumannii. *Nat. Rev. Microbiol.* **2007**, *5* (12), 939–951. https://doi.org/10.1038/nrmicro1789.

(51)   Parsek, M. R.; Singh, P. K. Bacterial Biofilms: An Emerging Link to Disease Pathogenesis. *Annu. Rev. Microbiol.* **2003**, *57*, 677–701. https://doi.org/10.1146/annurev.micro.57.030502.090720.

(52)   Götz, F. Staphylococcus and Biofilms. *Mol. Microbiol.* **2002**, *43*, 1367–1378. https://doi.org/10.1046/j.1365-2958.2002.02827.x.

(53)   Minandri, F.; Imperi, F.; Frangipani, E.; Bonchi, C.; Visaggio, D.; Facchini, M.; Pasquali, P.; Bragonzi, A.; Visca, P. Role of Iron Uptake Systems in Pseudomonas Aeruginosa Virulence and Airway Infection. *Infect. Immun.* **2016**, *84* (8), 2324–2335. https://doi.org/10.1128/IAI.00098-16.

(54)   Caza, M.; Kronstad, J. W. Shared and Distinct Mechanisms of Iron Acquisition by Bacterial and Fungal Pathogens of Humans. *Front. Cell. Infect. Microbiol.* **2013**, *3* (80), 1–23.

(55)   Hammer, N. D.; Skaar, E. P. Molecular Mechanisms of Staphylococcus Aureus Iron Acquisition. *Annu. Rev. Microbiol.* **2011**, *65*, 129–147.

(56)   Pendleton, J.; Gorman, S.; Gilmore, B. Clinical Relevance of the ESKAPE Pathogens. *Expert Rev Anti Infect Ther* **2013**, *11* (3), 297–308.

(57)   DiMasi, J. A.; Hansen, R. W.; Grabowski, H. G. The Price of Innovation: New Estimates of Drug Development Costs. *J. Health Econ.* **2002**, *22* (2), 151–185.

(58)   Spellberg, B.; Guidos, R.; Gilbert, D.; Bradley, J.; Boucher, H. W.; Scheld, W. M.; Bartlett, J. G.; Edwards, J.; Diseases, I. The Epidemic of Antibiotic-Resistant Infections : A Call to Action for the Medical Community from the Infectious Diseases Society of America. *Clin. Infect. Dis.* **2008**, *46*, 155–164. https://doi.org/10.1086/524891.

(59)   Bragg, R. R.; Meyburgh, C. M.; Lee, J. Y.; Coetzee, M. Potential Treatment Options in a Post-Antibiotic Era. *Adv. Exp. Med. Biol.* **2018**, *1052*, 51–61.

(60)   Theobald, E. J.; Hill, M. J.; Tran, E.; Agrawal, S.; Nicole Arroyo, E.; Behling, S.; Chambwe, N.; Cintrón, D. L.; Cooper, J. D.; Dunster, G.; Grummer, J. A.; Hennessey, K.; Hsiao, J.; Iranon, N.; Jones, L.; Jordt, H.; Keller, M.; Lacey, M. E.; Littlefield, C. E.; Lowe, A.; Newman, S.; Okolo, V.; Olroyd, S.; Peecook, B. R.; Pickett, S. B.; Slager, D. L.; Caviedes-Solis, I. W.; Stanchak, K. E.; Sundaravardan, V.; Valdebenito, C.; Williams, C. R.; Zinsli, K.; Freeman, S. Active Learning Narrows Achievement Gaps for Underrepresented Students in Undergraduate Science, Technology, Engineering, and Math. *Proc. Natl. Acad. Sci. U. S. A.* **2020**, *117* (12), 6476–6483. https://doi.org/10.1073/pnas.1916903117.

(61)   Atanasov, A.; … B. W.-B.; 2015, undefined. Discovery and Resupply of Pharmacologically Active Plant-Derived Natural Products: A Review. *Elsevier*.

(62)   Feher, M.; Schmidt, J. M. Property Distributions: Differences between Drugs, Natural Products, and Molecules from Combinatorial Chemistry. *J. Chem. Inf. Comput. Sci.* **2003**, *43* (1), 218–227. https://doi.org/10.1021/CI0200467.

(63)   Barnes, E.; Kumar, R.; reports, R. D.-N. product; 2016, undefined. The Use of Isolated Natural Products as Scaffolds for the Generation of Chemically Diverse Screening Libraries for Drug Discovery. *pubs.rsc.org* **2013**, *00*, 1–3. https://doi.org/10.1039/x0xx00000x.

(64)   Clardy, J.; Nature, C. W.-; 2004, undefined. Lessons from Natural Molecules. *nature.com*.

(65)   Atanasov, A. G.; Zotchev, S. B.; Dirsch, V. M.; Orhan, I. E.; Banach, M.; Rollinger, J. M.; Barreca, D.; Weckwerth, W.; Bauer, R.; Bayer, E. A.; Majeed, M.; Bishayee, A.;

Bochkov, V.; Bonn, G. K.; Braidy, N.; Bucar, F.; Cifuentes, A.; D'Onofrio, G.; Bodkin, M.; Diederich, M.; Dinkova-Kostova, A. T.; Efferth, T.; El Bairi, K.; Arkells, N.; Fan, T.-P.; Fiebich, B. L.; Freissmuth, M.; Georgiev, M. I.; Gibbons, S.; Godfrey, K. M.; Gruber, C. W.; Heer, J.; Huber, L. A.; Ibanez, E.; Kijjoa, A.; Kiss, A. K.; Lu, A.; Macias, F. A.; Miller, M. J. S.; Mocan, A.; Müller, R.; Nicoletti, F.; Perry, G.; Pittalà, V.; Rastrelli, L.; Ristow, M.; Russo, G. L.; Silva, A. S.; Schuster, D.; Sheridan, H.; Skalicka-Woźniak, K.; Skaltsounis, L.; Sobarzo-Sánchez, E.; Bredt, D. S.; Stuppner, H.; Sureda, A.; Tzvetkov, N. T.; Vacca, R. A.; Aggarwal, B. B.; Battino, M.; Giampieri, F.; Wink, M.; Wolfender, J.-L.; Xiao, J.; Yeung, A. W. K.; Lizard, G.; Popp, M. A.; Heinrich, M.; Berindan-Neagoe, I.; Stadler, M.; Daglia, M.; Verpoorte, R.; Supuran, C. T.; Taskforce, the I. N. P. S. Natural Products in Drug Discovery: Advances and Opportunities. *Nat. Rev. Drug Discov.* **2021**, *20* (3), 200–216. https://doi.org/10.1038/s41573-020-00114-z.

(66) Kho, Z. Y.; Lal, S. K. The Human Gut Microbiome – A Potential Controller of Wellness and Disease . *Frontiers in Microbiology* . 2018, p 1835.

(67) Hudault, S.; Guignot, J.; Servin, A. L. Escherichia Coli Strains Colonising the Gastrointestinal Tract Protect Germfree Mice against Salmonella Typhimurium Infection. *Gut* **2001**. https://doi.org/10.1136/gut.49.1.47.

(68) Den Besten, G.; Van Eunen, K.; Groen, A. K.; Venema, K.; Reijngoud, D. J.; Bakker, B. M. The Role of Short-Chain Fatty Acids in the Interplay between Diet, Gut Microbiota, and Host Energy Metabolism. *Journal of Lipid Research*. American Society for Biochemistry and Molecular Biology September 2013, pp 2325–2340. https://doi.org/10.1194/jlr.R036012.

(69) Reid, G.; Howard, J.; Gan, B. S. Can Bacterial Interference Prevent Infection? *Trends Microbiol.* **2001**, *9* (9), 424–428. https://doi.org/10.1016/S0966-842X(01)02132-1.

(70) Bentley, R.; Meganathan, R. Biosynthesis of Vitamin K (Menaquinone) in Bacteria. *Microbiological Reviews*. 1982.

(71) Yatsunenko, T.; Rey, F. E.; Manary, M. J.; Trehan, I.; Dominguez-Bello, M. G.; Contreras, M.; Magris, M.; Hidalgo, G.; Baldassano, R. N.; Anokhin, A. P.; Heath, A. C.; Warner, B.; Reeder, J.; Kuczynski, J.; Caporaso, J. G.; Lozupone, C. A.; Lauber, C.; Clemente, J. C.; Knights, D.; Knight, R.; Gordon, J. I. Human Gut Microbiome Viewed across Age and Geography. *Nature* **2012**, *486*, 222–227. https://doi.org/10.1038/nature11053.

(72) Ley, R. E.; Turnbaugh, P. J.; Klein, S.; Gordon, J. I. Microbial Ecology: Human Gut Microbes Associated with Obesity. *Nature* **2006**, *444* (7122), 1022–1023. https://doi.org/10.1038/4441022a.

(73) Kau, A. L.; Ahern, P. P.; Griffin, N. W.; Goodman, A. L.; Gordon, J. I. Human Nutrition, the Gut Microbiome and the Immune System. *Nature* **2011**, *474* (7351), 327–336. https://doi.org/10.1038/nature10213.

(74) Partridge, A. H.; Burstein, H. J.; Winer, E. P. Side Effects of Chemotherapy and Combined Chemohormonal Therapy in Women with Early-Stage Breast Cancer. *J. Natl. Cancer Inst. Monogr.* **2001**, No. 30, 135–142. https://doi.org/10.1093/OXFORDJOURNALS.JNCIMONOGRAPHS.A003451.

(75) Blagosklonny, M. V. Analysis of FDA Approved Anticancer Drugs Reveals the Future of Cancer Therapy. *Cell Cycle* **2004**, *3* (8), 1035–1042. https://doi.org/10.4161/cc.3.8.1023.

(76) Peters, B. S.; Conway, K. Therapy for HIV: Past, Present, and Future. *Adv. Dent. Res.* **2011**, *23* (1), 23–27. https://doi.org/10.1177/0022034511399082.

(77) Akanbi, M. O.; Scarci, K.; Taiwo, B.; Murphy, R. L. Combination Nucleoside/Nucleotide Reverse Transcriptase Inhibitors for Treatment of HIV Infection. *http://dx.doi.org/10.1517/14656566.2012.642865* **2011**, *13* (1), 65–79. https://doi.org/10.1517/14656566.2012.642865.

(78) Cihlar, T.; Fordyce, M. Current Status and Prospects of HIV Treatment. *Curr. Opin. Virol.* **2016**, *18*, 50–56. https://doi.org/10.1016/J.COVIRO.2016.03.004.

(79) Shyr, Z. A.; Cheng, Y.-S.; Lo, D. C.; Zheng, W. Drug Combination Therapy for Emerging Viral Diseases. *Drug Discov. Today* **2021**, *26* (10), 2367–2376. https://doi.org/10.1016/j.drudis.2021.05.008.

(80) Kumar, A.; Safdar, N.; Kethireddy, S.; Chateau, D. A Survival Benefit of Combination Antibiotic Therapy for Serious Infections Associated with Sepsis and Septic Shock Is Contingent Only on the Risk of Death: A Meta-Analytic/Meta-Regression Study. *Crit. Care Med.* **2010**, *38* (8), 1651–1664. https://doi.org/10.1097/CCM.0B013E3181E96B91.

(81) Paul M; Lador A; Leibovici, G.-G. S. Cochrane Library Cochrane Database of Systematic Reviews Beta Lactam Antibiotic Monotherapy versus Beta Lactam-Aminoglycoside Antibiotic Combination Therapy for Sepsis (Review). *Cochrane Database Syst. Rev.* **2014**, 3344. https://doi.org/10.1002/14651858.CD003344.pub3.

(82) Safdar, N.; Handelsman, J.; Maki, D. G. Does Combination Antimicrobial Therapy Reduce Mortality in Gram-Negative Bacteraemia? A Meta-Analysis. *Lancet Infect. Dis.* **2004**, *4* (8), 519–527. https://doi.org/10.1016/S1473-3099(04)01108-9.

(83) Tamma, P. D.; Cosgrove, S. E.; Maragakis, L. L. Combination Therapy for Treatment of Infections with Gram-Negative Bacteria. **2012**. https://doi.org/10.1128/CMR.05041-11.

(84) Kumar, A.; Zarychanski, R.; Light, B.; Parrillo, J.; Maki, D.; Simon, D.; Laporta, D.; Lapinsky, S.; Ellis, P.; Mirzanejad, Y.; Martinka, G.; Keenan, S.; Wood, G.; Arabi, Y.; Feinstein, D.; Kumar, A.; Dodek, P.; Kravetsky, L.; Doucette, S. Early Combination Antibiotic Therapy Yields Improved Survival Compared with Monotherapy in Septic Shock: A Propensity-Matched Analysis. *Crit. Care Med.* **2010**, *38* (9), 1773–1785. https://doi.org/10.1097/CCM.0B013E3181EB3CCD.

(85) DiMasi, J. A.; Hansen, R. W.; Grabowski, H. G. The Price of Innovation: New Estimates of Drug Development Costs. *J. Health Econ.* **2003**, *22*, 151–185. https://doi.org/10.1016/S0167-6296(02)00126-1.

(86) Albain, K. S.; Nag, S. M.; Calderillo-Ruiz, G.; Jordaan, J. P.; Llombart, A. C.; Pluzanska, A.; Rolski, J.; Melemed, A. S.; Reyes-Vidal, J. M.; Sekhon, J. S.; Simms, L.; O'Shaughnessy, J. Gemcitabine plus Paclitaxel versus Paclitaxel Monotherapy in Patients with Metastatic Breast Cancer and Prior Anthracycline Treatment. *J. Clin. Oncol.* **2008**, *26* (24), 3950–3957. https://doi.org/10.1200/JCO.2007.11.9362.

(87) Mokhtari, R. B.; Kumar, S.; Islam, S. S.; Yazdanpanah, M.; Adeli, K.; Cutz, E.; Yeger, H. Combination of Carbonic Anhydrase Inhibitor, Acetazolamide, and Sulforaphane, Reduces the Viability and Growth of Bronchial Carcinoid Cell Lines. **2013**. https://doi.org/10.1186/1471-2407-13-378.

(88) Melnyk, A. H.; Wong, A.; Kassen, R. The Fitness Costs of Antibiotic Resistance Mutations. *Evol. Appl.* **2015**, *8* (3), 273. https://doi.org/10.1111/EVA.12196.

(89) Clatworthy, A. E.; Pierson, E.; Hung, D. T. Targeting Virulence : A New Paradigm for Antimicrobial Therapy. *Nat. Chem. Biol.* **2007**, *3* (9), 541–548. https://doi.org/10.1038/nchembio.2007.24.

(90) Bullen, J. J.; Rogers, H. J.; Spalding, P. B.; Ward, C. G. Iron and Infection: The Heart of

the Matter. *FEMS Immunol. Med. Microbiol.* **2005**, *43*, 325–330. https://doi.org/10.1016/j.femsim.2004.11.010.

(91)   Griffiths, E. Iron in Biological Systems. In *Iron and infection: molecular, physiological and clinical aspects*; Bullen, D. J., Griffiths, E., Eds.; John Wiley & Sons Ltd: Chichester, 1999; pp 1–26.

(92)   Hider, R. C.; Kong, X. Chemistry and Biology of Siderophores. *Nat. Prod. Rep.* **2010**, *27* (5), 637–657. https://doi.org/10.1039/b906679a.

(93)   Johnstone, T. C.; Nolan, E. M. Beyond Iron: Non-Classical Biological Functions of Bacterial Siderophores. *Dalt. Trans.* **2015**, *44* (14), 6320–6339. https://doi.org/10.1039/c4dt03559c.

(94)   Kloepper, J. W.; Leong, J.; Teintze, M.; Schroth, M. N. Enhanced Plant Growth by Siderophores Produced by Plant Growth-Promoting Rhizobacteria. *Nature* **1980**, *286*, 885–886. https://doi.org/10.1038/286885a0.

(95)   Haas, H.; Eisendle, M.; Turgeon, B. G. Siderophores in Fungal Physiology and Virulence. *Annu. Rev. Phytopathol.* **2008**, *46*, 149–187. https://doi.org/10.1146/annurev.phyto.45.062806.094338.

(96)   Singh, S.; Singh, S. K.; Chowdhury, I.; Singh, R. Understanding the Mechanism of Bacterial Biofilms Resistance to Antimicrobial Agents. *Open Microbiol. J.* **2017**, *11*, 53–62. https://doi.org/10.2174/1874285801711010053.

(97)   Cutler, P. Deferoxamine Therapy in High-Ferritin Diabetes. *Diabetes* **1989**, *38*, 1207–1210.

(98)   Bergeron, R.; Wiegand, J.; Dionis, J.; Al, E. Evaluation of Desferrithiocin and Its Synthetic Analogues as Orally Effective Iron Chelators. *J. Med. Chem.* **1991**, *34*, 2072–2078.

(99)   Buss, J.; Greene, B.; Turner, J.; Torti, F.; Torti, S. Iron Chelators in Cancer Chemotherapy. *Curr. Top. Med. Chem.* **2004**, *4*, 1623–1635.

(100) Borgna-Pignatti, C.; Cappellini, M.; De Stefano, P.; Del Vecchio, G.; Forni, G.; Gamberini, M.; Ghilardi, R.; Piga, A.; Romeo, M.; Zhao, H.; Cnaan, A. Cardiac Morbidity and Mortality in Deferoxamine- or Deferiprone-Treated Patients with Thalassemia Major. *Blood* **2006**, *107* (9), 3733–3737.

(101) Meng, L.; Cai, W.; Qu, H.; Liu, J.; Lan, J.; Lu, J.; Lan, T.; Li, J. Inhibition of Ethylenediaminetetraacetic Acid (EDTA) on Biofilm Formation of Staphylococcus Aureus. *Food Sci. Technol. Res.* **2013**, *19* (2), 323–330.

(102) Moreau-Marquis, S.; O'Toole, G. A.; Stanton, B. A. Tobramycin and FDA-Approved Iron Chelators Eliminate Pseudomonas Aeruginosa Biofilms on Cystic Fibrosis Cells. *Am. J. Respir. Cell Mol. Biol.* **2009**, *41*, 305–313. https://doi.org/10.1165/rcmb.2008-0299OC.

(103) O'May, C. Y.; Sanderson, K.; Roddam, L. F.; Kirov, S. M.; Reid, D. W. Iron-Binding Compounds Impair Pseudomonas Aeruginosa Biofilm Formation, Especially under Anaerobic Conditions. *J. Med. Microbiol.* **2009**, *58*, 765–773. https://doi.org/10.1099/jmm.0.004416-0.

(104) Gentile, V.; Frangipani, E.; Bonchi, C.; Minandri, F.; Runci, F.; Visca, P. Iron and Acinetobacter Baumannii Biofilm Formation. *Pathogens* **2014**, *3*, 704–719. https://doi.org/10.3390/pathogens3030704.

(105) Windus, D. W.; Stokes, T. J.; Julian, B. A.; Fenves, A. Z. Fatal Rhizopus Infections in Hemodialysis Patients Receiving Deferoxamine. *Ann. Intern. Med.* **1987**, *107*, 678–680. https://doi.org/10.7326/0003-4819-107-5-678.

(106) García-Quintanilla, M.; Pulido, M. R.; López-Rojas, R.; Pachón, J.; McConnell, M. J. Emerging Therapies for Multidrug Resistant Acinetobacter Baumannii. *Trends Microbiol.* **2013**, *21* (3), 157–163. https://doi.org/10.1016/j.tim.2012.12.002.

(107) De Léséleuc, L.; Harris, G.; KuoLee, R.; Chen, W. In Vitro and in Vivo Biological Activities of Iron Chelators and Gallium Nitrate against Acinetobacter Baumannii. *Antimicrob. Agents Chemother.* **2012**, *56* (10), 5397–5400. https://doi.org/10.1128/AAC.00778-12.

(108) Antunes, L. C. S.; Imperi, F.; Minandri, F.; Visca, P. In Vitro and In Vivo Antimicrobial Activities of Gallium Nitrate against Multidrug-Resistant Acinetobacter Baumannii. *Antimicrob. Agents Chemother.* **2012**, *56* (11), 5961–5970. https://doi.org/10.1128/AAC.01519-12.

(109) Kaneko, Y.; Thoendel, M.; Olakanmi, O.; Britigan, B. E.; Singh, P. K. The Transition Metal Gallium Disrupts Pseudomonas Aeruginosa Iron Metabolism and Has Antimicrobial and Antibiofilm Activity. *J. Clin. Invest.* **2007**, *117* (4), 877–888. https://doi.org/10.1172/JCI30783.

(110) Runci, F.; Bonchi, C.; Frangipani, E.; Visaggio, D.; Visca, P. Acinetobacter Baumannii Biofilm Formation in Human Serum and Disruption by Gallium. *Antimicrob. Agents Chemother.* **2017**, *61* (1), 1–8. https://doi.org/10.1128/AAC.01563-16.

(111) Garcia, R. A.; Tennent, D. J.; Chang, D.; Wenke, J. C.; Sanchez, C. J. An in Vitro Comparison of PMMA and Calcium Sulfate as Carriers for the Local Delivery of Gallium(III) Nitrate to Staphylococcal Infected Surgical Sites. *Biomed Res. Int.* **2016**, 1–11. https://doi.org/10.1155/2016/7078989.

(112) Banin, E.; Lozinski, A.; Brady, K. M.; Berenshtein, E.; Butterfield, P. W.; Moshe, M.; Chevion, M.; Greenberg, E. P.; Banin, E. The Potential of Desferrioxamine-Gallium as an Anti-Pseudomonas Therapeutic Agent. *Proc. Natl. Acad. Sci.* **2008**, *105* (43), 16761–16766. https://doi.org/10.1073/pnas.0808608105.

(113) Alvarez-Ortega, C.; Wiegand, I.; Olivares, J.; Hancock, R. E. W.; Martínez, J. L. The Intrinsic Resistome of Pseudomonas Aeruginosa to β-Lactams. *Virulence* **2011**, *2*, 144–146. https://doi.org/10.4161/viru.2.2.15014.

(114) Costa, S. S.; Viveiros, M.; Amaral, L.; Couto, I. Multidrug Efflux Pumps in Staphylococcus Aureus: An Update. *Open Microbiol. J.* **2013**, *7*, 59–71. https://doi.org/10.2174/1874285801307010059.

(115) Chitambar, C. R. Medical Applications and Toxicities of Gallium Compounds. *Int. J. Environ. Res. Public Health* **2010**, *7* (5), 2337–2361. https://doi.org/10.3390/ijerph7052337.

(116) Bernstein, L. R. Mechanisms of Therapeutic Activity for Gallium. *Pharmacol. Rev.* **1998**, *50*, 665–682. https://doi.org/10.1021/la8038335.

(117) Lamb, A. L. Breaking a Pathogen's Iron Will: Inhibiting Siderophore Production as an Antimicrobial Strategy. *Biochim Biophys Acta* **2015**, *1854* (8), 1054–1070.

(118) Bleuel, C.; Grosse, C.; Taudte, N.; Scherer, J.; Wesenberg, D.; Krauss, G. J.; Nies, D. H.; Grass, G. TolC Is Involved in Enterobactin Efflux across the Outer Membrane of Escherichia Coli. *J. Bacteriol.* **2005**, *187*, 6701–6707.

(119) Vinella, D.; Albrecht, C.; Cashel, M.; D'Ari, R. Iron Limitation Induces SpoT-Dependent Accumulation of PpGpp in Escherichia Coli. *Mol. Microbiol.* **2005**, *56*, 958–970.

(120) Theriault, J.; Wurst, J.; Jewett, I.; Verplank, L.; Perez, J.; Gulick, A.; Drake, E.; Palmer, M.; Moskowitz, S.; Dasgupta, N.; Brannon, M.; Dandapani, S.; Munoz, B.; Schreiber, S.

Identification of a Small Molecule Inhibitor of Pseudomonas Aeruginosa PvdQ Acylase, an Enzyme Involved in Siderophore Pyoverdine Synthesis. *Probe Reports from NIH Mol. Libr. Progr.* **2010**.

(121) Eijkelkamp, B. A.; Hassan, K. A.; Paulsen, I. T.; Brown, M. H. Investigation of the Human Pathogen Acinetobacter Baumannii under Iron Limiting Conditions. *BMC Genomics* **2011**, *12* (126), 1–14. https://doi.org/10.1186/1471-2164-12-126.

(122) Häußler, S. Biofilm Formation by the Small Colony Variant Phenotype of Pseudomonas Aeruginosa. *Environ. Microbiol.* **2004**, *6*, 546–551. https://doi.org/10.1111/j.1462-2920.2004.00618.x.

(123) Waksman, G.; Hultgren, S. J. Structural Biology of the Chaperone-Usher Pathway of Pilus Biogenesis. *Nat. Rev. Microbiol.* **2009**, *7*, 765–774. https://doi.org/10.1038/nrmicro2220.

(124) Nudleman, E.; Kaiser, D. Pulling Together with Type IV Pili. *J. Mol. Microbiol. Biotechnol.* **2004**, *7*, 52–62. https://doi.org/10.1159/000077869.

(125) Moche, M.; Schlüter, R.; Bernhardt, J.; Plate, K.; Riedel, K.; Hecker, M.; Becher, D. Time-Resolved Analysis of Cytosolic and Surface-Associated Proteins of Staphylococcus Aureus HG001 under Planktonic and Biofilm Conditions. *J. Proteome Res.* **2015**, *14* (9), 3804–3822. https://doi.org/10.1021/acs.jproteome.5b00148.

(126) Lin, M. H.; Shu, J. C.; Huang, H. Y.; Cheng, Y. C. Involvement of Iron in Biofilm Formation by Staphylococcus Aureus. *PLoS One* **2012**, *7* (3), 1–7. https://doi.org/10.1371/journal.pone.0034388.

(127) Johnson, M.; Cockayne, A.; Williams, P. H.; Morrissey, J. A. Iron-Responsive Regulation of Biofilm Formation in Staphylococcus Aureus Involves Fur-Dependent and Fur-Independent Mechanisms. *J. Bacteriol.* **2005**, *187*, 8211–8215. https://doi.org/10.1128/JB.187.23.8211-8215.2005.

(128) Johnson, M.; Cockayne, A.; Morrissey, J. A. Iron-Regulated Biofilm Formation in Staphylococcus Aureus Newman Requires Ica and the Secreted Protein Emp. *Infect. Immun.* **2008**, *76*, 1756–1765. https://doi.org/10.1128/IAI.01635-07.

(129) Leonov, V. V; Mironov, A. Y. The Formation of Biofilm in Opportunistic Microorganisms in Blood Plasma Depending on Content of Iron. *Klin. Lab. Diagnostika* **2016**, *61* (1), 52–54.

(130) Kang, D.; Kirienko, N. V. Interdependence between Iron Acquisition and Biofilm Formation in Pseudomonas Aeruginosa. *J. Microbiol.* **2018**, *56* (7), 449–457. https://doi.org/10.1007/s12275-018-8114-3.

(131) Meyer, J. M.; Neely, A.; Stintzi, A.; Georges, C.; Holder, I. A. Pyoverdin Is Essential for Virulence of Pseudomonas Aeruginosa. *Infect. Immun.* **1996**, *64* (2), 518–523. https://doi.org/10.4081/ijfs.2014.2112.

(132) Takase, H.; Nitanai, H.; Hoshino, K.; Otani, T. Impact of Siderophore Production on Pseudomonas Aeruginosa Infections in Immunosuppressed Mice. *Infect. Immun.* **2000**, *68*, 1834–1839. https://doi.org/10.1128/IAI.68.4.1834-1839.2000.

(133) Minandri, F.; Imperi, F.; Frangipani, E.; Bonchi, C.; Visaggio, D.; Facchini, M.; Pasquali, P.; Bragonzi, A.; Visca, P. Role of Iron Uptake Systems in Pseudomonas Aeruginosa Virulence and Airway Infection. *Infect. Immun.* **2016**, *84*, 2324–2335. https://doi.org/10.1128/IAI.00098-16.

(134) Ankenbauer, R.; Skiyosachati, S.; Cox, C. D. Effects of Siderophores on the Growth of Pseudomonas Aeruginosa in Human Serum and Transferrin. *Infect. Immun.* **1985**, *45*, 132–140.

(135) Banin, E.; Vasil, M. L.; Greenberg, E. P. Iron and Pseudomonas Aeruginosa Biofilm Formation. *Proc. Natl. Acad. Sci. U. S. A.* **2005**, *102* (31), 11076–11081. https://doi.org/10.1073/pnas.0504266102.

(136) Lamont, I. L.; Beare, P. A.; Ochsner, U.; Vasil, A. I.; Vasil, M. L. Siderophore-Mediated Signaling Regulates Virulence Factor Production in Pseudomonas Aeruginosa. *Proc. Natl. Acad. Sci. U. S. A.* **2002**, *99* (10), 7072–7077.

(137) de Chial, M.; Ghysels, B.; Beatson, S. A.; Geoffroy, V.; Meyer, J. M.; Pattery, T.; Baysse, C.; Chablain, P.; Parsons, Y. N.; Winstanley, C.; Cordwell, S. J.; Cornelis, P. Identification of Type II and Type III Pyoverdine Receptors from Pseudomonas Aeruginosa. *Microbiology* **2003**, *149*, 821–831. https://doi.org/10.1099/mic.0.26136-0.

(138) Denayer, S.; Matthijs, S.; Cornelis, P. Pyocin S2 (Sa) Kills Pseudomonas Aeruginosa Strains via the FpvA Type I Ferripyoverdine Receptor. *J. Bacteriol.* **2007**, *189* (21), 7663–7668. https://doi.org/10.1128/JB.00992-07.

(139) Elfarash, A.; Wei, Q.; Cornelis, P. The Soluble Pyocins S2 and S4 from Pseudomonas Aeruginosa Bind to the Same FpvAI Receptor. *Microbiologyopen* **2012**, *1* (3), 268–275. https://doi.org/10.1002/mbo3.27.

(140) Kang, D.; Kirienko, N. V. High-Throughput Genetic Screen Reveals That Early Attachment and Biofilm Formation Are Necessary for Full Pyoverdine Production by Pseudomonas Aeruginosa. *Front. Microbiol.* **2017**, *8*, 1707. https://doi.org/10.3389/fmicb.2017.01707.

(141) Lawlor, M. S.; O'Connor, C.; Miller, V. L. Yersiniabactin Is a Virulence Factor for Klebsiella Pneumoniae during Pulmonary Infection. *Infect. Immun.* **2007**, *75* (3), 1463–1472. https://doi.org/10.1128/IAI.00372-06.

(142) Russo, T. A.; Shon, A. S.; Beanan, J. M.; Olson, R.; MacDonald, U.; Pomakov, A. O.; Visitacion, M. P. Hypervirulent K. Pneumoniae Secretes More and More Active Iron-Acquisition Molecules than "Classical" k. Pneumoniae Thereby Enhancing Its Virulence. *PLoS One* **2011**, *6* (10), 1–13. https://doi.org/10.1371/journal.pone.0026734.

(143) Lisiecki, P. Antibiotic Resistance and Siderophore Production in Enterococci. *Med Dosw Mikrobiol* **2014**, *66* (1), 1–10.

(144) Park, S. R.; Tripathi, A.; Wu, J.; Schultz, P. J.; Yim, I.; McQuade, T. J.; Yu, F.; Arevang, C. J.; Mensah, A. Y.; Tamayo-Castillo, G.; Xi, C.; Sherman, D. H. Discovery of Cahuitamycins as Biofilm Inhibitors Derived from a Convergent Biosynthetic Pathway. *Nat. Commun.* **2016**, *7*, 1–11. https://doi.org/10.1038/ncomms10710.

Chapter 2. Synthesis and Biological Investigation of Promysalin Alkyl Analogs

Chapter 2 has been adapted with permission from (**Post, S. J.**[‡]; Keohane, C. E.[‡]; Rossiter, L. M.; Kaplan, A. R.; Khowsathit, J.; Karanicolas, J.; Wuest, W. M.* "Target-based design of promysalin analogs identifies a new putative binding cleft in succinate dehydrogenase." *ACS Infectious Disease.* **2020**, 6, 6, 1372-1377.). **Copyright © 2018 American Chemical Society**

The work for the alkyl analogs was completed in collaboration with Dr. Colleen Keohane, a former graduate student in our lab.

2.1. Introduction

Since the introduction of penicillin into hospitals in 1943, antibiotics have played an instrumental role in the treatment of bacterial infections.[146] Despite this success, the threat of antibiotic-resistant microbes continues to increase. According to the recent report by the CDC, there are over 2.8 million cases of antibiotic-resistant infections reported annually, resulting in more than 35,000 deaths.[147] One cause of antibiotic resistance is the misuse and over-prescription of clinical antibiotics, most of which are broad-spectrum, meaning they target a wide range of bacterial species.[148] While broad spectrum therapeutics are beneficial when the identity of the infecting pathogen is unknown, their use eradicates all susceptible bacteria, increasing nutrient availability to resistant microbes, and enabling them to proliferate rapidly.[149,150] This is particularly problematic for patients with compromised immune systems, as they are unable to fend off infections without heavy, prolonged use of broad-spectrum antibiotics.

Particularly at risk by this extensive use of broad-spectrum antibiotics are those with cystic fibrosis (CF), which is caused by a defect in the gene encoding the CFTR (cystic fibrosis transmembrane regulator) protein. This disease results in the build-up of thick mucus layers in the lungs,[151] providing harmful pathogens such as *Staphylococcus aureus* and *Pseudomonas aeruginosa* with an ideal environment for colonization and infection. Once colonized, patients are required to continuously take high doses of antibiotics for the entirety of their lives.[152] Accompanying this extensive antibiotic treatment is the

emergence of multidrug-resistant *P. aeruginosa*, with an estimated 32,600 cases reported in hospitalized patients, resulting in 2,700 deaths, and costing the public $767 million in 2017.[153]

These problems have triggered a renewed effort to develop narrow-spectrum antibiotics, defined as being active against only Gram-positive or only Gram-negative bacteria, to combat these resistant microbes.[154] An even more effective tactic to avoid both resistance development and collateral damage to commensal species would be the use of species-specific antibiotics, especially for colonized CF patients, for which 80% are infected by *P. aeruginosa* by the age of 18.[155] As a result, our group has become interested in the prospect of developing an antibiotic that is active solely against *P. aeruginosa*. This goal is quite daunting, due to the complex nature of bacteria, their ability to rapidly adapt, and the significant overlap in biological targets. We expected to find such specificity in nature, particularly in the rhizosphere where Gram-negative pathogens like *P. aeruginosa* thrive. We sought inspiration from recently characterized natural products to fill this scientific gap.[156–158]

In 2011 De Mot and coworkers isolated a new metabolite from *Pseudomonas putida*, promysalin ((–)-**1**, Figure 2.1A), which was shown to selectively inhibit growth of *P. aeruginosa*, despite being tested against wide variety of other Gram-negative and Gram-positive species.[159] Intrigued by this highly selective nature, our lab soon published the first total synthesis of the natural product.[160] We subsequently reported the diverted total synthesis of a number of structural analogs and their biological activity as summarized in
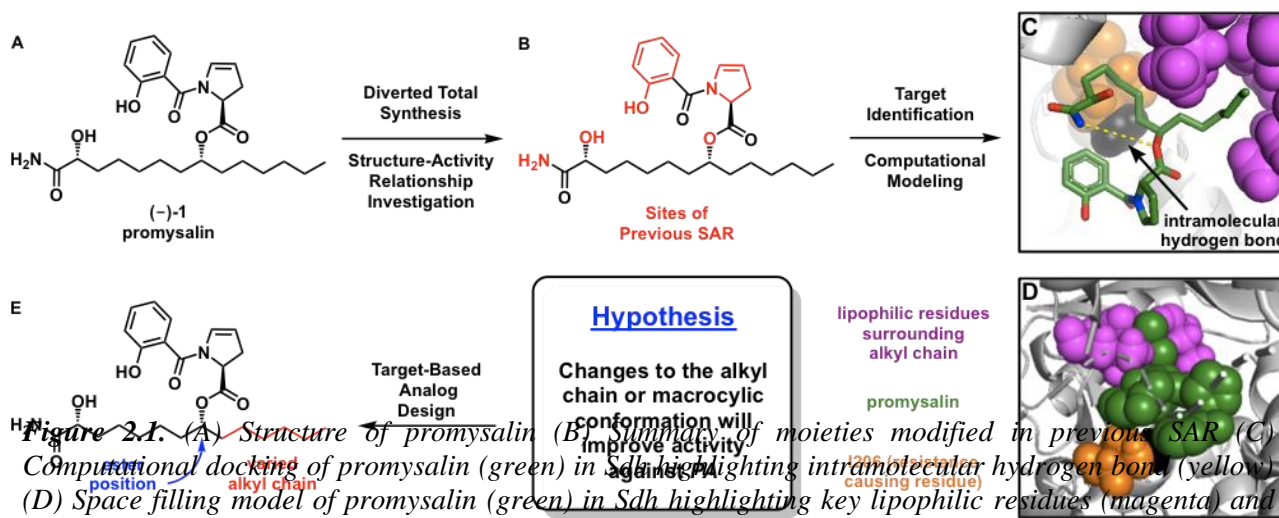
Figure 2.1. *(A) Structure of promysalin (B) Summary of moieties modified in previous SAR (C) Computational docking of promysalin (green) in Sdh highlighting intramolecular hydrogen bond (yellow) (D) Space filling model of promysalin (green) in Sdh highlighting key lipophilic residues (magenta) and resistance mutation (orange) (E) Summary of structural changes in new promysalin analogs.*

Figure 2.1B.[161,162] Based on these findings and competing studies that postulated that promysalin targeted the cell membrane of *S. aureus*,[163] we sought to definitively identify the biological target. Our SAR investigation enabled the synthesis of a probe compound utilizing the Yao minimalist probe[164], facilitating our subsequent target identification studies. Using affinity-based protein profiling, we identified succinate dehydrogenase (Sdh) as the biological target of promysalin in *P. aeruginosa*.[165] This mechanism was validated by a resistance selection assay followed by whole genome sequencing of two resulting mutants, revealing the mutation of I206V in Sdh via an identical single nucleotide point mutation. We had previously described the ability of promysalin to chelate iron[161] but further transcriptomic studies by our group rationalized the anti-virulence activity to also correlate to inhibition of Sdh.[166] Interestingly, the activity and structure of promysalin is reminiscent to that of siccanin, a fungal Sdh inhibitor that was rediscovered as an antibiotic that specifically inhibits *P. aeruginosa*.[167,168]

With the protein target identified, we then sought to use this information to strategically design new analogs based on the structure of Sdh. Both of our target identification experiments indicated that promysalin was interacting in the ubiquinone binding site, which is in line with the mechanism of known Sdh inhibitors.[169,170] Based on this information, we carried out computational docking of promysalin using a previously characterized homologous *E. coli* model of Sdh[171] along with known binding models of other previously characterized inhibitors.[172] (Figure 2.1C, 2.1D). This model indicated that promysalin binds with a macrocyclic conformation dictated by an intramolecular hydrogen bond between the ester and the amide, which has been reaffirmed by previous structure activity relationships (Figure 2.1C).[165] The model also revealed that I206 (Figure 2.1D, orange) has increased hydrophobic contacts with promysalin (green) as compared to ubiquinone, the native substrate. Mutation of this isoleucine to valine eliminates these key interactions (black) and results in a ~50-fold reduction in activity, revealing the importance of these contacts. With this information in hand, we wanted to design synthetic analogs that would potentially restore these interactions. Accordingly, we hypothesized that changing the position of the ester on the carbon side chain would impact this macrocyclic conformation of the molecule thereby potentially regaining contacts in the resistant strain. Additional inspection of the model showed that the aliphatic tail

of promysalin is positioned in a pocket containing several hydrophobic residues (Figure 2.1D, magenta) that could contribute to positive binding interactions. We postulated that although nature has provided a fantastic lead compound in promysalin, it is limited in the molecular building blocks at its disposal, wherein the side chain of promysalin is derived from myristic acid. However, as organic chemists, we are limited solely by the synthetic buildings blocks available. The flexibility of our synthetic strategy provided us with the ability to manipulate the alkyl chain in order to optimize the biological activity, pharmacological profile, and potentially identify new binding modes.

2.2.   Synthesis

To assess these hypotheses, we now synthesized a series of rationally designed structural analogs with side chains of varying length (Table 2.1, **11e-11j**) and steric bulk (**11c-11d**). Two additional analogs would retain the overall 14-carbon sidechain but move the position of the ester from C_8 (**1**) to C_7 (**11a**) or C_9 (**11b**), which would serve to manipulate the macrocyclic conformation. Employing our previously reported synthetic route,[160] we began by installing an Evans chiral auxiliary to commercially available *n*-eneoic acids (Scheme 2.1). This enabled a stereoselective Davis oxidation followed by TBS protection affording various fragments with general structure **4**, where n = 0, 1, or 2. Cross metathesis with homoallylic alcohols (**5**), synthesized to accommodate a wide range of alkyl substituents, followed by hydrogenation and subsequent auxiliary removal afforded fragments with general structure **8**, where R corresponds to the alkyl tail of the final analogs (Table 2.1). EDC-mediated esterification with compound **9** (synthesis reported previously[160]) followed by global deprotection afforded analogs **11a-11j**, which were obtained in overall yields ranging from 15-42%.
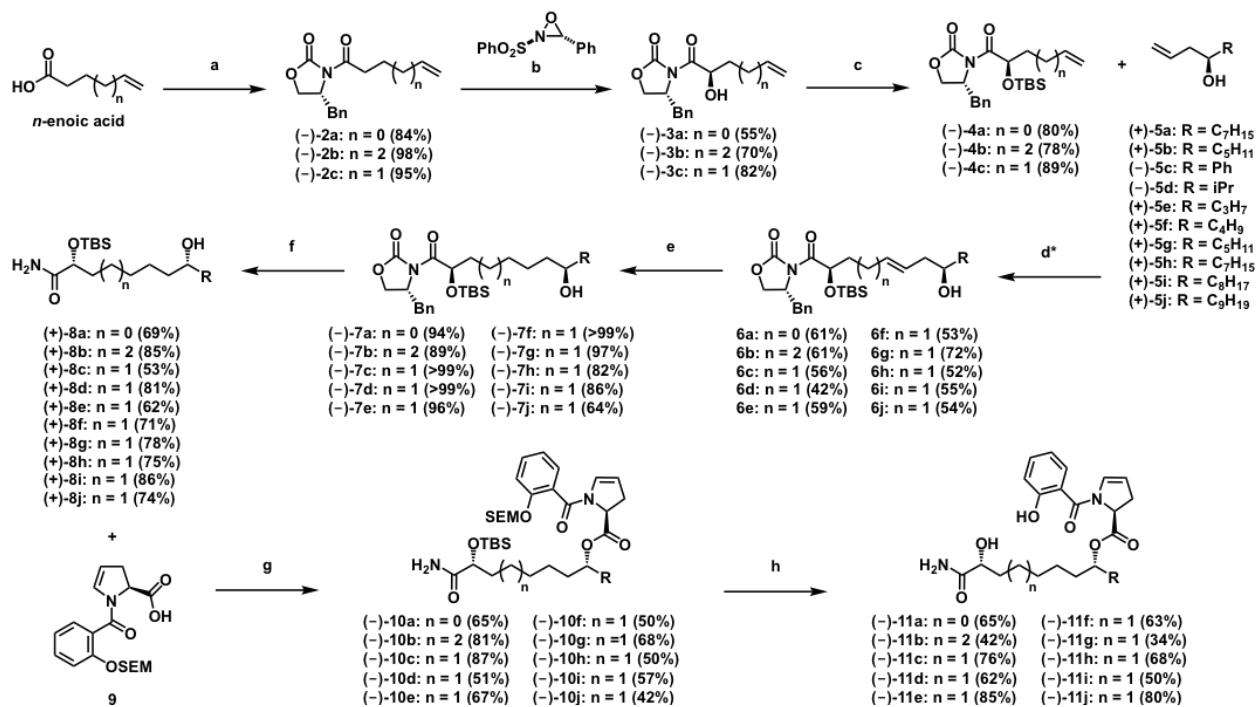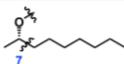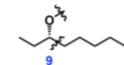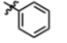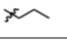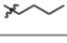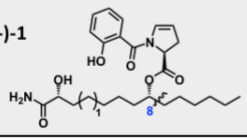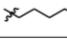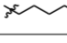
Scheme 2.1. *General synthetic route for the synthesis of new promysalin analogs. Reaction Conditions: (a) i) NEt₃, PivCl, THF ii) LiCl, (R)-4-Benzyl-2-oxazolidinone; (b) NaHMDS, CSA; (c) TBSCl, imidazole, DMF; (d) Grubbs Catalyst C711, DCM; *4c used to make 6c-6j; (e) H₂, Pd/C, EtOAc; (f) NH₄OH, THF/H₂O; (g) EDC, DMAP, DCM; (h) TBAF, DMPU, THF*

2.3.   Growth Inhibition

With 10 new analogs in hand, we evaluated their inhibitory activity against the *P. aeruginosa* strains, PA14 and PAO1, and the resistant *P. aeruginosa* strain selected for in our laboratory, RO5 (Table 2.1, Table 5.1.1). As we expected, the activity of the linear alkyl chain analogs varied significantly with chain length. Generally, those with truncated chains relative to promysalin were less active (Table 2.1, **11e-11g**), while extending the chain by one or two carbons increased activity (**11h, 11i**). These results indicate that the hydrophobic interactions with the alkyl tail are important for binding affinity. However, if too many carbons were added (**11j**), activity diminished, suggesting that we had achieved optimal chain length in analog **11h**. Alternatively, adding sterically hindered or rigid groups such as phenyl (**11c**) or isopropyl (**11d**) to a truncated chain greatly reduced activity, suggesting that the binding pocket does not easily

accommodate nonlinear tails. Finally, changing the position of the ester, and presumably disrupting the intramolecular hydrogen bonding network, decreased activity (**11a, 11b**), indicating that this structural feature is critical for an optimized conformation within the binding pocket. Interestingly, the activity of most analogs decreased only marginally in the resistant strain (5-12-fold decrease) relative to promysalin (~50-fold decrease) (Table 5.1.1). However, other analogs had a greater reduction in activity compared to promysalin. Overall, a general trend was not observed between chain length and differential inhibitory activity between resistant and susceptible strains.

	Structure	PA14 IC$_{50}$ (μM)	PA14 IC$_{90}$ (μM)	Overall Yield
Connectivity (-)-11a n = 0		3.1	12	27%
Connectivity (-)-11b n = 2		5.7	22	22%
Bulky (-)-11c n = 1		38	140	42%
Bulky (-)-11d n = 1		130	200	20%
Truncated (-)-11e n = 1		9.4	22	36%
Truncated (-)-11f n = 1		5.7	21	20%
Truncated (-)-11g n = 1		2.5	12	15%
Gentamicin		3.6	17	--
(-)-1		0.065	4.6	39%
Elongated (-)-11h n = 1		0.026	0.89	22%
Elongated (-)-11i n = 1		0.035	1.0	18%
Elongated (-)-11j n = 1		0.15	1.6	21%

Table 2.1*. Summary of overall yield for promysalin and analogs and growth inhibition against PA14. Gentamicin was used as a positive control. IC$_{50}$ and IC$_{90}$ values are the average of three trials.*
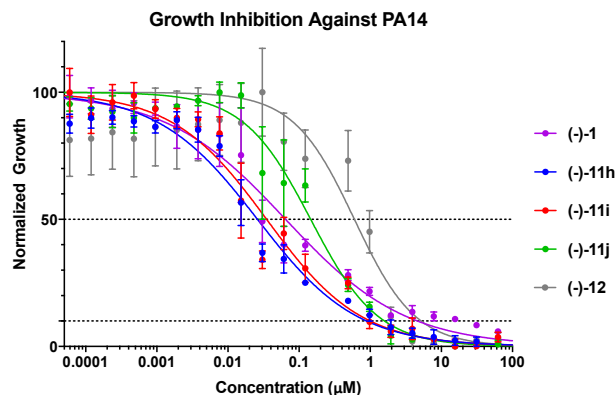
Figure 2.2. *Inhibitory activity of promysalin and extended chain analogs against PA14. Best fit lines and data points are the average of three trials (error bars indicate SEM). Dotted lines indicate IC_{50} and IC_{90}.*

2.4.   Computational Modeling

In order to rationalize the observed biological activity, we built computational models of these analogs in complex with Sdh. We were surprised to find that the positioning of the alkyl chain in these models was not always the same as in promysalin. All analogs with shorter alkyl chains resulted in conformations very similar to that observed with promysalin (Figure 2.3A, green). However, all analogs with increased tail length were positioned such that their tail was oriented into a previously unidentified binding cleft (Figure 2.3A, orange), as the native orientation would unfavorably extend the hydrophobic side chain into a solvent-exposed region. We postulated that this is the driving force for the longer analogs to occupy this new area of the binding pocket.

We also identified a tryptophan residue (Figure 2.3B, blue) in proximity to the alkyl chain terminus in the new binding orientation. We speculated that installing a terminal aromatic group on the side chain would induce π-stacking interactions with the protein resulting in a higher binding affinity.[173] Additional computational analysis revealed that an ideal chain length would contain six carbons between the aromatic moiety the ester linker arriving at analog **12** (Figure 2.3B, purple; 3C). Anna Kaplan, a former graduate student in our lab, subsequently synthesized **12** in 21% overall yield, via our previously described synthetic sequence with only minor modifications (Scheme 5.1.1). We then examined its inhibitory activity against

PA14. These results revealed that **12** an $IC_{50} = 0.75$ µM and an $IC_{90} = 1.8$ µM. Although this is less potent than the parent compound, it is >200 fold more active than the truncated aryl analog **11c**. This indicates that this new binding cleft is more amenable to changes, and this analog provides a promising starting point for further optimization.
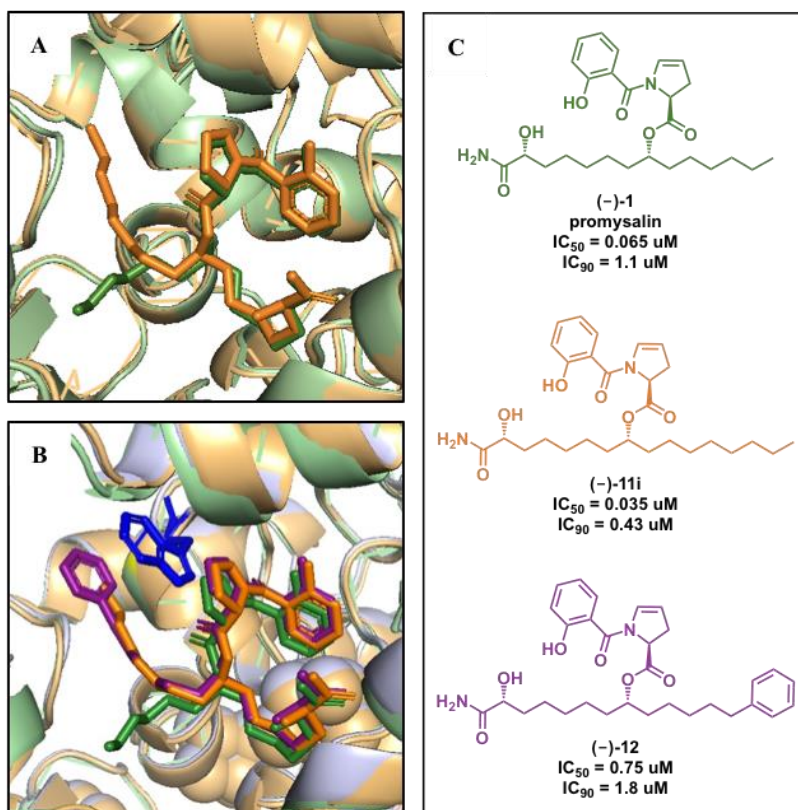
Figure 2.3. *(A) Computational model of promysalin (green) and extended chain analog 11i (orange). (B) Model of promysalin, analog 11i, and extended aromatic analog 12 (purple). TRP161 residue on Sdh shown in blue. (C) Structures of promysalin and analogs 11i and 12, and their inhibitory activity against PA14.*

2.5. Conclusions

In conclusion, we have synthesized eleven promysalin analogs based on its computationally predicted binding mode in Sdh. Biological investigation of these analogs revealed that manipulating the hydrophobic character on the alkyl chain has a direct effect on growth inhibition, resulting in two analogs more potent than the natural product. Notably, a new binding cleft was revealed through computational modeling of Sdh, which has the ability to accommodate greater structural diversity, including both linear

and rigid aromatic moieties, and leads to improved IC$_{90}$ values. This provides the basis for future work focused on optimization of binding interactions in the newly discovered cleft combined with other improvements previously reported by our group toward the development of a potent *P. aeruginosa*-specific antimicrobial.

2.6. References

(146) Ventola, C. L. The Antibiotic Resistance Crisis: Causes and Threats. *P T J.* **2015**, *40*, 277–283. https://doi.org/Article.

(147) Biggest Threats and Data. *CDC's Antibiotic Resistance Threats Report*. 2019.

(148) Lewis, K. Platforms for Antibiotic Discovery. *Nat. Rev. Drug Discov.* **2013**, *12*, 371–387. https://doi.org/10.1038/nrd3975.

(149) Garland, M.; Loscher, S.; Bogyo, M. Chemical Strategies To Target Bacterial Virulence. *Chem. Rev.* **2017**, *117*, 4422–4461. https://doi.org/10.1021/acs.chemrev.6b00676.

(150) Cantón, R.; Morosini, M. I. Emergence and Spread of Antibiotic Resistance Following Exposure to Antibiotics. *FEMS Microbiol. Rev.* **2011**, *35*, 977–991. https://doi.org/10.1111/j.1574-6976.2011.00295.x.

(151) Heijerman, H. Infection and Inflammation in Cystic Fibrosis: A Short Review. *J. Cyst. Fibros.* **2005**, *4* (2), 3–5. https://doi.org/10.1016/j.jcf.2005.05.005.

(152) Bhagirath, A. Y.; Li, Y.; Somayajula, D.; Dadashi, M.; Badr, S.; Duan, K. Cystic Fibrosis Lung Environment and Pseudomonas Aeruginosa Infection. *BMC Pulm. Med.* **2016**, *16*, 17. https://doi.org/10.1186/s12890-016-0339-5.

(153) Multidrug-Resistant Pseudomonas Aeruginosa. *CDC's Antibiotic Resistance Threats Report*. 2019.

(154) Hopkins, S. J. *Drugs and Pharmacology for Nurses*, 12th ed.; Churchill Livingstone, 1997.

(155) Crull, M. R.; Ramos, K. J.; Caldwell, E.; Mayer-Hamblett, N.; Aitken, M. L.; Goss, C. H. Change in Pseudomonas Aeruginosa Prevalence in Cystic Fibrosis Adults over Time. *BMC Pulm. Med.* **2016**, *16*, 176. https://doi.org/10.1186/s12890-016-0333-y.

(156) Keohane, C. E.; Steele, A. D.; Wuest, W. M. The Rhizosphere Microbiome: A Playground for Natural Product Chemists. *Synlett* **2015**, *26* (20), 2739–2744. https://doi.org/10.1055/s-0035-1560711.

(157) Rossiter, S. E.; Fletcher, M. H.; Wuest, W. M. Natural Products as Platforms to Overcome Antibiotic Resistance. *Chem. Rev.* **2017**, *117* (19), 12415–12474. https://doi.org/10.1021/acs.chemrev.7b00283.

(158) Abouelhassan, Y.; Garrison, A. T.; Yang, H.; Chávez-Riveros, A.; Burch, G. M.; Huigens, R. W. Recent Progress in Natural-Product-Inspired Programs Aimed to Address Antibiotic Resistance and Tolerance. *J. Med. Chem.* **2019**, *62* (17), 7618–7642. https://doi.org/10.1021/acs.jmedchem.9b00370.

(159) Li, W.; Estrada-De Los Santos, P.; Matthijs, S.; Xie, G. L.; Busson, R.; Cornelis, P.; Rozenski, J.; De Mot, R. Promysalin, a Salicylate-Containing Pseudomonas Putida Antibiotic, Promotes Surface Colonization and Selectively Targets Other Pseudomonas. *Chem. Biol.* **2011**, *18* (10), 1320–1330. https://doi.org/10.1016/j.chembiol.2011.08.006.

(160) Steele, A. D.; Knouse, K. W.; Keohane, C. E.; Wuest, W. M. Total Synthesis and Biological

Investigation of (-)-Promysalin. *J. Am. Chem. Soc.* **2015**, *137* (23), 7314–7317. https://doi.org/10.1021/jacs.5b04767.

(161) Steele, A. D.; Keohane, C. E.; Knouse, K. W.; Rossiter, S. E.; Williams, S. J.; Wuest, W. M. Diverted Total Synthesis of Promysalin Analogs Demonstrates That an Iron-Binding Motif Is Responsible for Its Narrow-Spectrum Antibacterial Activity. *J. Am. Chem. Soc.* **2016**, *138* (18), 5833–5836. https://doi.org/10.1021/jacs.6b03373.

(162) Knouse, K. W.; Wuest, W. M. The Enantioselective Synthesis and Biological Evaluation of Chimeric Promysalin Analogs Facilitated by Diverted Total Synthesis. *J. Antibiot. (Tokyo).* **2016**, *69*, 337–339. https://doi.org/10.1038/ja.2016.4.

(163) Kaduskar, R. D.; Scala, G. Della; Al Jabri, Z. J. H.; Arioli, S.; Musso, L.; Oggioni, M. R.; Dallavalle, S.; Mora, D. Promysalin Is a Salicylate-Containing Antimicrobial with a Cell-Membrane-Disrupting Mechanism of Action on Gram-Positive Bacteria. *Sci. Rep.* **2017**, *7* (8861), 1–11. https://doi.org/10.1038/s41598-017-07567-0.

(164) Li, Z.; Hao, P.; Li, L.; Tan, C. Y. J.; Cheng, X.; Chen, G. Y. J.; Sze, S. K.; Shen, H. M.; Yao, S. Q. Design and Synthesis of Minimalist Terminal Alkyne-Containing Diazirine Photo-Crosslinkers and Their Incorporation into Kinase Inhibitors for Cell- and Tissue-Based Proteome Profiling. *Angew. Chemie - Int. Ed.* **2013**, *52* (33), 8551–8556. https://doi.org/10.1002/anie.201300683.

(165) Keohane, C. E.; Steele, A. D.; Fetzer, C.; Khowsathit, J.; Van Tyne, D.; Moynié, L.; Gilmore, M. S.; Karanicolas, J.; Sieber, S. A.; Wuest, W. M. Promysalin Elicits Species-Selective Inhibition of Pseudomonas Aeruginosa by Targeting Succinate Dehydrogenase. *J. Am. Chem. Soc.* **2018**, *140* (5), 1774–1782. https://doi.org/10.1021/jacs.7b11212.

(166) Giglio, K. M.; Keohane, C. E.; Stodghill, P. V; Steele, A. D.; Fetzer, C.; Sieber, S. A.; Filiatrault, M. J.; Wuest, W. M. Transcriptomic Profiling Reveals That Promysalin Alters Metabolic Flux , Motility , and Iron Regulation in Pseudomonas Putida KT2440. 1–15.

(167) Mogi, T.; Kawakami, T.; Arai, H.; Igarashi, Y.; Matsushita, K.; Mori, M.; Shiomi, K.; Omura, S.; Harada, S.; Kita, K. Siccanin Rediscovered as a Species-Selective Succinate Dehydrogenase Inhibitor. *J. Biochem.* **2009**, *146* (3), 383–387. https://doi.org/10.1093/jb/mvp085.

(168) Nose, K.; Endo, A. Mode of Action of the Antibiotic Siccanin on Intact Cells and Mitochondria of Trichophyton Mentagrophytes. *J. Bacteriol.* **1971**, *105* (1), 176–184.

(169) Zhu, X. L.; Xiong, L.; Li, H.; Song, X. Y.; Liu, J. J.; Yang, G. F. Computational and Experimental Insight into the Molecular Mechanism of Carboxamide Inhibitors of Succinate-Ubiquinone Oxidoreductase. *ChemMedChem* **2014**, *9* (7), 1512–1521. https://doi.org/10.1002/cmdc.201300456.

(170) Xiong, L.; Li, H.; Jiang, L. N.; Ge, J. M.; Yang, W. C.; Zhu, X. L.; Yang, G. F. Structure-Based Discovery of Potential Fungicides as Succinate Ubiquinone Oxidoreductase Inhibitors. *J. Agric. Food Chem.* **2017**, *65*, 1021−1029. https://doi.org/10.1021/acs.jafc.6b05134.

(171) Yankovskaya, V.; Horsefield, R.; Törnroth, S.; Luna-Chavez, C.; Miyoshi, H.; Léger, C.; Byrne, B.; Cecchini, G.; Iwata, S. Architecture of Succinate Dehydrogenase and Reactive Oxygen Species Generation. *Science (80-.).* **2003**, *299* (5607), 700–704. https://doi.org/10.1126/science.1079605.

(172) Sierotzki, H.; Scalliet, G. A Review of Current Knowledge of Resistance Aspects for the Next-Generation Succinate Dehydrogenase Inhibitor Fungicides. *Phytopathology* **2013**, *103* (9), 880–887. https://doi.org/10.1094/PHYTO-01-13-0009-RVW.

(173) da Silva, C. H. T. P.; Campo, V. L.; Carvalho, I.; Taft, C. A. Molecular Modeling, Docking and ADMET Studies Applied to the Design of a Novel Hybrid for Treatment of Alzheimer's Disease. *J. Mol. Graph. Model.* **2006**, *25* (2), 169–175. https://doi.org/10.1016/j.jmgm.2005.12.002.

(174) Post, S. J.; Keohane, C. E.; Rossiter, L. M.; Kaplan, A. R.; Khowsathit, J.; Matuska, K.; Karanicolas, J.; Wuest, W. M. Target-Based Design of Promysalin Analogues Identifies a New Putative Binding Cleft in Succinate Dehydrogenase. **2020**, *6*, 1372–1377. https://doi.org/10.1021/acsinfecdis.0c00024.

Chapter 3. Investigation of a Simplified Promysalin Analog for Antibiotic Synergy

The promysalin synergy experiments were completed in collaboration with Renata Rivera, a former undergraduate researcher, and Martina Golden, a current graduate student.

3.1.   Introduction

Over the years, our lab has done much synthetic work toward the optimization of promysalin's activity against *P. aeruginosa*.[161,174] Through these analog series, nearly every portion of the scaffold had been investigated. While some structural changes resulted in modest improvement in activity, many had no effect or mitigated promysalin's activity. Through this, we realized that nature's scaffold had already been tuned for optimal activity in its native environment, where *P. putida*, the producer of promysalin, must protect itself against *P. aeruginosa*. As such, we considered an alternative approach wherein we sought to investigate manipulations in a biological context, rather than continued modifications to the chemical structure. To that end, we considered the possibility of a combination with promysalin and existing antibiotics to improve activity.

As discussed in Section 1.2.2., combination therapy presents many advantages as a strategy for overcoming and preventing antibiotic resistance. One successful combination in antibiotics is sulfamethoxazole (SMX) and trimethoprim (TMP). SMX and TMP have a synergistic effect when used in combination, and as such, have been widely administered clinically as a co-therapy for the treatment of many bacterial infections.[175] SMX and TMP both act by inhibiting different steps in the synthesis and derivatization of folate (Figure 3.1),[8] which is required for bacterial metabolism.[11] It is therefore generally accepted that this synergistic relationship arises from the fact that two subsequent steps in the same pathway are being inhibited.[176] As such, we thought that by combining promysalin with an antibiotic whose target is upstream or downstream of Sdh, promysalin's protein target, we could identify a new synergistic pair. Furthermore, recent investigations have revealed promise of combination therapies in *P. aeruginosa* specifically.[177,178] We thus began our investigation by testing a broad panel of antibiotics that satisfy this requirement and target *P. aeruginosa*.
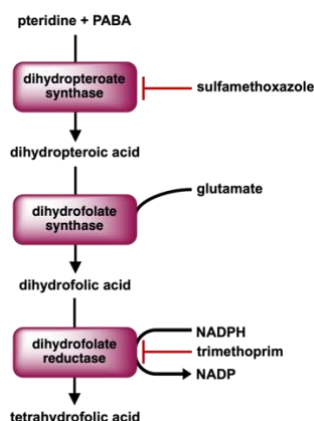
Figure 3.1. Overview of folate synthesis including inhibition by sulfamethoxazole and trimethoprim.

While utilizing two existing antibiotics would be a more streamlined entry into the clinic, there is a major drawback with this strategy. Namely, clinical isolates exist that display high levels of resistance to nearly all antibiotics on the market, and multi-drug resistant (MDR) strains exhibiting resistance to multiple antibiotics are becoming prevalent.[18] As such, using promysalin, which has a novel mechanism of action, in combination with an existing antibiotic would reduce the likelihood of treatment failure due to previously existing MDR strains. Furthermore, combination therapies are less likely to induce new resistance,[88] so this strategy would also reduce the risk of promysalin resistance in the clinic.

Additionally, some characteristics of promysalin's activity alone would preclude its clinical application, which we thought could be overcome through the use of a combination strategy. Specifically, although promysalin exhibits a very potent IC_{50} against *P. aeruginosa* (67nM – PA14), the MIC is much higher, making it difficult to fully inhibit all cells in a culture. As we considered possible explanations for this, several possibilities came to mind. Traditional resistance mechanisms including target modification, compound inactivation, decreased uptake, and efflux were initially considered as *P. aeruginosa* has been reported to possess innate resistance through these mechanisms.[179] Target modification and compound inactivation seemed improbable, as these would likely result in complete loss of activity. However, we see that concentrations above the IC_{50} only exhibit low levels of growth compared to the negative control.

Therefore, we considered the use of membrane-targeting antibiotics to mitigate potential membrane alterations that may be preventing promysalin's uptake. Additionally, we sought to employ efflux pump inhibitors as well as genetically modified strains devoid of efflux pumps to investigate this final mechanism as the cause of decreased susceptibility.

In addition to innate resistance, *P. aeruginosa* can exhibit adaptive resistance, wherein it makes transient changes to expression in specific genes or proteins in response to an external stimulus or threat.[180] The most common adaptive resistance in *P. aeruginosa* are the formation of biofilms and persister cells.[181] Biofilms have been shown to decrease antibiotic efficacy 10-1000-fold,[182] and an important aspect of biofilm regulation is the production of quorum sensing (QS) molecules. These are small molecules excreted by bacteria used to sense cell density to regulate the formation of biofilms, among other things.[183,184] As such, QS pathways have become a target of interest, and many inhibitors have been identified and developed, including against *P. aeruginosa*.[185–188] We thus wondered if biofilm formation was hindering promysalin activity and sought to examine the effects of a combination therapy with known QS inhibitors.

As for persister cells, their existence and role in infection has been more debated. Opposed to resistance as conventionally defined, tolerance and persistence are both transient states, which can be altered under certain conditions. Tolerance is described as a *transient* ability to survive antibiotic exposure which is a characteristic of an entire population. Given enough time, a tolerant population would *eventually* be killed completely, it would just take longer than that of a susceptible population (Figure 3.2, blue). On the other hand, persistence is defined as the ability of a subpopulation to evade antibiotic treatment.[189] As such, the susceptible subpopulation is rapidly killed, whereas the persistent subpopulation is largely unaffected, even given extended antibiotic exposure (Figure 3.2, yellow).
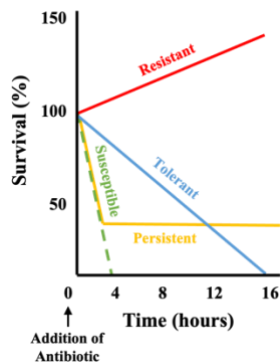
Figure 3.2. Graph depicting the survival of different cell populations over time (susceptible – green; resistant – red; tolerant – blue; persistent – yellow).

Based on what we have observed in growth inhibition assays, it seemed as though persistence could be an explanation for our observations. Furthermore, persister cells are often the result of decreased cell growth or dormancy, as a defense mechanism for antibiotics whose targets are only present during cell replication.[47] Since promysalin targets an enzyme in primary metabolism, we saw this as a likely resistance mechanism for *P. aeruginosa*. Finally, since we were utilizing laboratory strains that are generally susceptible to promysalin, we knew the entire initial population was not resistant or tolerant. Additionally, it is unlikely that the entire population would lose susceptibility upon a single antibiotic treatment. As such, a heterogeneous subpopulation (whether pre-existing or induced by exposure), seemed the most likely explanation. Based on all these factors, we sought to determine whether promysalin was inducing persister cells and identified known methods for quantifying the induction of persister cells to carry out these experiments.[190]

Finally, thinking more about promysalin's mechanism more specifically, in that it targets Sdh, an enzyme in the TCA cycle, we looked to the literature for other examples of metabolism inhibitors. One of the key challenges in targeting bacterial metabolism is the complexity and connection of various metabolic pathways.[191] When it comes to the TCA cycle specifically, there is a shunt pathway, known as the glyoxylate shunt, which bypasses part of the TCA cycle (Figure 3.3).[192] Importantly, it bypasses Sdh, promysalin's target. As such, we wondered if *P. aeruginosa* was diverting through this alternative pathway

in the presence of promysalin. Of note, Sdh is also utilized in the electron transport chain and is critical for the production of ATP. We therefore presumed that diverting around Sdh would come at a high fitness cost, which could explain the low levels of growth relative to negative controls. We postulated that if we could inhibit both pathways simultaneously, we could fully inhibit primary metabolism and achieve full inhibition at lower concentrations. Furthermore, other reports have indicated a link between TCA shunting and a tolerant cell state, giving further credence to our hypothesis.[193] We thus found reported glyoxylate shunt inhibitors[194] to test in combination with promysalin.
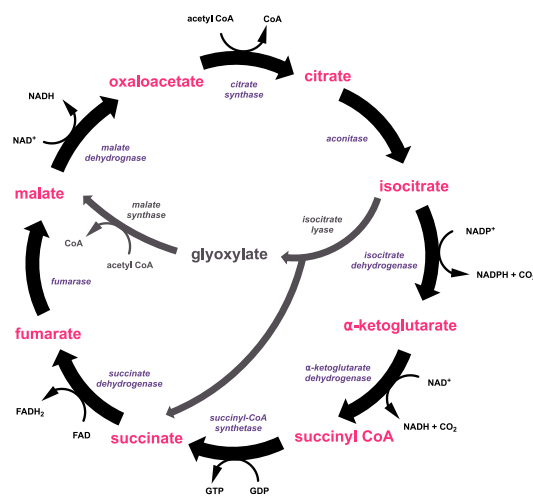
Figure 3.3. *Overview of the TCA cycle including the glyoxylate shunt pathway.*

Overall, bacterial resistance is a complex, multifaceted problem, for which multiple solutions must be explored. As such, the work discussed herein utilizes two parallel approaches, in which we investigated possible synergy of promysalin with both traditional antibiotics and alternative compounds with two goals in mind: (1) identifying novel synergistic pairs with improved activity against *P. aeruginosa*; (2) determining underlying mechanisms of *P. aeruginosa* evasion of promysalin treatment.

3.2. Synthesis & Growth Inhibition of Simplified Analog

The synthesis of promysalin is highly convergent and amenable to analog synthesis.[160] Consequently, it can be difficult to obtain large quantities. We anticipated needing significant quantities of material of the natural product for an in-depth biological investigation. We therefore identified a simplified compound with similar activity for the purposes of these studies (Figure 3.4, **3.2**). Compound **3.2** only differs from promysalin, **3.1**, in the absence of the side chain α-hydroxyl (Figure 3.4). This analog, which was previously synthesized and tested in our group,[161] is equipotent to promysalin and can be obtained in five fewer synthetic steps. We therefore proceeded through the previously reported synthesis of this analog (Scheme 3.1), producing large quantities of **3.2**, enabling the plethora of experiments described below. Upon completion, we confirmed that its IC$_{50}$ against *P. aeruginosa* matched reported data[161] through a standard growth inhibition assay.
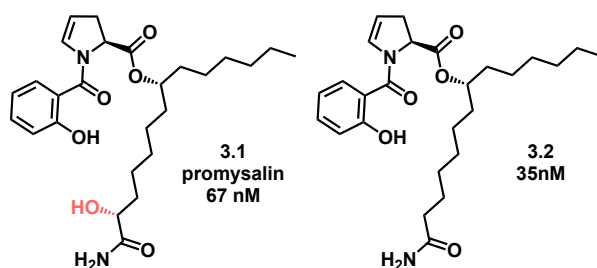
Figure 3.4. *Promysalin (left) and deoxy-promysalin (right) and their respective IC$_{50}$ values against PA14.*
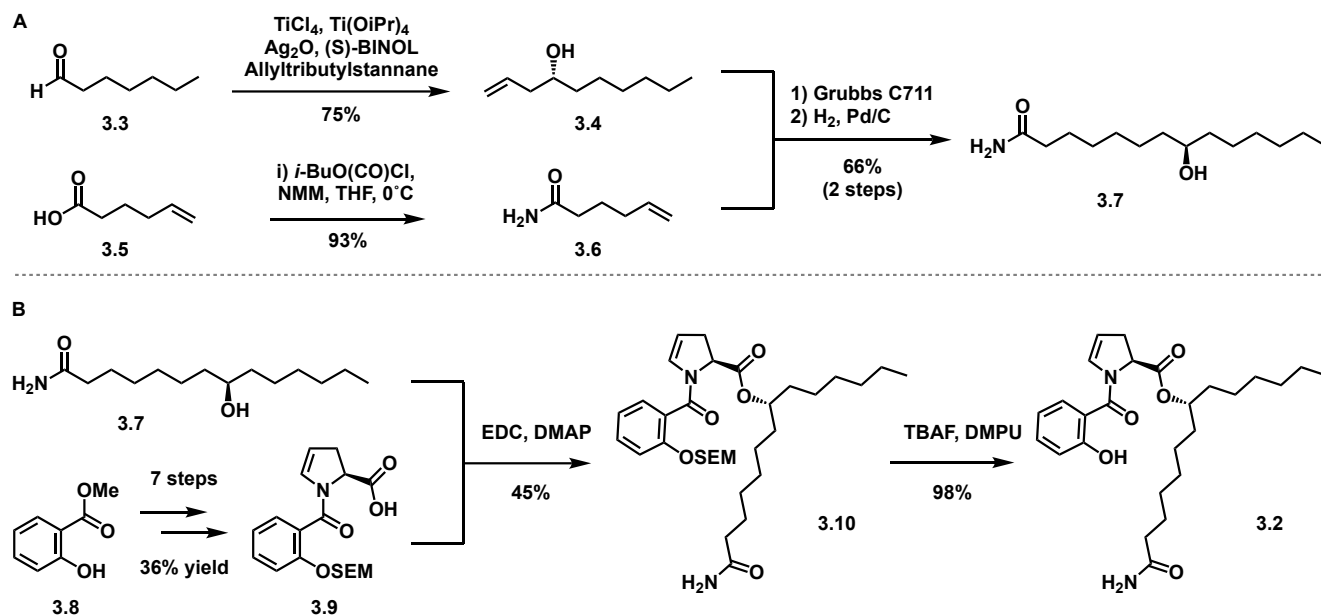
Scheme 3.1. *Synthesis of deoxy-promysalin, **3.2**. (A) Synthesis of deoxy side chain, **3.7**. (B) End game synthesis. *Synthesis of fragment **3.9** is in the experimental section (Scheme 5.2.1.)*

3.3. Screen for Synergy with Traditional Antibiotics

Our initial investigation included a panel of traditional antibiotics spanning all major mechanisms of action (Table 3.1). Each of these was tested in combination with **3.2** against PA14 in a standard checkerboard assay. In this assay, one compound is serially diluted across each column in a 96-well plate, while the other is serially diluted down each row in the same plate (Figure 3.5). After incubation with bacteria, growth can be visualized, and optical density is measured at 600 nm (OD_{600}) for quantification. Most commonly, synergy is determined based on minimum inhibitory concentrations (MICs), from which a fractional inhibitory concentration (FIC) index is calculated. To do so, a single well containing the MIC is selected. Within each selected well, the following equation is used to calculate the FIC index (Equation 3.1), where A and B are the concentrations of compounds 1 and 2 in the well, respectively, and MIC_A and MIC_B are the MICs of each compound individually.

$$\frac{A}{MIC_A} + \frac{B}{MIC_B} = FIC_A + FIC_B = FIC\ Index$$

Equation 3.1. Equation for calculating the FIC index from a checkerboard assay.

However, since an MIC for promysalin is not easily obtained, we instead used IC_{50} values. As such, we calculated FIC_{50} values for each of our combinations using Equation 3.2.

$$\frac{A}{IC_{50_A}} + \frac{B}{IC_{50_B}} = FIC_{50_A} + FIC_{50_B} = FIC_{50}\ Index$$

Equation 3.2. Equation for calculating the FIC_{50} index from a checkerboard assay.

Since this is a two-dimensional assay, there may be multiple wells containing an MIC, so the process can be repeated for multiple wells. As such, the values reported in Table 3.1 indicate the range of FIC_{50} values obtained for all selected wells for a given combination.
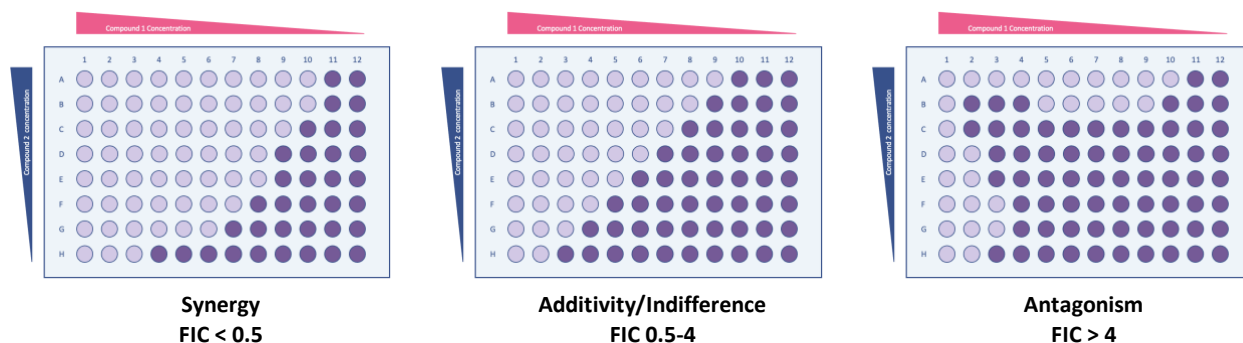
Figure 3.5. *Visual and numerical depictions of possible results of a checkerboard assay.*

Upon optimization of our data collection and processing, we completed checkerboard assays for each of the designated antibiotics in combination with **3.2** (Table 3.1).[1] As stated, we chose antibiotics that spanned all major mechanisms of action to assess a breadth of possible combinations. However, we found

---

[1] Each checkerboard assay was completed in biological triplicate.

that all combinations resulted in an additive or indifferent effect. Although these results were unexpected, they illustrate the resilience of *P. aeruginosa* and urge further to work understand this complex pathogen.

Antibiotic	Class	Mechanism	FIC_{50} Index
Vancomycin	Glycopeptide	Cell wall synthesis	0.8 - 1.2
Kanamycin	Aminoglycoside	Protein synthesis (30S)	1.5 - 2.1
Tobramycin	Aminoglycoside	Protein synthesis (30S)	1.3
Gentamicin	Aminoglycoside	Protein synthesis (30S)	1.8
Amikacin	Aminoglycoside	Protein synthesis (30S)	1.0
Chloramphenicol		Protein synthesis (50S)	0.6 - 1.7
Erythromycin	Macrolide	Protein synthesis (50S)	0.9 - 1.5
Tetracycline	Tetracycline	Protein synthesis (30S)	1.2 - 2.2
Ciprofloxacin	Fluoroquinolone	DNA synthesis	1.4 - 1.9
Levofloxacin	Fluoroquinolone	DNA synthesis	1.0
Trimethoprim		Folate synthesis	0.8 - 2.2
Colistin	Polymyxin	Cell Membrane	0.6 – 1.0

Table 3.1. List of traditional antibiotics tested in combination with 3.2, including their antibiotic class and mechanism of action, as well as our results from synergy experiments (FIC_{50} index).

3.4. Alternative Approaches to Bacterial Synergism

Seeing that **3.2** did not synergize with any traditional antibiotics, we turned our attention to compounds inhibiting alternate pathways including efflux, quorum sensing, and the glyoxylate shunt (Table 3.2). As these compounds do not exhibit bacterial inhibition or killing on their own, an FIC index could not be calculated for these combinations. Instead, we assessed whether the IC_{50} of **3.2** changed in their presence.

Toward the investigation of efflux mechanisms, we began by testing synergy with carbonyl cyanide m-chlorophenyl hydrazone (CCCP, **3.12**, Figure 3.6) a ubiquitous efflux pump inhibitor. This compound is known to decrease efflux pump effectiveness through the destruction of the proton gradient, which is required for the function of most efflux pumps. However, we saw no improvement to the activity of **3.2**. Ongoing work to verify this finding includes testing **3.2** against a panel of *P. aeruginosa* strains containing various efflux pump knockouts.
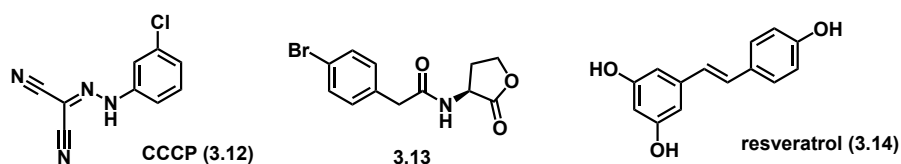
Figure 3.6. *Structures of alternative compounds tested in combination with **3.2**.*

In the meantime, we turned our attention to quorum sensing (QS) and biofilm. We first considered N-acyl L-homoserine lactones (AHLs), which are small molecules used by many Gram-negative bacteria including *P. aeruginosa* for various signaling purposes. We selected a derivative identified by the Blackwell lab, **3.13**[*] (Figure 3.6), as it was shown to be a more potent analog, and was specifically classified as a biofilm inhibitor in *P. aeruginosa*.[195] However, when tested in a checkerboard assay, it had no effect on the activity of **3.2**, indicating that biofilms are not impeding the activity of promysalin. We then considered alternative QS pathways, as these signaling pathways have been implicated in a number of other virulence mechanisms. Resveratrol (**3.14**, Figure 3.6) was selected to investigate this possibility, as it has shown inhibition of several different QS pathways in *P. aeruginosa*.[196] Again, no effect was observed, suggesting that some other common signaling pathways are not responsible for promysalin resistance.

Compound	Mechanism	Result
CCCP	Protonophore (Efflux Inhibitor)	No effect

---

[*] Synthesized by Ingrid Wilt, a graduate student in our lab.

3.13	QS Inhibitor	No effect
Resveratrol	QS Inhibitor	No effect
SB-002	Glyoxylate Shunt Inhibitor	Antagonistic

Table 3.2. List of alternative compounds tested in combination with 3.2, including their mechanism of action and their effect on the activity of 3.2.

With initial QS investigations being unfruitful, we set out to identify glyoxylate shunt inhibitors for our investigation. Itaconate (**3.15**, Scheme 3.2A) was initially considered, as it is commercially available. This compound is produced by human cells and inhibits isocitrate lyase, the first enzyme in the glyoxylate shunt, in some bacteria, including *Pseudomonas*.[197,198] However, upon further investigation, we found that *P. aeruginosa* has the ability to degrade this molecule,[199] and so we searched for alternative molecules. SB-002 (**3.18**, Scheme 3.2B) was then identified, which exhibited potent inhibition of malate synthase and isocitrate lyase, both enzymes comprising the glyoxylate shunt.[194] Subsequently, SB-002 was synthesized in a single step from 2-amino-4-chloropyridine (**3.16**) and 2-tert-butyl-1,3-diisopropylisourea (**3.17**) according to the reported procedure (Scheme 3.2B),[194] and was tested in a checkerboard assay with **3.2**. To our surprise, SB-002 mitigated the activity of **3.2** in a concentration dependent manner (Figure 3.7). We postulate that the presence of SB-002 could be triggering the upregulation of metabolism, resulting in increased expression of Sdh, mitigating the effect of **3.2**. We are currently exploring ways in which this hypothesis could be tested.
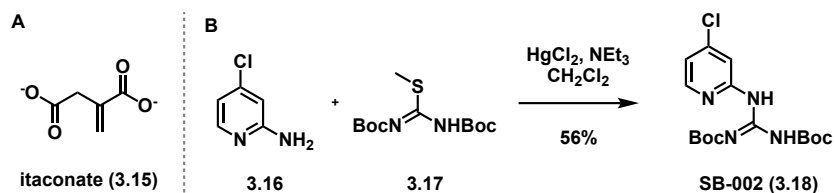
Scheme 3.2. (A) Structure of itaconate. (B) Synthesis of SB-002.
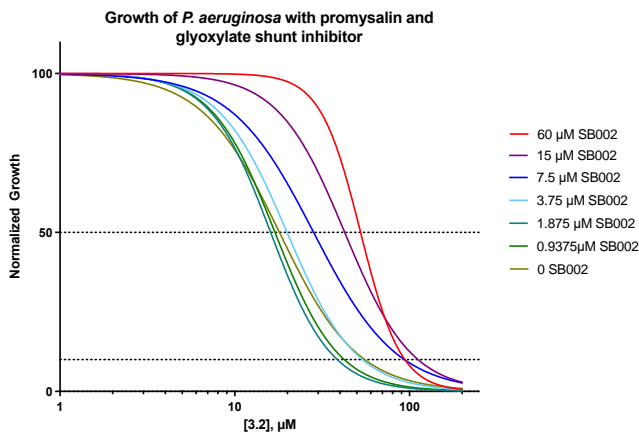
Figure 3.7. *Growth of P. aeruginosa in the presence of **3.2** and SB-002 at varying concentrations.*

3.5.   Conclusions & Future Directions

In all, the only compound to have any effect in combination with **3.2** was SB-002, a glyoxylate shunt inhibitor. Specifically, it showed an antagonistic effect, and ongoing investigations are underway in order to better understand this relationship. Namely, feeding experiments are in progress in which carbon source is control in the media, which will allow us to force *P. aeruginosa* to either utilize or bypass the glyoxylate shunt. We hope to use these experiments to mimic the effects of SB-002 and will then treat with **3.2** under those conditions. Additionally, as a final attempt to rule out resistance through efflux mechanisms, we obtained two genetically engineered *P. aeruginosa* strains from Genentech which had various efflux pumps knocked out. Experiments assessing the activity of **3.2** in these strains is currently in progress. Finally, the last remaining question to be investigated is whether promysalin induces persister cells. Initial

experiments replicating the assay with CCCP, which is known to induce persister cells, were successful. Additional experiments are underway toward optimizing the persister inducing assay using **3.2**.

Based on all of our experiments, *P. aeruginosa* has proven to be very resilient and impervious to further optimization. However, we wondered if this would hold true in resistant strains, opposed to laboratory strains. As it stands, most clinical antibiotics have good activity against laboratory strains but fall short in clinical isolates. Therefore, promysalin could hold promise in such circumstances when existing treatments fail. As such, we have begun exploring some of the experiments described herein using a library of resistant clinical *P. aeruginosa* isolates obtained from the Department of Defense. This will serve to test promysalin's efficacy and potential as a combination therapy under more clinically relevant conditions.

3.6.   References

(174) Post, S. J.; Keohane, C. E.; Rossiter, L. M.; Kaplan, A. R.; Khowsathit, J.; Matuska, K.; Karanicolas, J.; Wuest, W. M. Target-Based Design of Promysalin Analogues Identifies a New Putative Binding Cleft in Succinate Dehydrogenase. **2020**, *6*, 1372–1377. https://doi.org/10.1021/acsinfecdis.0c00024.

(175) Proceedings, J. S.-M. C.; 1999, undefined. Trimethoprim-Sulfamethoxazole. *Elsevier*.

(176) Journal, S. B.-C. M. A.; 1975, undefined. Synergy of Trimethoprim-Sulfamethoxazole. *ncbi.nlm.nih.gov*.

(177) Park, S. Y.; Park, H. J.; Moon, S. M.; Park, K. H.; Chong, Y. P.; Kim, M. N.; Kim, S. H.; Lee, S. O.; Kim, Y. S.; Woo, J. H.; Choi, S. H. Impact of Adequate Empirical Combination Therapy on Mortality from Bacteremic Pseudomonas Aeruginosa Pneumonia. *BMC Infect. Dis.* **2012**, *12*. https://doi.org/10.1186/1471-2334-12-308.

(178) El Solh, A. A.; Alhajhusain, A. Update on the Treatment of Pseudomonas Aeruginosa Pneumonia. *J. Antimicrob. Chemother.* **2009**, *64* (2), 229–238. https://doi.org/10.1093/JAC/DKP201.

(179) Pang, Z.; Raudonis, R.; Glick, B. R.; Lin, T. J.; Cheng, Z. Antibiotic Resistance in Pseudomonas Aeruginosa: Mechanisms and Alternative Therapeutic Strategies. *Biotechnol. Adv.* **2019**, *37* (1), 177–192. https://doi.org/10.1016/J.BIOTECHADV.2018.11.013.

(180) Sandoval-Motta, S.; Aldana, M. Adaptive Resistance to Antibiotics in Bacteria: A Systems Biology Perspective. *Wiley Interdiscip. Rev. Syst. Biol. Med.* **2016**, *8* (3), 253–267. https://doi.org/10.1002/WSBM.1335.

(181) Taylor, P. K.; Yeung, A. T. Y.; Hancock, R. E. W. Antibiotic Resistance in Pseudomonas Aeruginosa Biofilms: Towards the Development of Novel Anti-Biofilm Therapies. *J. Biotechnol.* **2014**, *191*, 121–130. https://doi.org/10.1016/j.jbiotec.2014.09.003.

(182) Hoyle, B. D.; Costerton, J. W. Bacterial Resistance to Antibiotics: The Role of Biofilms. *Prog. Drug Res.* **1991**, *37*, 91–105. https://doi.org/10.1007/978-3-0348-7139-6_2.

(183) De Kievit, T. R.; Gillis, R.; Marx, S.; Brown, C.; Iglewski, B. H. Quorum-Sensing Genes in Pseudomonas Aeruginosa Biofilms: Their Role and Expression Patterns. *Appl. Environ. Microbiol.* **2001**, *67* (4), 1865–1873. https://doi.org/10.1128/AEM.67.4.1865-1873.2001.

(184)   Davies, D. G.; Parsek, M. R.; Pearson, J. P.; Iglewski, B. H.; Costerton, J. W.; Greenberg, E. P. The Involvement of Cell-to-Cell Signals in the Development of a Bacterial Biofilm. *Science (80-.).* **1998**, *280* (5361), 295–298. https://doi.org/10.1126/SCIENCE.280.5361.295/ASSET/FB9F64D1-C794-46CC-BAF6-518822A5C195/ASSETS/GRAPHIC/SE1486404003.JPEG.

(185)   Welsh, M. A.; Blackwell, H. E. Chemical Probes of Quorum Sensing: From Compound Development to Biological Discovery. *FEMS Microbiol. Rev.* **2016**, *40* (5), 774–794. https://doi.org/10.1093/FEMSRE/FUW009.

(186)   Waters, C. M.; Bassler, B. L. Quorum Sensing: Cell-to-Cell Communication in Bacteria. **2005**. https://doi.org/10.1146/annurev.cellbio.21.012704.131001.

(187)   Amara, N.; Krom, B. P.; Kaufmann, G. F.; Meijler, M. M. Macromolecular Inhibition of Quorum Sensing: Enzymes, Antibodies, and Beyond Contents 1. Introduction 195 1.1. Coordination of Gene Expression 195 2. Enzymatic Quenching of Quorum Sensing 196 2.1. AHL Degrading Enzymes 197 2.1.1. AHL Lactonases 197 2.1.2. AHL Acylases 199 2.2. Interkingdom Quorum Quenching 201 2.2.1. AHL-Degrading Enzymes in Eukaryotes 202 2.3. Quorum Quenching As an Antivirulence Strategy. https://doi.org/10.1021/cr100101c.

(188)   Mcdougald, D.; Rice, S. A.; Kjelleberg, S. Bacterial Quorum Sensing and Interference by Naturally Occurring Biomimics. https://doi.org/10.1007/s00216-006-0761-2.

(189)   Gefen, O.; reviews, N. B.-F. microbiology; 2009, undefined. The Importance of Being Persistent: Heterogeneity of Bacterial Populations under Antibiotic Stress. *academic.oup.com*.

(190)   Grassi, L.; Di Luca, M.; Maisetta, G.; Rinaldi, A. C.; Esin, S.; Trampuz, A.; Batoni, G. Generation of Persister Cells of Pseudomonas Aeruginosa and Staphylococcus Aureus by Chemical Treatment and Evaluation of Their Susceptibility to Membrane-Targeting Agents. *Front. Microbiol.* **2017**, *8* (OCT), 1917. https://doi.org/10.3389/FMICB.2017.01917/BIBTEX.

(191)   Heinemann, M.; Sauer, U. Systems Biology of Microbial Metabolism. *Curr. Opin. Microbiol.* **2010**, *13* (3), 337–343. https://doi.org/10.1016/J.MIB.2010.02.005.

(192)   Kornberg, H. L.; Krebs, H. A. Synthesis of Cell Constituents from C2-Units by a Modified Tricarboxylic Acid Cycle. *Nat. 1957 1794568* **1957**, *179* (4568), 988–991. https://doi.org/10.1038/179988a0.

(193)   Meylan, S.; Porter, C. B. M.; Yang, J. H.; Belenky, P.; Gutierrez, A.; Lobritz, M. A.; Park, J.; Kim, S. H.; Moskowitz, S. M.; Collins, J. J. Carbon Sources Tune Antibiotic Susceptibility in Pseudomonas Aeruginosa via Tricarboxylic Acid Cycle Control. *Cell Chem. Biol.* **2017**, *24* (2), 195–206. https://doi.org/10.1016/J.CHEMBIOL.2016.12.015.

(194)   McVey, A. C. The Glyoxylate Shunt as a Target for Antibacterial Intervention in Pseudomonas Aeruginosa, 2019.

(195)   Geske, G. D.; Wezeman, R. J.; Siegel, A. P.; Blackwell, H. E. Small Molecule Inhibitors of Bacterial Quorum Sensing and Biofilm Formation. **2005**. https://doi.org/10.1021/ja0530321.

(196)   Sheng, J. Y.; Chen, T. T.; Tan, X. J.; Chen, T.; Jia, A. Q. The Quorum-Sensing Inhibiting Effects of Stilbenoids and Their Potential Structure–Activity Relationship. *Bioorg. Med. Chem. Lett.* **2015**, *25* (22), 5217–5220. https://doi.org/10.1016/J.BMCL.2015.09.064.

(197)   Luan, H. H.; Medzhitov, R. Food Fight: Role of Itaconate and Other Metabolites in Antimicrobial Defense. *Cell Metab.* **2016**, *24* (3), 379–387. https://doi.org/10.1016/J.CMET.2016.08.013.

(198)   McFadden, B. A.; Purohit, S. Itaconate, an Isocitrate Lyase-Directed Inhibitor in Pseudomonas Indigofera. *J. Bacteriol.* **1977**, *131* (1), 136–144. https://doi.org/10.1128/JB.131.1.136-144.1977.

(199)   Sasikaran, J.; Zadora, P. K.; Fleig, A.; Berg, I. A. Bacterial Itaconate Degradation Promotes Pathogenicity. *Nat. Chem. Biol.* **2014**. https://doi.org/10.1038/nCHeMBIO.1482.

Chapter 4. Total Synthesis of the Reported Structure of the Cahuitamycins and Structural Isomers

The work for the reported structure of cahuitamycin A and structural analogs was completed in collaboration with Dr. Justin Shapiro, a former post-doctoral fellow in our lab.

4.1. Introduction

4.1.1. *Acinetobacter baumannii*

Another devastating Gram-negative pathogen that continues to have tremendous impact on society is *Acinetobacter baumannii*. Also an ESKAPE pathogen, *A. baumannii* was upgraded from "serious threat" in the 2013 CDC report to "urgent threat" in 2019 due to the ease with which resistance determinants can spread amongst this species and the lack of antibiotics in the clinic or pipeline to treat infections.[18] *A. baumannii* is an opportunistic pathogen commonly found in lung, wound, bloodstream, and urinary tract infections amongst immune-compromised patients and those in hospitals or military treatment facilities.[200] Isolates are routinely found with resistance to drugs of last resort such as the carbapenems and polymyxins[201] and resistant strains accounted for over 8,500 infections of hospitalized patients in the United States in 2017.[202] With effective treatment options dwindling, new drugs with novel mechanisms that are less likely to succumb to existing resistance mechanisms are desperately needed to combat this increasing threat.

Like other ESKAPE pathogens, an important method by which *A. baumannii* evades treatment is through the formation of biofilms,[203] which are known to lay dormant on medical equipment.[204] Targeting biofilm formation is advantageous as it would evade existing resistance mechanisms. Furthermore, there would be reduced risk of novel resistance mechanisms because this strategy targets virulence rather than vital life processes. As discussed in Chapter 1, the literature has revealed a connection between biofilm formation and iron acquisition, but the investigation of this relationship has been limited in *A. baumannii*. Therefore, the prospect of manipulating iron homeostasis as a means to inhibit biofilm formation represents an intriguing strategy for novel therapeutics. Some work has been executed studying the effects on biofilm

from direct manipulation of iron concentration, through either exogenous iron chelators or redox inactive iron mimics (refs from chapter 1). However, if these strategies were implemented therapeutically, they could have harmful effects on the host, as iron homeostasis is also vital to many human biological processes (refs). As such, a more indirect, bacteria-specific approach is needed. In particular, a small molecule that specifically inhibits some aspect of bacterial iron acquisition represents an ideal and novel approach to specific bacterial biofilm inhibition.

4.1.2. Cahuitamycin Prior Work

In a 2016 screen of a natural product extract library containing nearly 10,000 samples, the Sherman group at the University of Michigan identified an extract that showed selective inhibition of biofilm formation in *A. baumannii*, with minimal effect on planktonic growth.[144] Through ribosomal engineering of *Streptomyces gandocaensis* they were able to enhance production of the active compounds, and isolated the cahuitamycins A-C (Figure 4.1), a novel group of natural products. Using high-resolution time-of-flight electrospray ionization mass spectrometry (HRESIMS), they deduced the molecular formula of cahuitamycin A to be $C_{27}H_{37}N_7O_{11}$, indicating three degrees of unsaturation. Using initial 1D and 2D NMR experiments they determined the fundamental presence of a peptide scaffold. Analysis of correlated spectroscopy (COSY), total correlation spectroscopy (TOCSY), and heteronuclear multiple bond correlation (HMBC) NMR indicated an *N*-terminal *ortho*-phenol substituted with an oxazoline at the 2-position. They also identified the presence of four additional spin systems: serine, two modified ornithines, and alanine. Through further examination, they determined the C-terminus to be a beta-alanine and defined one of the modified ornithines as N^{δ}-hydroxy-N^{δ}-formylornithine (*N*-OH-*N*-fOrn). The last ornithine residue proved to be the most ambiguous but using a single long-range HMBC correlation they assigned this spin system as a piperazic acid, completing their linear assignment of cahuitamycin A (**4.1**).

4.1: cahuitamycin A, R = H
4.2: cahuitamycin C, R = Me
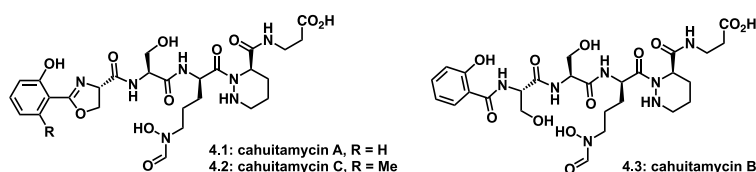
4.3: cahuitamycin B

Figure 4.1. Reported structures of the natural products cahuitamycins A-C.

With one structure resolved, they moved onto characterization of cahuitamycins B (**4.2**) and C (**4.3**) through a similar process. HRESIMS indicated a molecular formula $C_{28}H_{39}N_7O_{11}$ for cahuitamycin C, again revealing 13 degrees of unsaturation. 1D and 2D NMR analysis indicated a high degree of similarity to cahuitamycin A, and HMBC easily revealed the only difference to be methylation of the 6-position on the phenol. HRESIMS was again used to determine the molecular formula and degrees of unsaturation for cahuitamycin B to be $C_{27}H_{39}N_7O_{12}$ and 12, respectively, one fewer degree of unsaturation than A and C. NMR analysis revealed several common spin systems to cahuitamycin A including beta-alanine, piperazic acid, *N*-OH-*N*-fOrn, serine, and *ortho*-phenol. However, COSY and HMBC correlations precluded the presence of the oxazoline, indicating in its place a linear serine, which would account for the loss of a single degree of unsaturation. These analyses concluded their assignment of the linear structure for all three natural products.

Toward the stereochemical assignment of these compounds, they utilized advanced Marfey's analysis,[205] which is commonplace for the determination of absolute stereochemistry in peptides. This method employs a chiral reagent, 1-fluoro-2,4-dinitrobenzene-5-alanine amide (FDAA), which contains a fluorine that is reactive toward amino acids. Subsequent HPLC of the resulting diastereomers can be used to determine the absolute stereochemistry of the amino acid, based on differential retention time.[206] This difference is due to stronger intramolecular hydrogen bonding of the diastereomer resulting from reaction with D- amino acids, resulting in greater interaction with reverse-phase silica, increasing retention times. This analysis was completed on the hydrolyzed cahuitamycin B, which indicated the following stereochemical arrays: L-Ser, L-Ser, D-Pip, and D-*N*-OH-Orn. The same procedure was followed for cahuitamycins A and C to reveal the same stereochemistry for common amino acids (L-Ser, D-Pip, and D-*N*-OH-*N*-fOrn), while the oxazoline stereochemistry was determined to be D- based on extrapolation from NMR shifts in cahuitamycin B. Furthermore, the lack of an epimerization domain in the oxazoline-forming domain suggests that all three compounds possess the same stereochemistry at that position.

With full linear and stereochemical assignments complete, they sought to investigate the biosynthetic origins of these natural products, especially the methylated cahuitamycin C. Using antibiotics & Secondary Metabolite Analysis Shell (antiSMASH)[207] to analyze the *S. gandocaensis* genome, they identified the core nonribosomal peptide synthetase (NRPS)-encoding gene cluster to be *cahA-D*, which encodes for four non-colinear proteins, CahA-D, respectively. (Figure 4.2). Furthermore, they proposed that CahA is responsible for loading of the first L-Ser unit and subsequent cyclization with the existing salycilate to form the key oxazoline ring. From there, CahB loads the second L-Ser unit followed by L-*N*-OH-*N*-fOrn, which is then epimerized. The latter is proposed to be synthesized off scaffold by CahMO and CahFT, before being appended to the growing peptide. The piperazic acid is proposed to originate from either L-*N*-OH-Orn or L-glutamine, which loaded and epimerized by CahC, and then cyclized by nucleophilic attack of the amino group, although no cyclization domain is present. Finally, ß-Ala is loaded by CahD and peptide termination is carried out by CahG.
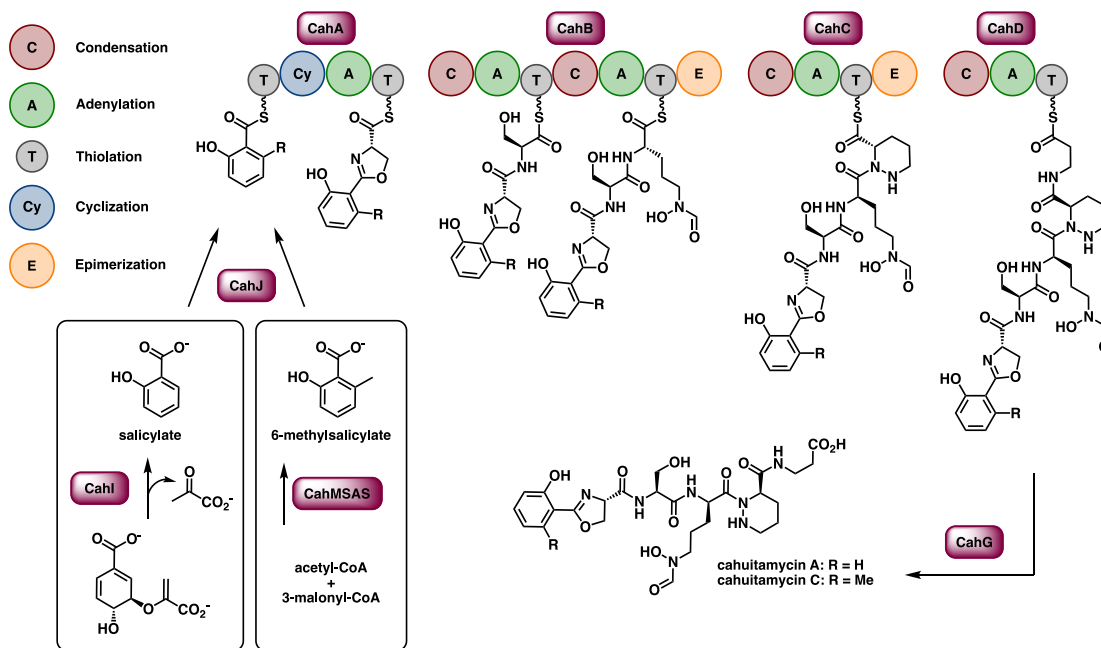
Figure 4.2. *Proposed biosynthesis of the cahuitamycins.*

60

With the core biosynthetic machinery assigned, they were interested in how methylation of cahuitamycin C was carried out. To that end, they generated a Δ*cahI S. gandocaensis* mutant, which would be incapable of synthesizing the salicylate precursor. They found that this mutant still produced cahuitamycin C, but production of cahuitamycins A and B were completely mitigated. This finding suggested an alternative source for the methylated salicylate, rather than post-assembly methylation. Subsequent Basic Local Alignment Search Tool (BLAST) analysis led to the identification of a separate gene cluster that encoded a 6-methyl salicylate synthase, CahMSAS.

Being that cahuitamycin C was a more potent and selective *A. baumannii* biofilm inhibitor, and their initial data suggested that the NRPS could accept alternative salicylate scaffolds, they wondered if they could generate mutasynthetic derivatives with improved activity. They conducted various feeding studies with unnatural starter units and found that 5-methylsalicylic acid was the only unit incorporated sufficiently enough to produce isolatable quantities, which resulted in a new analog, cahuitamycin D (Figure 4.3). In parallel, they isolated another analog from the same extract, cahuitamycin E. Following the same characterization process described above, cahuitamycin D was confirmed to differ from cahuitamycins A and C only in its salicylate methylation. Furthermore, based on the absence of certain HMBC correlations, they concluded that cahuitamcyin E differed from D in that the piperazate was replaced with a linear L-*N*-OH-Orn. These findings suggest that either the cyclization to form the piperazate occurs after loading of L-*N*-OH-Orn onto the NRPS, or that CahC can accept both the linear and cyclized precursors.
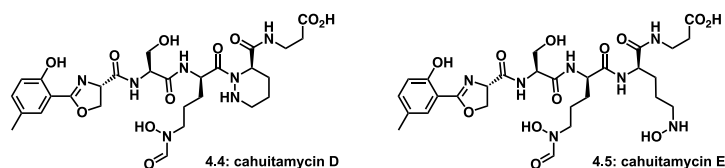
Figure 4.3. *Reported structures of the mutasynthetic derivatives cahuitamycins D and E.*

With all five compounds in hand, they looked to investigate more in-depth biological activity. Specifically, they confirmed that all derivatives had negligible effect on *A. baumannii* growth, despite

significant biofilm inhibition by most compounds (Table 4.1). Additionally, through the use of a secondary flow cell assay, they determined that these molecules had minimal effect on initial attachment of planktonic cells and are specifically inhibiting some part of biofilm maturation following cell attachment (Figure 4.4A). Furthermore, they determined minimal effect on eradication of preexisting biofilms, further indicating their specific mechanism as inhibition of biofilm formation.

Compound	IC_{50}	Biofilm IC_{50}	Biofilm Eradication	pFe^{III}
4.1	>1 mM			18.34
4.1-Fe	No activity	No activity		--
4.2	No activity	No activity		20.42
4.3	>1 mM	14.5 µM		17.52
4.4	>1 mM	8.4 µM	692 µM	
4.5		10.5 µM	535 µM	

Table 4.1. *Biological activity and iron binding of the cahuitamycins.*

It was also apparent that these molecules possess several canonical iron-chelating moieties, namely, a phenolate-oxazoline and a hydroxamate. These motifs have been identified in many *A. baumannii* siderophores including fimsbactin A (**4.6**) and pre-acinetobactin (**4.7**)[208,209] (Figure 4.4B) and are known to contribute to their iron chelating properties. As such, the authors carried out additional assays to investigate the iron-chelating properties of these compounds. They report moderate iron-chelating ability (Table 4.1), but the relatively low affinity compared to other hydroxamate siderophores make a primary mechanism of action as siderophores unlikely. Additionally, when *A. baumannii* was treated with desferrioxamine (**4.8**, Figure 4.4B), a strong iron chelator,[210] biofilm inhibition similar to that induced by the cahuitamycins was not observed. Furthermore, cahuitamycin B (**4.2**), which does not contain the oxazoline ring, retains iron affinity, but loses all biofilm activity. Together, these data indicate that iron depletion alone is not responsible for the anti-biofilm activity of these molecules.
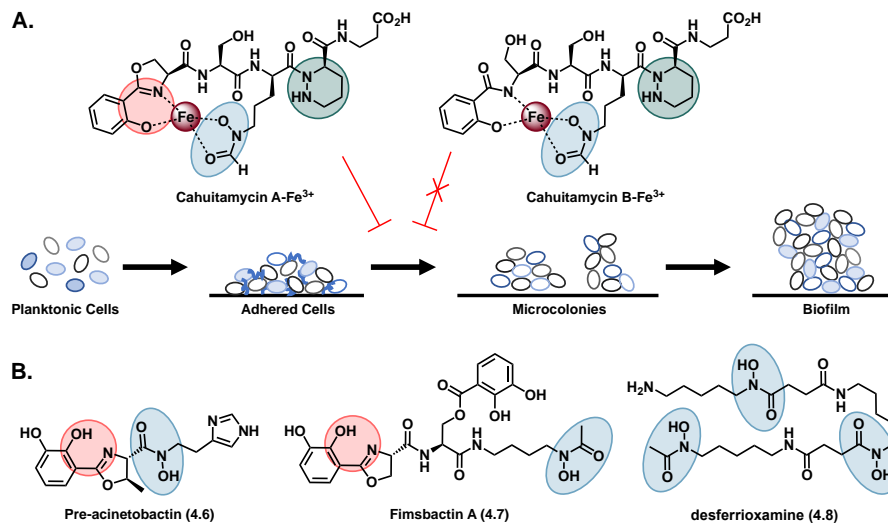
Figure 4.4. *(A) Proposed cahuitamycin-iron complexes (top). The cahuitamycins inhibit biofilm formation, without affecting planktonic growth or cell surface adhesion (bottom). (B) Structures of pre-acinetobactin and fimsbactin, A. baumannii siderophores, and desferrioxamine, a strong iron chelator. Iron-chelating motifs shown in red (phenolate-oxazoline) and blue (hydroxamate).*

However, the presence of chemical motifs common to native *A. baumannii* siderophores suggest that these moieties are still important for biological function, especially considering the inactivity of cahuitamycin B. One possible explanation is that these molecules utilize siderophore uptake machinery to gain entrance into the cell, and these motifs are required for recognition by such proteins. Furthermore, the presence of the piperazate moieties prompts additional questions, as cahuitamycin E, which does not contain this motif, and the other natural products which do, display similar bioactivity. Piperazates have been observed in a few other natural products[211–216] (Figure 4.5), but are not widespread, and therefore the reason for incorporation into some cahuitamycin scaffolds warrants investigation. Due to these interesting structural motifs and the ambiguous iron-biofilm relationship, as well as the implications of both in microbial infections, our lab was interested in exploring these molecules as tools to study this relationship in *A. baumannii*. Toward that end, we sought to synthesize these molecules along with structural analogs

to further investigate necessary chemical motifs for activity, as well as elucidate the mechanism of action. Toward that end, we began with the total synthesis of the natural products.
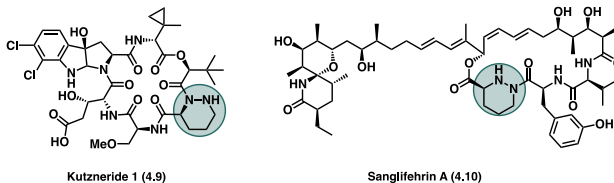
Figure 4.5. *Piperazate-containing natural products.*

4.2.   Total Synthesis & Structural Evaluation

4.2.1. Cahuitamycin E

Cahuitamycin E was selected as a first synthetic target due to its unique structural features, despite similar biological activity. Namely, the piperazic acid derivative present in cahuitamycins A-D is not present in cahuitamycin E, which instead contains a linear ornithine derivative. Despite this significant structural change, cahuitamycin E retained similar levels of biofilm inhibition to the other natural products (Table 4.1). As such, synthetic efforts were commenced following a straightforward retrosynthetic approach utilizing several amides as key disconnections for the construction of amino acid derived intermediates in a convergent manner (Scheme 4.1). These intermediates could be obtained through derivatization of salicylic acid, two serine units, two ornithine units, and one beta-alanine unit.
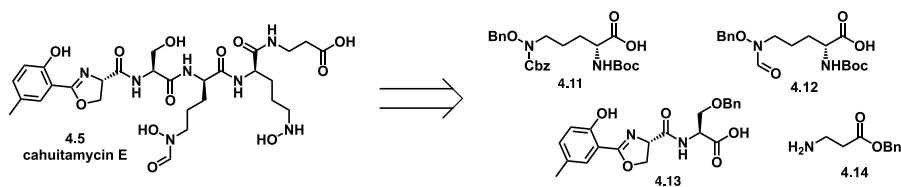
Scheme 4.1. *Retrosynthesis of cahuitamycin E.*

Toward this end, **4.13** was accessed from aldehyde **4.15** in six steps (Scheme 4.2). Conversion to the corresponding nitrile (**4.16**) followed by imidate formation and condensation of benzyl protected L-serine afforded intermediate **4.17**, installing the key oxazoline ring. Deprotection of the benzyl ester, followed by condensation of a benzyl protected L-serine methyl ester and subsequent ester hydrolysis provided access to key fragment **4.13**.
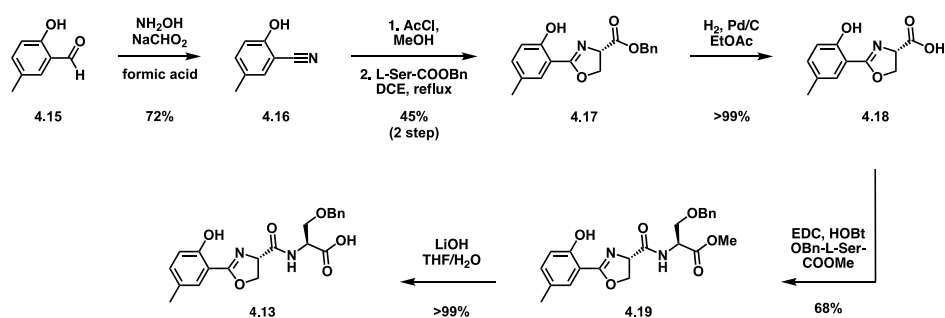
Scheme 4.2. *Synthesis of oxazoline fragment, **4.13**.*

In parallel, fragments **4.11** and **4.12** were prepared in a divergent manner from a single commercial reagent (**4.20**, Scheme 4.3). Initial esterification was achieved via a commercial isourea, followed by carboxybenzyl (Cbz) removal and installation of the key hydroxamate functionality using benzoyl peroxide, to afford the common intermediate **4.22**. From there, intermediate **4.22** was subjected to Cbz protection, followed again by several protecting group manipulations to afford fragment **4.11**. Simultaneously, fragment **4.12** was obtained through coupling of **4.22** with formic acid followed by several protecting group manipulations, which primed the intermediate for later couplings.
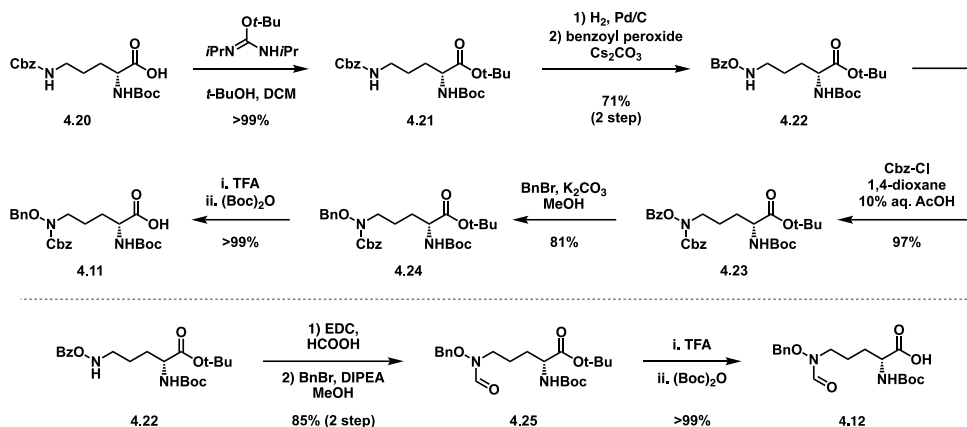
Scheme 4.3. *Synthesis of ornithine fragment, **4.11**, and hydroxamate fragment, **4.12**.*

With all key intermediates in hand, assembly began with the coupling of beta-alanine onto fragment **4.11** (Scheme 4.4). Boc deprotection enabled the subsequent coupling onto fragment **4.12**, which was then subjected to an additional boc deprotection, facilitating coupling of oxazoline fragment **4.13**. This afforded the fully protected cahuitamycin E scaffold (**4.29**) in 11 LLS and 13% overall yield.
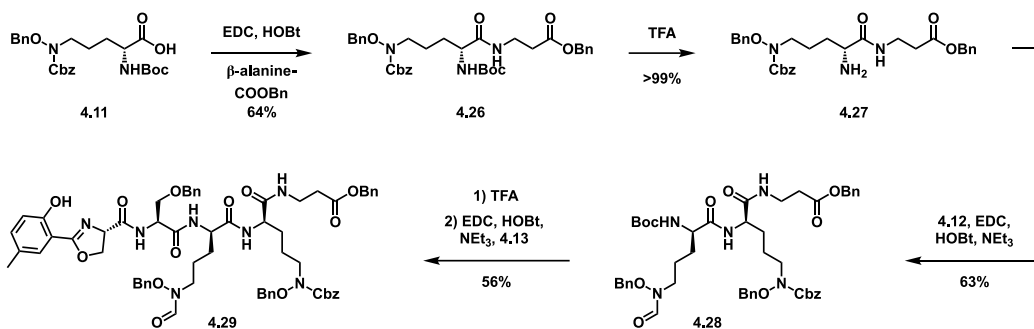
Scheme 4.4. *Synthesis of protected cahuitamycin E scaffold, **4.29**.*

Initial attempts at global deprotection (Scheme 4.5) using standard conditions resulted in incomplete removal of protecting groups and some degradation (Table 4.2, entry 1). Slightly more forcing conditions (entries 2-3) gave the same result. Upon turning to the literature in search of alternate conditions, I found that cyclohexadiene could be used as a substitute for hydrogen gas in hydrogenations,[217] and

specifically these types of methods had been used to deprotect peptides previously.[218] However, attempts at deprotections using these methods were also unsuccessful (entries 4-5).
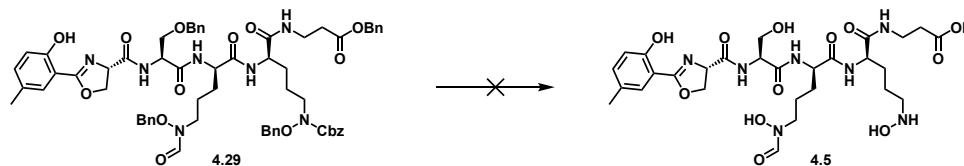
Scheme 4.5. *Deprotection of cahuitamycin E, 4.5.*

Entry	Hydrogen Source	Solvent	Additive	Temp.
1	H$_2$	EtOAc	--	rt
2	H$_2$	THF	--	50 °C
3	H$_2$	EtOAc	AcOH	rt
4	Cyclohexadiene	EtOAc	microwave	100 °C
5	Cyclohexadiene	MeOH	microwave	100 °C

Table 4.2. *Conditions for the deprotection of cahuitamycin E.*

In the literature, it has been noted that benzyl ethers can be more difficult to remove than benzyl esters and carbamates, and often require harsher conditions. As such, I wondered if intermediate **4.13** could be utilized without the need for a protecting group on the serine alcohol, as the amine should be more reactive in nucleophilic addition than the alcohol. I thus synthesized alternative intermediate **4.30** in 11% overall yield using the route in scheme 4.2 (Scheme 4.6, left). Subsequent coupling onto **4.28** proved successful in 27% yield, affording the protected scaffold bearing the unprotected serine (**4.31**, Scheme 4.6, right) in 11 LLS and 11% overall yield.
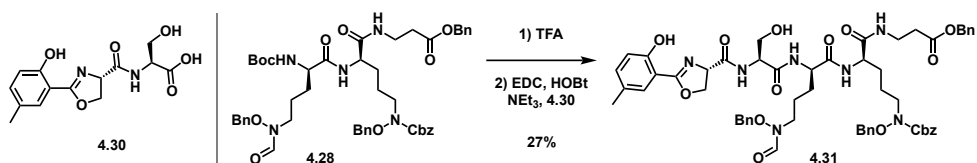
Scheme 4.6. *Structure of alternative, unprotected oxazoline fragment,* ***4.30*** *(left). Synthesis of alternative protected cahuitamycin E scaffold,* ***4.31*** *(right).*

Initial attempts at global deprotection using standard hydrogenation conditions now resulted in complete removal of all protecting groups. However, only degradation byproducts were able to be isolated. I hypothesized that this was the result of innate reactivity within the molecule. Namely, the hydroxyl amine could act as a nucleophile toward the electrophilic carboxylic acid. As such, I began considering alternative protecting group strategies to enable selective removal of some protecting groups, toward a stepwise deprotection that would provide more information regarding the cause of the degradation.

Concurrent to my efforts toward cahuitamycin E, Dr. Justin Shapiro, a post-doctoral fellow in our lab, was progressing toward the synthesis of cahuitamycin A. While I was amidst troubleshooting the deprotection of cahuitamycin E, he successfully completed this synthesis utilizing a similar route, save the piperazic acid fragment (Scheme 4.7). At that time, he observed discrepancies between the spectral data for his synthetic material and the reported structure. For that reason, we both shifted our attention to the structural characterization and elucidation of cahuitamycin A.
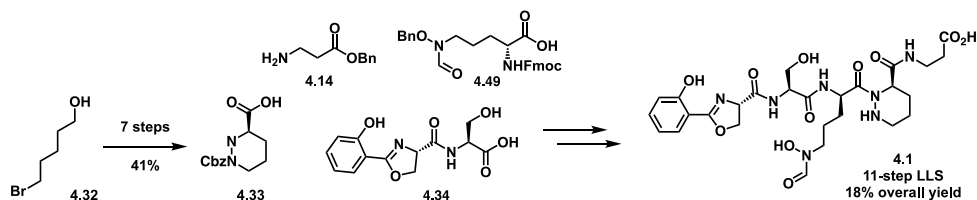
Scheme 4.7. *Overview of the synthesis of the reported structure of cahuitamycin A,* ***4.1***.

68

4.2.2. Structural Evaluation of Cahuitcamycin A

Spectral data for the authentic cahuitamycin A sample and the synthetic material displayed significant differences (Figure 4.6). Specifically, some chemical shifts in the ^{1}H NMR differed by up to ~1.0 ppm, indicating structural disparities between the two molecules. Following extensive characterization (^{1}H NMR, ^{13}C NMR, 2D NMR, MS, IR, optical rotation) of our final compound and all intermediates we confirmed the structural identity of the synthetic material, and specifically assigned peaks in the ^{1}H and ^{13}C NMR (Table 5.3.2). To further confirm these observations, and the distinct identities of the authentic and synthetic material, we obtained a sample of the isolated cahuitamycin A from the Sherman lab. Upon co-injection on HPLC, we observed distinct retention times (Figure 5.3.2), supporting the notion of differing structures. Furthermore, we found that the growth inhibition of the authentic sample aligned closely to the reported data, while the synthetic material differed drastically (Figure 4.7). Based on this spectral, chromatographic, and biological data, we concluded that the isolated material did not match the reported structure, and we set out toward determining the true natural product structure.
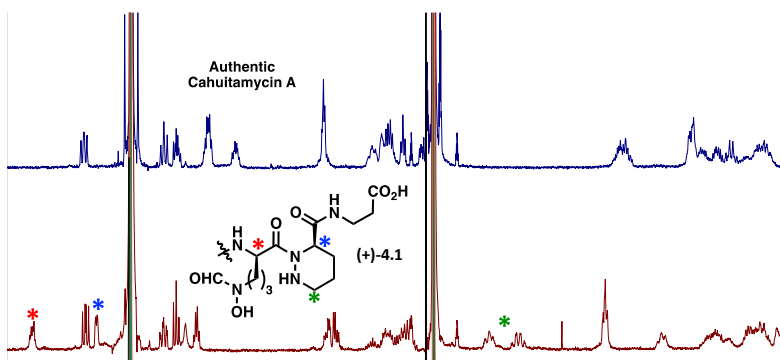
Figure 4.6. *^{1}H NMR of isolated (top) and synthetic (bottom) cahuitamycin A. Key differences highlighted.*
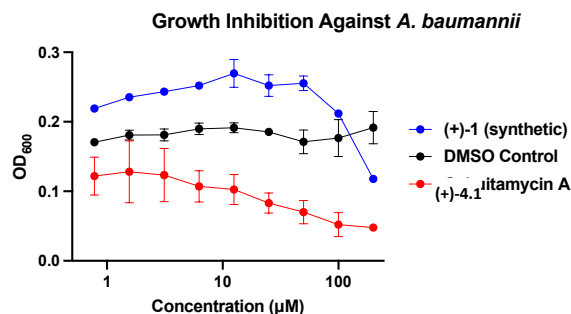
Figure 4.7. *A. baumannii growth inhibition of isolated (red) and synthetic (blue) cahuitamycin A.*

Based upon the spectral observations, we concluded that the N-terminus was correct as reported, namely the phenol, oxazoline, and serine portions, while the spectral inconsistencies were the result of some variation on the C-terminus. Toward elucidating possibilities for the true structure of cahuitamycin A, we turned to the reported biosynthesis for inspiration and identified several possibilities. First, there were two reported epimerase domains, one for each of the ornithine and piperazic acid portions. As such, we concluded that an inactive domain for either of those, would result in the corresponding diastereomers, and proposed **4.35** and **4.36** as potential revisions to the structure (Figure 4.8). As stereocenters can confer significant changes to three-dimensional conformation, we concluded that a single inversion could account for the many spectral inconsistencies observed.
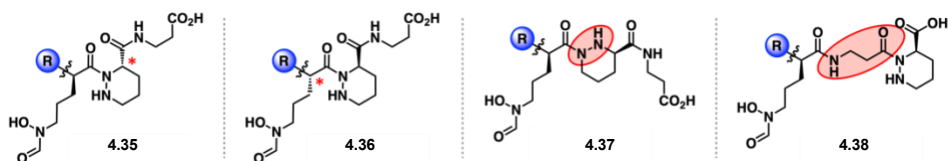
Figure 4.8. *Proposed corrections to the corrected structure of cahuitamycin A.*

We also noticed that the piperazic acid was proposed to be synthesized via a different pathway and joined onto the growing peptide after cyclization. We therefore conjectured that perhaps the piperazic was joined to the N-terminus through the N-2 amine, rather than the N-1 amine as reported (**4.37**, Figure 4.8).

This connectivity is not unprecedented as it has been reported in other natural products like the sanglifehrins (Figure 4.5). Furthermore, ambiguity in the reported HMBC correlations on the piperazic acid portion would make it difficult to distinguish between N-1 and N-2 connected structures. Finally, we noticed that the biosynthesis was composed of four modules, namely CahA, CahB, CahC, and CahD, where CahC is responsible for loading of the piperazic acid, and CahD is responsible for loading the beta-alanine. Being that these modules are reported to be non-colinear, it is possible for them to be assembled in an alternate order. Specifically, if CahD came before CahC, the beta-alanine would be loaded onto the N-terminus prior to the piperazic acid, which led us to the proposed isomer **4.38** (Figure 4.8). Again, this structure would explain the observed spectral data, as the protons attributed to the piperazic acid exhibited large discrepancies in chemical shift and those for the beta-alanine showed vastly different *J*-coupling values.

4.3.   Analog Synthesis

On these grounds, we set out toward the synthesis of each of these four structural isomers. Routes were envisioned where common oxazoline ((−)-**4.34**) and ornithine ((−)-**4.49**) fragments could be utilized, requiring only changes to the synthetic route toward the piperazic acid portion (Scheme 4.8). In brief, the piperazate diastereomer ((−)-**4.35**) was achieved in 12 LLS and 13% overall yield, following the same route as the reported structure of cahuitamycin A, merely using the alternative catalyst for the setting of the piperazate stereocenter (Scheme 4.8, A). Similarly, the ornithine diastereomer (**4.36**) was obtained in 12 LLS and 3% overall yield via the same route, beginning with the opposite commercial ornithine stereoisomer and using the opposite catalyst for setting the piperazate stereocenter (Scheme 4.8, B). A simplified route was utilized for the N-2 connected piperazate isomer ((+)-**4.37**, Scheme 4.8, C), enabled by the innate reactivity of the N-2 position, no longer requiring complex protecting group manipulations to force coupling at the less reactive N-1 position. This allowed the synthesis of (+)-**4.37** in 12 LLS and 21% overall yield. Finally, the inverted beta-alanine-piperazate isomer ((+)-**4.38**) was obtained from the same piperazate intermediate (+)-**4.45** used in the synthesis of the reported structure (Scheme 4.8, D). Subsequent

rearrangement of coupling steps and protecting group manipulations afforded **(+)-4.38** in 14 LLS and 13% overall yield.

Scheme 4.8. *Synthesis of cahuitamycin A structural isomers.*

With all four isomers in hand, we proceeded through the same rigorous characterization process as before (Tables 5.3.3-5.3.5), and unfortunately determined that none of the revised structures corresponded to the isolated material. Going back to the drawing board once more, we envisioned yet another possibility for the true structure. In the proposed biosynthetic pathway, cahuitamycin A and cahuitamycin E were synthesized separately, via loading alternative intermediates onto CahC (Figure 4.9), followed by similar loading of beta-alanine in CahD and termination from the module via hydrolysis. However, realizing that there was a nucleophilic hydroxylamine in proximity to the C-terminus, we proposed that an intramolecular cyclization could be responsible for cleavage, resulting in a 10-membered macrocylic structure.

Figure 4.9. *Proposed biosynthetic termination of reported structure of cahuitamycin A (left) and proposed structure (right).*

Upon searching the literature for similar scaffolds in other natural products, the fuscachelins were identified,[219] which possess a similar 10-membered macrocycle bearing a cyclic hydroxyl amine (Figure 4.10). This macrocycle possesses remarkable similarity to the newly proposed cahuitamycin A structure, save the replacement of the lactone with a lactam. Furthermore, they reported the isolation of cyclized (fuscachelin A, **4.50**) and linear (fuscachelin B, **4.51**) structures, which would align with a similar isolation of cyclized and linear cahuitamycins molecules (A and E, respectively). Additionally, this innate reactivity and propensity for cyclization would explain difficulties in isolating cahuitamycin E synthetically. Based upon this collective evidence, efforts toward the synthesis of this macrocyclic structure are currently underway by Gavin Smith and Marina Michaud, junior graduate students in our lab.
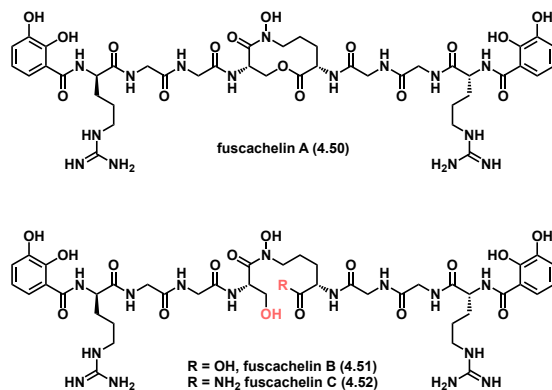
Figure 4.10. *Structure of macrocycle-containing natural products, fuscachelins.*

4.4. Conclusions & Future Directions

In conclusion, the first total synthesis of the reported structure of cahuitamycin A was completed in 11 LLS and 18% overall yield. Additionally, synthesis of the protected scaffold of cahuitamycin E was completed in 11 LLS and 11% overall yield. However, challenges with isolation due to hypothesized innate reactivity of the natural product precluded its isolation and characterization. Extensive characterization and analysis of cahuitamycin A revealed structural inconsistencies from the isolated material. As such, four structural isomers were proposed based on the reported biosynthesis, and subsequent synthesis and characterization indicated that these too were distinct from the natural product. Current hypotheses predict a 10-membered macrocylic structure in the natural product, for which the synthesis is currently underway. Upon confirmation of the true natural product structure, synthesis of other analogs and biological evaluation thereof will be performed to determine which structural motifs are important for their activity in *A. baumannii*. These investigations will enable eventual probe development, which will be utilized to identify the target of the cahuitamycins in *A. baumannii*. This information will lay the groundwork for a better understanding of the interplay between iron chelation and biofilm formation in this and other species.

4.5. References

(200) Peleg, A. Y.; Seifert, H.; Paterson, D. L. Acinetobacter Baumannii: Emergence of a Successful Pathogen. *Clin. Microbiol. Rev.* **2008**, *21* (3), 538–582. https://doi.org/10.1128/CMR.00058-07.

(201) Li, Z.; Cao, Y.; Yi, L.; Liu, J. H.; Yang, Q. Emergent Polymyxin Resistance: End of an Era? *Open Forum Infect. Dis.* **2019**, *6* (10), 1–10. https://doi.org/10.1093/ofid/ofz368.

(202) Frieden, T. Antibiotic Resistance Threats in the United States, 2013. *Centers Dis. Control Prev.* **2013**. https://doi.org/CS239559-B.

(203) Eze, E. C.; Chenia, H. Y.; El Zowalaty, M. E. Acinetobacter Baumannii Biofilms: Effects of Physicochemical Factors, Virulence, Antibiotic Resistance Determinants, Gene Regulation, and Future Antimicrobial Treatments. *Infect. Drug Resist.* **2018**, *11*, 2277–2299. https://doi.org/10.2147/IDR.S169894.

(204) Veerachamy, S.; Yarlagadda, T.; Manivasagam, G.; Yarlagadda, P. K. Bacterial Adherence and Biofilm Formation on Medical Implants: A Review. *Proc. Inst. Mech. Eng. Part H J. Eng. Med.* **2014**, *228* (10), 1083–1099. https://doi.org/10.1177/0954411914556137.

(205) Fujii, K.; Ikai, Y.; Mayumi, T.; Oka, H.; Suzuki, M.; Harada, K. I. A Nonempirical Method Using LC/MS for Determination of the Absolute Configuration of Constituent Amino Acids in a Peptide: Elucidation of Limitations of Marfey's Method and of Its Separation Mechanism. *Anal. Chem.* **1997**, *69* (16), 3346–3352. https://doi.org/10.1021/AC9701795.

(206) Marfey, P. Determination OfD-Amino Acids. II. Use of a Bifunctional Reagent, 1,5-Difluoro-2,4-Dinitrobenzene. *Carlsb. Res. Commun. 1984 496* **1984**, *49* (6), 591–596. https://doi.org/10.1007/BF02908688.

(207) Blin, K.; Medema, M. H.; Kazempour, D.; Fischbach, M. A.; Breitling, R.; Takano, E.; Weber, T. AntiSMASH 2.0-a Versatile Platform for Genome Mining of Secondary Metabolite Producers. *Nucleic Acids Res.* **2013**, *41* (Web Server issue), W204–W212. https://doi.org/10.1093/nar/gkt449.

(208) Proschak, A.; Lubuta, P.; Grün, P.; Löhr, F.; Wilharm, G.; De Berardinis, V.; Bode, H. B. Structure and Biosynthesis of Fimsbactins A-F, Siderophores from Acinetobacter Baumannii and Acinetobacter Baylyi. *ChemBioChem* **2013**, *14* (5), 633–638. https://doi.org/10.1080/14772000.2017.1375046.

(209) Shapiro, J. A.; Wencewicz, T. A. Acinetobactin Isomerization Enables Adaptive Iron Acquisition in Acinetobacter Baumannii through PH-Triggered Siderophore Swapping. *ACS Infect. Dis.* **2016**, *2* (2), 157–168. https://doi.org/10.1021/acsinfecdis.5b00145.

(210) Evers, A.; Hancock, R. D.; Martell, A. E.; Motekaitis, R. J. Metal Ion Recognition in Ligands with Negatively Charged Oxygen Donor Groups. Complexation of Iron(III), Gallium(III), Indium(III), Aluminum(III), and Other Highly Charged Metal Ions. *Inorg. Chem.* **1989**, *28* (11), 2189–2195. https://doi.org/10.1021/ic00310a035.

(211) Neumann, C. S.; Jiang, W.; Heemstra, J. R.; Gontang, E. A.; Kolter, R.; Walsh, C. T. Biosynthesis of Piperazic Acid via N5-Hydroxy-Ornithine in Kutzneria Spp. 744. *Chembiochem.* **2012**, *13* (7), 972–976. https://doi.org/10.1002/cbic.201200054.

(212) Broberg, A.; Menkis, A.; Vasiliauskas, R. Kutznerides 1-4, Depsipeptides from the Actinomycete Kutzneria Sp. 744 Inhabiting Mycorrhizal Roots of Picea Abies Seedlings. *J. Nat. Prod.* **2006**, *69* (1), 97–102. https://doi.org/10.1021/np050378g.

(213) Fehr, T.; Kallen, J.; Oberer, L.; Sanglier, J. J.; Schilling, W. Sanglifehrins A, B, C and D, Novel Cyclophilin-Binding Compounds Isolated from Streptomyces Sp. A92-308110. II. Structure Elucidation, Stereochemistry and Physico-Chemical Properties. *J. Antibiot.* **1999**, *52* (5), 474–479. https://doi.org/10.7164/antibiotics.52.474.

(214) Tao, T.; Alemany, L. B.; Parry, R. J. Valanimycin Biosynthesis: Investigations of the Mechanism of Isobutylhydroxylamineincorporation. *Org. Lett.* **2003**, *5* (8), 1213–1215. https://doi.org/10.1021/ol0340989.

(215) Oelke, A. J.; France, D. J.; Hofmann, T.; Wuitschik, G.; Ley, S. V; ; · Waldman, A. J.; Ng, T. L.;

Wang, P.; Balkus, E. P. *Piperazic Acid Synthesis*; 1998; Vol. 120.

(216) Umezawa, K.; Ikeda, Y.; Kawase, O.; Naganawa, H.; Kondo, S. Biosynthesis of Polyoxypeptin A: Novel Amino Acid 3-Hydroxy-3-Methylproline Derived from Isoleucine. *J. Chem. Soc. Perkin Trans.* **2001**, *1*, 1550–1553. https://doi.org/10.1039/b101942m.

(217) Quinn, J. F.; Razzano, D. A.; Golden, K. C.; Gregg, B. T. 1,4-Cyclohexadiene with Pd/C as a Rapid, Safe Transfer Hydrogenation System with Microwave Heating. *Tetrahedron Lett.* **2008**, *49* (42), 6137–6140. https://doi.org/10.1016/j.tetlet.2008.08.023.

(218) Felix, A. M.; Heimer, E. P.; Lambros, T. J.; Tzougraki, C.; Meienhofer, J. *Rapid Removal of Protecting Groups from Peptides by Catalytic Transfer Hydrogenation with 1,4-Cyclohexadiene*; 1978; Vol. 43.

(219) Dimise, E. J.; Widboom, P. F.; Bruner, S. D. Structure Elucidation and Biosynthesis of Fuscachelins, Peptide Siderophores from the Moderate Thermophile Thermobifida Fusca. *Proc. Natl. Acad. Sci. U. S. A.* **2008**, *105* (40), 15311–15316. https://doi.org/10.1073/PNAS.0805451105/SUPPL_FILE/0805451105SI.PDF.

(220) Kaliappan, K. P.; Ravikumar, V. Angucyclinone Antibiotics: Total Syntheses of YM-181741, (+)-Ochromycinone, (+)-Rubiginone B2, (-)-Tetrangomycin, and MM-47755. *J. Org. Chem.* **2007**, *72* (16), 6116–6126. https://doi.org/10.1021/jo070709p.

(221) Kerhervé, J.; Botuha, C.; Dubois, J. New Asymmetric Synthesis of Protein Farnesyltransferase Inhibitors via Palladium-Catalyzed Cross-Coupling Reactions of 2-Iodo-Imidazoles. *Org. Biomol. Chem.* **2009**. https://doi.org/10.1039/b902601k.

(222) Hon, Y. S.; Hsieh, C. H.; Liu, Y. W. Dibromomethane as One-Carbon Source in Organic Synthesis: Total Synthesis of (±)- and (-)-Methylenolactocin. *Tetrahedron* **2005**. https://doi.org/10.1016/j.tet.2005.01.057.

(223) Ruprecht, J.; Yankovskaya, V.; Maklashina, E.; Iwata, S.; Cecchini, G. Structure of Escherichia Coli Succinate: Quinone Oxidoreductase with an Occupied and Empty Quinone-Binding Site. *J. Biol. Chem.* **2009**. https://doi.org/10.1074/jbc.M109.010058.

(224) Leaver-Fay, A.; Tyka, M.; Lewis, S. M.; Lange, O. F.; Thompson, J.; Jacak, R.; Kaufman, K.; Renfrew, P. D.; Smith, C. A.; Sheffler, W.; Davis, I. W.; Cooper, S.; Treuille, A.; Mandell, D. J.; Richter, F.; Ban, Y. E. A.; Fleishman, S. J.; Corn, J. E.; Kim, D. E.; Lyskov, S.; Berrondo, M.; Mentzer, S.; Popović, Z.; Havranek, J. J.; Karanicolas, J.; Das, R.; Meiler, J.; Kortemme, T.; Gray, J. J.; Kuhlman, B.; Baker, D.; Bradley, P. Rosetta3: An Object-Oriented Software Suite for the Simulation and Design of Macromolecules. In *Methods in Enzymology*; 2011. https://doi.org/10.1016/B978-0-12-381270-4.00019-6.

(225) Hawkins, P. C. D.; Skillman, A. G.; Warren, G. L.; Ellingson, B. A.; Stahl, M. T. Conformer Generation with OMEGA: Algorithm and Validation Using High Quality Structures from the Protein Databank and Cambridge Structural Database. *J. Chem. Inf. Model.* **2010**. https://doi.org/10.1021/ci100031x.

(226) Hawkins, P. C. D.; Nicholls, A. Conformer Generation with OMEGA: Learning from the Data Set and the Analysis of Failures. *J. Chem. Inf. Model.* **2012**. https://doi.org/10.1021/ci300314k.

(227) Preparation of 2-pyridinylguanidines as urokinase inhibitors. Reference Detail | CAS SciFinder[n] https://scifinder-n.cas.org/searchDetail/reference/6254550daaa21311b5c3d3cd/referenceDetails (accessed Apr 11, 2022).

(228) Yokokawa, F.; Sugiyama, H.; Shioiri, T.; Katagiri, N.; Oda, O.; Ogawa, H. An Expeditious Synthesis of Pentosidine, an Advanced Glycation End Product. *Tetrahedron* **2001**, *57* (22), 4759–4766. https://doi.org/10.1016/S0040-4020(01)00399-4.

(229) Mashiach, R.; Meijler, M. M. Total Synthesis of Pyoverdin D. *Org. Lett.* **2013**, *15* (7), 1702–1705. https://doi.org/10.1021/ol400490s.

(230) Henmi, Y.; Makino, K.; Yoshitomi, Y.; Hara, O.; Hamada, Y. Highly Efficient Synthesis of (R)-

and (S)-Piperazic Acids Using Proline-Catalyzed Asymmetric α-Hydrazination. *Tetrahedron Asymmetry* **2004**, *15* (21), 3477–3481. https://doi.org/10.1016/j.tetasy.2004.09.025.

(231) Chen, Y.; Lu, Y.; Zou, Q.; Chen, H.; Ma, D. A Scalable Process to the Key Intermediate of Cilazapril, (S) - 1- Benzyloxycarbonylhexahydropyridazine-3-Carboxylic Acid, Through a Novel Cascade Course. **2013**, 1209–1213. https://doi.org/10.1021/op400155u.

5.1. Promysalin Alkyl Analogs

5.1.1. Supporting Figures
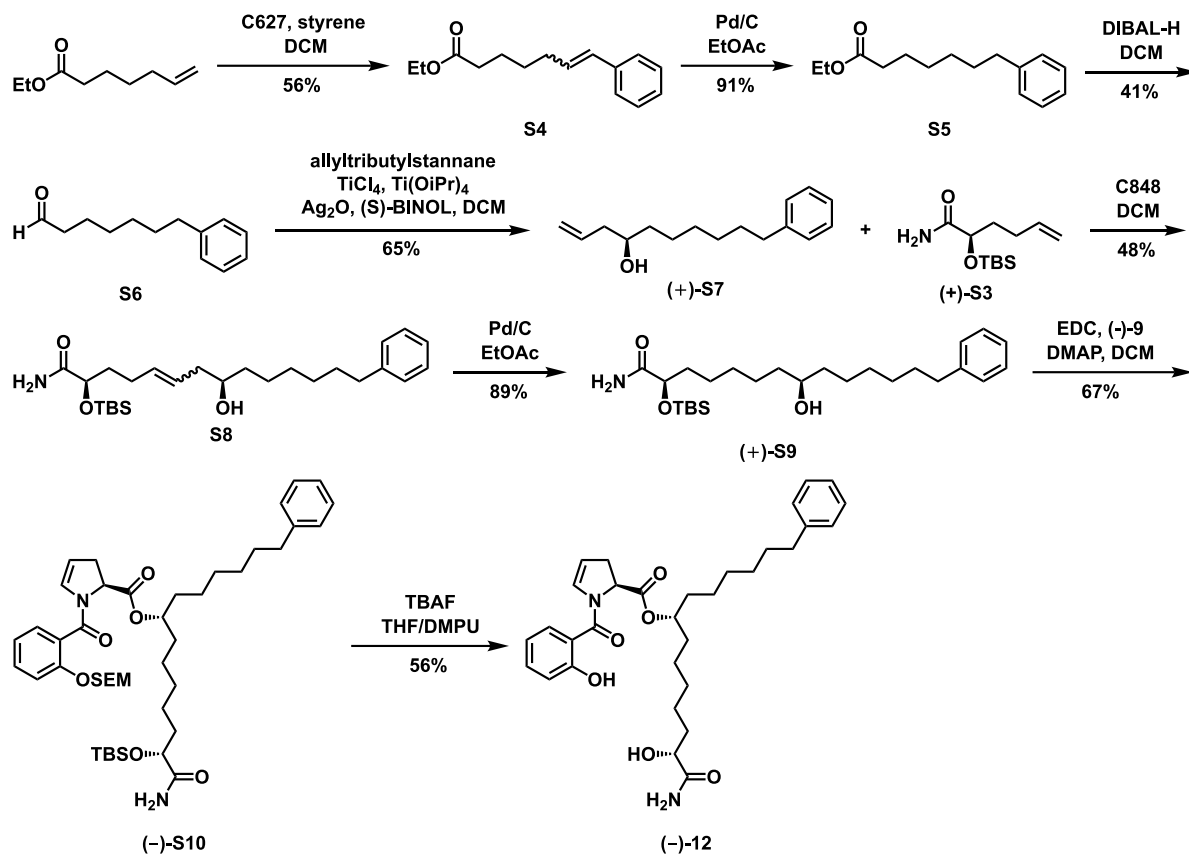
Scheme 5.1.1. *Modified synthetic route for the synthesis of (–)-12.*

	Structure	PAO1 IC$_{50}$ (µM)	PAO1 IC$_{90}$ (µM)	RO5 IC$_{50}$ (µM)	RO5 IC$_{90}$ (µM)
Connectivity	(-)-**11a** n = 0	32	190	15	43
	(-)-**11b** n = 2	37	130	40	120
Bulky	(-)-**11c** n = 1	--	--	--	--
	(-)-**11d** n = 1	--	--	--	--
Truncated	(-)-**11e** n = 1	85	150	77	210
	(-)-**11f** n = 1	27	>250	49	160
	(-)-**11g** n = 1	14	30	16	140
	(-)-**1**	6.9	73	2.9	15
Elongated	(-)-**11h** n = 1	1.8	>250	3.7	13
	(-)-**11i** n = 1	1.1	10	1.7	4.4
	(-)-**11j** n = 1	3.4	89	1.8	3.8
	(-)-**12** n = 1	2.4	4.3	1.7	9.4

Table 5.1.1. *Summary of growth inhibition against PAO1 and resistant mutant, RO5. IC$_{50}$ and IC$_{90}$ values are the average of 3 trials.*
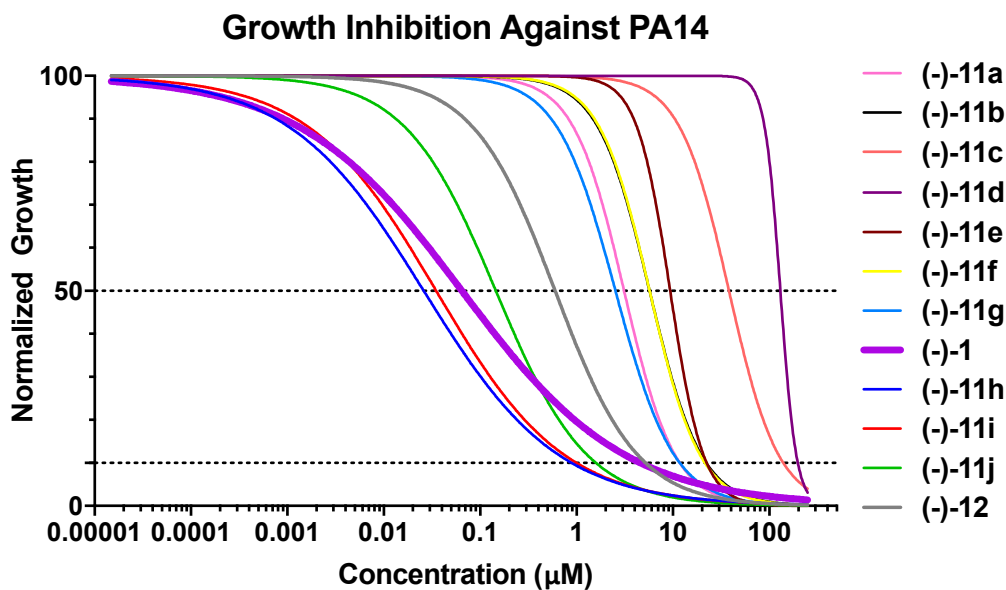
Figure 5.1.1. *Inhibitory activity of promysalin and all analogs against PA14. Best fit lines are the average of 3 trials (error bars indicate SEM). Dotted lines indicate IC_{50} and IC_{90}.*
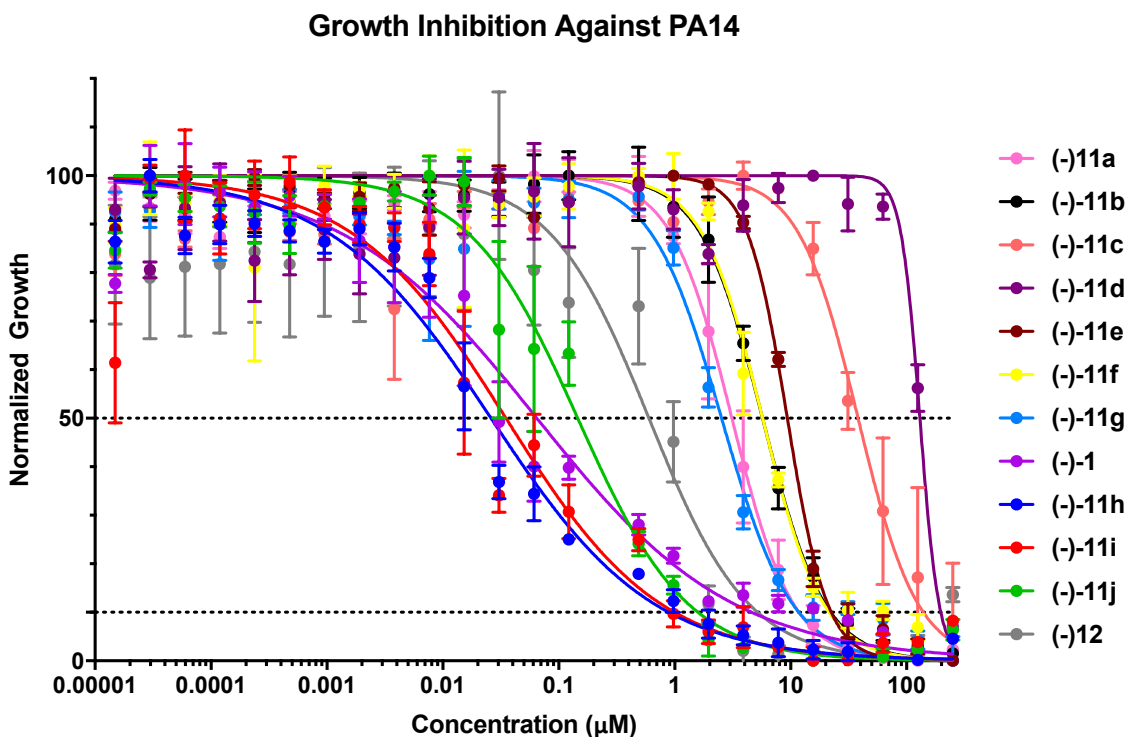
Figure 5.1.2. *Inhibitory activity of promysalin and all analogs against PA14. Best fit lines and data points are the average of 3 trials (error bars indicate SEM). Dotted lines indicate IC_{50} and IC_{90}.*

Growth Inhibition Against PAO1
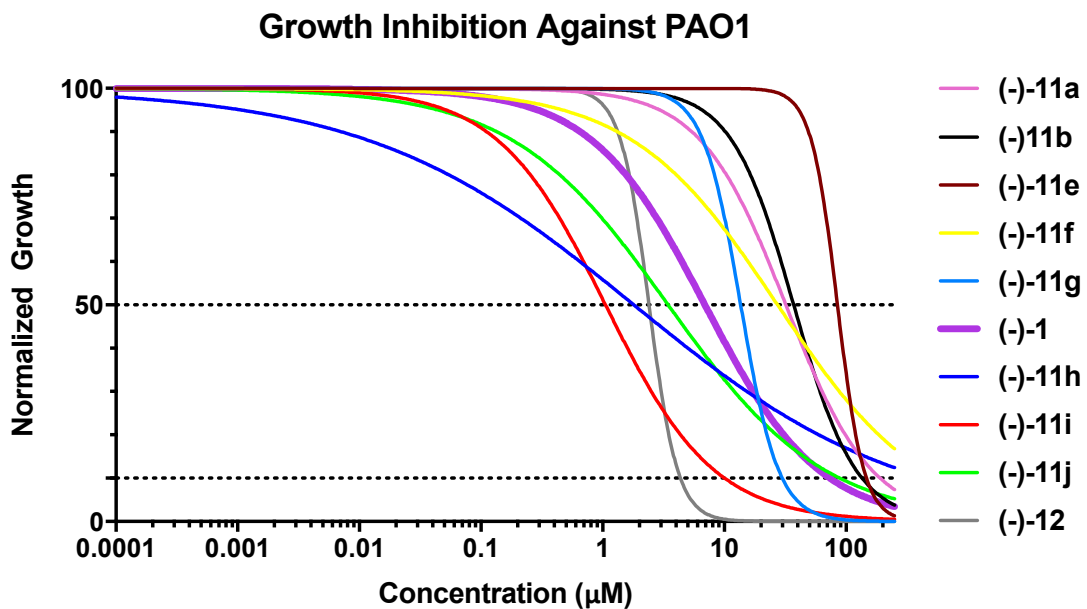
Figure 5.1.3. Inhibitory activity of promysalin and all analogs against PAO1. Best fit lines are the average of 3 trials (error bars indicate SEM). Dotted lines indicate IC_{50} and IC_{90}.

Growth Inhibition Against PAO1
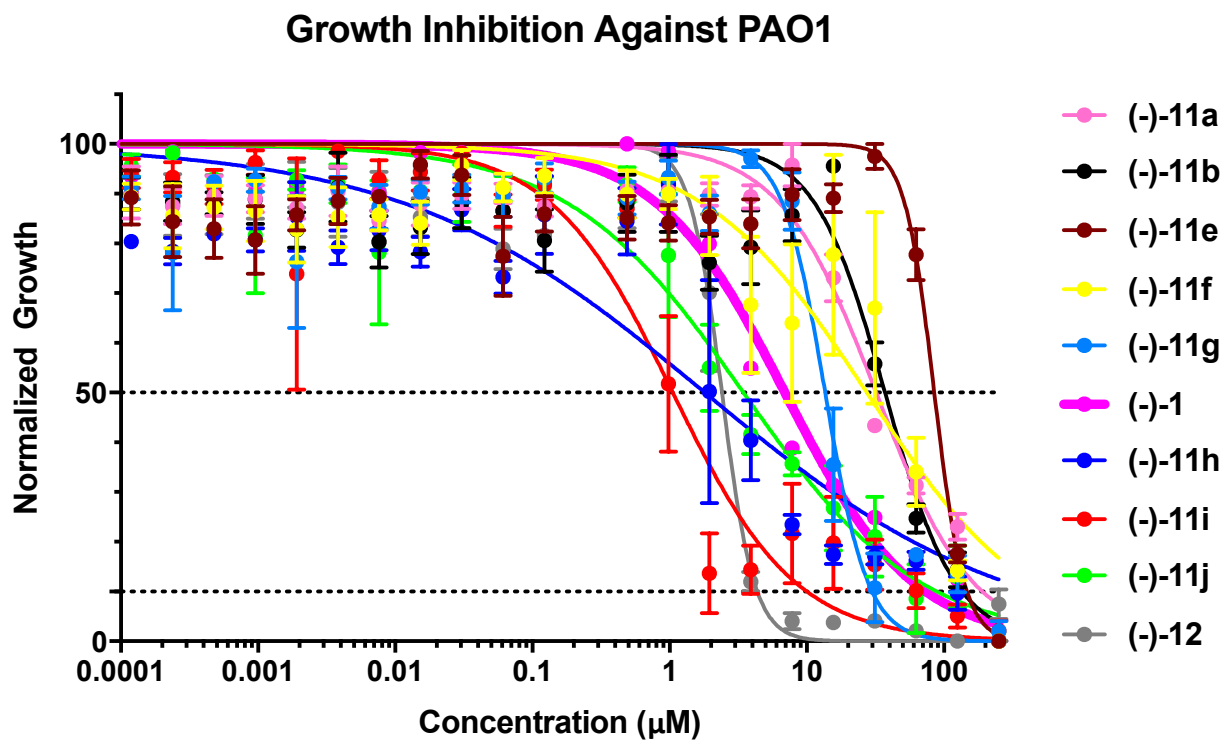
Figure 5.1.4. Inhibitory activity of promysalin and all analogs against PAO1. Best fit lines and data points are the average of 3 trials (error bars indicate SEM). Dotted lines indicate IC_{50} and IC_{90}.
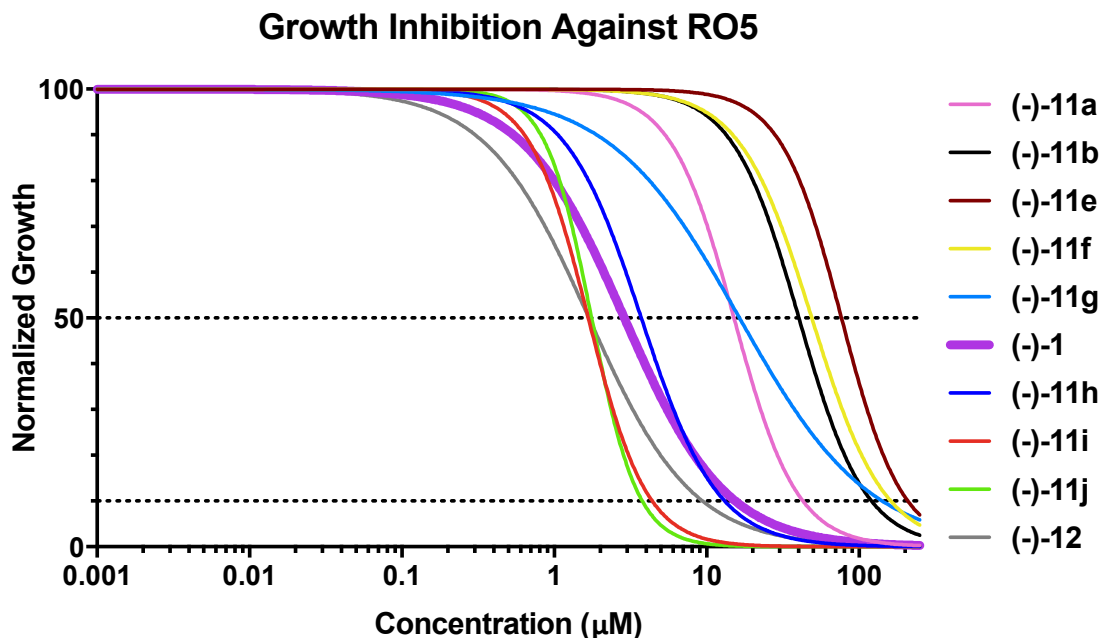
Figure 5.1.5. *Inhibitory activity of promysalin and all analogs against RO5. Best fit lines are the average of 3 trials (error bars indicate SEM). Dotted lines indicate IC$_{50}$ and IC$_{90}$.*
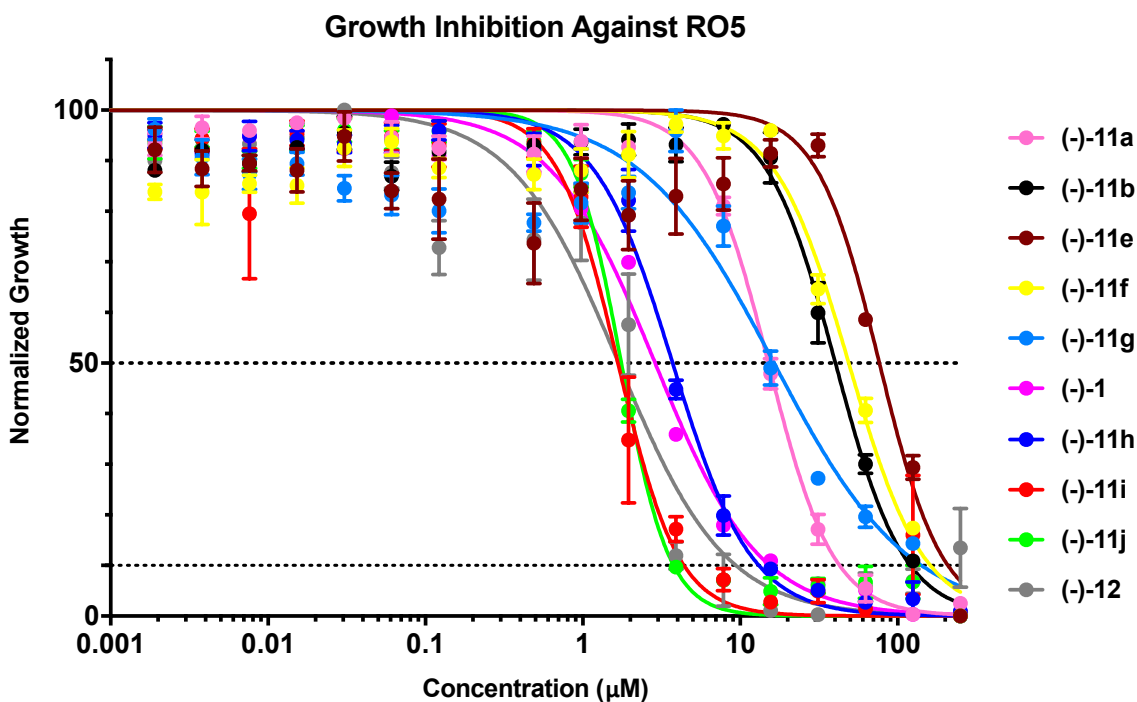
Figure 5.1.6. *Inhibitory activity of promysalin and all analogs against RO5. Best fit lines and data points are the average of 3 trials (error bars indicate SEM). Dotted lines indicate IC$_{50}$ and IC$_{90}$.*

5.1.1. Chemistry

5.1.1.1. General Methods

NMR spectra were recorded using the following spectrometers: Bruker Advance 500 (500/125 MHz) or Bruker Advance 400 (400/100 MHz). Chemical shifts are quoted in ppm relative to tetramethylsilane and with the indicated solvent as an internal reference. The following abbreviations are used to describe signal multiplicities: s (singlet), d (doublet), t (triplet), q (quartet), m (multiplet), br (broad), dd (doublet of doublets), dt (doublet of triplets), etc. Accurate mass spectra were recorded on an Agilent 6520 Accurate-Mass Q-TOF LC/MS, infrared spectra were obtained using a Thermo Nicolet Nexus 670 FTIR spectrophotometer and specific rotation measurements were made with a 1 dm path length using a Perkin Elmer 341 Polarimeter.

Non-aqueous reactions were performed under an atmosphere of argon, in flame- dried glassware, with HPLC-grade solvents dried by passage through activated alumina. 2,6-lutidine, triethylamine, and diisopropylethylamine were freshly distilled from CaH_2 prior to use. Brine refers to a saturated aqueous solution of sodium chloride, sat. $NaHCO_3$ refers to a saturated aqueous solution of sodium bicarbonate, sat. NH_4Cl refers to a saturated aqueous solution of ammonium chloride, etc. 3 Å molecular sieves were activated in a round-bottom flask under vacuum heating at 120°C in an oil bath overnight. "Column chromatography", unless otherwise indicated, refers to purification in a gradient of increasing EtOAc concentration in hexanes on a Biotage® flash chromatography purification system. Metathesis catalysts were obtained as generous gifts from Materia, Inc. All other chemicals were used as received from Oakwood, TCI America, Sigma-Aldrich, Alfa Aesar, or AK Scientific.

5.1.1.2. Procedures and Characterization

General procedure A: Cross metathesis. Homoallylic alcohol (5 eq) was combined with TBS protected alkene (1 eq) in CH_2Cl_2 (0.02M). The flask was charged with catalyst C711 (Materia, CAS [635679-242])

(10 mol%) and stirred under a static argon atmosphere for 24 hours. The solution was loaded directly onto a silica gel column and subjected to chromatography.

General procedure B: Hydrogenation of alkenes. Alkene (1 eq) was dissolved in EtOAc (0.05 M) and 10% Pd/C (5 mol%) then the reaction flask was vacuum and backfilled with H_2 5x and stirred under a H_2 balloon overnight. The reaction was filtered through celite and concentrated.

General procedure C: Removal of Evans oxazolidinone. Alcohol (1 eq) was dissolved in THF (0.03 M) and ammonium hydroxide (0.02 M) was added. The flask was tightly sealed and the biphasic mixture was stirred for 48 hours. The reaction was carefully vented, concentrated, and azeotroped with methanol 3x. The crude reaction was purified with column chromatography (20% Et_2O/DCM $\rightarrow$ 30% Et_2O/DCM $\rightarrow$ 5%MeOH/30%Et_2O/65% DCM).

General procedure D: EDC Esterification. An acid (1.3 eq) was dissolved in DCM (0.2 M), cooled to 0°C and EDC (2 eq) was added. A solution of alcohol (1 eq) and DMAP (0.5 eq) were dissolved in an equal volume of DCM and added to the first solution. The reaction was allowed to warm to room temperature and stir overnight. The resulting mixture was poured into water and extracted with DCM 3x. The combined organic layers were washed with brine, dried over $MgSO_4$, concentrated, and purified by column chromatography (0 $\rightarrow$ 30% EtOAc/DCM).

General procedure E: Global Deprotection. The protected ester was dissolved in DMPU (1:1 v/v TBAF, dried over 3Å molecular sieves). Tetrabutylammonium fluoride (20 eq, 1M solution in THF, dried over 3Å molecular sieves for 1 - 2 days) was added dropwise. The reaction was quenched with sat. NH_4Cl after 30 minutes. The mixture was extracted with Et_2O (5 times, TLC analysis of aqueous layer to confirm full extraction), and the combined organic layers were washed with sat'd NH_4Cl 5x followed by brine. The

solution was dried over Na₂SO₄, concentrated, and purified by column chromatography (0 → 5% MeOH/CH₂Cl₂).
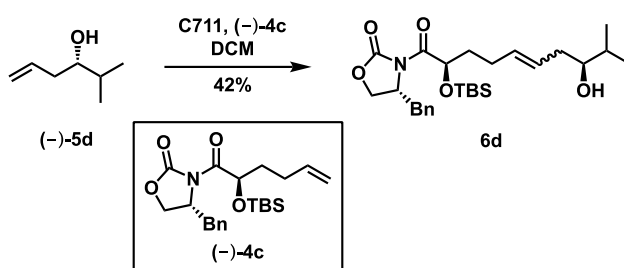
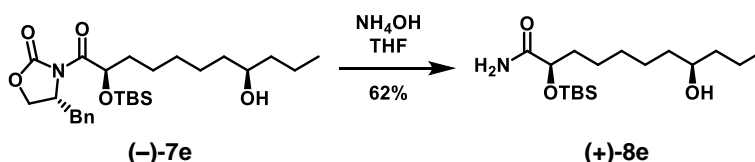**(R)-4-benzyl-3-((2R,8S,E)-2-((tert-butyldimethylsilyl)oxy)-8-hydroxy-9-methyldec-5-enoyl)oxazolidin-2-one (6d).** Following general procedure A, homoallylic alcohol **(–)-5d** (0.546 g, 01.35 mmol) yielded the title compound as a brown oil (0.278 g, 42% yield). **¹H NMR** (500 MHz, CDCl₃ mixture of E/Z isomers) δ 7.36 – 7.31 (m, 2H), 7.31 – 7.27 (m, 1H), 7.25 – 7.22 (m, 2H), 5.63 – 5.52 (m, 1H), 5.51 – 5.43 (m, 1H), 5.37 (dd, J = 8.4, 3.3 Hz, 1H), 4.66 – 4.58 (m, 1H), 4.24 – 4.14 (m, 2H), 3.43 – 3.31 (m, 2H), 2.74 – 2.65 (m, 1H), 2.29 – 2.14 (m, 3H), 2.08 – 2.00 (m, 1H), 1.82 – 1.61 (m, 4H), 0.94 (s, 9H), 0.92 (dd, J = 9.7, 6.8 Hz, 6H), 0.11 (d, J = 3.6 Hz, 3H), 0.09 (d, J = 3.6 Hz, 3H).; **¹³C NMR** (126 MHz, CDCl₃) δ 174.44, 153.24, 135.35, 132.89, 129.58, 129.13, 127.74, 127.53, 75.64, 70.86, 66.69, 55.75, 55.74, 37.84, 37.72, 35.27, 33.16, 28.56, 25.95, 18.88, 18.45, 17.81, -4.44, -4.92.; **IR** (film) 3538 (br O-H), 2955, 2928, 2856, 1778 (C=O), 1710 (C=O), 1471, 1387, 1348, 1249, 1210, 1196, 1109, 1006 ,972, 836, 777, 701; **HRMS** Accurate mass (ES⁺): Found 490.2989, C₂₇H₄₄NO₅Si (M+H) requires 490.2989.
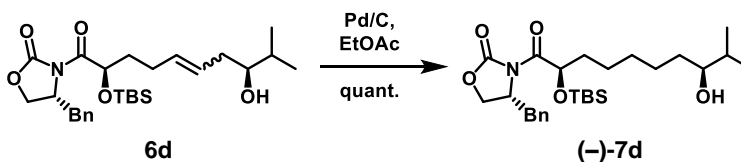
(R)-4-benzyl-3-((2R,8S)-2-((tert-butyldimethylsilyl)oxy)-8-hydroxy-9-methyldecanoyl)oxazolidin-2-one (–)-7d. Following general procedure B, alkene **6d** (278 mg, 0.568 mmol) yielded the title compound as a clear oil (281 mg, quant.). **¹H NMR** (500 MHz, CDCl₃) δ 7.36 – 7.32 (m, 2H), 7.30 – 7.27 (m, 1H), 7.25 – 7.23 (m, 2H), 5.36 (dd, J = 8.3, 3.3 Hz, 1H), 4.62 (qd, J = 6.3, 3.0 Hz, 1H), 4.24 – 4.14 (m, 2H), 3.40 (dd, J = 13.3, 3.2 Hz, 1H), 3.34 (ddd, J = 8.3, 5.0, 3.1 Hz, 1H), 2.70 (dd, J = 13.3, 10.1 Hz, 1H), 1.72 – 1.59

(m, 3H), 1.56 – 1.42 (m, 5H), 1.41 – 1.27 (m, 4H), 0.94 (s, 9H), 0.90 (t, J = 6.5 Hz, 6H), 0.11 (s, 3H), 0.09 (s, 3H).; ^{13}**C NMR** (126 MHz, CDCl$_3$) δ 174.53, 153.24, 135.37, 129.55, 129.10, 127.49, 71.44, 66.63, 55.72, 37.83, 35.26, 34.14, 33.60, 29.35, 25.94, 25.92, 25.57, 18.97, 18.46, 17.20, -4.50, -4.96.; **[α]^{25}$_D$** -2.7 (c = 0.51 in CHCl$_3$); **IR** (film) 3522 (br O-H), 2928, 2856, 1779 (C=O), 1710 (C=O), 1462, 1387, 1348, 1249, 1210, 1195, 1107, 1007, 976, 835, 777, 701; **HRMS** Accurate mass (ES$^+$): Found 492.3135, C$_{27}$H$_{46}$NO$_5$Si (M+H) requires 492.3145.

(–)-7d   (+)-8d
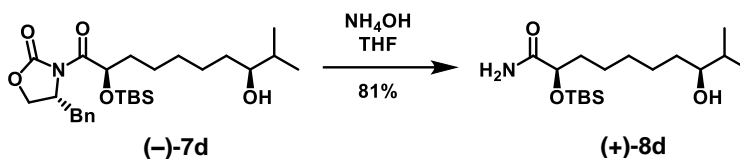
(2R,8S)-2-((tert-butyldimethylsilyl)oxy)-8-hydroxy-9-methyldecanamide (+)-8d. Following general procedure C, oxazolidinone **(–)-7d** (84 mg, 0.171 mmol) yielded the title compound as a clear oil (46 mg, 81% yield). ^{1}**H NMR** (500 MHz, CDCl$_3$) δ 6.52 (d, J = 4.6 Hz, 1H), 5.94 (d, J = 4.5 Hz, 1H), 4.15 – 4.10 (m, 1H), 3.36 – 3.30 (m, 1H), 1.81 – 1.71 (m, 1H), 1.70 – 1.58 (m, 2H), 1.49 – 1.40 (m, 3H), 1.40 – 1.26 (m, 6H), 0.91 (s, 9H), 0.89 (dd, J = 6.8, 5.5 Hz, 6H), 0.09 (s, 3H), 0.08 (s, 3H).; ^{13}**C NMR** (126 MHz, CDCl$_3$) δ 177.24, 76.75, 73.57, 35.23, 34.16, 33.58, 29.73, 25.99, 25.86, 24.27, 18.99, 18.14, 17.21, -4.71, -5.12.; **[α]^{25}$_D$** +2.3 (c = 0.85 in CHCl$_3$); **IR** (film) 3478 (N-H), 3350 (br O-H), 2928, 2857, 1680 (C=O), 1583, 1463, 1388, 1361, 1253, 1101, 1005, 835, 777, 669; **HRMS** Accurate mass (ES$^+$): Found 332.2615, C$_{17}$H$_{38}$NO$_3$Si (M+H) requires 332.2621.

(+)-8d   (–)-9   (–)-10d
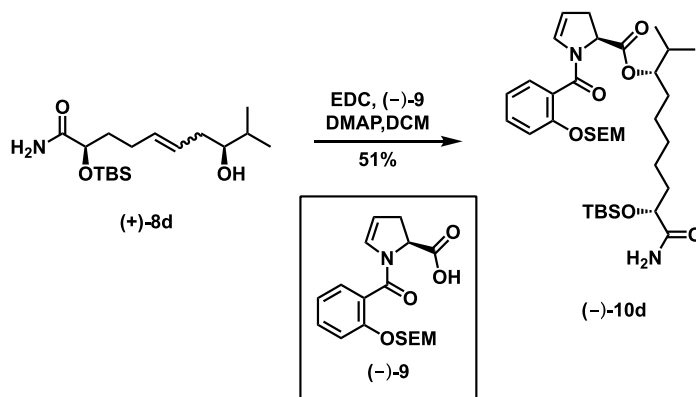
**(3S,9R)-10-amino-9-((tert-butyldimethylsilyl)oxy)-2-methyl-10-oxodecan-3-yl** **(S)-1-(2-((2-(trimethylsilyl)ethoxy)methoxy)benzoyl)-2,3-dihydro-1H-pyrrole-2-carboxylate (–)-10d.** Following general procedure D, alcohol **(+)-8d** (34 mg, 0.102 mmol) yielded the title compound as a clear oil (35 mg, 51% yield). **^{1}H NMR** (500 MHz, CDCl$_3$) δ 7.37 – 7.33 (m, 2H), 7.20 (dd, J = 8.9, 1.0 Hz, 1H), 7.03 (td, J = 7.5, 1.0 Hz, 1H), 6.52 (d, J = 4.6 Hz, 1H), 6.18 – 6.14 (m, 1H), 5.62 (d, J = 4.6 Hz, 1H), 5.26 – 5.18 (m, 2H), 5.05 – 4.99 (m, 2H), 4.86 – 4.81 (m, 1H), 4.11 (t, J = 5.1 Hz, 1H), 3.76 – 3.71 (m, 2H), 3.17 – 3.08 (m, 1H), 2.73 – 2.65 (m, 1H), 1.91 – 1.83 (m, 1H), 1.76 – 1.70 (m, 1H), 1.69 – 1.61 (m, 1H), 1.59 – 1.49 (m, 2H), 1.44 – 1.22 (m, 7H), 0.95 – 0.92 (m, 6H), 0.91 (s, 9H), 0.78 (dd, J = 14.2, 6.8 Hz, 1H), 0.08 (s, 3H), 0.07 (s, 3H), -0.01 (s, 9H).; **^{13}C NMR** (126 MHz, CDCl$_3$) δ 176.97, 170.96, 164.96, 153.92, 131.24, 131.07, 129.03, 125.98, 121.98, 115.27, 110.14, 108.34, 93.38, 79.59, 73.62, 66.63, 58.33, 35.16, 34.53, 31.40, 31.03, 29.54, 25.88, 25.24, 24.15, 18.69, 18.18, 17.70, -1.27, -4.71, -5.13.; **[α]$^{25}_D$** -3.5 (c = 1.30 in CHCl$_3$); **IR** (film) 3481 (N-H), 2929, 2857, 1734 (C=O), 1688 (C=O), 1649 (C=O), 1455, 1406, 1249, 1195, 1087, 988, 835, 778, 755, 731, 696; **HRMS** Accurate mass (ES$^+$): Found 677.4009, C$_{35}$H$_{61}$N$_2$O$_7$Si$_2$ (M+H) requires 677.4017.

(–)-10d   **(–)-11d**
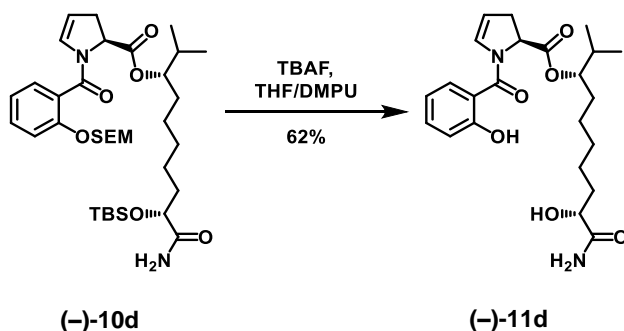
(3S,9R)-10-amino-9-hydroxy-2-methyl-10-oxodecan-3-yl **(S)-1-(2-hydroxybenzoyl)-2,3-dihydro-1H-pyrrole-2-carboxylate (–)-11d.** Following general procedure E, silyl ether **(–)-10d** (18 mg, 0.026 mmol) yielded the title compound as a clear oil (7 mg, 62% yield). **^{1}H NMR** (600 MHz, CDCl$_3$) δ 9.48 (s, 1H), 7.41 – 7.34 (m, 2H), 6.99 (d, J = 7.6 Hz, 1H), 6.91 (t, J = 7.1 Hz, 1H), 6.71 (s, 1H), 6.61 (s, 1H), 5.40 (s, 1H), 5.32 – 5.24 (m, 1H), 5.04 (dd, J = 11.3, 4.7 Hz, 1H), 4.88 (s, 1H), 4.13 – 4.06 (m, 1H), 3.44 (s, 1H), 3.19 – 3.11 (m, 1H), 2.72 (d, J = 17.1 Hz, 1H), 1.89 – 1.76 (m, 2H), 1.71 – 1.61 (m, 4H), 1.52 – 1.37 (m,

5H), 0.91 (d, J = 6.7 Hz, 6H).; ^{13}**C NMR** (151 MHz, CDCl$_3$) δ 177.03, 171.42, 167.41, 157.89, 133.50, 130.86, 128.31, 119.48, 118.03, 117.85, 111.11, 80.29, 71.35, 59.34, 34.26, 31.97, 31.30, 29.84, 28.38, 25.08, 24.60, 18.84, 17.86.; $[\alpha]^{25}_D$ -50.7 (c = 0.71 in CHCl$_3$); **IR** (film) 3338 (br O-H), 2927, 2859, 1729 (C=O), 1664 (C=O), 1594 (C=O), 1459, 1428, 1377, 1294, 1198, 1153, 1110, 1015, 945, 859, 817, 755, 727, 653, 617; **HRMS** Accurate mass (ES$^+$): Found 433.2330, C$_{23}$H$_{33}$N$_2$O$_6$ (M+H) requires 433.2339.
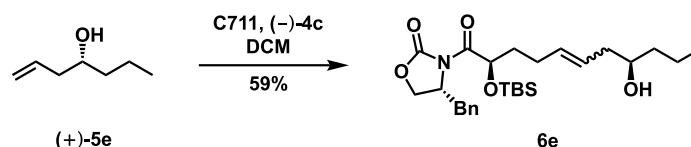
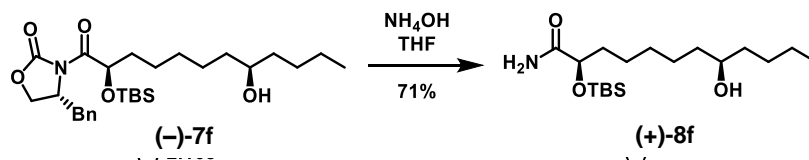**(R)-4-benzyl-3-((2R,8R)-2-((tert-butyldimethylsilyl)oxy)-8-hydroxyundec-5-enoyl)oxazolidin-2-one 6e.** Following general procedure A, homoallylic alcohol **(+)-5e** (460 mg, 3.85 mmol) yielded the title compound as a brown oil (222 mg, 59% yield). ^{1}**H NMR** (400 MHz, CDCl$_3$, mixture of E/Z isomers) δ 7.37 – 7.22 (m, 5H), 5.63 – 5.40 (m, 2H), 5.37 (dd, J = 8.3, 3.4 Hz, 1H), 4.70 – 4.54 (m, 1H), 4.25 – 4.13 (m, 2H), 3.60 (s, 1H), 3.39 (dd, J = 13.2, 3.1 Hz, 1H), 2.68 (dd, J = 13.2, 10.2 Hz, 1H), 2.22 (s, 3H), 2.11 – 1.99 (m, 1H), 1.87 – 1.66 (m, 3H), 1.48 – 1.36 (m, 4H), 0.94 (s, 9H), 0.91 (s, 3H), 0.10 (s, 3H), 0.09 (s, 3H); ^{13}**C NMR** (100 MHz, CDCl$_3$) δ 174.41, 153.20, 135.27, 132.93, 129.54, 129.08, 127.48, 127.24, 70.79, 70.58, 66.65, 55.68, 40.82, 39.00, 37.75, 35.17, 28.53, 25.91, 19.02, 18.42, 14.23, -4.48, -4.96; **IR** (film) 3514 (br O-H), 2954, 2856, 1778 (C=O), 1710 (C=O), 1388, 1348, 1249, 1209, 1108, 1011 ,971, 835, 776, 700; **HRMS** Accurate mass (ES$^+$): Found 490.2985, C$_{27}$H$_{44}$NO$_5$Si (M+H) requires 490.2989.
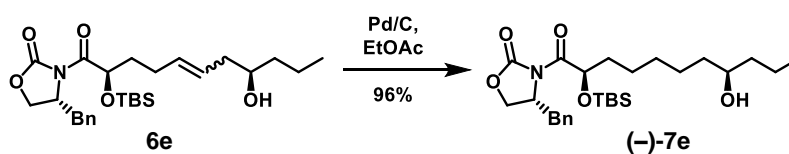
(R)-4-benzyl-3-((2R,8R)-2-((tert-butyldimethylsilyl)oxy)-8-hydroxyundecanoyl)oxazolidin-2-one (–)-7e. Following general procedure B, alkene **6e** (80 mg, 0.16 mmol) yielded the title compound as a clear oil (76 mg, 96% yield). ^{1}**H NMR** (400 MHz, CDCl$_3$) δ 7.41 – 7.20 (m, 5H), 5.40 – 5.32 (m, 1H), 4.62 (ddt, J = 10.1, 6.6, 3.1 Hz, 1H), 4.25 – 4.14 (m, 2H), 3.59 (d, J = 4.2 Hz, 1H), 3.40 (dd, J = 13.2, 3.2 Hz, 1H), 2.69 (dd, J = 13.2, 10.2 Hz, 1H), 1.82 – 1.18 (m, 15H), 0.94 (s, 9H), 0.93 – 0.88 (m, 3H), 0.11 (s, 3H), 0.09 (s,

3H); **¹³C NMR** (100 MHz, CDCl₃) δ 174.51, 153.22, 135.31, 129.53, 129.06, 127.46, 71.71, 71.39, 66.60, 55.67, 39.76, 37.76, 37.43, 35.21, 29.29, 25.90, 25.55, 25.50, 18.91, 18.43, 14.23, -4.54, -5.00; **[α]²⁵_D** -1.7 (c = 0.59 in CHCl₃); **IR** (film) 3572 (br O-H), 2928, 2856, 1778 (C=O), 1710 (C=O), 1389, 1348, 1248, 1210, 1195, 1105, 1006, 976, 835, 776, 700; **HRMS** Accurate mass (ES⁺): Found 492.3145, C₂₇H₄₆NO₅Si (M+H) requires 492.3145.

(–)-7e   (+)-8e

(2R,8R)-2-((tert-butyldimethylsilyl)oxy)-8-hydroxyundecanamide (+)-8e. Following general procedure C, oxazolidinone **(–)-7e** (70 mg, 0.14 mmol) yielded the title compound as a clear oil (29 mg, 62% yield). **¹H NMR** (600 MHz, CDCl₃) δ 6.51 (d, *J* = 4.6 Hz, 1H), 5.96 (d, *J* = 5.1 Hz, 1H), 4.12 (dd, *J* = 5.7, 4.6 Hz, 1H), 3.60 – 3.54 (m, 1H), 1.79 – 1.71 (m, 1H), 1.69 – 1.62 (m, 1H), 1.46 – 1.35 (m, 7H), 1.36 – 1.26 (m, 5H), 0.91 (s, 9H), 0.91 (t, *J* = 6.6 Hz, 3H), 0.09 (s, 3H), 0.07 (s, 3H).; **¹³C NMR** (151 MHz, CDCl₃) δ 177.29, 73.54, 71.69, 39.78, 37.49, 35.18, 29.67, 25.85, 25.58, 24.23, 18.95, 18.13, 14.24, -4.71, -5.13.; **[α]²⁵_D** +57.8 (c = 0.45 in CHCl₃); **IR** (film) 3479 (N-H), 3300 (br O-H), 2928, 2857, 1680 (C=O), 1582, 1463, 1389, 1361, 1339, 1253, 1096, 1005, 835, 777, 668; **HRMS** Accurate mass (ES⁺): Found 332.2613, C₁₇H₃₈NO₃Si (M+H) requires 332.2621.

(+)-8e   (–)-10e
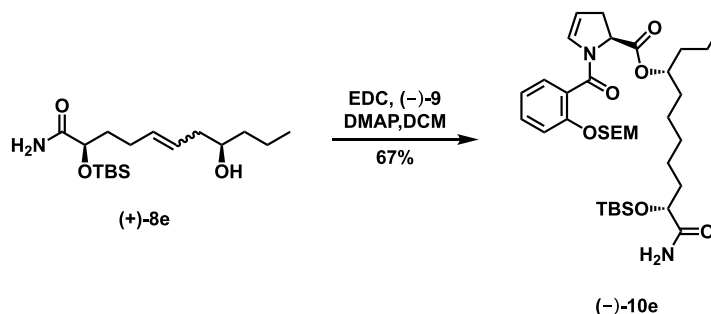
**(4R,10R)-11-amino-10-((tert-butyldimethylsilyl)oxy)-11-oxoundecan-4-yl**   **(S)-1-(2-((2-(trimethylsilyl)ethoxy)methoxy)benzoyl)-2,3-dihydro-1H-pyrrole-2-carboxylate (–)-10e.**

Following general procedure D, alcohol **(+)-8e** (34 mg, 0.103 mmol) yielded the title compound as a clear oil (30 mg, 67% yield). **^{1}H NMR** (600 MHz, CDCl$_3$) δ 7.37 – 7.31 (m, 2H), 7.19 (d, J = 8.3 Hz, 1H), 7.04 (t, J = 7.4 Hz, 1H), 6.53 (dd, J = 15.8, 4.6 Hz, 1H), 6.18 – 6.13 (m, 1H), 5.55 (s, 1H), 5.23 (q, 2H), 5.04 – 4.93 (m, 2H), 4.12 (t, J = 5.3 Hz, 1H), 3.74 (t, J = 8.3 Hz, 2H), 3.17 – 3.06 (m, 2H), 2.71 – 2.61 (m, 1H), 1.79 – 1.62 (m, 3H), 1.61 – 1.54 (m, 3H), 1.54 – 1.46 (m, 1H), 1.43 – 1.27 (m, 7H), 1.24 – 1.10 (m, 1H), 0.96 – 0.92 (m, 2H), 0.93 – 0.88 (m, 11H), 0.08 (s, 3H), 0.07 (s, 3H), -0.01 (s, 9H).; **^{13}C NMR** (151 MHz, CDCl$_3$) δ 176.97, 170.81, 165.00, 153.87, 131.23, 131.06, 129.00, 126.01, 122.00, 115.28, 108.37, 93.38, 75.23, 73.60, 66.64, 58.24, 36.30, 35.14, 34.44, 34.11, 29.50, 25.88, 25.07, 24.13, 18.66, 18.19, 18.15, 14.14, -1.27, -4.69, -5.12.; **[α]^{25}$_D$** -29.5 (c = 0.39 in CHCl$_3$); **IR** (film) 3480 (N-H), 2928, 2857, 1738 (C=O), 1687 (C=O), 1649 (C=O), 1454, 1407, 1249, 1194, 1087, 988, 834, 778, 754, 696; **HRMS** Accurate mass (ES$^+$): Found 677.4020, C$_{35}$H$_{61}$N$_2$O$_7$Si$_2$ (M+H) requires 677.4017.
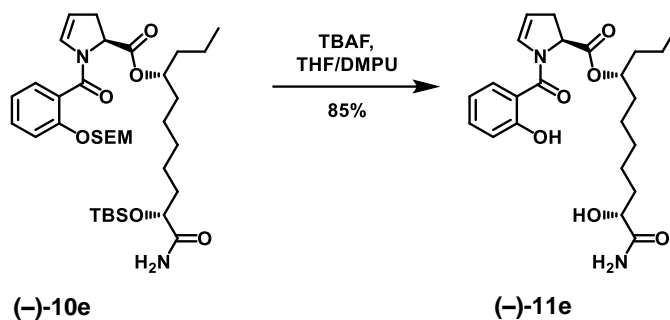
(4R,10R)-11-amino-10-hydroxy-11-oxoundecan-4-yl **(S)-1-(2-hydroxybenzoyl)-2,3-dihydro-1H-pyrrole-2-carboxylate (–)-11e.** Following general procedure E, silyl ether **(–)-10e** (17 mg, 0.025 mmol) yielded the title compound as a clear oil (9.2 mg, 85% yield). **^{1}H NMR** (400 MHz, CDCl$_3$) δ 9.51 (s, 1H), 7.42 – 7.33 (m, 2H), 6.99 (d, J = 8.2 Hz, 1H), 6.94 – 6.87 (m, 1H), 6.71 (s, 1H), 6.61 (s, 1H), 5.41 (s, 1H), 5.30 – 5.26 (m, 1H), 5.09 – 4.97 (m, 2H), 4.14 – 4.05 (m, 1H), 3.46 (s, 1H), 3.20 – 3.07 (m, 1H), 2.70 (d, J = 16.9 Hz, 1H), 1.86 – 1.75 (m, 1H), 1.71 – 1.65 (m, 2H), 1.64 – 1.55 (m, 3H), 1.51 – 1.38 (m, 5H), 1.36 – 1.27 (m, 3H), 0.90 (t, J = 7.3 Hz, 3H).; **^{13}C NMR** (151 MHz, CDCl$_3$) δ 176.97, 171.32, 167.42, 158.02, 133.49, 130.86, 128.32, 119.42, 118.02, 117.78, 111.08, 75.76, 71.42, 64.53, 59.34, 36.70, 34.33, 34.21,

28.35, 24.83, 24.57, 18.85, 14.03.; $[\alpha]^{25}_D$ -72.8 (c = 0.32 in CHCl$_3$); **IR** (film) 3338 (br O-H), 2927, 2859, 1729 (C=O), 1664 (C=O), 1594 (C=O), 1459, 1428, 1377, 1294, 1198, 1153, 1110, 1015, 945, 859, 817, 755, 727, 653, 617; **HRMS** Accurate mass (ES$^+$): Found 433.2329, C$_{23}$H$_{33}$N$_2$O$_6$ (M+H) requires 433.2339.

(+)-5f   6f
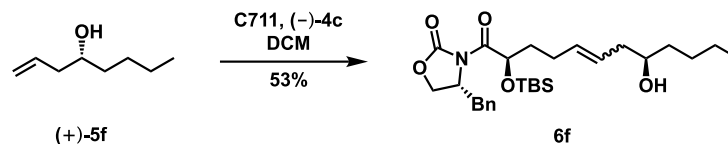
(R)-4-benzyl-3-((2R,8R,E)-2-((tert-butyldimethylsilyl)oxy)-8-hydroxydodec-5-enoyl)oxazolidin-2-one 6f. Following general procedure A, homoallylic alcohol **(+)-5f** (385 mg, 3.0 mmol) yielded the title compound as a brown oil (161 mg, 53% yield). **^{1}H NMR** (400 MHz, CDCl$_3$, mixture of E/Z isomers) 7.33 (d, J = 7.5 Hz, 2H), 7.31 – 7.27 (m, 1H), 7.23 (s, 2H). 5.64 – 5.41 (m, 2H), 5.37 (dd, J = 8.3, 3.4 Hz, 1H), 4.68 – 4.56 (m, 1H), 4.24 – 4.13 (m, 2H), 3.59 (s, 1H), 3.40 (dd, J = 13.2, 2.9 Hz, 1H), 2.68 (dd, J = 13.2, 10.2 Hz, 1H), 2.32 – 2.13 (m, 3H), 2.11 – 2.00 (m, 1H), 1.77 – 1.64 (m, 2H), 1.49 – 1.40 (m, 2H), 1.38 – 1.24 (m, 5H), 0.94 (s, 9H), 0.92 – 0.87 (m, 3H), 0.11 (s, 3H), 0.09 (s, 3H); **^{13}C NMR** (101 MHz, CDCl$_3$) δ 174.35, 153.14, 135.21, 132.79, 129.48, 129.01, 127.42, 127.22, 70.80, 70.72, 66.59, 55.61, 40.75, 37.68, 36.47, 35.12, 28.47, 27.96, 25.85, 22.79, 18.35, 14.16, -4.54, -5.01; **IR** (film) 3514 (br O-H), 2954, 2856, 1778 (C=O), 1710 (C=O), 1389, 1348, 1249, 1209, 1110, 1007 ,971, 836, 777, 700; **HRMS** Accurate mass (ES$^+$): Found 504.31431 (+0.43 ppm), C$_{28}$H$_{46}$NO$_5$Si (M+H$^+$) requires 504.314527.

6f   (–)-7f
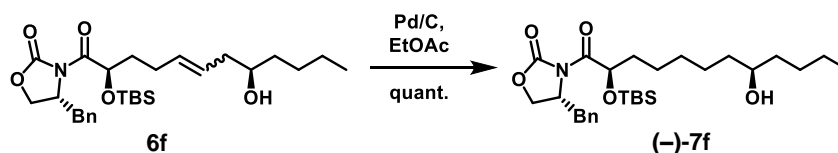
(R)-4-benzyl-3-((2R,8R)-2-((tert-butyldimethylsilyl)oxy)-8-hydroxydodecanoyl)oxazolidin-2-one (–)-7f. Following general procedure B, alkene **6f** (155 mg, 0.31 mmol) yielded the title compound as a clear oil (155 mg, quant.). **^{1}H NMR** (400 MHz, CDCl$_3$) δ 7.42 – 7.19 (m, 5H), 5.36 (dd, J = 8.3, 3.4 Hz, 1H), 4.62 (qd, J = 6.5, 3.1 Hz, 1H), 4.26 – 4.15 (m, 2H), 3.58 (s, 1H), 3.45 – 3.36 (m, 1H), 2.69 (dd, J = 13.2, 10.2 Hz, 1H), 1.75 – 1.59 (m, 4H), 1.55 – 1.19 (m, 15H), 0.97 – 0.92 (m, 9H), 0.90 (ddd, J = 9.6, 4.1, 2.1 Hz, 3H), 0.10 (s, 3H), 0.09 (s, 3H); **^{13}C NMR** (100 MHz, CDCl$_3$) δ 174.40, 153.12, 135.23, 129.43, 128.95,

127.35, 71.78, 71.30, 66.50, 55.56, 37.64, 37.31, 37.18, 35.11, 29.20, 27.83, 25.82, 25.46, 25.42, 22.77, 18.33, 14.11, -4.63, -5.09; $[\alpha]^{25}_D$ -2.3 (c = 0.7 in CHCl$_3$); **IR** (film) 3572 (br O-H), 2927, 2856, 1779 (C=O), 1710 (C=O), 1389, 1348, 1249, 1210, 1195, 1106, 1012, 976, 836, 777, 701; **HRMS** Accurate mass (ES$^+$): Found 506.33011 (+0.13 ppm), C$_{28}$H$_{48}$NO$_5$Si (M+H$^+$) requires 506.330177.

(2R,8R)-2-((tert-butyldimethylsilyl)oxy)-8-hydroxydodecanamide (+)-8f. Following general procedure C, oxazolidinone **(–)-7f** (134 mg, 0.26 mmol) yielded the title compound as a clear oil (65 mg, 71% yield). **^{1}H NMR** (400 MHz, CDCl$_3$) δ 6.50 (s, 1H), 6.38 (s, 1H), 4.09 (t, J = 5.0 Hz, 1H), 3.53 (dd, J = 6.8, 4.2 Hz, 1H), 1.91 – 1.56 (m, 3H), 1.50 – 1.21 (m, 14H), 0.89 (s, 9H), 0.86 (t, J = 10.6 Hz, 3H), 0.07 (s, 3H), 0.06 (s, 3H); **^{13}C NMR** (100 MHz, CDCl$_3$) δ 177.47, 73.47, 71.86, 37.43, 37.23, 35.13, 29.66, 27.93, 25.81, 25.57, 24.20, 22.85, 18.09, 14.18, -4.76, -5.17; $[\alpha]^{25}_D$ +49 (c = 0.49 in CHCl$_3$); **IR** (film) 3479 (N-H), 3290 (br O-H), 2928, 2857, 1681 (C=O), 1581, 1463, 1389, 1361, 1339, 1253, 1097, 1005, 836, 778, 669; **HRMS** Accurate mass (ES$^+$): Found 346.27731 (+1.27 ppm), C$_{18}$H$_{40}$NO$_3$Si (M+H$^+$) requires 346.277747.
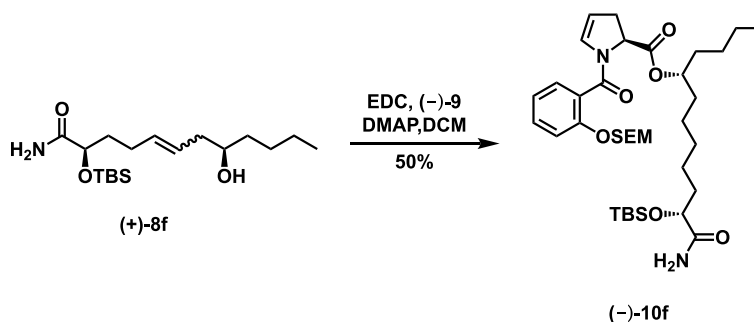
(5R,11R)-12-amino-11-((tert-butyldimethylsilyl)oxy)-12-oxododecan-5-yl **(S)-1-(2-((2-(trimethylsilyl)ethoxy)methoxy)benzoyl)-2,3-dihydro-1H-pyrrole-2-carboxylate (–)-10f.** Following general procedure D, alcohol **(+)-8f** (19 mg, 0.05 mmol) yielded the title compound as a clear oil (19 mg, 50% yield). **^{1}H NMR** (600 MHz, CDCl$_3$) δ 7.35 (dd, J = 12.3, 4.6 Hz, 2H), 7.19 (dd, J = 10.5, 4.9 Hz, 1H), 7.03 (td, J = 7.5, 0.8 Hz, 1H), 6.52 (d, J = 4.0 Hz, 1H), 6.16 (dd, J = 5.3, 3.1 Hz, 1H), 5.53 (d, J = 3.8 Hz, 1H), 5.28 – 5.17 (m, 2H), 5.04 – 4.91 (m, 2H), 4.12 (t, J = 5.1 Hz, 1H), 3.77 – 3.71 (m, 2H), 3.11 (ddt, J =

16.6, 11.6, 2.3 Hz, 1H), 2.71 – 2.62 (m, 1H), 1.78 – 1.73 (m, 1H), 1.74 – 1.69 (m, 2H), 1.68 – 1.62 (m, 1H), 1.61 – 1.52 (m, 3H), 1.44 – 1.21 (m, 9H), 0.94 (m, 2H), 0.91 (s, 9H), 0.88 (t, J = 9.0, 4.3 Hz, 3H), 0.08 (s, 3H), 0.07 (s, 3H), -0.01 (s, 9H); ^{13}C NMR (151 MHz, CDCl$_3$) δ 176.98, 170.81, 165.02, 153.87, 131.24, 131.07, 129.02, 126.01, 122.00, 115.28, 108.38, 93.39, 75.47, 73.60, 66.64, 58.23, 35.13, 34.43, 34.05, 33.78, 29.50, 27.51, 25.88, 25.06, 24.11, 22.71, 18.18, 18.16, 14.13, -1.27, -4.70, -5.12; [α]$^{25}_D$ -24.4 (c = 1.6 in CHCl$_3$); IR (film) 3481 (N-H), 2928, 2858, 1737 (C=O), 1689 (C=O), 1650 (C=O), 1455, 1249, 1194, 1087, 987, 834, 778, 754, 696; HRMS Accurate mass (ES$^+$): Found 713.39935, C$_{36}$H$_{62}$N$_2$ O$_7$Si$_2$Na (M+Na$^+$) requires 713.399329.

(–)-10f (–)-11f
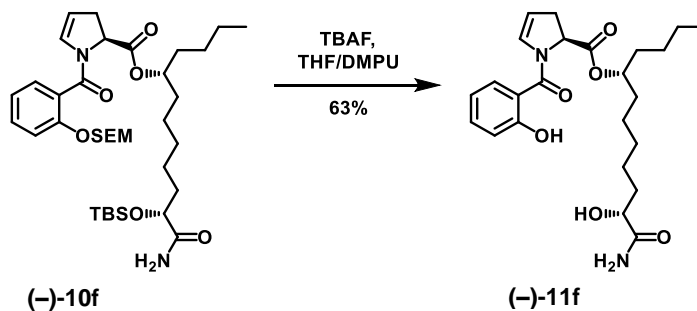
(5R,11R)-12-amino-11-hydroxy-12-oxododecan-5-yl **(S)-1-(2-hydroxybenzoyl)-2,3-dihydro-1H-pyrrole-2-carboxylate (–)-11f.** Following general procedure E; silyl ether **(–)-10f** (12 mg, 0.017 mmol) yielded the title compound as a clear oil (5 mg, 63% yield). ^{1}H NMR (600 MHz, CDCl$_3$) δ 9.51 (s, 1H), 7.35 (dd, J = 12.3, 4.6 Hz, 2H), 6.99 (dd, J = 10.5, 4.9 Hz, 1H), 6.91 (td, J = 7.5, 0.8 Hz, 1H), 6.72 (s, 1H), 6.59 (s, 1H), 5.39 (s, 1H), 5.28 (s, 1H), 5.12 – 4.95 (m, 2H), 4.10 (t, J = 5.1 Hz, 1H), 3.45 – 3.35 (m, 1H), 3.13 (t, J = 16.6 1H), 2.71 – 2.69 (m, 1H), 1.85 – 1.75 (m, 1H) 1.74 – 1.53 (m, 6H), 1.50 – 1.38 (m, 4H), 1.35 – 1.20 (m, 5H), 0.88 (t, J = 9.0, 4.3 Hz, 3H); ^{13}C NMR (151 MHz, CDCl$_3$) δ 176.99, 171.33, 167.43, 158.04, 133.50, 130.86, 128.32, 119.42, 118.03, 117.76, 111.08, 76.01, 71.42, 59.37, 34.33, 34.23, 34.18, 29.84, 28.34, 27.71, 24.84, 24.57, 22.63, 14.09; [α]$^{25}_D$ -44.9 (c = 0.35 in CHCl$_3$); IR (film) 3338 (br O-H), 2922, 2853, 1731 (C=O), 1665 (C=O), 1592 (C=O), 1460, 1430, 1378, 1294, 1196, 1153, 1110, 1017, 946, 857, 817, 755, 721, 656, 617, 500; HRMS Accurate mass (ES$^+$): Found 447.24936 (+0.34 ppm), C$_{24}$H$_{35}$N$_2$O$_6$ (M+H$^+$) requires 447.24951.

C711, (−)-4c
DCM
72%

(+)-5g

6g
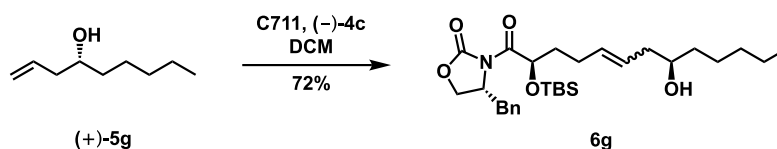
(R)-4-benzyl-3-((2R,8R)-2-((tert-butyldimethylsilyl)oxy)-8-hydroxytridec-5-enoyl)oxazolidin-2-one

6g. Following general procedure A; homoallylic alcohol **(+)-5g** (245 mg, 1.7 mmol) yielded the title compound as a brown oil (126 mg, 72% yield). **¹H NMR** (500 MHz, CDCl₃, mixture of E/Z isomers) δ 7.36 – 7.31 (m, 2H), 7.30 – 7.27 (m, 1H), 7.25 – 7.22 (m, 2H), 5.60 – 5.43 (m, 2H), 5.37 (dd, J = 8.4, 3.4 Hz, 1H), 4.66 – 4.59 (m, 1H), 4.24 – 4.15 (m, 2H), 3.63 – 3.55 (m, 1H), 3.43 – 3.35 (m, 1H), 2.69 (dd, J = 13.3, 10.1 Hz, 1H), 2.31 – 2.15 (m, 3H), 2.10 – 1.99 (m, 1H), 1.82 – 1.67 (m, 2H), 1.49 – 1.39 (m, 3H), 1.38 – 1.23 (m, 5H), 0.94 (s, 9H), 0.89 (t, J = 7.0 Hz, 3H), 0.11 (s, 3H), 0.09 (s, 3H); **¹³C NMR** (126 MHz, CDCl₃) δ 174.46, 153.24, 135.35, 133.04, 129.59, 129.14, 127.55, 127.30, 70.94, 70.85, 66.70, 55.74, 40.87, 37.83, 36.89, 35.24, 32.04, 28.57, 25.95, 25.56, 22.79, 18.46, 14.20, -4.44, -4.91; **IR** (film) 3510 (br O-H), 2928, 2857, 1778 (C=O), 1711 (C=O), 1387, 1348, 1250, 1210, 1109, 1015 ,973, 908, 836, 729, 701; **HRMS** Accurate mass (ES⁺): Found 540.3120, C₂₉H₄₇NO₅SiNa (M+Na) requires 540.3121.

Pd/C,
EtOAc
97%

6g

(−)-7g
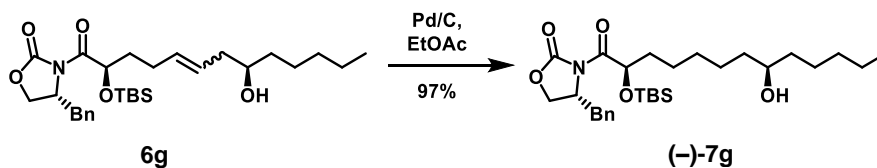
(R)-4-benzyl-3-((2R,8R)-2-((tert-butyldimethylsilyl)oxy)-8-hydroxytridecanoyl)oxazolidin-2-one (−)-7g. Following general procedure B; alkene **6g** (126 mg, 0.243 mmol) yielded the title compound as a clear oil (122 mg, 97% yield). **¹H NMR** (500 MHz, CDCl₃) δ 7.25 – 7.21 (m, 2H), 7.19 – 7.16 (m, 1H), 7.13 (d, 2H), 5.25 (dd, J = 8.3, 3.3 Hz, 1H), 4.54 – 4.48 (m, 1H), 4.12 – 4.05 (m, 2H), 3.46 (s, 1H), 3.29 (dd, J = 13.3, 3.3 Hz, 1H), 2.59 (dd, J = 13.3, 10.1 Hz, 1H), 1.62 – 1.49 (m, 2H), 1.45 – 1.24 (m, 9H), 1.24 – 1.16 (m, 8H), 0.83 (s, 9H), 0.80 – 0.75 (m, 3H), 0.00 (s, 3H), -0.02 (s, 3H).; **¹³C NMR** (126 MHz, CDCl₃) δ 174.59, 153.28, 135.40, 129.60, 129.14, 127.54, 72.11, 71.47, 66.65, 55.74, 37.84, 37.63, 37.50, 35.27, 32.05, 29.35, 25.95, 25.61, 25.58, 25.46, 22.79, 18.49, 14.20, -4.49, -4.95.; **[α]²⁵_D** -7.5 (c = 0.65 in CHCl₃);

IR (film) 3390 (br O-H), 2927, 2856, 1779 (C=O), 1711 (C=O), 1388, 1348, 1250, 1210, 1196, 1107, 1012, 974, 910, 836, 776, 731, 701; **HRMS** Accurate mass (ES$^+$): Found 520.3470, $C_{29}H_{50}NO_5Si$ (M+H) requires 520.3458.
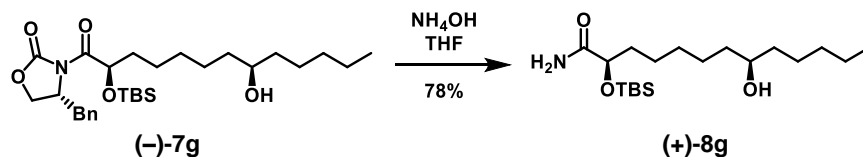
(2R,8R)-2-((tert-butyldimethylsilyl)oxy)-8-hydroxytridecanamide (+)-8g. Following general procedure C; oxazolidinone **(−)-7g** (77 mg, 0.14 mmol) yielded the title compound as a clear oil (42 mg, 78% yield).

^{1}H NMR (400 MHz, CDCl$_3$) δ 6.52 (d, J = 3.5 Hz, 1H), 6.01 (s, 1H), 4.11 (t, J = 5.1 Hz, 1H), 3.55 (s, 1H), 1.97 (s, 1H), 1.82 – 1.51 (m, 3H), 1.49 – 1.19 (m, 15H), 0.91 (s, 9H), 0.87 (t, J = 6.8 Hz, 3H), 0.09 (s, 3H), 0.07 (s, 3H); **^{13}C NMR** (100 MHz, CDCl$_3$) δ 177.31, 73.50, 71.98, 37.54, 37.45, 35.16, 32.03, 29.67, 25.85, 25.59, 25.45, 24.23, 22.77, 18.13, 14.18, -4.71, -5.13; **[α]$^{25}_D$** +28 (c = 2.0 in CHCl$_3$); **IR** (film) 3479 (N-H), 3297 (br O-H), 2928, 2857, 1681 (C=O), 1583, 1463, 1389, 1361, 1339, 1253, 1097, 1005, 835, 778, 669; **HRMS** Accurate mass (ES$^+$): Found 360.2953, $C_{19}H_{42}NO_3Si$ (M+H) requires 360.2934.
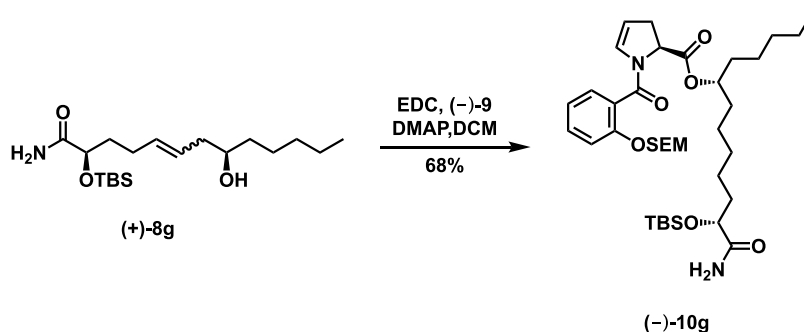
(6R,12R)-13-amino-12-((tert-butyldimethylsilyl)oxy)-13-oxotridecan-6-yl **(S)-1-(2-((2-(trimethylsilyl)ethoxy)methoxy)benzoyl)-2,3-dihydro-1H-pyrrole-2-carboxylate (−)-10g.** Following general procedure D; alcohol **(+)-8g** (25 mg, 0.07 mmol) yielded the title compound as a clear oil (33 mg, 68% yield). **^{1}H NMR** (600 MHz, CDCl$_3$) δ 7.35 (t, J = 7.6 Hz, 2H), 7.20 (d, J = 8.6 Hz, 1H), 7.04 (t, J = 7.5 Hz, 1H), 6.52 (d, J = 4.7 Hz, 1H), 6.18 – 6.14 (m, 1H), 5.50 (d, J = 23.8 Hz, 1H), 5.26 – 5.19 (m, 2H), 5.04 – 4.93 (m, 2H), 4.12 (t, J = 5.1 Hz, 1H), 3.74 (t, J = 8.3 Hz, 2H), 3.15 – 3.08 (m, 1H), 2.70 – 2.63 (m,

1H), 1.79 – 1.72 (m, 1H), 1.69 – 1.61 (m, 2H), 1.60 – 1.51 (m, 4H), 1.44 – 1.26 (m, 12H), 0.96 – 0.93 (m,

2H), 0.91 (s, 9H), 0.87 (t, J = 6.6 Hz, 3H), 0.09 (s, 3H), 0.07 (s, 3H), -0.01 (s, 9H).; **13C NMR** (151 MHz,

CDCl3) δ 176.96, 170.80, 165.00, 153.88, 131.23, 131.08, 129.04, 126.04, 122.00, 115.29, 108.34, 93.39,

75.48, 73.61, 66.64, 58.23, 35.15, 34.43, 34.07, 31.84, 29.52, 25.89, 25.08, 25.04, 24.13, 22.67, 18.19,

18.16, 14.15, -1.26, -4.68, -5.11.; **[α]$^{25}_D$** -38.8 (c = 0.75 in CHCl3); **IR** (film) 3480 (N-H), 2928, 2857, 1734

(C=O), 1683 (C=O), 1463, 1389, 1251, 1189, 1089, 989, 909, 836, 778, 731; **HRMS** Accurate mass (ES$^+$):

Found 705.4357, $C_{37}H_{65}N_2O_7Si_2$ (M+H$^+$) requires 705.4330.

(–)-10g   **(–)-11g**
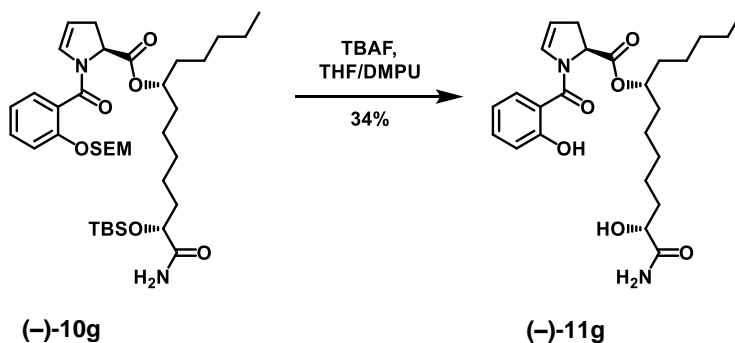
(6R,12R)-13-amino-12-hydroxy-13-oxotridecan-6-yl   **(S)-1-(2-hydroxybenzoyl)-2,3-dihydro-1H-**

pyrrole-2-carboxylate (–)-11g. Following general procedure E; silyl ether **(–)-10g** (18 mg, 0.026 mmol)

yielded the title compound as a clear oil (4 mg, 34% yield). **1H NMR** (600 MHz, CDCl3) δ 9.52 (s, 1H),

7.42 – 7.35 (m, 2H), 6.99 (d, J = 8.3 Hz, 1H), 6.91 (t, J = 7.6 Hz, 1H), 6.72 (s, 1H), 6.57 (s, 1H), 5.28 (s,

1H), 5.01 (dd, J = 11.5, 4.8 Hz, 2H), 4.11 (d, J = 3.7 Hz, 1H), 3.31 (s, 1H), 3.14 (dd, J = 17.1, 11.5 Hz,

1H), 2.70 (d, J = 17.1 Hz, 1H), 1.85 – 1.78 (m, 1H), 1.70 – 1.51 (m, 9H), 1.48 – 1.40 (m, 4H), 1.33 – 1.27

(m, 5H), 0.87 (t, J = 6.5 Hz, 3H).; **13C NMR** (151 MHz, CDCl3) δ 176.85, 171.33, 167.45, 158.08, 133.52,

130.88, 128.32, 119.42, 118.04, 117.74, 111.09, 76.02, 71.42, 59.37, 34.51, 34.34, 34.18, 31.71, 29.85,

28.33, 25.22, 24.84, 24.56, 22.63, 14.10.; **[α]$^{25}_D$** -49.7 (c = 0.41 in CHCl3); **IR** (film) 3339 (br O-H), 2923,

2853, 1730 (C=O), 1665 (C=O), 1594 (C=O), 1461, 1428, 1377, 1294, 1196, 1153, 1111, 1017, 945, 857,

817, 756, 720, 658, 617; **HRMS** Accurate mass (ES$^+$): Found 461.26471, $C_{25}H_{37}N_2O_6$ (M+H$^+$) requires

461.26516.
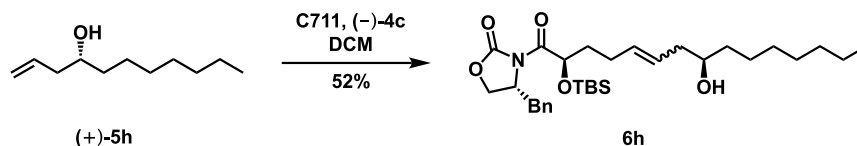
(R)-4-benzyl-3-((2R,8R)-2-((tert-butyldimethylsilyl)oxy)-8-hydroxypentadec-5-enoyl)oxazolidin-2-one 6h. Following general procedure A; homoallylic alcohol **(+)-5h** (527 mg, 3.1 mmol) yielded the title compound as a brown oil (175 mg, 52% yield). **^{1}H NMR** (500 MHz, CDCl$_3$, mixture of E/Z isomers) δ 7.34 (t, J = 7.2 Hz, 2H), 7.29 (d, J = 7.2 Hz, 1H), 7.24 (d, J = 7.0 Hz, 2H), 5.59 – 5.43 (m, 2H), 5.40 – 5.35 (m, 1H), 4.66 – 4.59 (m, 1H), 4.24 – 4.15 (m, 2H), 3.63 – 3.55 (m, 1H), 3.44 – 3.37 (m, 1H), 2.74 – 2.64 (m, 1H), 2.28 – 2.15 (m, 3H), 2.12 – 1.99 (m, 1H), 1.88 – 1.60 (m, 3H), 1.45 (s, 3H), 1.28 (s, 10H), 0.94 (s, 9H), 0.88 (t, J = 6.8 Hz, 3H), 0.11 (s, 3H), 0.09 (s, 3H); **^{13}C NMR** (126 MHz, CDCl$_3$) δ 174.46, 153.24, 135.34, 133.03, 129.58, 129.14, 127.54, 127.29, 70.93, 70.84, 66.69, 55.73, 40.86, 37.82, 36.92, 35.23, 31.97, 29.79, 29.43, 28.56, 25.95, 25.88, 22.79, 18.46, 14.24, -4.45, -4.92; **IR** (film) 3510 (br O-H), 2928, 2855, 1778 (C=O), 1711 (C=O), 1387, 1348, 1250, 1210, 1112, 1012 ,971, 909, 836, 731, 701; **HRMS** Accurate mass (ES$^+$): Found 546.3617, C$_{31}$H$_{52}$NO$_5$Si (M+H$^+$) requires 546.3615.
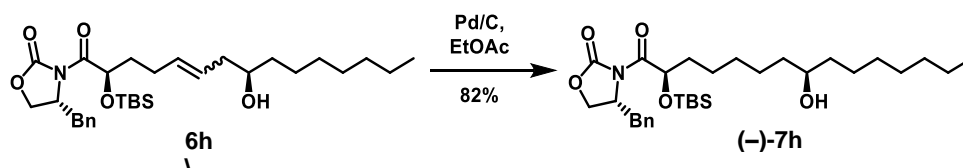
(R)-4-benzyl-3-((2R,8R)-2-((tert-butyldimethylsilyl)oxy)-8-hydroxypentadecanoyl)oxazolidin-2-one (–)-7h. Following general procedure B; alkene **6h** (175 mg, 0.32 mmol) yielded the title compound as a clear oil (144 mg, 82% yield). **^{1}H NMR** (500 MHz, CDCl$_3$) δ 7.37 – 7.31 (m, 2H), 7.31 – 7.27 (m, 1H), 7.25 – 7.22 (m, 2H), 5.36 (dd, J = 8.4, 3.3 Hz, 1H), 4.62 (qd, J = 6.3, 3.1 Hz, 1H), 4.24 – 4.14 (m, 2H), 3.57 (s, 1H), 3.41 (dd, J = 13.2, 3.2 Hz, 1H), 2.70 (dd, J = 13.3, 10.2 Hz, 1H), 1.74 – 1.59 (m, 2H), 1.49 – 1.35 (m, 8H), 1.34 – 1.22 (m, 14H), 0.94 (s, 9H), 0.90 – 0.85 (m, 3H), 0.11 (s, 3H), 0.09 (s, 3H); **^{13}C NMR** (126 MHz, CDCl$_3$) δ 174.58, 153.27, 135.40, 129.60, 129.14, 127.54, 72.12, 71.47, 66.66, 55.75, 37.85, 37.68, 37.51, 35.28, 31.98, 29.82, 29.45, 29.37, 25.96, 25.80, 25.62, 25.60, 22.81, 18.50, 14.26, -4.48, -4.94.; **[α]^{25}$_D$** -7.4 (c = 0.96 in CHCl$_3$); **IR** (film) 3400 (br O-H), 2926, 2855, 1781 (C=O), 1711 (C=O), 1388,

1348, 1249, 1210, 1195, 1106, 1012, 976, 836, 777, 732, 701; **HRMS** Accurate mass (ES⁺): Found 570.3602, $C_{31}H_{53}NO_5SiNa$ (M+Na) requires 570.3791.

(–)-7h → **(+)-8h**
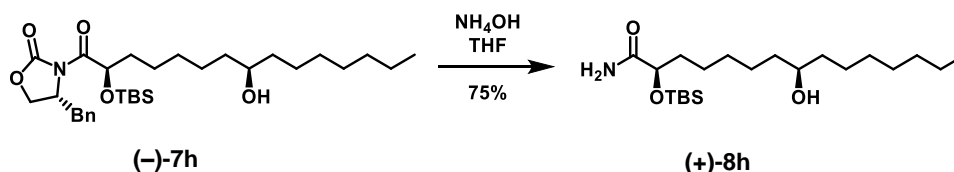
(2R,8R)-2-((tert-butyldimethylsilyl)oxy)-8-hydroxypentadecanamide (+)-8h. Following general procedure C; oxazolidinone **(–)-7h** (144 mg, 0.26 mmol) yielded the title compound as a clear oil (77 mg, 75% yield). **¹H NMR** (400 MHz, CDCl₃) δ 6.52 (d, J = 4.1 Hz, 1H), 5.99 (d, J = 3.9 Hz, 1H), 4.12 (s, 1H), 3.55 (s, 1H), 1.73 (s, 4H), 1.33 (d, J = 58.3 Hz, 19H), 0.91 (s, 9H), 0.86 (s, 3H), 0.09 (s, 3H), 0.07 (s, 3H); ¹³C NMR (126 MHz, CDCl₃) δ 177.27, 73.55, 71.99, 37.61, 37.49, 35.20, 31.95, 29.80, 29.69, 29.41, 25.86, 25.79, 25.60, 24.26, 22.77, 18.13, 14.21, -4.71, -5.12.; $[\alpha]^{25}_D$ +10.8 (c = 0.84 in CHCl₃); **IR** (film) 3479 (N-H), 3001 (br O-H), 2926, 2855, 1682 (C=O), 1583, 1463, 1389, 1361, 1339, 1253, 1098, 1005, 835, 778, 772, 668; **HRMS** Accurate mass (ES⁺): Found 388.3261, $C_{21}H_{46}NO_3Si$ (M+H⁺) requires 388.3247.

(+)-8h → **(–)-10h**
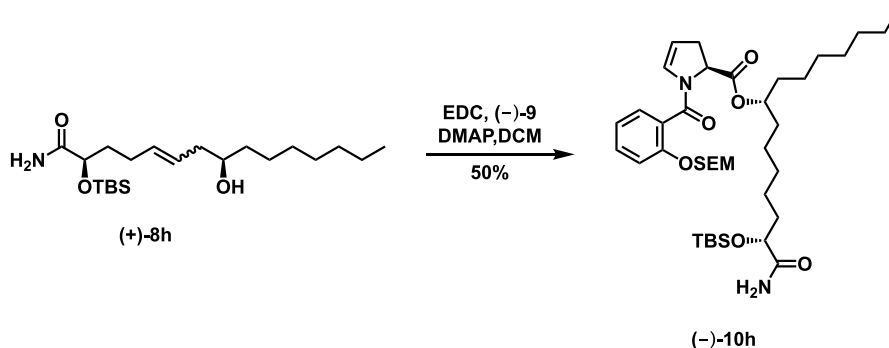
(2R,8R)-1-amino-2-((tert-butyldimethylsilyl)oxy)-1-oxopentadecan-8-yl **(S)-1-(2-((2-(trimethylsilyl)ethoxy)methoxy)benzoyl)-2,3-dihydro-1H-pyrrole-2-carboxylate (–)-10h.** Following general procedure D; alcohol **(+)-8h** (18 mg, 0.046 mmol) yielded the title compound as a clear oil (17 mg, 50% yield). **¹H NMR** (400 MHz, CDCl₃) δ 7.39 – 7.32 (m, 2H), 7.22 – 7.17 (m, 1H), 7.03 (td, J = 7.5, 0.8 Hz, 1H), 6.53 (d, J = 4.3 Hz, 1H), 6.14 (t, J = 4.2 Hz, 1H), 5.55 (d, J = 4.2 Hz, 1H), 5.22 (q, J = 7.1 Hz, 2H), 5.05 – 4.91 (m, 3H), 4.12 (t, J = 5.1 Hz, 1H), 3.78 – 3.71 (m, 2H), 3.12 (ddt, J = 16.6, 11.6, 2.3 Hz, 1H), 2.71 – 2.62 (m, 1H), 1.80 – 1.70 (m, 1H), 1.72 – 1.45 (m, 7H), 1.39 – 1.19 (m, 19H), 0.91 (m, 12H),

0.86 (t, 3H), 0.08 (d, J = 4.7 Hz, 6H), -0.02 (s, 9H); ^{13}**C NMR** (151 MHz, CDCl$_3$) δ 176.95, 170.80, 164.99, 153.88, 131.23, 131.09, 129.04, 126.04, 122.00, 115.29, 108.33, 93.40, 75.49, 73.61, 66.64, 58.23, 35.15, 34.43, 34.12, 34.06, 31.94, 29.84, 29.63, 29.52, 29.33, 25.89, 25.39, 25.07, 24.13, 22.77, 18.19, 18.16, 14.23, -1.26, -4.68, -5.12; **[α]^{25}$_D$** -8.3 (c = 0.30 in CHCl$_3$); **IR** (film) 3343 (N-H), 2927, 2857, 1734 (C=O), 1645 (C=O), 1489, 1455, 1409, 1249, 1162, 1089, 983, 914, 834, 755, 731, 602; **HRMS** Accurate mass (ES$^+$): Found 755.4483, C$_{39}$H$_{68}$N$_2$O$_7$Si$_2$Na (M+Na) requires 744.4463.

(–)-10h   **(–)-11h**
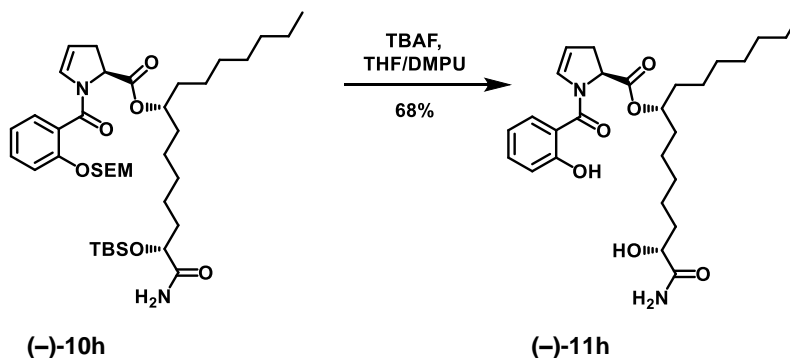
(2R,8R)-1-amino-2-hydroxy-1-oxopentadecan-8-yl   **(S)-1-(2-hydroxybenzoyl)-2,3-dihydro-1H-pyrrole-2-carboxylate (–)-11h.** Following general procedure E; silyl ether **(–)-10h** (18 mg, 0.024 mmol) yielded the title compound as a clear oil (8 mg, 68% yield). ^{1}**H NMR** (400 MHz, CDCl$_3$) δ 9.52 (s, 1H), 7.42 – 7.32 (m, 2H), 6.98 (d, J = 8.2 Hz, 1H), 6.90 (t, J = 7.5 Hz, 1H), 6.71 (s, 1H), 6.62 (s, 1H), 5.42 (s, 1H), 5.30 – 5.26 (m, 1H), 5.01 (dd, J = 11.4, 4.8 Hz, 2H), 4.13 – 4.05 (m, 1H), 3.48 (q, J = 7.0 Hz, 1H), 3.20 – 3.07 (m, 1H), 2.69 (d, J = 16.9 Hz, 1H), 1.85 – 1.75 (m, 1H), 1.73 – 1.65 (m, 2H), 1.62 – 1.52 (m, 3H), 1.49 – 1.36 (m, 4H), 1.32 – 1.21 (m, 12H), 0.87 (t, J = 6.8 Hz, 3H).; ^{13}**C NMR** (151 MHz, CDCl$_3$) δ 176.98, 171.29, 167.42, 158.04, 133.48, 130.86, 128.31, 119.40, 118.02, 117.76, 111.05, 76.02, 71.42, 59.36, 34.54, 34.34, 34.18, 31.89, 29.84, 29.52, 29.29, 28.37, 25.56, 24.86, 24.59, 22.76, 14.23.; **[α]^{25}$_D$** -47.3 (c = 0.82 in CHCl$_3$); **IR** (film) 3326 (br O-H), 2921, 2859, 1741 (C=O), 1665 (C=O), 1597 (C=O), 1459, 1437, 1201, 1105, 1098, 754, 722, 619; **HRMS** Accurate mass (ES$^+$): Found 489.2959, C$_{27}$H$_{41}$N$_2$O$_6$ (M+H$^+$) requires 489.2964.
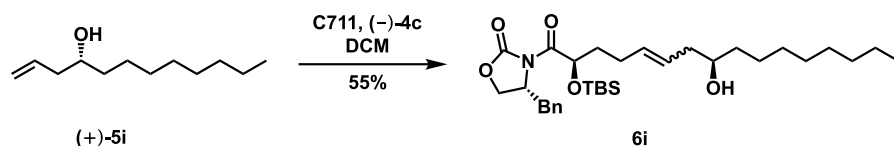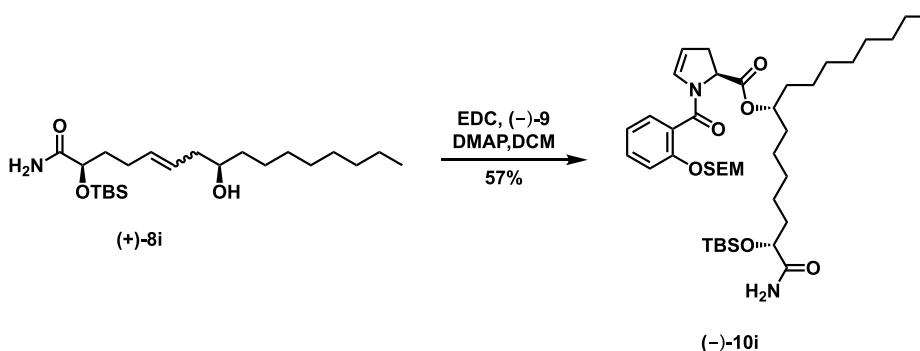
(R)-4-benzyl-3-((2R,8R,E)-2-((tert-butyldimethylsilyl)oxy)-8-hydroxyhexadec-5-enoyl)oxazolidin-2-one 6i. Following general procedure A, homoallylic alcohol **(+)-5i** (500 mg, 2.7 mmol) yielded the title compound as a brown oil (167 mg, 55% yield). ^{1}**H NMR** (400 MHz, CDCl$_3$, mixture of E/Z isomers) δ 7.37 – 7.27 (m, 3H), 7.22 (d, J = 9.1 Hz, 2H), 5.51 (ddd, J = 21.2, 15.1, 8.5 Hz, 2H), 5.37 (dd, J = 8.2, 3.4 Hz, 1H), 4.67 – 4.57 (m, 1H), 4.24 – 4.13 (m, 2H), 3.59 (d, J = 3.9 Hz, 1H), 3.40 (dd, J = 13.3, 3.1 Hz, 1H), 2.68 (dd, J = 13.3, 10.2 Hz, 1H), 2.28 – 2.17 (m, 3H), 2.10 – 1.98 (m, 1H), 1.69 (ddd, J = 29.0, 14.8, 8.0 Hz, 4H), 1.43 (s, 3H), 1.33 – 1.21 (m, 10H), 0.96 – 0.93 (m, 9H), 0.88 (dd, J = 12.0, 5.5 Hz, 3H), 0.11 (s, 3H), 0.09 (s, 3H); ^{13}**C NMR** (126 MHz, CDCl$_3$) δ 174.46, 153.24, 135.35, 133.04, 129.59, 129.14, 127.55, 127.30, 70.94, 70.85, 66.70, 55.74, 40.87, 37.83, 36.94, 35.24, 32.03, 29.85, 29.74, 29.43, 28.57, 25.96, 25.89, 22.82, 18.46, 14.26, -4.44, -4.91; **IR** (film) 3510 (br O-H), 2926, 2854, 1779 (C=O), 1711 (C=O), 1388, 1348, 1250, 1210, 1113, 1010, 971, 908, 777, 701; **HRMS** Accurate mass (ES$^+$): Found 560.3800, C$_{32}$H$_{54}$NO$_5$Si (M+H$^+$) requires 560.3797.
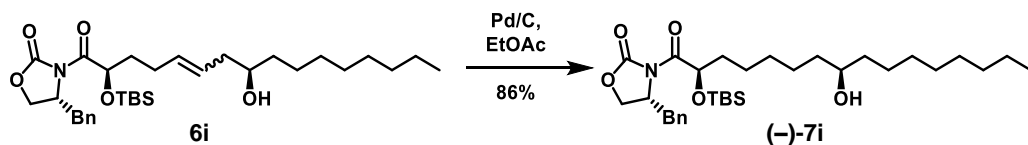
(R)-4-benzyl-3-((2R,8R)-2-((tert-butyldimethylsilyl)oxy)-8-hydroxyhexadecanoyl)oxazolidin-2-one (–)-7i. Following general procedure B, alkene **6i** (166 mg, 0.30 mmol) yielded the title compound as a clear oil (145 mg, 86% yield). ^{1}**H NMR** 500 MHz, CDCl$_3$) δ 7.37 – 7.31 (m, 2H), 7.30 – 7.27 (m, 1H), 7.25 – 7.21 (m, 2H), 5.36 (dd, J = 8.3, 3.3 Hz, 1H), 4.62 (qd, J = 6.5, 3.1 Hz, 1H), 4.25 – 4.14 (m, 2H), 3.57 (s, 1H), 3.40 (dd, J = 13.3, 3.2 Hz, 1H), 2.73 – 2.67 (m, 1H), 1.76 – 1.57 (m, 3H), 1.54 – 1.35 (m, 8H), 1.35 – 1.23 (m, J = 20.4, 13.9 Hz, 14H), 0.94 – 0.92 (m, 9H), 0.88 (t, J = 6.9 Hz, 3H), 0.11 (s, J = 2.7 Hz, 3H), 0.09 (s, J = 2.1 Hz, 3H); ^{13}**C NMR** (126 MHz, CDCl$_3$) δ 174.58, 153.27, 135.39, 129.59, 129.14, 127.53, 72.11, 71.46, 66.65, 55.74, 37.84, 37.68, 37.51, 35.28, 32.03, 29.86, 29.74, 29.43, 29.36, 25.96, 25.80,

25.61, 25.59, 22.82, 18.49, 14.26, -4.49, -4.95; $[\alpha]^{25}_D$ -8.1 (c = 1.1 in CHCl$_3$); **IR** (film) 3390 (br O-H), 2926, 2855, 1779 (C=O), 1711 (C=O), 1388, 1348, 1249, 1210, 1196, 1107, 1012, 909, 836, 777, 731, 701; **HRMS** Accurate mass (ES$^+$): Found 584.3755, C$_{32}$H$_{55}$NO$_5$SiNa (M+Na$^+$) requires 584.3747.
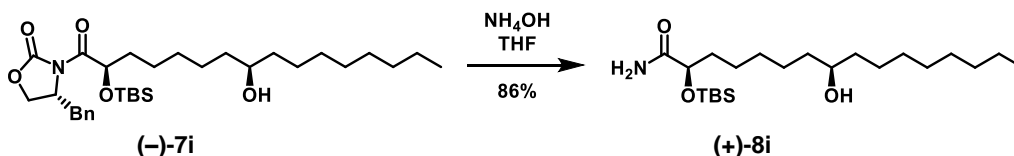
(2R,8R)-2-((tert-butyldimethylsilyl)oxy)-8-hydroxyhexadecanamide **(+)-8i.** Following general procedure C, oxazolidinone **(–)-7i** (93 mg, 0.17 mmol) yielded the title compound as a clear oil (57 mg, 86% yield). **^{1}H NMR** (400 MHz, CDCl$_3$) δ 6.55 (s, 1H), 5.57 (s, 1H), 4.13 (t, J = 12.1, 6.6 Hz, 1H), 3.57 (s, 1H), 1.83 – 1.63 (m, 4H), 1.50 – 1.18 (m, 21H), 0.93 (s, 9H), 0.88 (t, J = 6.8 Hz, 3H), 0.10 (s, 3H), 0.09 (s, 3H); **^{13}C NMR** (100 MHz, CDCl$_3$) δ 177.40, 73.46, 71.95, 37.58, 37.45, 35.15, 31.99, 29.83, 29.71, 29.68, 29.40, 25.83, 25.78, 25.60, 24.23, 22.78, 18.11, 14.24, -4.73, -5.14; $[\alpha]^{25}_D$ +18.7 (c = 1.1 in CHCl$_3$); **IR** (film) 3479 (N-H), 3295 (br O-H), 2926, 2855, 1681 (C=O), 1463, 1389, 1251, 1079, 1005, 835, 778, 668; **HRMS** Accurate mass (ES$^+$): Found 402.3414, C$_{22}$H$_{48}$NO$_3$Si (M+H$^+$) requires 402.3403.

(2R,8R)-1-amino-2-((tert-butyldimethylsilyl)oxy)-1-oxohexadecan-8-yl **(S)-1-(2-((2-(trimethylsilyl)ethoxy)methoxy)benzoyl)-2,3-dihydro-1H-pyrrole-2-carboxylate** **(–)-10i.** Following general procedure D, alcohol **(+)-8i** (30 mg, 0.07 mmol) yielded the title compound as a clear oil (32 mg, 57% yield). **^{1}H NMR** (600 MHz, CDCl$_3$) δ 7.35 (dd, J = 12.1, 4.6 Hz, 2H), 7.21 – 7.18 (m, 1H), 7.03 (td, J = 7.5, 0.9 Hz, 1H), 6.51 (d, J = 4.3 Hz, 1H), 6.16 (dt, J = 4.2, 2.1 Hz, 1H), 5.57 (s, 1H), 5.25 – 5.19 (m,

2H), 5.03 – 4.93 (m, 3H), 4.12 (t, J = 5.1 Hz, 1H), 3.76 – 3.72 (m, 2H), 3.11 (ddt, J = 16.6, 11.6, 2.3 Hz, 1H), 2.70 – 2.62 (m, 1H), 1.79 – 1.71 (m, 3H), 1.69 – 1.61 (m, 1H), 1.61 – 1.49 (m, 4H), 1.44 – 1.17 (m, J = 81.1 Hz, 21H), 0.95 – 0.90 (m, 11H), 0.86 (t, J = 7.0 Hz, 3H), 0.08 (s, 2H), 0.07 (s, 2H), -0.02 (s, 6H); ^{13}C NMR (151 MHz, CDCl$_3$) δ 176.99, 170.79, 165.00, 153.86, 131.23, 131.07, 129.03, 126.01, 121.99, 115.28, 108.35, 93.38, 75.49, 73.60, 66.63, 58.22, 35.13, 34.41, 34.11, 34.05, 31.98, 29.66, 29.62, 29.50, 29.37, 25.88, 25.37, 25.06, 24.12, 22.78, 18.17, 18.15, 14.23, -1.27, -4.70, -5.13; $[\alpha]^{25}_{D}$ -32.7 (c = 1.57 in CHCl$_3$); IR (film) 3481 (N-H), 2927, 2856, 1741 (C=O), 1689 (C=O), 1455, 1406, 1250, 1194, 1087, 989, 835, 777, 731; HRMS Accurate mass (ES$^+$): Found 747.4781, C$_{40}$H$_{71}$N$_2$O$_7$Si$_2$ (M+H$^+$) requires 747.4800.
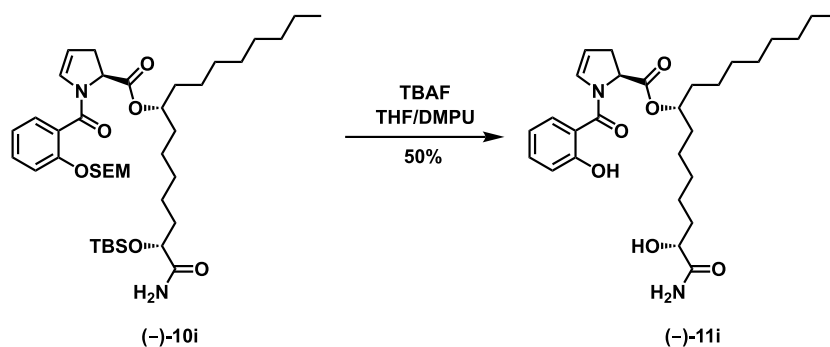
(2R,8R)-1-amino-2-hydroxy-1-oxohexadecan-8-yl (S)-1-(2-hydroxybenzoyl)-2,3-dihydro-1H-pyrrole-2-carboxylate (–)-11i. Following general procedure E; silyl ether (–)-10i (16 mg, 0.020 mmol) yielded the title compound as a clear oil (5 mg, 50% yield). ^{1}H NMR (400 MHz, CDCl$_3$) δ 9.52 (s, 1H), 7.38 (t, J = 9.0 Hz, 2H), 6.99 (d, J = 8.1 Hz, 1H), 6.91 (t, J = 7.5 Hz, 1H), 6.72 (s, 1H), 6.60 (s, 1H), 5.36 (s, 1H), 5.28 (d, J = 4.0 Hz, 1H), 5.01 (dd, J = 11.3, 4.7 Hz, 2H), 4.10 (s, 1H), 3.40 (s, 1H), 3.19 – 3.08 (m, 1H), 2.75 – 2.64 (m, J = 16.9 Hz, 1H), 1.86 – 1.74 (m, 1H), 1.72 – 1.50 (m, 7H), 1.42 (s, 5H), 1.30 – 1.19 (m, J = 3.2 Hz, 11H), 0.87 (t, J = 6.8 Hz, 3H); ^{13}C NMR (151 MHz, CDCl$_3$) δ 176.89, 171.32, 167.43, 158.04, 133.50, 130.86, 128.31, 119.42, 118.04, 117.75, 111.08, 76.04, 71.42, 59.37, 34.56, 34.34, 34.19, 31.98, 29.84, 29.59, 29.56, 29.34, 28.34, 25.57, 24.85, 24.57, 22.80, 14.25; $[\alpha]^{25}_{D}$ -30.6 (c = 0.32 in CHCl$_3$); IR (film) 3339 (br O-H), 2923, 2854, 1737 (C=O), 1664 (C=O), 1592 (C=O), 1459, 1430, 1376, 1294, 1196, 1153, 1098, 1017, 945, 858, 817, 755, 721, 654, 616; HRMS Accurate mass (ES$^+$): Found 503.3134, C$_{28}$H$_{43}$N$_2$O$_6$ (M+H$^+$) requires 503.3121.
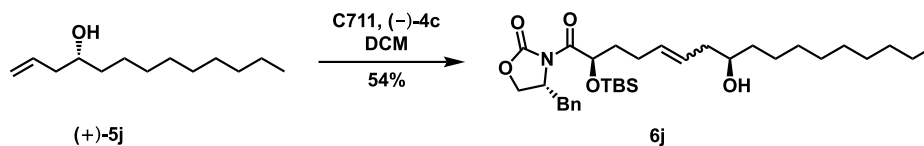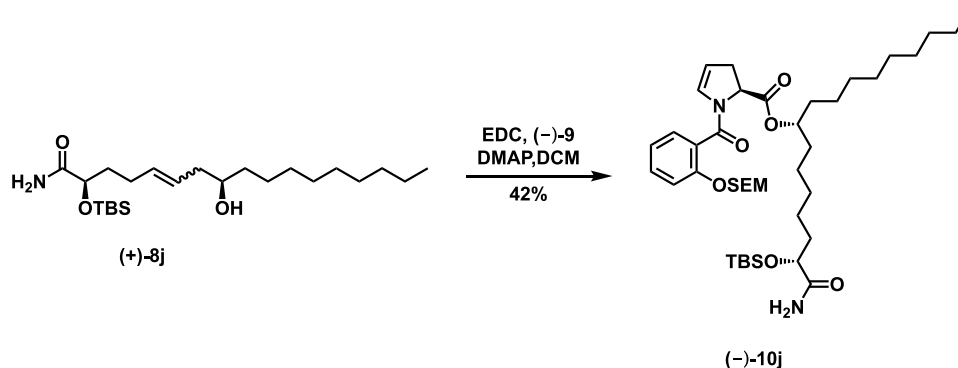
(R)-4-benzyl-3-((2R,8R)-2-((tert-butyldimethylsilyl)oxy)-8-hydroxyheptadec-5-enoyl)oxazolidin-2-one 6j. Following general procedure A; homoallylic alcohol **(+)-5j** (713 mg, 3.6 mmol) yielded the title compound as a brown oil (222 mg, 54% yield). **^{1}H NMR** (500 MHz, CDCl$_3$, mixture of E/Z isomers) δ 7.34 (dd, J = 9.9, 4.5 Hz, 2H), 7.30 – 7.27 (m, J = 7.9, 1.9 Hz, 1H), 7.25 – 7.22 (m, 2H), 5.61 – 5.41 (m, 2H), 5.37 (dt, J = 12.4, 4.8 Hz, 1H), 4.65 – 4.58 (m, 1H), 4.25 – 4.15 (m, 2H), 3.64 – 3.54 (m, 1H), 3.40 (dt, J = 13.2, 3.5 Hz, 1H), 2.74 – 2.63 (m, 1H), 2.30 – 2.14 (m, 3H), 2.08 – 2.01 (m, 1H), 1.80-1.64 (m, 3H), 1.47 – 1.39 (m, 3H), 1.33 – 1.22 (m, 13H), 0.94 (s, 9H), 0.87 (t, J = 7.0 Hz, 3H), 0.11 (s, 3H), 0.09 (s, 3H); **^{13}C NMR** (126 MHz, CDCl$_3$) δ 174.45, 153.23, 135.34, 133.01, 129.58, 129.13, 127.53, 127.30, 70.93, 70.84, 66.68, 55.73, 40.85, 37.82, 36.93, 35.23, 32.03, 29.83, 29.77, 29.71, 29.46, 28.56, 25.94, 25.88, 22.81, 18.45, 14.25, -4.45, -4.92; **IR** (film) 3510 (br O-H), 2925, 2854, 1779 (C=O), 1711 (C=O), 1388, 1348, 1250, 1210, 1115, 971, 908, 836, 777, 700; **HRMS** Accurate mass (ES$^+$): Found 596.3749, C$_{33}$H$_{55}$NO$_5$SiNa (M+Na$^+$) requires 596.3747.
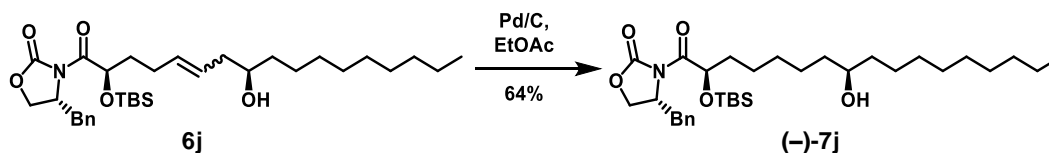
(R)-4-benzyl-3-((2R,8R)-2-((tert-butyldimethylsilyl)oxy)-8-hydroxyheptadecanoyl)oxazolidin-2-one (−)-7j. Following general procedure B; alkene **6j** (220 mg, 0.38 mmol) yielded the title compound as a brown oil (140 mg, 64% yield). **^{1}H NMR** (500 MHz, CDCl$_3$) δ 7.36 – 7.31 (m, 2H), 7.30 – 7.27 (m, 1H), 7.25 – 7.22 (m, 2H), 5.39 – 5.33 (m, 1H), 4.62 (qd, J = 6.3, 3.0 Hz, 1H), 4.24 – 4.14 (m, 2H), 3.60 – 3.54 (m, 1H), 3.40 (dd, J = 13.3, 3.2 Hz, 1H), 2.70 (dd, J = 13.3, 10.1 Hz, 1H), 1.74 – 1.58 (m, 2H), 1.53 – 1.35 (m, 8H), 1.33 – 1.23 (m, 16H), 0.93 (s, 9H), 0.87 (t, J = 7.0 Hz, 3H), 0.11 (s, J = 3.2 Hz, 3H), 0.09 (s, J = 6.9 Hz, 3H); **^{13}C NMR** (126 MHz, CDCl$_3$) δ 174.56, 153.25, 135.37, 129.57, 129.11, 127.50, 72.07, 71.44, 66.63, 55.72, 37.81, 37.65, 37.47, 35.25, 32.02, 29.84, 29.77, 29.70, 29.45, 29.34, 25.94, 25.78, 25.59,

25.56, 22.80, 18.46, 14.25, -4.51, -4.97; **[α]^{25}$_D$** -4.2 (c = 1.1 in CHCl$_3$); **IR** (film) 3390 (br O-H), 2926,

2854, 1780 (C=O), 1711 (C=O), 1388, 1348, 1249, 1210, 1195, 1106, 1012, 976, 909, 836, 776, 731, 701;

HRMS Accurate mass (ES$^+$): Found 598.3904, C$_{33}$H$_{57}$NO$_5$SiNa (M+Na$^+$) requires 598.3909.

(−)-7j → **(+)-8j**
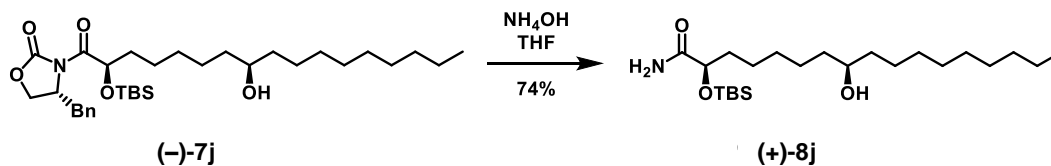
(2R,8R)-2-((tert-butyldimethylsilyl)oxy)-8-hydroxyheptadecanamide **(+)-8j.** Following general

procedure C; oxazolidinone **(−)-7j** (140 mg, 0.24 mmol) yielded the title compound as a clear oil (74 mg,

74% yield). **^{1}H NMR** (400 MHz, CDCl$_3$) δ 6.56 − 6.45 (m, J = 4.1 Hz, 1H), 6.31 (d, J = 3.8 Hz, 1H), 4.09

(t, J = 5.1 Hz, 1H), 3.53 (d, J = 2.9 Hz, 1H), 1.79 − 1.55 (m, 4H), 1.46 − 1.32 (m, 9H), 1.32 − 1.19 (m, 14H),

0.90 (s, 9H), 0.85 (t, J = 6.8 Hz, 3H), 0.07 (s, 3H), 0.06 (s, 3H); **^{13}C NMR** (100 MHz, CDCl$_3$) δ 177.45,

73.46, 71.90, 37.56, 37.43, 35.13, 31.99, 29.82, 29.74, 29.67, 29.42, 25.82, 25.77, 25.57, 24.21, 22.77,

18.09, 14.21, -4.75, -5.16.; **[α]^{25}$_D$** +13.6 (c = 0.56 in CHCl$_3$); **IR** (film) 3479 (N-H), 3300 (br O-H), 2953,

2854, 1682 (C=O), 1583, 1463, 1389, 1361, 1253, 1100, 1005, 836, 778, 667; **HRMS** Accurate mass (ES$^+$):

Found 416.3552, C$_{23}$H$_{50}$NO$_3$Si (M+H$^+$) requires 416.3560.

(+)-8j → **(−)-10j**

(2R,8R)-1-amino-2-((tert-butyldimethylsilyl)oxy)-1-oxoheptadecan-8-yl **(S)-1-(2-((2-(trimethylsilyl)ethoxy)methoxy)benzoyl)-2,3-dihydro-1H-pyrrole-2-carboxylate** **(−)-10j.** Following

general procedure D; alcohol **(+)-8j** (36 mg, 0.09 mmol) yielded the title compound as a clear oil (29 mg,

42% yield). **^{1}H NMR** (400 MHz, CDCl$_3$)) δ 7.35 (t, J = 7.4 Hz, 2H), 7.19 (d, J = 8.9 Hz, 1H), 7.03 (t, J =

7.5 Hz, 1H), 6.53 (d, J = 4.3 Hz, 1H), 6.16 (d, J = 4.3 Hz, 1H), 5.57 (s, 1H), 5.22 (q, J = 7.1 Hz, 2H), 5.06

– 4.89 (m, 3H), 4.12 (t, J = 5.0 Hz, 1H), 3.79 – 3.68 (m, 2H), 3.19 – 3.06 (m, 1H), 2.72 – 2.61 (m, 1H), 1.73 (m, 4H), 1.65 (m, 1H), 1.55 (m, 4H), 1.24 (m, 19H), 0.91 (s, 9H), 0.86 (t, J = 6.8 Hz, 3H), 0.08 (s, 3H), 0.07 (s, 3H), 0.00 – -0.03 (m, 9H) ; **^{13}C NMR** (100 MHz, CDCl$_3$) δ 177.05, 170.77, 164.99, 153.82, 131.22, 131.03, 129.00, 125.94, 121.97, 115.22, 108.39, 93.34, 75.49, 73.55, 66.62, 58.20, 35.11, 34.41, 34.10, 34.04, 32.01, 29.66, 29.49, 29.42, 25.87, 25.37, 25.05, 24.11, 22.80, 18.16, 14.24, -1.27, -4.70, -5.14; **[α]$^{25}_D$** -31.0 (c = 1.3 in CHCl$_3$); **IR** (film) 3480 (N-H), 2926, 2855, 1738 (C=O), 1690 (C=O), 1455, 1406, 1249, 1194, 1087, 988, 939, 835, 778, 754, 697; **HRMS** Accurate mass (ES$^+$): Found 761.4991, C$_{41}$H$_{73}$N$_2$O$_7$Si$_2$ (M+H$^+$) requires 761.4956.

(–)-10j   (–)-11j
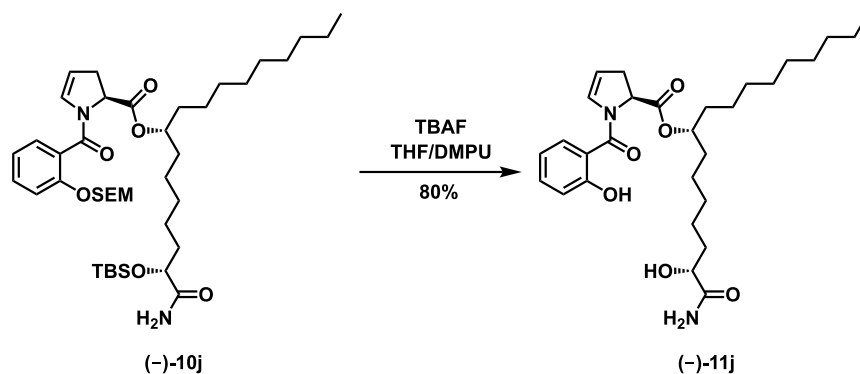
(2R,8R)-1-amino-2-hydroxy-1-oxoheptadecan-8-yl   **(S)-1-(2-hydroxybenzoyl)-2,3-dihydro-1H-pyrrole-2-carboxylate (–)-11j.** Following general procedure E; silyl ether **(–)-10j** (13 mg, 0.017 mmol) yielded the title compound as a clear oil (7 mg, 80% yield). **^{1}H NMR** (400 MHz, CDCl$_3$) δ 7.41 – 7.34 (m, 1H), 6.99 (d, J = 8.1 Hz, 1H), 6.91 (t, J = 7.5 Hz, 1H), 6.71 (s, 1H), 6.63 (s, 1H), 5.53 (s, 1H), 5.30 – 5.26 (m, 1H), 5.01 (dd, J = 11.3, 4.7 Hz, 2H), 4.10 (dd, J = 7.9, 3.6 Hz, 1H), 3.19 – 3.08 (m, 1H), 2.70 (d, J = 17.3 Hz, 1H), 1.86 – 1.75 (m, 1H), 1.68 – 1.52 (m, 6H), 1.48 – 1.38 (m, 5H), 1.31 – 1.19 (m, 17H), 0.88 (t, J = 6.8 Hz, 3H); **^{13}C NMR** (151 MHz, CDCl$_3$) δ 177.02, 171.16, 167.27, 157.83, 133.32, 130.73, 128.19, 119.27, 117.87, 117.70, 110.89, 75.90, 71.29, 59.21, 34.40, 34.18, 34.04, 33.56, 31.88, 29.70, 29.50, 29.42, 29.28, 28.24, 25.42, 24.72, 24.46, 22.67, 14.11; **[α]$^{25}_D$** -28.1 (c = 0.32 in CHCl$_3$); **IR** (film) 3338 (br O-H), 2922, 2853, 1734 (C=O), 1662 (C=O), 1593 (C=O), 1458, 1431, 1376, 1294, 1196, 1153, 1098, 1017, 945, 858, 817, 756, 721, 654, 616; **HRMS** Accurate mass (ES$^+$): Found 517.3276, C$_{29}$H$_{45}$N$_2$O$_6$ (M+H$^+$) requires 517.3277.
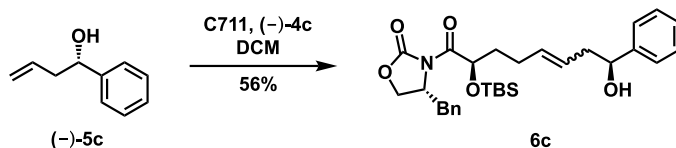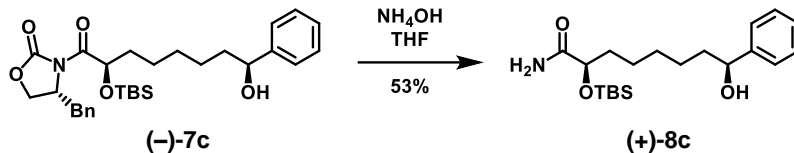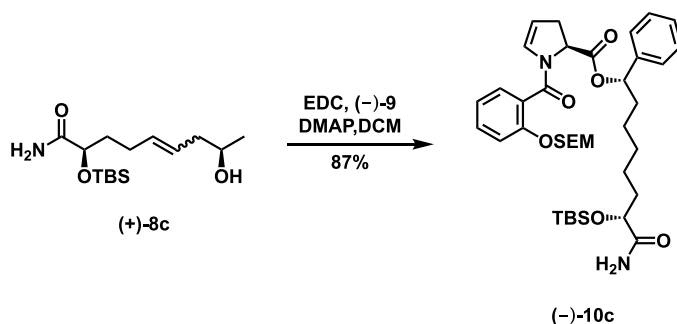
(R)-4-benzyl-3-((2R,8S)-2-((tert-butyldimethylsilyl)oxy)-8-hydroxy-8-phenyloct-5-enoyl)oxazolidin-2-one 6c. Following general procedure A; homoallylic alcohol **(−)-5c** (500 mg, 3.42 mmol) yielded the title compound as a brown oil (200 mg, 56% yield). ^{1}**H NMR** (500 MHz, CDCl$_3$, mixture of E/Z isomers) δ 7.37 – 7.32 (m, 6H), 7.31 – 7.27 (m, 2H), 7.26 – 7.22 (m, 2H), 5.67 – 5.43 (m, 2H), 5.40 – 5.33 (m, 1H), 4.72 – 4.68 (m, 1H), 4.67 – 4.58 (m, 1H), 4.24 – 4.15 (m, 2H), 3.43 – 3.39 (m, 1H), 2.73 – 2.65 (m, 1H), 2.51 – 2.35 (m, 2H), 2.31 – 2.15 (m, 3H), 1.82 – 1.66 (m, 2H), 0.94 (s, 9H), 0.11 (s, 3H), 0.08 (s, 3H); ^{13}**C NMR** (126 MHz, CDCl$_3$) δ 174.30, 153.13, 144.11, 135.21, 133.52, 129.47, 129.02, 128.35, 127.43, 127.34, 126.76, 125.79, 73.26, 70.76, 66.59, 55.62, 42.95, 37.71, 35.08, 28.45, 25.83, 18.33, -4.57, -5.04; **IR** (film) 3400 (br O-H), 2928, 2856, 1777 (C=O), 1710 (C=O), 1388, 1349, 1250, 1210, 1127, 1050 ,971, 909, 835, 777, 700; **HRMS** Accurate mass (ES^{+}): Found 546.2653, C$_{30}$H$_{41}$NO$_5$SiNa (M+Na) requires 546.2652.
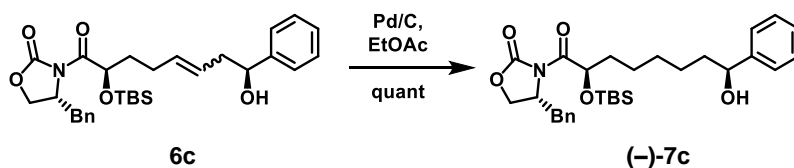
(R)-4-benzyl-3-((2R,8S)-2-((tert-butyldimethylsilyl)oxy)-8-hydroxy-8-phenyloctanoyl)oxazolidin-2-one (−)-7c. Following general procedure B; alkene **6c** (260 mg, 0.5 mmol) yielded the title compound as a clear oil (262 mg, quant.). ^{1}**H NMR** (500 MHz, CDCl$_3$) δ 7.37 – 7.32 (m, 4H), 7.30 – 7.26 (m, 2H), 7.24 (d, J = 8.4 Hz, 2H), 7.17 (d, J = 6.7 Hz, 2H), 5.36 (td, J = 7.9, 3.4 Hz, 1H), 4.68 – 4.59 (m, 2H), 4.22 – 4.15 (m, 2H), 3.40 (dt, J = 13.3, 2.7 Hz, 1H), 2.69 (ddd, J = 13.3, 10.1, 1.9 Hz, 1H), 2.62 – 2.57 (m, 1H), 1.84 – 1.75 (m, 1H), 1.73 – 1.57 (m, 4H), 1.45 (s, 2H), 1.33 (s, 3H), 0.93 (s, 9H), 0.11 (d, J = 3.4 Hz, 3H), 0.08 (d, J = 4.9 Hz, 3H).; ^{13}**C NMR** (126 MHz, CDCl$_3$) δ 174.53, 153.24, 145.02, 142.98, 135.39, 129.59, 129.14, 128.58, 128.53, 128.35, 127.63, 127.53, 126.02, 125.68, 77.41, 77.16, 76.91, 74.75, 71.47, 71.45, 66.64, 55.74, 39.15, 37.84, 36.05, 35.39, 35.25, 31.51, 29.27, 29.22, 25.96, 25.77, 25.53, 18.49, -4.49, -

4.94.; $[\alpha]^{25}_D$ -11.5 (c = 1.0 in CHCl$_3$); **IR** (film) 3500 (br O-H), 2928, 2856, 1779 (C=O), 1711 (C=O), 1454, 1387, 1348, 1249, 1210, 1195, 1105, 1121, 1010, 977, 835, 777, 699; **HRMS** Accurate mass (ES$^+$): Found 526.2998, C$_{30}$H$_{44}$NO$_5$Si (M+H$^+$) requires 526.2989.


(−)-7c   (+)-8c

(2R,8S)-2-((tert-butyldimethylsilyl)oxy)-8-hydroxy-8-phenyloctanamide (+)-8c. Following general procedure C; oxazolidinone **(−)-7c** (197 mg, 0.375 mmol) yielded the title compound as a clear oil (72 mg, 53% yield). **^{1}H NMR** (500 MHz, CDCl$_3$) δ 7.29 – 7.24 (m, 4H), 7.22 – 7.17 (m, 1H), 6.43 (d, J = 3.7 Hz, 1H), 5.73 – 5.65 (m, 1H), 4.58 (t, J = 5.9 Hz, 1H), 4.04 (t, J = 5.1 Hz, 1H), 2.00 (s, 1H), 1.76 – 1.52 (m, 4H), 1.39 – 1.15 (m, 6H), 0.85 (s, 9H), 0.02 (s, 3H), 0.01 (s, 3H).; **^{13}C NMR** (126 MHz, CDCl$_3$) δ 177.12, 145.05, 128.55, 127.59, 126.02, 74.67, 73.55, 39.13, 35.17, 29.53, 25.87, 25.77, 24.17, 18.14, -4.70, -5.12.; $[\alpha]^{25}_D$ +3.2 (c = 1.1 in CHCl$_3$); **IR** (film) 3475 (N-H), 3300 (br O-H), 2928, 2856, 1780, 1681 (C=O), 1582, 1463, 1389, 1361, 1253, 1005, 909, 836, 778, 730, 700; **HRMS** Accurate mass (ES$^+$): Found 366.2465, C$_{20}$H$_{36}$NO$_3$Si (M+H$^+$) requires 366.2464.

(+)-8c   (−)-10c

(1S,7R)-8-amino-7-((tert-butyldimethylsilyl)oxy)-8-oxo-1-phenyloctyl (S)-1-(2-((2-(trimethylsilyl)ethoxy)methoxy)benzoyl)-2,3-dihydro-1H-pyrrole-2-carboxylate (−)-10c. Following general procedure D; alcohol **(+)-8c** (30 mg, 0.082 mmol) yielded the title compound as a clear oil (51 mg, 87% yield). **^{1}H NMR** (300 MHz, CDCl$_3$) δ 7.36 – 7.26 (m, 7H), 7.18 (d, J = 8.3 Hz, 1H), 7.01 (t, J = 7.5 Hz, 1H), 6.51 (d, J = 4.6 Hz, 1H), 6.16 – 6.09 (m, 1H), 5.87 – 5.70 (m, 2H), 5.25 – 5.17 (m, 2H), 5.05 (dd,

J = 11.6, 4.6 Hz, 1H), 4.99 – 4.92 (m, 1H), 4.10 (t, *J* = 5.0 Hz, 1H), 3.79 – 3.65 (m, 2H), 3.15 – 2.98 (m, 1H), 2.61 – 2.47 (m, 1H), 2.05 – 1.90 (m, 1H), 1.82 – 1.54 (m, 4H), 1.38 – 1.21 (m, 9H), 0.90 (s, 9H), 0.07 (d, *J* = 1.8 Hz, 6H), -0.03 (s, 6H).; **^{13}C NMR** (126 MHz, CDCl$_3$) δ 176.94, 170.07, 165.10, 153.81, 140.52, 131.22, 130.94, 129.04, 128.55, 127.99, 126.65, 121.97, 115.22, 108.40, 93.34, 77.25, 73.53, 66.61, 57.92, 36.22, 35.10, 33.90, 29.81, 29.35, 25.86, 25.30, 24.05, 18.16, 18.13, -1.29, -4.71, -5.14.; **[α]$^{25}_D$** -21.3 (c = 1.10 in CHCl$_3$); **IR** (film) 3500 (N-H), 2925, 2854, 2362, 1735 (C=O), 1653 (C=O), 1601 (C=O), 1456, 1398, 1249, 1193, 1086, 986, 830, 756; **HRMS** Accurate mass (ES$^+$): Found 711.3856, C$_{38}$H$_{59}$N$_2$O$_7$Si$_2$ (M+H$^+$) requires 711.3861.
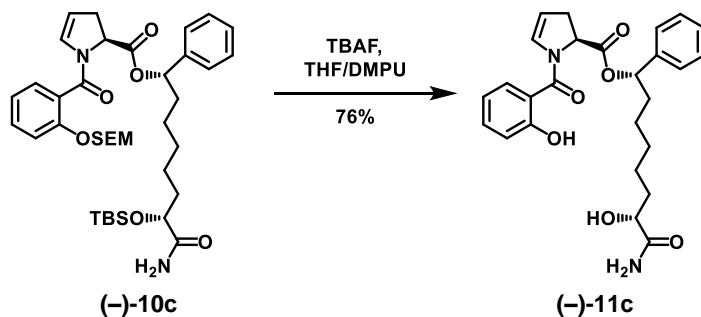
(1S,7R)-8-amino-7-hydroxy-8-oxo-1-phenyloctyl (S)-1-(2-hydroxybenzoyl)-2,3-dihydro-1H-pyrrole-2-carboxylate (–)-11c. Following general procedure E; silyl ether **(–)-10c** (18 mg, 0.025 mmol) yielded the title compound as a clear oil (9 mg, 76% yield). **^{1}H NMR** (600 MHz, CDCl$_3$) δ 9.55 (s, 1H), 7.41 – 7.37 (m, 2H), 7.35 – 7.29 (m, 5H), 6.99 (dd, *J* = 8.3, 1.1 Hz, 1H), 6.90 (t, *J* = 7.5 Hz, 1H), 6.72 (s, 1H), 6.55 (s, 1H), 5.89 (s, 1H), 5.47 (s, 1H), 5.23 – 5.18 (m, 1H), 5.07 (dd, *J* = 11.4, 4.7 Hz, 1H), 4.11 (dd, *J* = 8.0, 3.7 Hz, 1H), 3.12 – 3.03 (m, 1H), 2.57 (d, *J* = 17.1 Hz, 1H), 2.04 – 1.96 (m, 1H), 1.86 – 1.78 (m, 2H), 1.70 – 1.61 (m, 3H), 1.50 – 1.40 (m, 3H), 1.36 – 1.30 (m, 2H).; **^{13}C NMR** (151 MHz, CDCl$_3$) δ 176.95, 170.52, 167.53, 158.34, 140.26, 133.56, 130.80, 128.70, 128.62, 128.24, 126.54, 119.33, 118.05, 117.52, 111.06, 77.29, 71.50, 59.20, 36.24, 34.47, 29.84, 28.36, 25.22, 24.68.; **[α]$^{25}_D$** -63.5 (c = x0.49 in CHCl$_3$); **IR** (film) 3326 (br O-H), 2930, 2859, 1738 (C=O), 1663 (C=O), 1586 (C=O), 1456, 1428, 1354, 1294, 1190, 1153, 1097, 908, 856, 817, 755, 727, 669; **HRMS** Accurate mass (ES$^+$): Found 489.2019, C$_{26}$H$_{30}$N$_2$O$_6$Na (M+Na) requires 489.2002.
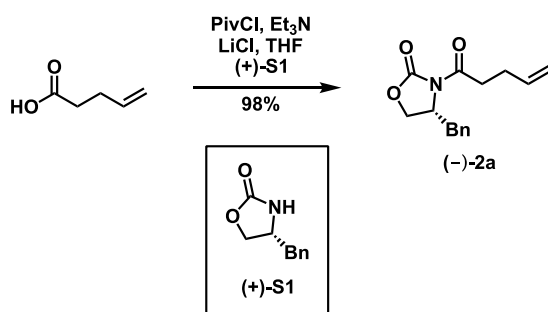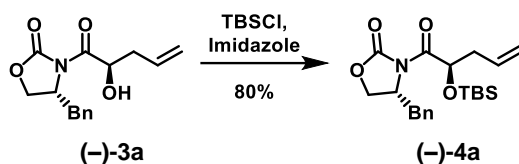
(R)-4-benzyl-3-(pent-4-enoyl)oxazolidin-2-one (–)-2a Based on the procedure by Kaliappan, et. al.[1]: To

a solution of 5-pentenoic acid (1.05 mL, 7.8 mmol) and triethylamine (2.9 mL, 20.4 mmol) in THF (40 mL)

at - 10°C was added pivaloyl chloride (0.961 mL, 7.8 mmol) dropwise, and stirred at this temperature for

an hour. Then, LiCl (0.362 g, 8.54 mmol) and **(+)-S1** (1.32 g, 7.43 mmol) were each quickly added in one

portion, and the reaction was allowed to warm to room temperature, and stirred for 16 hours. Reaction was

quenched with saturated NaHCO$_3$ and extracted with EtOAc 3x. The combined organic layers were washed

with brine, dried (Na$_2$SO$_4$), concentrated, and purified by column chromatography, yielding the title

compound as a clear oil (2.1 g, 98%). **^{1}H NMR**, **^{13}C NMR**, optical rotation, IR, and HRMS all matched

previously reported characterization data.[2,3]
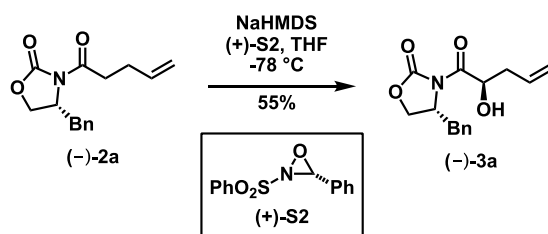
(R)-4-benzyl-3-((R)-2-hydroxypent-4-enoyl)oxazolidin-2-one (–)-3a. NaHMDS (6.6 mL, 1M soln. in

THF, 6.6 mmol) was diluted with anhydrous THF (42 mL) and cooled to -78°C. **(-)-2a** (1.47 g, 5.7 mmol)

was dissolved in THF (8.5 mL), cooled to -78°C, and slowly added to the NaHMDS solution via cannula.

The resulting solution was stirred for an hour at -78°C. Davis oxaziridine (**(±)-S2**, 1.58 g, 6.04 mmol) was

dissolved in THF (8.5 mL) and added via syringe pump to the reaction over a 25-minute period. The reaction

was stirred for an additional hour at -78°C. (±)-Camphorsulfonic acid (CSA) (6.4 g, 27.5 mmol) dissolved

in THF (53 mL) was added, and the reaction was warmed up to room temperature. H$_2$O was added, and the

solution was extracted 3x EtOAc. The combined organic layers were washed with brine, dried (MgSO$_4$), filtered, concentrated, and purified by column chromatography (0→10% EtOAc in hexanes) to yield the title compound as a yellow oil (0.853 g, 55%). **^{1}H NMR** (400 MHz, CDCl$_3$) δ 7.38 – 7.32 (m, 2H), 7.32 – 7.27 (m, 1H), 7.24 – 7.20 (m, 2H), 5.87 (ddt, J = 17.2, 10.2, 7.1 Hz, 1H), 5.23 – 5.07 (m, 3H), 4.66 (ddt, J = 9.8, 6.6, 3.4 Hz, 1H), 4.32 – 4.22 (m, 2H), 3.32 (dd, J = 13.5, 3.3 Hz, 1H), 2.84 (dd, J = 13.5, 9.4 Hz, 1H), 2.62 (dddd, J = 6.9, 4.7, 4.1, 1.2 Hz, 1H), 2.45 (dt, J = 14.2, 7.1 Hz, 1H). **^{13}C NMR** (100 MHz, CDCl$_3$) δ 174.09, 153.38, 134.87, 132.96, 129.59, 129.19, 127.68, 118.76, 70.42, 67.13, 55.70, 38.43, 37.64.; **[α]$^{25}_D$** -57.3 (c = 0.77 in CHCl$_3$); **IR** (film) 3496 (br O-H), 3069, 3030, 2977, 2920, 1774 (C=O), 1698 (C=O), 1389, 1350, 1291, 1212, 1117, 763, 704; **HRMS** Accurate mass (ES$^+$): Found 298.1053, C$_{15}$H$_{17}$NO$_4$Na (M+H) requires 298.1055.

(R)-4-benzyl-3-((R)-2-((tert-butyldimethylsilyl)oxy)pent-4-enoyl)oxazolidin-2-one (–)-4a. To a solutin of **(–)-3a** (0.336 g, 1.22 mmol) in DMF (6 mL) at 0°C was added tert-butyldimethylsilyl chloride (0.276 g, 1.83 mmol) and imidiazole (0.108 g, 1.59 mmol). The reaction was allowed to warm to room temperature and stirred for 16 hours. The nexr day, the reaction was poured over H$_2$O (10 mL) and extracted with 1:1 EtOAc:hexanes (3x50mL). The combined organic layers were washed with water then brine, dried over Na$_2$SO$_4$, filtered and concentrated. The product was purified by column chromatography to give the title compound as a clear oil (0.379 g, 80%). **^{1}H NMR** (400 MHz, CDCl$_3$) δ 7.37 – 7.31 (m, J = 7.8, 6.4 Hz, 2H), 7.28 (t, J = 5.1 Hz, 1H), 7.25 – 7.21 (m, 2H), 5.88 (ddt, J = 17.1, 10.0, 7.1 Hz, 1H), 5.47 (dd, J = 7.2, 4.5 Hz, 1H), 5.16 – 5.05 (m, 2H), 4.62 (dt, J = 9.9, 4.4 Hz, 1H), 4.19 (d, J = 4.5 Hz, 2H), 3.39 (dd, J = 13.3, 3.3 Hz, 1H), 2.76 – 2.68 (m, 1H), 2.57 – 2.35 (m, 2H), 0.94 – 0.91 (m, 9H), 0.11 (s, 3H), 0.09 (s, 3H).**^{13}C NMR** (100 MHz, CDCl$_3$173.59, 153.26, 135.29, 133.59, 129.55, 129.09, 127.50, 118.27, 71.10, 66.69, 55.69, 40.00, 37.80, 25.89, 18.46, -4.58, -4.90.; **[α]$^{25}_D$** -23.6 (c = 0.95 in CHCl$_3$); **IR** (film) 3075, 2960,

2926, 2856, 1777 (C=O), 1712 (C=O), 1386, 1347, 1257, 1209, 1144, 1105, 984, 920, 838, 777, 706;

HRMS Accurate mass (ES⁺): Found 390.2099, $C_{21}H_{32}NO_4Si$ (M+H) requires 390.2101.
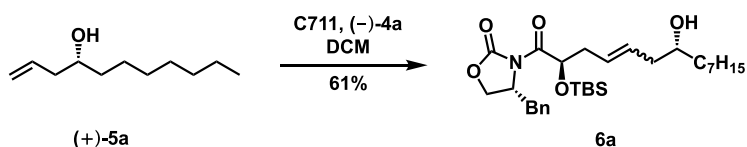
(R)-4-benzyl-3-((2R,7R)-2-((tert-butyldimethylsilyl)oxy)-7-hydroxytetradec-4-enoyl)oxazolidin-2-one 6a. Following general procedure A, homoallylic alcohol **(+)-5a** (833 mg, 4.9 mmol) yielded the title compound as a brown oil (54 mg, 61% yield). **¹H NMR** (600 MHz, CDCl₃, mixture of E/Z isomers) δ 7.35 (t, J = 7.6 Hz, 2H), 7.30 (d, J = 7.3 Hz, 1H), 7.25 (d, J = 7.1 Hz, 2H), 5.77 – 5.54 (m, 2H), 5.53 – 5.49 (m, 1H), 4.68 – 4.61 (m, 1H), 4.28 – 4.16 (m, 2H), 3.59 (s, 1H), 3.39 (dd, J = 13.3, 3.3 Hz, 1H), 2.80 – 2.70 (m, 1H), 2.60 – 2.40 (m, 2H), 2.30 – 2.00 (m, 2H), 1.79 (d, J = 43.0 Hz, 1H), 1.50 – 1.41 (m, 3H), 1.38 – 1.23 (m, 9H), 0.95 (s, 9H), 0.92 – 0.88 (m, 3H), 0.13 (s, 3H), 0.11 (s, 3H).; **¹³C NMR** (126 MHz, CDCl₃) δ 173.49, 153.19, 135.19, 130.61, 129.49, 129.01, 128.15, 127.43, 70.93, 70.67, 66.60, 55.57, 40.74, 38.44, 37.68, 36.86, 31.85, 29.66, 29.31, 25.83, 25.80, 22.68, 18.33, 14.12, -4.70, -5.02.; **IR** (film) 3510 (br O-H), 2926, 2855, 1781 (C=O), 1712 (C=O), 1388, 1348, 1250, 1210, 1109, 1007, 975, 938, 836, 778, 732, 701;

HRMS Accurate mass (ES⁺): Found 532.3457, $C_{30}H_{50}NO_5Si$ (M+H) requires 532.3458.
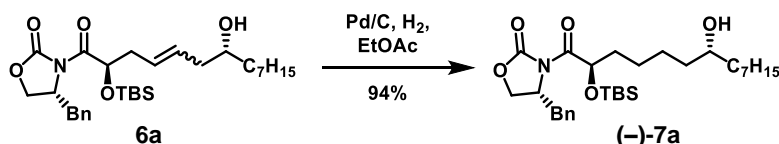
(R)-4-benzyl-3-((2R,7R)-2-((tert-butyldimethylsilyl)oxy)-7-hydroxytetradecanoyl)oxazolidin-2-one (–)-7a. Following general procedure B; alkene **6a** (456 mg, 0.85 mmol) yielded the title compound as a clear oil (430 mg, 94% yield). **¹H NMR** (400 MHz, CDCl₃) δ 7.37 – 7.27 (m, 3H), 7.26 – 7.22 (m, 2H), 5.37 (dd, J = 8.1, 3.4 Hz, 1H), 4.66 – 4.59 (m, 1H), 4.24 – 4.15 (m, 2H), 3.58 (s, 1H), 3.40 (dd, J = 13.2, 3.4 Hz, 1H), 2.70 (dd, J = 13.2, 10.2 Hz, 1H), 1.76 – 1.59 (m, 2H), 1.52 – 1.35 (m, 8H), 1.33 – 1.23 (m, 11H), 0.94 (s, 9H), 0.90 – 0.85 (m, 3H), 0.11 (s, 3H), 0.09 (s, 3H).; **¹³C NMR** (126 MHz, CDCl₃) δ 174.44, 153.17, 135.30, 129.50, 129.03, 127.43, 71.30, 66.58, 55.64, 37.72, 37.48, 37.28, 35.18, 31.90, 29.73,

29.37, 25.87, 25.74, 25.53, 25.15, 22.72, 18.39, 14.17, -4.58, -5.03.; $[\alpha]^{25}_D$ -4.5 (c = 0.83 in CHCl$_3$); **IR** (film) 3390 (br O-H), 2925, 2855, 1781 (C=O), 1711 (C=O), 1388, 1349, 1249, 1210, 1196, 1107, 1051, 1011, 977, 835, 777, 701; **HRMS** Accurate mass (ES$^+$): Found 534.3622, C$_{30}$H$_{52}$NO$_5$Si (M+H) requires 534.3615.


(−)-7a   (+)-8a
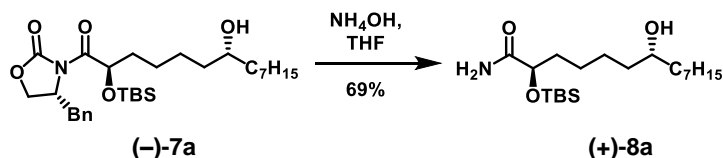
(2R,7R)-2-((tert-butyldimethylsilyl)oxy)-7-hydroxytetradecanamide   **(+)-8a.** Following general procedure C; oxazolidinone **(−)-7a** (430 mg, 0.8 mmol) yielded the title compound as a clear oil (208 mg, 69% yield). **¹H NMR** (500 MHz, CDCl$_3$) δ 6.53 (d, J = 4.0 Hz, 1H), 5.71 (d, J = 3.7 Hz, 1H), 4.17 – 4.09 (m, 1H), 3.56 (s, 1H), 1.83 – 1.64 (m, 3H), 1.49 – 1.35 (m, 9H), 1.33 – 1.22 (m, 9H), 0.92 (s, 9H), 0.87 (t, J = 7.0 Hz, 3H), 0.10 (s, 3H), 0.08 (s, 3H); **¹³C NMR** (126 MHz, CDCl$_3$) δ 177.20, 73.46, 71.88, 37.62, 37.39, 35.20, 31.95, 29.79, 29.42, 25.86, 25.78, 25.63, 24.24, 22.78, 18.13, 14.23, -4.71, -5.13; $[\alpha]^{25}_D$ +8.9 (c = 0.85 in CHCl$_3$); **IR** (film) 3480 (N-H), 3300 (br O-H), 2927, 2856, 1682 (C=O), 1582, 1463, 1361, 1253, 1096, 1005, 835, 778, 731, 669; **HRMS** Accurate mass (ES$^+$): Found 374.3098, C$_{20}$H$_{44}$NO$_3$Si (M+H) requires 374.3090.


(+)-8a   (−)-10a
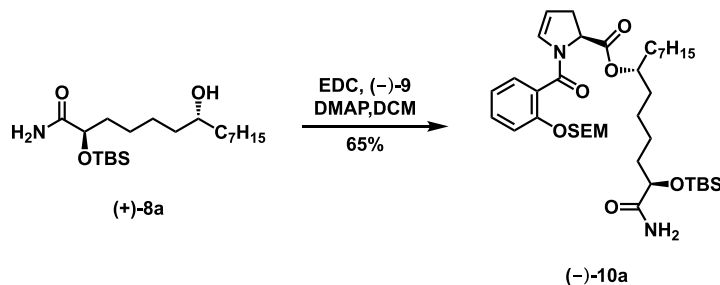
(2R,7R)-1-amino-2-((tert-butyldimethylsilyl)oxy)-1-oxotetradecan-7-yl   **(S)-1-(2-((2-(trimethylsilyl)ethoxy)methoxy)benzoyl)-2,3-dihydro-1H-pyrrole-2-carboxylate**   **(−)-10a.** Following general procedure D; alcohol **(+)-8a** (24 mg, 0.064 mmol) yielded the title compound as a clear oil (30 mg, 65% yield). **¹H NMR** (600 MHz, CDCl$_3$) δ 7.37 – 7.33 (m, 2H), 7.20 (dd, J = 8.9, 1.0 Hz, 1H), 7.04 (td, J = 7.5, 1.0 Hz, 1H), 6.54 (d, J = 4.5 Hz, 1H), 6.17 – 6.15 (m, 1H), 5.55 (d, J = 4.5 Hz, 1H), 5.25 – 5.20 (m,

1H), 5.03 – 4.98 (m, 2H), 4.97 – 4.92 (m, 1H), 4.14 (t, J = 5.1 Hz, 1H), 3.74 (t, J = 8.3 Hz, 2H), 3.16 – 3.08 (m, 1H), 2.70 – 2.63 (m, 1H), 1.82 – 1.74 (m, 1H), 1.71 – 1.62 (m, 3H), 1.62 – 1.51 (m, 4H), 1.43 – 1.36 (m, 3H), 1.31 – 1.20 (m, 12H), 0.91 (s, 9H), 0.86 (t, J = 7.0 Hz, 3H), 0.09 (s, 3H), 0.08 (s, 3H), -0.01 (s, 9H).; **^{13}C NMR** (151 MHz, CDCl$_3$) δ 176.90, 170.76, 165.04, 153.87, 131.25, 131.07, 129.05, 126.00, 122.00, 115.28, 108.41, 93.39, 75.51, 73.45, 66.65, 58.21, 34.97, 34.41, 34.20, 34.03, 31.93, 29.63, 29.33, 25.90, 25.37, 25.16, 24.08, 22.77, 18.19, 18.17, 14.23, -1.26, -4.68, -5.11.; **[α]^{25}$_D$** -27.3 (c = 0.97 in CHCl$_3$); **IR** (film) 3480 (N-H), 2928, 2857, 1740 (C=O), 1683 (C=O), 1456, 1406, 1250, 1195, 1087, 988, 915, 835, 779, 730; **HRMS** Accurate mass (ES$^+$): Found 719.4514, C$_{38}$H$_{67}$N$_2$O$_7$Si$_2$ (M+H$^+$) requires 719.4487.

(–)-10a   (–)-11a
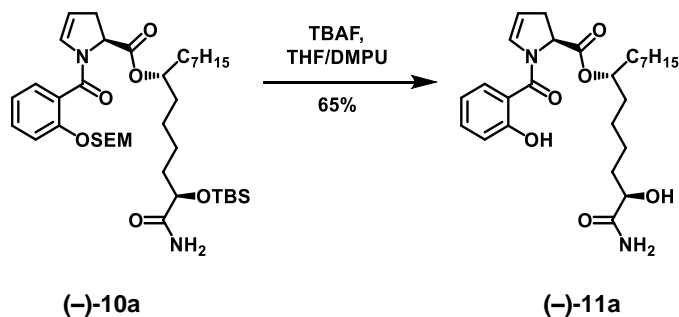
(2R,7R)-1-amino-2-hydroxy-1-oxotetradecan-7-yl   **(S)-1-(2-hydroxybenzoyl)-2,3-dihydro-1H-**

pyrrole-2-carboxylate (–)-11a. Following general procedure E; silyl ether **(–)-10a** (19 mg, 0.026 mmol) yielded the title compound as a clear oil (8 mg, 65% yield). **^{1}H NMR** (600 MHz, CDCl$_3$) δ 9.28 (s, 1H), 7.41 – 7.34 (m, 2H), 6.99 (d, J = 8.2 Hz, 1H), 6.90 (t, J = 7.5 Hz, 1H), 6.71 (s, 1H), 6.62 (s, 1H), 5.28 (s, 1H), 5.02 (dd, J = 11.4, 4.9 Hz, 2H), 4.10 (d, J = 5.2 Hz, 1H), 3.18 – 3.08 (m, 1H), 2.70 (d, J = 17.4 Hz, 1H), 1.90 – 1.80 (m, 1H), 1.73 – 1.56 (m, 9H), 1.55 – 1.37 (m, 8H), 1.36 – 1.25 (m, 3H), 0.87 (t, J = 7.1 Hz, 3H).; **^{13}C NMR** (151 MHz, CDCl$_3$) δ 177.11, 171.33, 167.44, 157.99, 133.52, 130.88, 128.38, 119.43, 118.07, 117.83, 111.07, 77.37, 77.16, 76.10, 71.52, 59.32, 34.66, 33.98, 32.07, 31.88, 29.84, 29.51, 29.29, 25.55, 24.83, 24.56, 22.76, 14.22.; **[α]^{25}$_D$** -27.8 (c = 0.83 in CHCl$_3$); **IR** (film) 3334 (br O-H), 2926, 2859, 1738 (C=O), 1665 (C=O), 1600 (C=O), 1459, 1431, 1370, 1198, 1153, 1099, 1035, 1015, 948, 861, 816, 757, 726, 619, 532.; **HRMS** Accurate mass (ES$^+$): Found 497.2645, C$_{26}$H$_{38}$N$_2$O$_6$Na (M+Na) requires 497.2628.
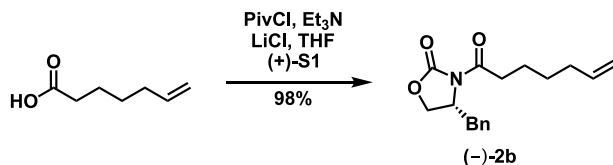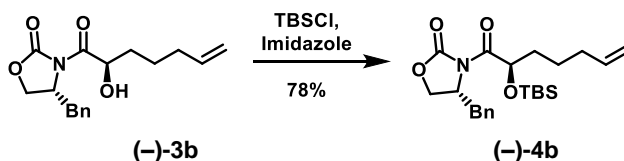
(R)-4-benzyl-3-(hept-6-enoyl)oxazolidin-2-one (–)-2b. Based on the procedure by Kaliappan, et. al.[1]: To

a solution of 6-heptenoic acid (1.05 mL, 7.8 mmol) and triethylamine (2.9 mL, 20.4 mmol) in THF (40 mL)

at - 10°C was added pivaloyl chloride (0.961 mL, 7.8 mmol) dropwise, and stirred at this temperature for

an hour. Then, LiCl (0.362 g, 8.54 mmol) and **(+)-S1** (1.32 g, 7.43 mmol) were each quickly added in one

portion, and reaction was allowed to warm to room temperature, and stirred for 16 hours. Reaction was

quenched with saturated $NaHCO_3$ and extracted with EtOAc 3x. The combined organic layers were washed

with brine, dried (Na_2SO_4), concentrated, and purified by column chromatography, yielding the title

compound as a clear oil (2.1 g, 98%). **^{1}H NMR** (400 MHz, CDCl$_3$) δ 7.34 – 7.27 (m, 2H), 7.25 – 7.21 (m,

1H), 7.18 (d, J = 7.0 Hz, 2H), 5.79 (ddt, J = 16.9, 10.2, 6.7 Hz, 1H), 5.04 – 4.91 (m, 2H), 4.64 (ddd, J =

13.0, 6.9, 3.3 Hz, 1H), 4.19 – 4.10 (m, 2H), 3.26 (dd, J = 13.4, 3.3 Hz, 1H), 3.00 – 2.82 (m, 2H), 2.75 (dd,

J = 13.3, 9.6 Hz, 1H), 2.08 (dd, J = 14.3, 7.1 Hz, 2H), 1.74 – 1.64 (m, 2H), 1.51 – 1.41 (m, 2H); **^{13}C NMR**

(101 MHz, CDCl$_3$) δ 173.22, 153.48, 138.45, 135.34, 129.45, 128.95, 127.34, 114.75, 66.19, 55.14, 37.90,

35.39, 33.51, 28.31, 23.72; **[α]$^{25}_D$** -50.8 (c = 0.59 in CHCl$_3$); **IR** (film) 2923, 2859, 1775 (C=O), 1696

(C=O), 1454, 1384, 1350, 1249, 1197, 1050, 992, 911, 748, 701; **HRMS** Accurate mass (ES$^+$): Found

288.1592, C$_{17}$H$_{22}$NO$_3$ (M+H$^+$) requires 288.1600.
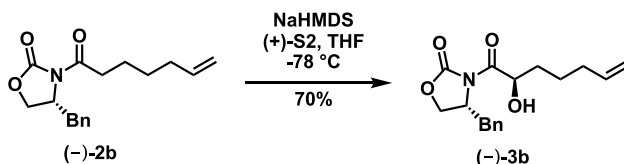
(R)-4-benzyl-3-((R)-2-hydroxyhept-6-enoyl)oxazolidin-2-one (–)-3b. NaHMDS (0.44 mL, 1M soln. in

THF, 0.44 mmol) was diluted with anhydrous THF (3 mL) and cooled to -78°C. **(-)-2b** (3.7 g, 13.53 mmol)

was dissolved in THF (20 mL), cooled to -78°C, and slowly added to the NaHMDS solution via cannula.

The resulting solution was stirred for an hour at -78°C. Davis oxaziridine ((±)-**S2**, 0.138 g, 0.44 mmol) was

dissolved in THF (1 mL) and added via syringe pump to the reaction over a 25 minute period. The reaction

was stirred for an additional hour at -78°C. (±)-Camphorsulfonic acid (CSA) (0.430 g, 1.85 mmol) dissolved in THF (3.5 mL) was added, and the reaction was warmed up to room temperature. H_2O was added, and the solution was extracted 3x EtOAc. The combined organic layers were washed with brine, dried (MgSO4), filtered, concentrated, and purified by column chromatography (0→10% EtOAc in hexanes) to yield the title compound as a yellow oil (0.078 g, 70%). **^{1}H NMR** (400 MHz, CDCl$_3$) δ 7.38 – 7.32 (m, 2H), 7.32 – 7.27 (m, 1H), 7.24 – 7.19 (m, 2H), 5.81 (ddt, J = 16.9, 10.2, 6.6 Hz, 1H), 5.08 – 4.92 (m, 3H), 4.67 (ddt, J = 10.3, 7.1, 3.1 Hz, 1H), 4.33 – 4.22 (m, 2H), 3.31 (dd, J = 13.5, 3.2 Hz, 1H), 2.84 (dd, J = 13.5, 9.4 Hz, 1H), 2.20 – 2.05 (m, 2H), 1.87 – 1.76 (m, 1H), 1.69 – 1.55 (m, 3H); **^{13}C NMR** (100 MHz, CDCl$_3$) δ 174.98, 153.27, 138.40, 134.86, 129.51, 129.09, 127.57, 114.89, 70.75, 66.99, 55.57, 37.51, 33.75, 33.35, 24.60; **[α]^{25}$_D$** -46.3 (c = 0.71 in CHCl$_3$); **IR** (film) 3490 (br O-H), 2923, 2861, 1777 (C=O), 1692 (C=O), 1454, 1387, 1351, 1293, 1210, 1197, 1109, 982, 912, 837, 752, 701; **HRMS** Accurate mass (ES$^+$): Found 304.1540, C$_{17}$H$_{22}$NO$_4$ (M+H$^+$) requires 304.1549.
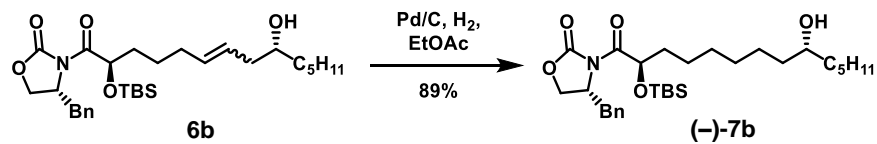

(R)-4-benzyl-3-((R)-2-((tert-butyldimethylsilyl)oxy)hept-6-enoyl)oxazolidin-2-one (–)-4b. To a solution of **(-)-3b** (0.074g, 0.24 mmol) in DMF (1.2 mL) at 0°C was added tert-Butyldimethylsilyl chloride (0.056g, 0.37 mmol) and imidazole (0.021g, 0.31 mmol). The solution was then allowed to warm to room temperature and stirred overnight. The following day, the reaction was poured into H_2O (2 mL) and extracted with 1:1 EtOAc:hexanes (4x20 mL). The combined organic layers were washed sequentially with H_2O and brine, dried (Na$_2$SO$_4$), filtered, concentrated, and purified by column chromatography to give the title compound as a clear oil (0.078 g, 78%). **^{1}H NMR** (400 MHz, CDCl$_3$) δ 7.37 – 7.30 (m, 2H), 7.32 – 7.25 (m, 1H), 7.27 – 7.21 (m, 2H), 5.79 (ddt, J = 16.9, 10.2, 6.6 Hz, 1H), 5.38 (dd, J = 7.8, 3.3 Hz, 1H), 5.05 – 4.91 (m, 2H), 4.62 (ddt, J = 10.1, 6.6, 3.3 Hz, 1H), 4.23 – 4.15 (m, 2H), 3.41 (dd, J = 13.2, 3.3 Hz, 1H), 2.69 (dd, J = 13.3, 10.2 Hz, 1H), 2.16 – 1.99 (m, 2H), 1.77 – 1.47 (m, 4H), 0.94 (s, 9H), 0.11 (s, 3H), 0.09 (s, 3H). **^{13}C NMR** (151 MHz, CDCl$_3$) δ 174.50, 153.26, 138.59, 135.41, 129.60, 129.15, 127.54,

114.85, 71.37, 66.67, 55.76, 37.86, 34.87, 33.42, 25.96, 24.90, 18.49, -4.49, -4.94; $[\alpha]^{25}_{D}$ -10.7 (c = 0.75 in CHCl$_3$); **IR** (film) 2928, 2856, 1778 (C=O), 1711 (C=O), 1453, 1386, 1348, 1247, 1209, 1194, 1106, 1006, 972, 835, 776, 700; **HRMS** Accurate mass (ES$^+$): Found 418.2408, C$_{23}$H$_{36}$NO$_4$Si (M+H$^+$) requires 418.2413.
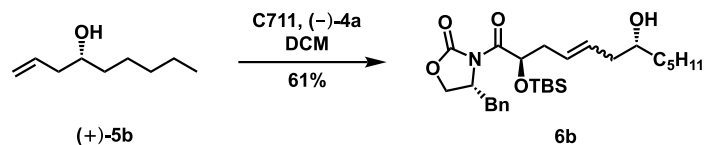
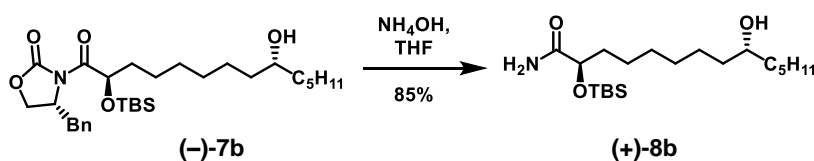**(R)-4-benzyl-3-((2R,9R)-2-((tert-butyldimethylsilyl)oxy)-9-hydroxytetradec-6-enoyl)oxazolidin-2-one 6b.** Following general procedure A, homoallylic alcohol **(+)-5b** (119 mg, 0.84 mmol) and oxazolidinone **(–)-2.215** (70 mg, 0.168 mmol) yielded the title compound as a brown oil (54 mg, 61% yield). **^{1}H NMR** (400 MHz, CDCl$_3$, mixture of E/Z isomers) δ 7.37 – 7.31 (m, 2H), 7.31 – 7.27 (m, 1H), 7.25 – 7.22 (m, 2H), 5.56 – 5.39 (m, 2H), 5.36 (dd, J = 8.0, 3.3 Hz, 1H), 4.62 (qd, J = 6.5, 3.1 Hz, 1H), 4.25 – 4.15 (m, 1H), 3.63 – 3.51 (m, 1H), 3.40 (dd, J = 13.2, 3.2 Hz, 1H), 2.69 (dd, J = 13.2, 10.2 Hz, 1H), 2.19 (dt, J = 11.9, 5.8 Hz, 1H), 2.14 – 1.99 (m, 3H), 1.76 – 1.51 (m, 4H), 1.47 – 1.39 (m, 3H), 1.37 – 1.22 (m, 6H), 0.93 (s, 9H), 0.88 (t, J = 6.8 Hz, 3H), 0.11 (s, 3H), 0.09 (s, 3H); **^{13}C NMR** (100 MHz, CDCl$_3$) δ 174.44, 153.25, 135.33, 133.86, 129.54, 129.09, 127.49, 126.62, 71.30, 71.11, 66.64, 55.70, 40.82, 37.78, 36.81, 34.74, 32.18, 31.99, 25.93, 25.48, 25.36, 22.75, 18.45, 14.18, -4.52, -4.98; **IR** (film) 3377 (br O-H), 2928, 2857, 1781 (C=O), 1712 (C=O), 1456, 1388, 1348, 1249, 1210, 1195, 1110, 1013, 970, 836, 777, 701; **HRMS** Accurate mass (ES$^+$): Found 554.3281, C$_{30}$H$_{49}$NO$_5$SiNa (M+Na$^+$) requires 554.3278.
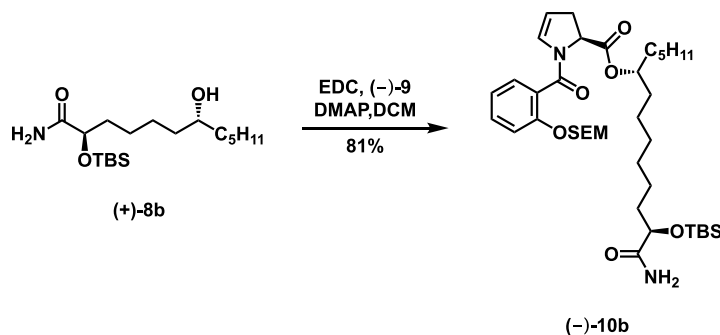

(R)-4-benzyl-3-((2R,9R)-2-((tert-butyldimethylsilyl)oxy)-9-hydroxytetradecanoyl)oxazolidin-2-one (–)-7b. Following general procedure B; alkene **6b** (54 mg, 0.10 mmol) yielded the title compound as a clear oil (48 mg, 89% yield). **^{1}H NMR** (400 MHz, CDCl$_3$) δ 7.37 – 7.27 (m, 3H), 7.26 – 7.22 (m, 2H), 5.36 (dd, J = 8.2, 3.4 Hz, 1H), 4.67 – 4.57 (m, 1H), 4.24 – 4.15 (m, 2H), 3.58 (s, 1H), 3.40 (dd, J = 13.3, 3.2 Hz, 1H),

2.69 (dd, J = 13.2, 10.2 Hz, 1H), 1.72 – 1.55 (m, 7H), 1.43 (dd, J = 24.1, 11.7 Hz, 4H), 1.36 – 1.23 (m, 9H), 0.93 (s, 9H), 0.89 (t, J = 6.9 Hz, 3H), 0.11 (s, 3H), 0.09 (s, 3H); **^{13}C NMR** (100 MHz, CDCl$_3$) δ 174.45, 153.13, 135.27, 129.46, 128.98, 127.38, 71.86, 71.32, 66.51, 55.60, 53.46, 37.69, 37.44, 37.43, 35.19, 29.45, 29.14, 25.82, 25.53, 25.35, 22.66, 18.35, 14.07, 4.62, 5.08; **[α]^{25}$_D$** -6.6 (c = 1.5 in CHCl$_3$); **IR** (film) 3400 (br O-H), 2926, 2855, 1781 (C=O), 1712 (C=O), 1455, 1388, 1348, 1249, 1210, 1195, 1106, 1011, 976, 835, 777, 700, 593; **HRMS** Accurate mass (ES$^+$): Found 556.3446, C$_{30}$H$_{51}$NO$_5$SiNa(M+H$^+$) requires 556.3434.


(2R,9R)-2-((tert-butyldimethylsilyl)oxy)-9-hydroxytetradecanamide (+)-8b. Following general procedeure C; oxazolidinone **(−)-7b** (48 mg, 0.09 mmol) yielded the title compound as a clear oil (29 mg, 85% yield). **^{1}H NMR** (300 MHz, CDCl$_3$) δ 6.52 (s, 1H), 5.81 (s, 1H), 4.12 (t, J = 5.0 Hz, 1H), 3.56 (s, 1H), 1.90 – 1.56 (m, 4H), 1.50 – 1.22 (m, 17H), 0.95 – 0.83 (m, 12H), 0.09 (s, 3H), 0.08 (s, 3H); **^{13}C NMR** (126 MHz, CDCl$_3$) δ 177.23, 73.58, 72.06, 37.58, 37.55, 35.24, 32.04, 29.65, 29.58, 25.86, 25.69, 25.46, 24.19, 22.77, 18.14, 14.19, -4.71, -5.12; **[α]^{25}$_D$** +19.6 (c = 0.27 in CHCl$_3$); **IR** (film) 3478 (N-H), 3300 (br O-H), 2927, 2856, 1682 (C=O), 1582, 1463, 1253, 1098, 908, 835, 778, 732, 669; **HRMS** Accurate mass (ES$^+$): Found 374.3101, C$_{20}$H$_{44}$NO$_3$Si (M+H$^+$) requires 374.3090.

(6R,13R)-14-amino-13-((tert-butyldimethylsilyl)oxy)-14-oxotetradecan-6-yl (S)-1-(2-((2-(trimethylsilyl)ethoxy)methoxy)benzoyl)-2,3-dihydro-1H-pyrrole-2-carboxylate (−)-10b. Following

general procedure D; alcohol **(+)-8b** (25 mg, 0.067 mmol) yielded the title compound as a clear oil (39 mg, 81% yield). **¹H NMR** (400 MHz, CDCl₃) δ 7.37 – 7.31 (m, 2H), 7.18 (d, J = 9.0 Hz, 1H), 7.02 (t, J = 7.4 Hz, 1H), 6.51 (s, 1H), 6.14 (d, J = 4.2 Hz, 1H), 5.51 – 5.42 (m, 1H), 5.21 (dd, J = 14.4, 7.1 Hz, 1H), 5.06 – 4.88 (m, 2H), 4.11 (t, J = 5.0 Hz, 1H), 3.77 – 3.68 (m, 1H), 3.11 (dd, J = 15.8, 12.9 Hz, 1H), 2.65 (d, J = 17.0 Hz, 1H), 1.78 – 1.69 (m, 1H), 1.66 – 1.51 (m, 9H), 1.31 – 1.23 (m, 13H), 0.95 – 0.89 (m, 11H), 0.85 (t, J = 6.1 Hz, 3H), 0.07 (d, J = 5.7 Hz, 6H), -0.03 (s, J = 0.9 Hz, 9H) ; **¹³C NMR** (126 MHz, CDCl₃) δ 177.00, 170.81, 165.01, 153.86, 131.23, 131.08, 129.03, 126.01, 121.99, 115.23, 108.36, 93.35, 75.58, 73.62, 66.63, 58.20, 35.17, 34.43, 34.12, 31.84, 29.84, 29.44, 25.88, 25.17, 25.03, 24.09, 22.67, 18.18, 18.16, 14.16, -1.26, -4.69, -5.11; **[α]²⁵_D** -28.3 (c = 0.86 in CHCl₃); **IR** (film) 3219 (N-H), 2927, 2857, 1740 (C=O), 1652 (C=O), 1456, 1405, 1250, 1087, 983, 915, 835, 779, 730, 668; **HRMS** Accurate mass (ES⁺): Found 741.4336, $C_{38}H_{66}N_2O_7Si_2Na$ (M+Na⁺) requires 741.4306.
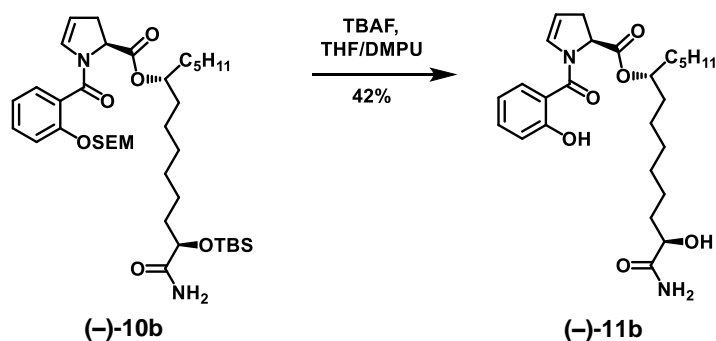

(6R,13R)-14-amino-13-hydroxy-14-oxotetradecan-6-yl **(S)-1-(2-hydroxybenzoyl)-2,3-dihydro-1H-pyrrole-2-carboxylate (–)-11b.** Following general procedure E; silyl ether **(–)-10b** (19 mg, 0.026 mmol) yielded the title compound as a clear oil (5 mg, 42% yield). **¹H NMR** (400 MHz, CDCl₃) δ 9.66 (s, 1H), 7.44 – 7.34 (m, 2H), 7.00 (s, J = 8.3 Hz, 1H), 6.90 (t, J = 7.5 Hz, 1H), 6.74 (s, 1H), 6.58 (s, 1H), 5.45 (s, 1H), 5.31 – 5.26 (m, 1H), 5.01 (dd, J = 11.2, 4.7 Hz, 2H), 4.04 (s, 1H), 3.40 (s, 1H), 3.20 – 3.07 (m, 1H), 2.70 (d, J = 15.0 Hz, 1H), 1.87 – 1.76 (m, J = 3.4 Hz, 1H), 1.73 – 1.48 (m, 6H), 1.47 – 1.21 (m, J = 43.7 Hz, 13H), 0.86 (t, J = 5.8 Hz, 3H); **¹³C NMR** (100 MHz, CDCl₃) δ 176.92, 171.32, 167.46, 158.30, 133.56, 130.93, 128.39, 119.35, 118.04, 117.55, 110.98, 76.14, 71.81, 59.43, 34.68, 34.51, 34.36, 31.72, 29.85,

28.85, 28.63, 25.19, 24.60, 24.26, 22.63, 14.10.; **[α]^{25}$_D$** -27.6 (c = 0.29 in CHCl$_3$); **IR** (film) 3338 (br O-H), 2924, 2855, 1734 (C=O), 1664 (C=O), 1616 (C=O), 1458, 1431, 1376, 1294, 1197, 1153, 1098, 1018, 858, 817, 756, 732, 654, 617; **HRMS** Accurate mass (ES$^+$): Found 497.2641, C$_{26}$H$_{38}$N$_2$O$_6$Na (M+Na$^+$) requires 497.2628.


(–)-4c → **(+)-S3**
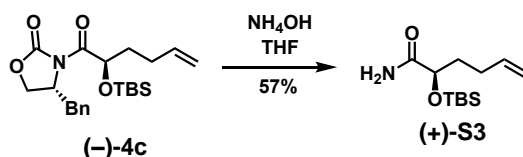
(_R_)-2-((_tert_-butyldimethylsilyl)oxy)hex-5-enamide **(+)-S3.** Following general procedure D, oxazolidinone **(–)-4c** (270 mg, 0.668 mmol) yielded the title compound as a white solid (93 mg, 57% yield). **^{1}H NMR** (400 MHz, CDCl$_3$) δ 6.53 (s, 1H), 5.81 (dt, _J_ = 10.2, 6.6 Hz, 1H), 5.64 (s, 1H), 4.99 (dd, _J_ = 3.2, 1.6 Hz, 2H), 4.16 (t, _J_ = 5.2 Hz, 1H), 2.22 – 2.06 (m, 2H), 1.92 – 1.74 (m, 2H), 0.93 (s, 9H), 0.11 (s, 3H), 0.09 (s, 3H); **^{13}C NMR** (151 MHz, CDCl$_3$) δ 176.74, 137.99, 115.09, 73.15, 34.59, 28.54, 25.87, 18.15, -4.69, -5.09; **[α]^{20}$_D$** +13.1 (c = 0.26 in CHCl$_3$); **IR** (film) 3478, 3224 (N-H), 2961, 2933, 2853, 1691 (C=O), 1653, 1252, 1098, 907, 834, 778, 555; **HRMS** Accurate mass (APCI$^+$): Found 244.1725 (-0.93 ppm), C$_{12}$H$_{26}$NO$_2$ ^{28}Si (M+H$^+$) requires 244.17273.


S4
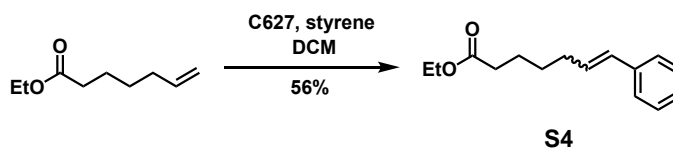
Ethyl (_E_)-7-phenylhept-6-enoate S4. Following general procedure B, ethyl heptenoate (2.00 mL, 11.4 mmol), styrene (2.61 mL, 22.8 mmol), and catalyst C627 (Materia, CAS[301224-40-8]) (**5 mol%**) yielded the title compound as a clear oil (1.49 g, 56% yield). **^{1}H NMR** (400 MHz, CDCl$_3$, mixture of E/Z isomers) δ 7.36 – 7.26 (m, 4H), 7.22 – 7.15 (m, 1H), 6.41 – 6.37 (dd, _J_ = 15.8, 4.1 Hz, 1H), 6.25-6.15 (dt, _J_ = 14.3, 6.9 Hz, 1H), 4.14 (q, _J_ = 7.1 Hz, 2H), 2.38-2.30 (t, _J_ = 7.5 Hz, 2H), 2.28 – 2.22 (dd, _J_ = 13.9, 6.7 Hz, 2H), 1.74-1.64 (m, 2H), 1.56-1.48 (m, 2H), 1.26 (t, _J_ = 7.1 Hz, 3H); **^{13}C NMR** (151 MHz, CDCl$_3$) δ 173.79, 137.88, 130.49, 130.30, 128.59, 126.98, 126.06, 60.34, 34.34, 32.76, 28.95, 24.65, 14.38; **IR** (film) 2955,

2876, 1708 (C=O), 1147, 964, 692; **HRMS** Accurate mass (APCI⁺): Found 233.15347 (-0.58 ppm), $C_{15}H_{21}O_2$ (M+H⁺) requires 233.15361.
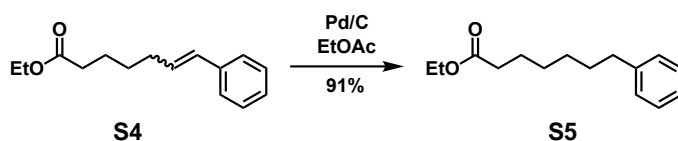

Ethyl 7-phenylheptanoate S5. Following general procedure C; alkene **S4** (1.49 g, 6.41 mmol) yielded the title compound as a clear oil (1.37 g, 91% yield). **¹H NMR** (400 MHz, CDCl₃) δ 7.30 – 7.26 (m, 2H), 7.19 – 7.16 (m, 3H), 4.13 (q, J = 7.2 Hz, 2H), 2.60 (t, J = 7.5 Hz, 2H), 2.29 (t, J = 7.6 Hz, 2H), 1.68 – 1.59 (m, 4H), 1.39-1.33 (m, 4H), 1.26 (t, J = 7.2 Hz, 3H); **¹³C NMR** (151 MHz, CDCl₃) δ 173.96, 142.84, 128.52, 128.37, 125.74, 60.30, 36.01, 34.48, 31.41, 29.12, 29.04, 25.04, 14.39; **IR** (film) 2933, 2857, 1734 (C=O), 698; **HRMS** Accurate mass (APCI⁺): Found 235.16908 (-0.77 ppm), $C_{15}H_{22}O_2$(M+H⁺) requires 235.16926.
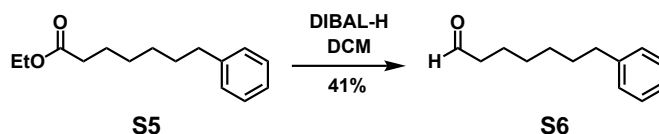

7-phenylheptanal S6. To a solution of ethyl ester **S5** (1.37 g, 5.85 mmol) in 25 mL of DCM cooled to -78 °C was added a 1.0 M solution of DIBAL-H (6.31 mL, 6.31 mmol) dropwise. The reaction mixture was stirred for 30 minutes, then quenched with a saturated solution of Rochelle's salt and stirred for 3 hours. This was then extracted with DCM (3x) washed with 1.0 M HCl (1x), dried over MgSO₄, concentrated under reduced pressure, then purified by column chromatography in 5% EtOAc/Hexanes, yielding the title compound as a clear oil (459 mg, 41%). **¹H NMR** (400 MHz, CDCl₃) δ 9.76 (s, 1H), 7.32-7.25 (m, 2H), 7.22 – 7.14 (m, 3H), 2.65-2.57 (m, 2H), 2.45-2.32 (m, 2H), 1.72-1.57 (m, 4H), 1.43-1.29 (m, 4H); **¹³C NMR** (151 MHz, CDCl₃) δ 203.04, 142.79, 128.52, 128.39, 125.77, 43.99, 35.99, 31.37, 29.03, 24.73, 22.13; **IR** (film) 2923, 2851, 1707 (C=O); **HRMS** Accurate mass (ES⁺): 191.14292 (-0.65 ppm), $C_{13}H_{19}O_5$ (M+H⁺) requires 191.304.
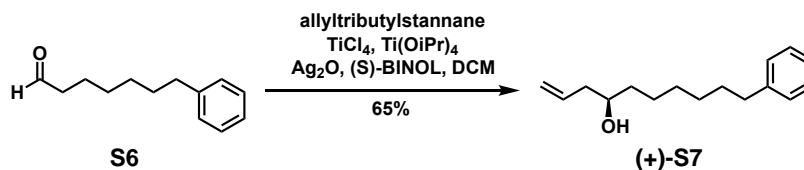
(+)-10-phenyldec-1-en-4-ol (+)-S7. Following general procedure A, aldehyde **S6** (459 mg, 2.41 mmol) yielded the title compound as a yellow oil (365 mg, 65%). **¹H NMR** (400 MHz, CDCl₃, trace amounts of aldehyde **2.224**) δ 7.32 – 7.25 (m, 2H), 7.22 – 7.15 (m, 3H), 5.89-5.77 (m, 1H), 5.19-5.09 (d, 2H), 3.68-3.60 (m, 1H), 2.65-2.56 (t, J = 7.6 Hz 2H), 2.36-2.25 (m, 1H), 2.19-2.08 (m, 1H), 1.69-1.56 (m, 4H), 1.51-1.42 (m, 2H), 1.41-1.29 (m, 6H); **¹³C NMR** (151 MHz, CDCl₃) δ 142.95, 135.02, 128.52, 128.36, 125.71, 118.21, 70.80, 42.06, 36.90, 36.08, 31.55, 29.63, 29.37, 25.72; **[α]²⁰_D** +1.9 (c = 0.69 in CHCl₃); **IR** (film) 3443 (br O-H), 3018, 2930, 2851, 1746, 1716 (C=O).
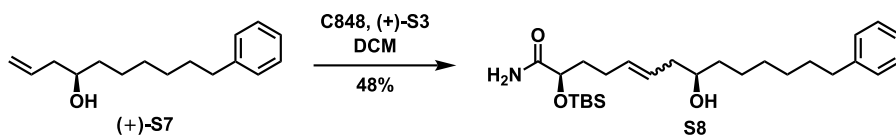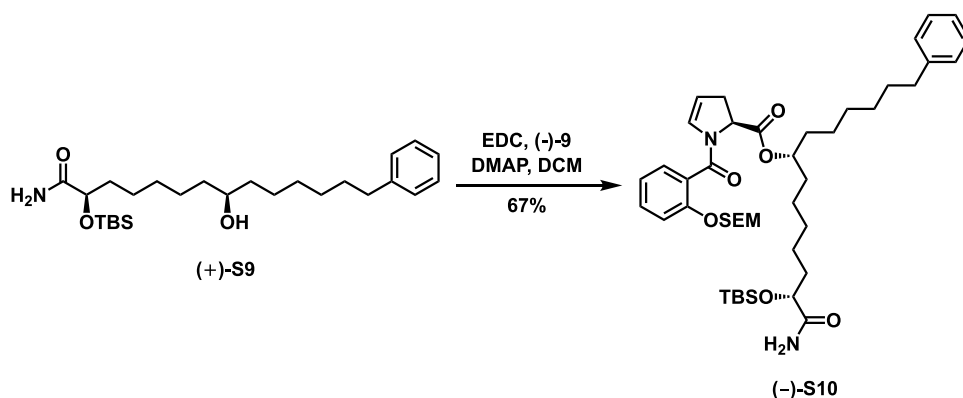

(2R,8R,E)-2-((tert-butyldimethylsilyl)oxy)-8-hydroxy-14-phenyltetradec-5-enamide S8. Following general procedure B, homoallylic alcohol **(+)-S7** (234 mg, 1.01 mmol) and catalyst C848 (Materia, CAS[246047-72-3]) (**20 mol%**) yielded the title compound as a dark purple oil (72 mg, 48% yield). **¹H NMR** (400 MHz, CDCl₃, mixture of E/Z isomers) δ 7.28-7.24 (m, 2H), 7.21-7.14 (m, 3H), 6.54 (d, J = 3.5 Hz, 1H), 5.61 (s, 1H), 5.57-5.39 (m, 2H), 4.16 (t, J = 5.0 Hz, 1H), 3.60-3.52 (m, 1H), 2.60 (t, J = 7.6 Hz, 2 H), 2.26-1.98 (m, 4H), 1.93-1.82 (m, 1H), 1.81-1.71 (m, 1H), 1.67-1.55 (m, 4H), 1.47-1.21 (m, 10H), 0.93 (s, 9H), 0.11 (s, 3H), 0.10 (s, 3H); **¹³C NMR** (151 MHz, CDCl₃) δ 176.78, 143.00, 133.37, 128.54, 128.36, 126.95, 125.70, 73.07, 71.05, 40.85, 36.91, 36.09, 34.99, 31.58, 29.67, 29.42, 27.42, 25.88, 25.79, 18.15, -4.67, -5.09; **IR** (film) 3484 (N-H), 3284 (br O-H), 2930, 2857, 1748, 1691 (C=O), 1103, 831, 780; **HRMS** Accurate mass (APCI⁺): Found 448.32399 (-0.34 ppm), $C_{26}H_{46}NO_3{}^{28}Si$ (M+H⁺) requires 448.32415.
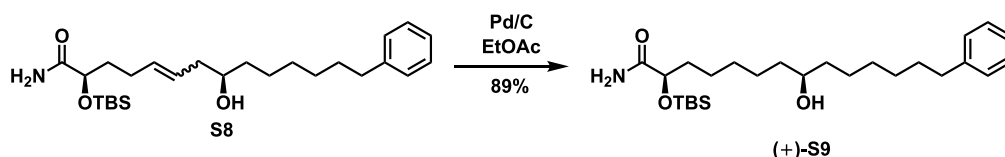
**(2R,8R)-2-((tert-butyldimethylsilyl)oxy)-8-hydroxy-14-phenyltetradecanamide (+) S9.** Following general procedure C; alkene **S8** (70 mg, 0.156 mmol) yielded the title compound as a brown oil (62 mg, 89% yield). **¹H NMR** (400 MHz, CDCl₃) δ 7.29 – 7.24 (m, 2H), 7.20 – 7.22-7.16 (m, 3H), 6.54 (s, 1H), 6.13 (s, 1H), 4.13 (t, J = 5.1 Hz, 1H), 3.60-3.53 (m, 1H), 2.60 (t, J = 7.8 Hz, 2H), 1.81-1.70 (m, 1H), 1.70-

1.66 (m, 1H), 1.66-1.56 (m, 3H), 1.47-1.21 (m, 17H), 0.93 (s, 9H), 0.10 (s, 3H), 0.09 (s, 3H); ^{13}**C NMR** (151 MHz, CDCl$_3$) δ 177.00, 142.99, 128.54, 128.37, 125.72, 73.61, 72.04, 37.61, 37.53, 36.10, 35.24, 31.58, 31.08, 29.71, 29.43, 25.89, 35.73, 25.63, 24.27, 18.17, -4.67, -5.09; **[α]^{20}$_D$** +0.7 (c = 0.83 in CHCl$_3$); **IR** (film) 3563 (N-H), 3240 (br O-H), 2955, 2864, 1748 (C=O), 1718, 1461, 1185, 1081, 1043, 1017, 986, 878, 727, 653; **HRMS** Accurate mass (ES$^+$): Found 450.33928 (-1.14 ppm), C$_{26}$H$_{48}$NO$_3$^{28}Si (M+H$^+$) requires 450.3398.

(7R,13R)-14-amino-13-((*tert*-butyldimethylsilyl)oxy)-14-oxo-1-phenyltetradecan-7-yl (S)-1-(2-((2-(trimethylsilyl)ethoxy)methoxy)benzoyl)-2,3-dihydro-1H-pyrrole-2-carboxylate (–)-S10. Following general procedure E; alcohol **(+)-S9** (56 mg, 0.124 mmol) yielded the title compound as a yellow oil (66 mg, 67% yield). ^{1}**H NMR** (400 MHz, CDCl$_3$) δ 7.44-3.37 (m, 2H), 7.31 (t, J = 7.5 Hz, 3H), 7.22 (t, J = 7.9 Hz, 3H), 7.08 (t, J = 7.4 Hz, 1 H), 6.57 (m, 1H), 6.21 (m, 1H), 5.67 (d, J = 4.0 Hz, 1H), 5.27 (q, J = 7.1 Hz, 2H), 5.08-5.04 (m, 1H), 5.04-4.97 (m, 1H), 4.17 (t, J = 4.9 Hz, 1H), 3.79 (t, J = 12.6 Hz, 2H), 3.22-3.10 (m, 1H), 2.76-2.67 (m, 1H), 2.63 (t, J = 11.7 Hz, 2H), 1.85-1.76 (m, 2H), 1.76-1.69 (m, 1H), 1.69-1.54 (m, 6H), 1.50-1.24 (m, 14H), 0.96 (s, 9H), 0.13 (s, 3H), 0.12 (s, 3H), 0.04 (s, 9H); ^{13}**C NMR** (151 MHz, CDCl$_3$) δ 176.93, 170.79, 164.97, 153.86, 142.94, 131.22, 131.06, 129.01, 128.51, 128.34, 126.02, 125.68, 121.98, 115.27, 108.32, 93.38, 75.40, 73.60, 66.63, 58.22, 36.04, 35.13, 34.42, 34.10, 34.06, 31.53, 29.50, 29.31, 25.88, 25.29, 25.06, 24.13, 18.17, 18.15, -1.27, -4.70, -5.13; **[α]^{20}$_D$** -7.8 (c = 0.80 in CHCl$_3$); **IR** (film) 3487 (N-H), 2961, 2854, 1746 (C=O), 1622, 1407, 831, 729; **HRMS** Accurate mass (APCI$^+$): Found 795.47917 (-0.33 ppm), C$_{44}$H$_{71}$N$_2$O$_7$^{28}Si$_2$ (M+H$^+$) requires 795.47943.
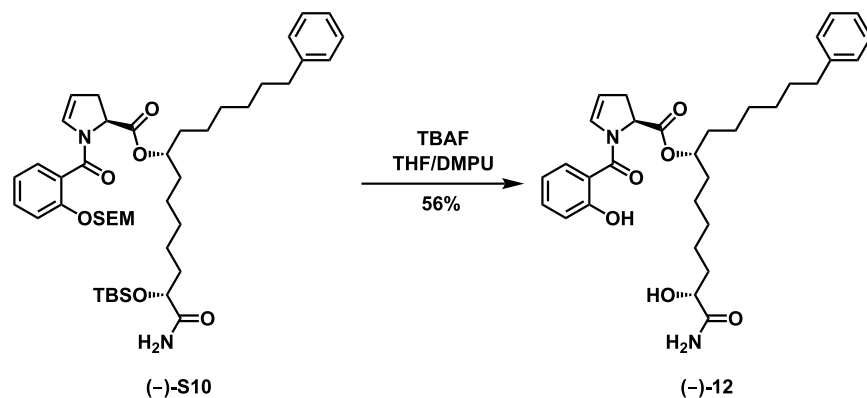
(7R,13R)-14-amino-13-hydroxy-14-oxo-1-phenyltetradecan-7-yl (S)-1-(2-hydroxybenzoyl)-2,3-dihydro-1H-pyrrole-2-carboxylate (–)-12. Following general procedure F; protected ester **(–)-S10** (9 mg, 0.011 mmol) yielded the title compound as a colorless oil (3 mg, 56% yield). **^{1}H NMR** (400 MHz, CDCl$_3$) δ 9.54 (s, 1H), 7.42-7.35 (m, 3H), 7.31-7.24 (m, 3H), 7.21-7.25 (m, 2H), 6.99 (d, J = 7.3 Hz, 1H), 6.91 (t, J = 7.3 Hz, 1H), 6.99 (s, 1H), 6.91 (s, 1H), 5.31- 5.23 (m, 2H), 5.06-4.96 (m, 2 H), 4.14-4.08 (m, 1H), 3.30 (s, 1H), 3.12 (m, 1H), 2.70 (m, 1H), 2.61-2.55 (m, 3H), 1.86-1.75 (m 1H), 1.72-1.11 (m, 17H); **^{13}C NMR** (151 MHz, CDCl$_3$) δ 176.75, 171.30, 158.13, 142.91, 133.54, 130.85, 128.54, 128.39, 128.30, 125.75, 119.41, 118.05, 117.66, 111.10, 75.94, 71.42, 59.38, 41.18, 36.04, 34.53, 34.35, 34.18, 31.49, 29.85, 29.40, 29.26, 28.36, 25.47, 28.84, 24.56; **[α]$^{20}_D$** -4.3 (c = 0.23 in CHCl$_3$); **IR** (film) 3481 (N-H), 3145 (br O-H), 2958, 2923, 1742 (C=O), 1717, 1407, 1195, 1087, 989, 834, 660; **HRMS** Accurate mass (ES$^+$): Found 551.31102 (-0.99 ppm), C$_{32}$H$_{43}$N$_2$O$_6$ (M+H$^+$) requires 551.31156.

5.1.3. Biology

5.1.3.1. Bacterial Strains and Culture Conditions

P. aeruginosa PAO1 was acquired from Prof. Bettina A. Buttaro (Lewis Katz School of Medicine, Temple University) and *P. aeruginosa* PA14 was acquired from Prof. Joanna B. Goldberg (School of Medicine, Emory University). *P. aeruginosa* RO5 was obtained via resistance selection assay from PA14 in our laboratory.[4] All three strains were grown from a freezer stock overnight (16-24 hr) with shaking at 37 °C, 200 rpm in Trypticase Soy Broth (TSB) media (5 mL).

5.1.3.2. IC$_{50}$ Assay

Compounds were dissolved in DMSO to give 10 mM stock solutions, which were serially diluted in flat-bottom 96-well microtiter plates yielding 24 test concentrations ranging from 500 $\square$M to 0.030 nM. Controls were prepared by dissolving in 10% DMSO/90% H$_2$O to 1mM stock solutions and serially diluting in the same manner as for test compounds. The positive control used in all cases was gentamicin and the negative control was a solution of 10% DMSO/90% H$_2$O. Overnight cultures were diluted 1:100 in 5 mL of fresh media and grown at 37 °C, 200 rpm to an OD$_{600}$ (measured on a Molecular Devices SpectraMax iD3 plate reader) reading of ~0.32. Bacteria were then diluted to a concentration of 0.004 according to the following equation:

(x $\square$L regrow culture)*(OD reading) = (0.004)*(volume of diluted bacteria culture needed).

Then 100 $\square$L was inoculated into each well of plate already containing 100 $\square$L of compound solution, giving final test concentrations of 250 $\square$M to 0.015 nM. Plates were then incubated statically at 37 °C for 24 hours. OD$_{600}$ readings were taken at this point, and IC$_{50}$ and IC$_{90}$ values were calculated by fitting OD readings vs. concentrations with a four-parameter logistic model. Compounds were tested in triplicate from three separate overnight cultures and averaged.

5.1.4. Computation

5.1.4.1. Computational pose prediction for promysalin analogs

To build structural models of promysalin analog in complex with succinate dehydrogenase (Sdh), we used a very similar protocol to that described in our earlier study.[4] Previously, we used the protein structure extracted from PDB ID 2WU5,[5] and used the ROCS software to overlay low-energy conformers of promysalin onto the carboxin inhibitor in the active site. From here, the model was refined using a gradient-based full atom minimization in Rosetta.[6] Finally, models were ranked on the basis of the protein-ligand interaction energy.

For the present study, we took advantage of the fact that diversity in the analogs was restricted to the alkyl chain. We therefore fixed the shared promysalin substructure in the active

conformation from our previous study, rather than build low-energy conformers from scratch. We built conformers using the OMEGA software,[7,8] with the following command line:

omega2 -in input_file.smi -out output_file.sdf.gz -prefix ligand_name -warts -maxconfs 1000000 -rms 0.01 –fixfile original_promysalin_model.pdb

Because structural diversity in the conformers was limited to the alkyl chain (i.e., the part of the chemical structure that was varied in this study), the number of conformers generated was much less than would be required if all internal degrees of freedom in the compound were explicitly modeled:

Analog	Number of conformers generated
(-)-11d	3
(-)-11e	8
(-)-11f	18
(-)-11g	36
(-)-1	113
(-)-11h	117
(-)-11i	178
(-)-11j	261
(-)-12	305

Having built these conformers, we replicated our earlier pipeline exactly, with the sole exception that we aligned each promysalin analog to our previous model of the promysalin/Sdh complex (rather than to carboxin from 2WU5). The resulting models were then refined and ranked using Rosetta, exactly as in our previous study.

5.2. Promysalin Synergy

5.2.1. Supporting Figures
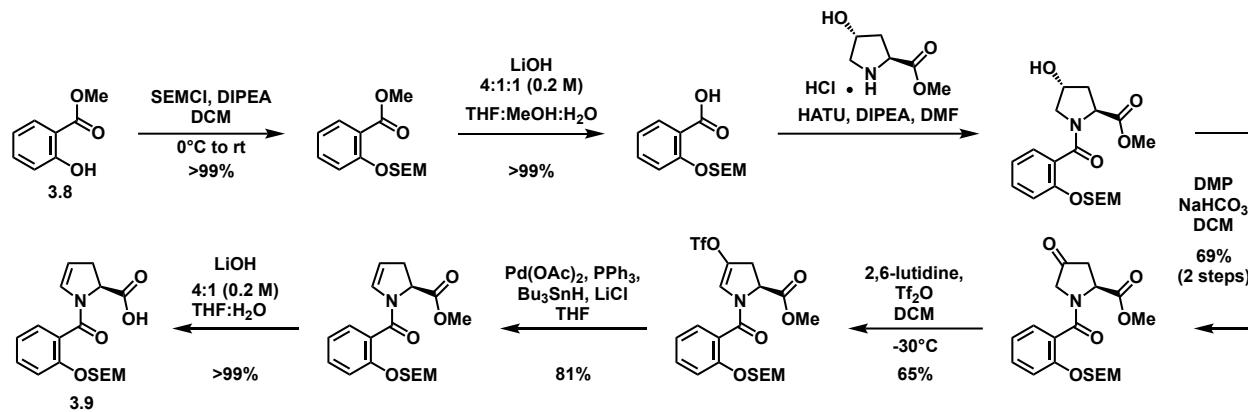
Scheme 5.2.1. Synthesis of acid fragment, **3.9**. Full procedures and characterization for **3.9** and **3.2** have been previously reported.[9]

5.2.2. Chemistry

5.2.2.1. General Methods

NMR spectra were obtained using the following spectrometers: Varian INOVA 600 (600/150 MHz), Varian INOVA 500 (500/125 MHz), Bruker 600 (600/125 MHz), or Varian INOVA 400 (400/100 MHz). Chemical shifts are in ppm relative to TMS and use the indicated solvent as an internal reference. The following abbreviations are used to describe signal multiplicities: s (singlet), d (doublet), t (triplet), q (quartet), m (multiplet), br (broad), dd (doublet of doublets), dt (doublet of triplets), etc. Accurate mass spectra were recorded on a ThermoScientific Exactive Plus Orbitrap MS.

Non-aqueous reactions were performed under an atmosphere of argon, in flame- dried glassware, with HPLC-grade solvents dried by passage through activated alumina. 2,6-lutidine, triethylamine, and diisopropylethylamine were freshly distilled from CaH_2 prior to use. Brine refers to a saturated aqueous solution of sodium chloride, sat. $NaHCO_3$ refers to a saturated aqueous solution of sodium bicarbonate, sat. NH_4Cl refers to a saturated aqueous solution of ammonium chloride, etc. 3Å molecular sieves were activated via heating to 220 °C overnight under vacuum, stored in a 120 °C oven, and flame-dried under

vacuum before use. "Column chromatography" refers to purification in a normal-phase gradient on a Biotage® flash chromatography purification system unless noted otherwise. All other chemicals were used as received from Oakwood, TCI America, Sigma-Aldrich, Alfa Aesar, CombiBlocks, or AK Scientific.

5.2.2.2. Procedures and Characterization
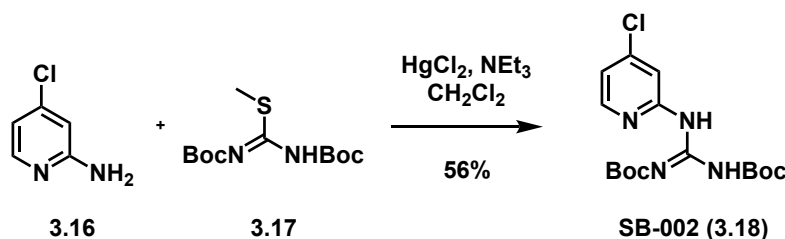
3.18: To a flask containing commercially available 2-amino-4-chloropyridine (0.100 g, 0.778 mmol) and 1,3-Bis(tert-butoxycarbonyl)-2-methyl-2-thiopseudourea (1.05 equiv, 0.237 g, 0.817 mmol) was added dichloromethane (0.1 M, 7.8 mL) under Argon. Cooled to 0°C and NEt$_3$ (4 equiv, 0.43 mL) was added followed by HgCl$_2$ (1.1 equiv, 0.232 g, 0.856 mmol). The reaction was stirred at 0°C for 1 hour and then at room temperature for 2 days. The reaction was diluted with ethyl acetate (10 mL per mmol of pyridine). Solution was filtered through celite and rinsed with ethyl acetate. Combined organics were washed with water then brine. Organics were dried over Na$_2$SO$_4$ and concentrated via rotary evaporation. The crude residue was purified by flash chromatography (gradient of 0->50% diethyl ether in hexanes) to yield pure **3.18** in 56% yield (0.162 g, 0.437 mmol). Characterization data matched those previously reported.[10]

1H NMR (500 MHz, cdcl3): δ 11.51 (s, 1H), 10.96 (s, 1H), 8.47 (s, 1H), 8.18 (d, J = 5.4 Hz, 1H), 7.02 (d, J = 5.4 Hz, 1H), 1.53 (s, 18H).

5.2.3. Biology

5.2.3.1. Bacteria Strains and Culture Conditions

P. aeruginosa PAO1 was acquired from Prof. Bettina A. Buttaro (Lewis Katz School of Medicine, Temple University) and *P. aeruginosa* PA14 was acquired from Prof. Joanna B. Goldberg (School of

Medicine, Emory University). All strains were grown from a freezer stock overnight (16-24 hr) with shaking at 37 °C, 200 rpm in Trypticase Soy Broth (TSB) media (5 mL) unless otherwise noted. Overnight cultures were diluted 1:100 in 5 mL of fresh media and grown at 37 °C, 200 rpm to an OD_{600} (measured on a Molecular Devices SpectraMax iD3 plate reader) reading of ~0.32 – mid-exponential growth. Bacteria were then diluted to a concentration of 0.004 according to the following equation: (x μL regrow culture)*(OD reading) = (0.004)*(volume of diluted bacteria culture needed).

5.2.3.2. IC_{50} Assay

Compounds were dissolved in water, 10% DMSO in water, or 5% Tween80 5% DMSO in water; vehicle and concentrations are indicated on respective data. Compounds were serially diluted 2-fold in water to produce 12 concentrations yielding 100 μL per well. Negative controls of each compounds respective vehicle were employed. 100 μL of diluted bacteria was plated into each well, then the plates were incubated statically for 24 hours at 37 °C. OD_{600} readings were taken at this point, and IC_{50} and IC_{90} values were calculated by fitting OD readings vs. concentrations with a four-parameter logistic S52 model. Compounds were tested in triplicate from three separate overnight cultures and averaged.

5.2.3.3. Checkerboard Assay

Compounds were dissolved in water, 10% DMSO in water, or 5% Tween80 5% DMSO in water; vehicle and concentrations are indicated on respective data. One compound was serially diluted 2-fold in vehicle 11 times so there was no compound in the final column (11 concentrations). The second compound was added to all wells in the first 7 rows in decreasing concentrations. Vehicle was added to bring final volume to 100 μL. 100 μL of diluted bacteria was plated into each well, then the plates were incubated statically for 24 hours at 37 °C. OD_{600} readings were taken at this point, and IC_{50} and IC_{90} values were calculated by fitting OD readings vs. concentrations with a four-parameter logistic S52 model. The

following equation was used to determine synergy ($FIC_{50} < 0.5$), antagonism ($FIC_{50} > 4$), or indifference ($FIC_{50} = 0.5\text{-}4$). The assay was tested in triplicate from three separate overnight cultures.
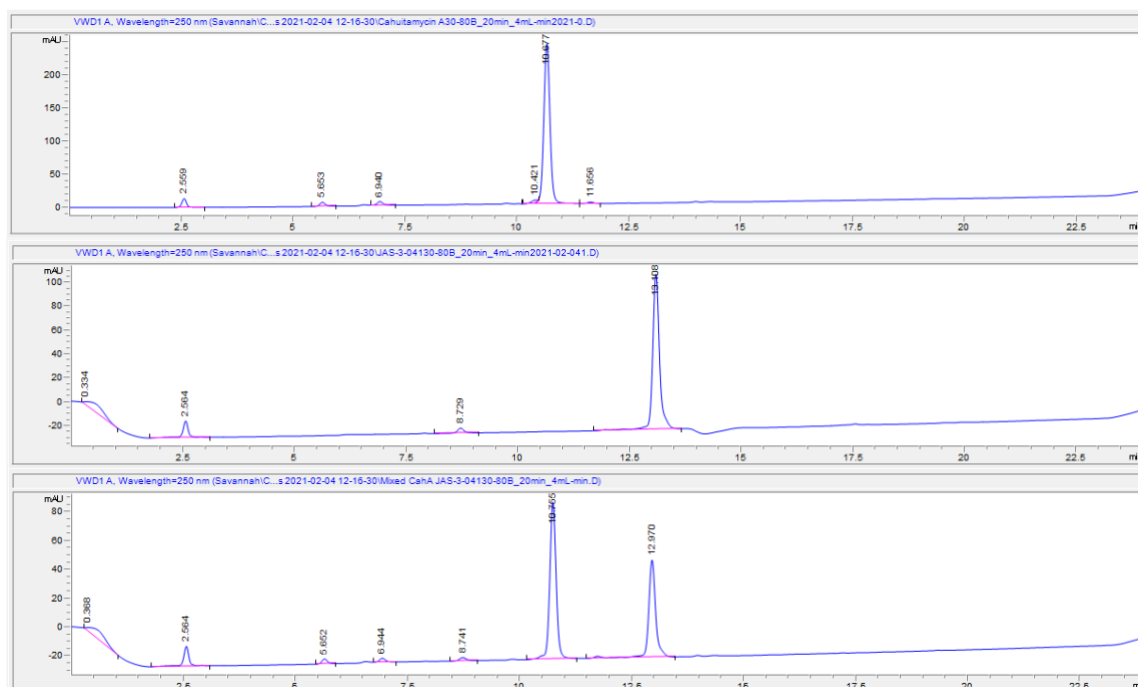
$$\frac{A}{IC_{50_A}} + \frac{B}{IC_{50_B}} = FIC_{50_A} + FIC_{50_B} = FIC_{50}\ Index$$

5.3. Cahuitamycins

5.3.1. Supporting Figures
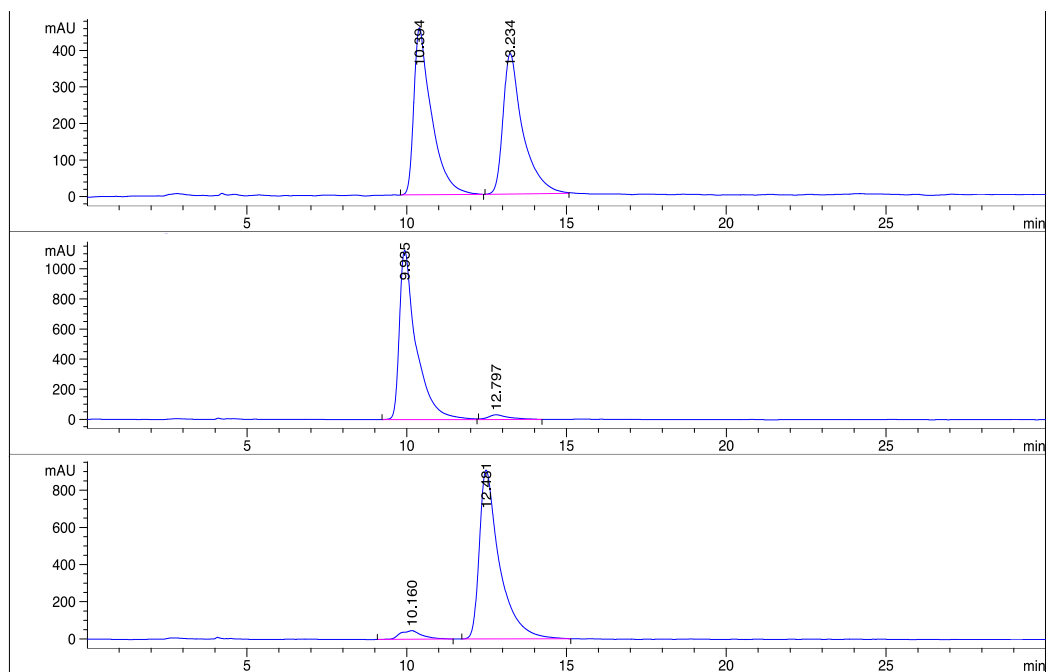
Figure 5.3.1: *Chiral HPLC chromatograms of racemic **4.39** (top), (+)-**4.39** (middle), and (−)-**4.39** (bottom).*

Figure 5.3.2: *Analytical C18-HPLC chromatogram of authentic cahuitamycin A (top), synthetic (+)-4.1 (middle), and a co-injecting of cahuitamycin A and (+)-4.1 (bottom).*

| Position	Authentic Cahuitamycin A	Synthetic (+)-4.1
1		
2	2.35 (m)	2.43 (t, 6.4)
3	3.37 (dd, 8.2, 5.2), 3.53 (m)	3.43 (m), 3.48 (m)
4		
5	4.45 (m)	5.02 (dd, 5.4, 1.3)
6	1.73 (m), 2.02 (m)	1.86 (m), 2.16 (m)
7	1.94 (m), 1.98 (m)	1.58 (m), 1.66 (m)
8	3.53 (m), 3.62 (m)	2.88 (q, 12.8), 3.03 (t, 12.7)
9		
10	4.31 (m)	5.35 (dd, 8.9, 4.3)
11	1.63 (m), 1.85 (m)	1.64 (m), 1.88 (m)
12	1.63 (m), 1.67 (m)	1.71 (m), 1.81 (m)
13	3.47 (t, 6.4)	3.54 (m)
14	8.25 (s)	8.29 (s)
15		
16	4.46 (m)	4.52 (q, 5.3)
17	3.87 (d, 4.8)	3.81 (dd, 11.1, 5.1), 3.85 (m)
18		
19	5.09 (dd, 10.5, 8.0)	5.08 (dd, 10.5, 8.0)
20	4.61 (td, 8.3, 5.3), 4.68 (t, 9.6)	4.62 (t, 8.2), 4.68 (td, 10.6, 2.7)
21		
22		
23	7.70 (d, 7.8)	7.70 (dd, 7.9, 1.7)
24	6.91 (t, 7.6)	6.90 (t, 7.6)
25	7.42 (t, 7.8)	7.42 (t, 7.9)
26	6.97 (d, 8.4)	6.97 (d, 8.3)
27		

Table 5.3.1. *Comparison of ^{1}H-NMR signals in CD$_3$OD of authentic cahuitamycin A* and synthetic (+)-4.1. Notable differences highlighted in yellow.*
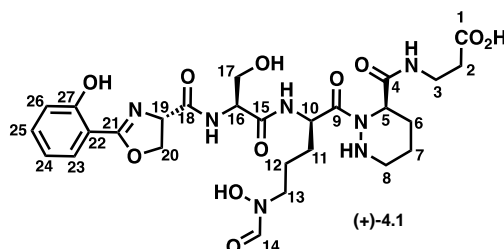
Position	^{1}H	^{13}C	COSY	TOCSY	HMBC
1		177.76			2, 3
2	2.43 (t, 6.4)	35.48	3	3	1, 3
3	3.43 (m), 3.48 (m)	35.42	2	2	1, 2, 4
4		171.57			3, 5
5	5.02 (dd, 5.4, 1.3)	51.31	6	6, 7, 8	4, 6, 7
6	1.92 (m), 2.16 (m)	25.76	5, 7	5, 7, 8	5, 7
7	1.58 (m), 1.66 (m)	20.72	6, 8	5, 6, 8	5, 6
8	2.88 (q, 12.8), 3.03 (t, 12.7)	46.5	7	5, 6, 7	6, 7
9		173.94			10
10	5.35 (dd, 8.9, 4.3)	49.03	11	11, 12, 13	9, 11
11	1.68 (m), 1.88 (m)	27.85	10, 12	10, 12, 13	10, 12, 13
12	1.72 (m), 1.82 (m)	22.4	11, 13	10, 11, 13	11, 13
13	3.54 (m)	45.8	12	10, 11, 12	11, 12, 14
14	8.29 (s)	162.59			13
15		170.53			16, 17
16	4.52 (q, 5.3)	55.33	17	17	15, 17
17	3.81 (dd, 11.1, 5.1), 3.85 (m)	61.65	16	16	15, 16
18		171.87			19, 20
19	5.08 (dd, 10.5, 8.0)	68.08	20	20	18, 20
20	4.62 (t, 8.2), 4.68 (td, 10.6, 2.7)	69.27	19	19	19, 21
21		167.42			19, 20, 23, 26
22		110.31			24, 26
23	7.70 (dd, 7.9, 1.7)	128.11	24	24, 25, 26	21, 22, 24, 25, 27
24	6.90 (t, 7.6)	118.65	23, 25	23, 25, 26	22, 23, 25, 26, 27
25	7.42 (t, 7.9)	133.62	24, 26	23, 24, 26	23, 24, 27
26	6.97 (d, 8.3)	116.33	25	23, 24, 25	22, 23, 24, 25
27		159.6			23, 25, 26

Table 5.3.2. *2D-NMR characterization of synthetic (+)-**4.1***.
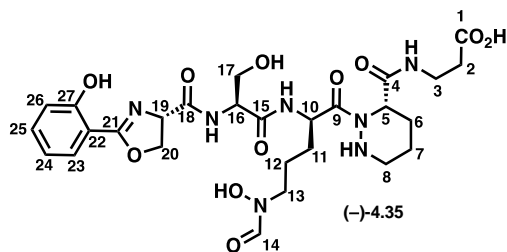
Position	¹H	¹³C	COSY	TOCSY	HMBC
1		175.44			
2	2.53 (s)	34.36	3	3	1, 3
3	3.49 (m)	35.71	2	2	1, 2, 4
4		170.49			
5	5.02 (d, 5.6)	51.72	6	6, 7, 8	4, 6, 7
6	1.81 (m), 2.30 (13.2)	24.83	5, 7	5, 7, 8	5, 8
7	1.54 (m), 1.79 (m)	20.8	6, 8	5, 6, 8	4, 5
8	2.77 (q, 12.8), 3.07 (d, 13.7)	46.81	7	5, 6, 7	6
9					
10	5.35 (d, 9.4)	49.09	11	11, 12, 13	
11	1.69 (m)	22.36	10, 12	10, 12, 13	12, 13
12	1.80 (m)	28.07	11, 13	10, 11, 13	11, 13
13	3.57 (m)	45.7	12	10, 11, 12	11, 12, 14
14	8.29 (s)	45.83			
15		170.58			
16	4.52 (q, 5.5)	55.15	17	17	15, 17
17	3.82 (m)	61.45	16	16	15, 16
18		171.89			
19	5.10 (dd, 10.5, 7.9)	67.94	20	20	18, 20, 21
20	4.61 (t, 8.3), 4.68 (t, 9.6)	69.31	19	19	18, 19, 21
21		167.34			
22		110.03			
23	7.69 (dd, 7.9, 1.7)	128.11	24, 25	24, 25, 26	21, 25, 27
24	6.90 (t, 7.6)	118.54	23, 25, 26	23, 25, 26	22, 26
25	7.39 (t, 8.2)	133.61	23, 24, 26	23, 24, 26	23, 27
26	6.97 (d, 8.3)	116.31	24, 25	23, 24, 25	22, 24, 27
27		159.53			

Table 5.3.3. *2D-NMR characterization of synthetic (−)-**4.35**.*
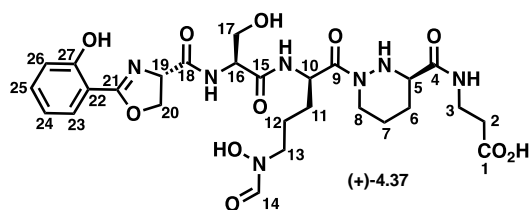
Position	^{1}H	^{13}C	COSY	TOCSY	HMBC
1		174.65			
2	2.50 (t, 6.5)	33.71	3	3	1, 3
3	3.50 (m)	35.25	2	2	1, 2
4					
NH(piz)	2.85 (d, 9.6)		5, 6	6	
5	4.23 (m)	41.41	NH(piz), 6	NH(piz), 6, 8	7, 8
6	1.65 (m), 1.90 (m)	22.3	NH(piz) 5, 7	NH(piz), 5, 7, 8	5, 7, 8
7	1.90 (m), 2.01 (m)	26.91	6, 8	5, 6, 8	5, 6, 8
8	3.47 (m), 3.41 (m)	59.67	7	NH(piz), 5, 6, 7	5, 7, 8, 9
9		172.44			
10	5.28 (m)	49.44	11	11, 12, 13	9, 11, 12, 15
11	1.67 (m), 1.77 (m)	22.35	10, 12	10, 12, 13	10, 12, 13
12	1.73 (m), 1.65 (m)	27.73	11, 13	10, 11, 13	11, 13
13	3.57 (m), 3.65 (m)	45.81	12	10, 11, 12	11, 12, 14
14	8.30 (s)	171.45			
15		170.39			
16	4.44 (q, 5.2)	55.4	17	17	15, 17
17	3.82 (m)	61.61	16	16	15, 16
18		171.89			
19	5.04 (dd, 10.5, 7.9)	67.92	20	20	18, 20, 21, 22
20	4.57 (t, 8.2), 4.64 (t, 8.2)	69.25	19	19	18, 20, 21
21		167.36			
22		110.14			
23	7.65 (dd, 7.9, 1.7)	128.15	24	24, 25, 26	21, 25, 26, 27
24	6.86 (t, 7.5)	118.59	23, 25	23, 25, 26	22, 23, 25, 26, 27
25	7.38 (ddd, 8.6, 7.2, 1.7)	133.66	24, 26	23, 24, 26	22, 23, 24, 26, 27
26	6.93 (dd, 8.4, 1.1)	116.35	25	23, 24, 25	22, 24, 25, 26, 27
27		159.79			

Table 5.3.4. *2D-NMR characterization of synthetic* **(+)-4.37**.
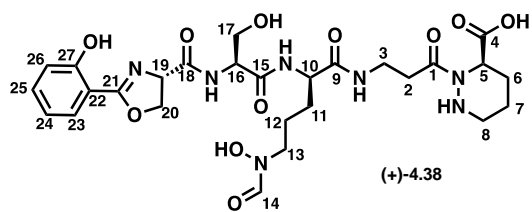
Position	¹H	¹³C	COSY	TOCSY	HMBC
1		173.97			
2	2.89 (m), 2.80 (m)	31.87	3	3	1, 3
3	3.46 (dt, 7.0, 3.7)	35.56	2	2	2, 9
4		171.97			
5	5.10 (m)	51.93	6	6, 7, 8	1, 4, 6, 7
6	1.82 (dt, 13.4, 5.7), 2.26 (d, 13.5)	25.44	5, 7	5, 7, 8	4, 7, 8
7	1.55 (m), 1.63 (m)	21.57	6, 8	5, 6, 8	6, 8
8	2.97 (d, 13.8), 2.78 (m)	46.7	7	6, 7, 8	1, 7
9		172.2			
10	4.38 (m)	52.83	11	11, 12, 13	9, 11, 12, 15
11	1.68 (m), 1.88 (m)	22.74	10, 12	10, 12, 13	10, 12, 13
12	1.64 (m), 1.94 (m)	27.96	11, 13	10, 12, 13	10, 11, 13
13	3.58 (td, 6.4, 2.5), 3.52 (m)	45.6	12	10, 11, 12	11, 12, 14
14	8.29 (s)	157.92			13
15		171.2			
16	4.42 (m)	55.76	17	17	15, 17, 18
17	3.84 (qd, 11.1, 5.2)	61.39	16	16	15, 16
18		172.3			
19	5.09 (m)	67.97	20	20	18, 20, 21
20	4.66 (m)	69.14	19	19	19, 21
21		166.98			
22		159.3			
23	7.70 (dd, 7.9, 1.7)	128.49	24	24, 25, 26	21, 22, 25, 26
24	6.90 (t, 7.8)	118.55	23, 25	23, 25, 26	22, 23, 25, 26, 27
25	7.42 (ddd, 8.8, 7.3, 1.7)	133.56	24, 26	23, 24, 26	22, 23, 26, 27
26	6.97 (dd, 8.4, 1.1)	116.44	25	24, 25, 26	21, 22, 23, 24, 27
27		110.05			

Table 5.3.5. 2D-NMR characterization of synthetic (+)-*4.38*.

Reagents (eq.)	Solvent	Temp.	Time	eq. (+)-20	% yield
DCC (1.5), DMAP (0.1)	DCC	0 C -> RT	16 hr	1.1	0
EDC (3.0), HOBt (3.0), NEt3 (6.0)	DMF	0 C -> RT	16 hr	1.1	0
HATU (1.2), DIPEA (4.5)	DMF	0 C -> RT	16 hr	1.1	0
PyBroP (1.0), DIPEA (3.0)	DCM	0 C -> RT	16 hr	1.1	0
1.) SOCl2 (xs), then 2.) NaHCO3 (3.0)	1.) DCM, then 2.) DCM/H2O	1.) reflux, then 2.) 0 C -> RT	1.) 30 min, then 2.) 16 hr	1.1	0
1.) (COCl)2 (2.0), DMF (cat.), then 2.) AgCN (0.1)	1.) DCM, then 2.) benzene	1.) 0 C, then 2.) reflux	1.) 30 min, then 2.) 1 hr	1.1	0
1.) PivCl (1.0) NEt3 (1.0), then 2.) LiCl (cat.), NEt3 (3.0)	1.) DCM, then 2.) DCM	1.) 0 C, then 2.) RT -> reflux	1.) 30 min, then 2.) 12 hr	1.5	0
1.) DAST (1.5), then 2.) NEt3 (2.0)	1.) DCM, then 2.) DCM	1.) 0 C, then 2.) reflux	1.) 1 hr, then 2.) 16 hr	0.5	0
BTFFH (1.15) DIPEA (3.5)	DCM	RT -> 80 C (sealed tube)	16 hr	1	0
TCFH (1.0), NMI (2.0)	CH3CN	RT -> 60 C	16 hr	1	0
1.) Cyanuric Chloride (0.33), NEt3 (cat.), then 2.) NaHCO3 (xs)	1.) DCM, then 2.) DCM/H2O	1.) RT, then 2.) 0 C -> RT	1.) 3 hr, then 2.) 16 hr	1.1	trace
1.) Ghosez's reagent (1.4), then 2.) Sc(Otf)3 (0.1)	toluene	1.) 0 C, then 2.) RT	1.) 30 min, then 2.) 2 hr	0.5	trace
1.) Ghosez's reagent (1.4), then 2.) AgCN (0.5)	benzene	1.) 0 C, then 2.) reflux	1.) 30 min, then 2.) 1 hr	0.5	57%
1.) Ghosez's reagent (1.4), then 2.) AgCN (0.33)	benzene	1.) 0 C, then 2.) reflux	1.) 30 min, then 2.) 1 hr	0.33	80%

Table 5.3.6. *Reaction screen for the synthesis of key intermediate (+)-**5.3.8**. All reactions are done relative to 1.0 equivalents of (−)-**4.49**. For all two-step sequences, (−)-**4.49** was added in the first step and (+)-**4.39** was added in the second step.*

Scheme 5.3.1. *Synthesis of key intermediate (+)-**5.3.8**, featuring compounds not shown in main text.*

a.) O-tert-buty-N,N'-diisopropylisourea, tert-BuOH, reflux b.) Pd/C, H2, EtOAc c.) 75% BPO, Cs2CO3, DCM d.) EDC, formic acid, DCM, 0° C to RT e.) BnBr, Hünig's base, MeOH f.) TFA, DCM g.) Fmoc-OSu, H2O, THF, NaHCO3 h.) PCC, DCM i.) Dibenzyl azodicarboxylate, L-proline, CH3CN, 0° C, then NaBH4, EtOH j.) TBSCl, imidazole, DMF k.) NaH, DMF, 0° C l.) TBAF, THF, 0° C m.) TEMPO, NaClO2, NaClO, CH3CN n.) KOH, THF o.) EDC, HOBt, DMF, NEt3, β-alanine benzyl ester TsOH, 0° C to RT p.) (−)-15, Ghosez's reagent, DCM, 0° C, then (+)-20, AgCN, benzene, reflux
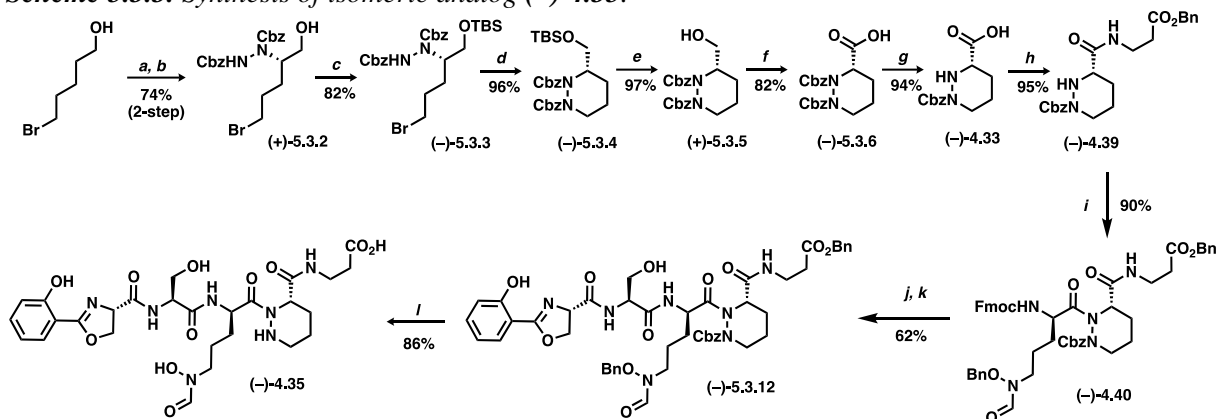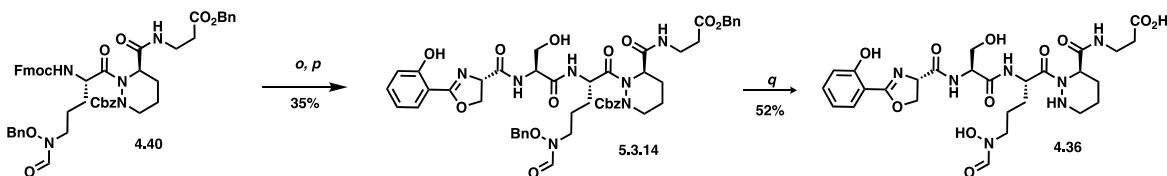
Scheme 5.3.2. *Synthesis of (+)-**4.1***
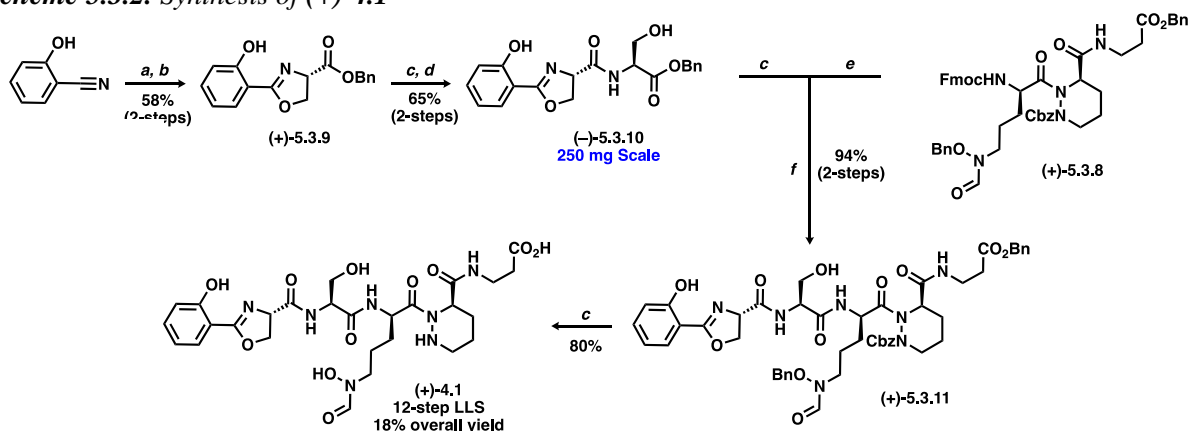
Conditions: a.) AcCl, MeOH b.) 1,2-DCE, L-serine benzyl ester HCl, reflux c.) Pd/C, H2, MeOH d.) EDC, HOBt, DMF, NEt3, L-serine benzyl ester HCl, 0° C to RT e.) 4-(aminomethyl)piperidine, DCM, then pH 5.5 buffer f.) EDC, HOBt, CH3CN, NEt3, 0° C to RT

135

Scheme 5.3.3. *Synthesis of isomeric analog (−)-4.35.*

a.) PCC, DCM *b.)* Dibenzyl azodicarboxylate, D-proline, CH₃CN, 0° C, *then* NaBH₄, EtOH *c.)* TBSCl, imidazole, DMF *d.)* NaH, DMF, 0° C *e.)* TBAF, THF, 0° C *f.)* TEMPO, NaClO₂, NaClO, CH₃CN *g.)* KOH, THF *h.)* EDC, HOBt, DMF, NEt₃, β-alanine benzyl ester TsOH, 0° C to RT *i.)* (−)-15, Ghosez's reagent, DCM, 0°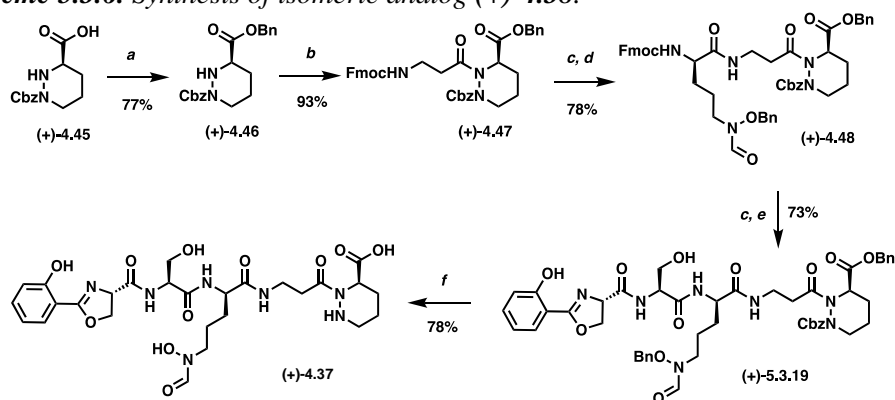 C, then (+)-20, AgCN, benzene, reflux *j.)* 4-(aminomethyl)piperidine, DCM, then pH 5.5 buffer *k.)* EDC, HOBt, CH₃CN, NEt₃, Hydrogenation Product of (−)-18 (see Supporting Scheme 2) *l.)* Pd/C, MeOH, H₂

Scheme 5.3.4. *Synthesis of isomeric analog 4.36.*
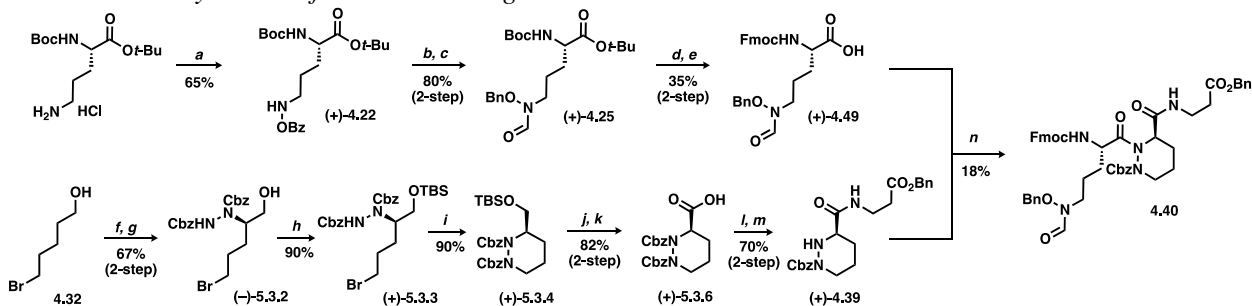
a.) 75% BPO, Cs₂CO₃, DCM *b.)* EDC, formic acid, DCM, 0° C to RT *c.)* BnBr, Hünig's base, MeOH *d.)* TFA, DCM *e.)* Fmoc-OSu, H₂O, THF, NaHCO₃ *f.)* PCC, DCM *g.)* Dibenzyl azodicarboxylate, L-proline, CH₃CN, 0° C, *then* NaBH₄, EtOH *h.)* TBSCl, imidazole, DMF *i.)* NaH, DMF, 0° C *j.)* TBAF, THF, 0° C *k.)* TEMPO, NaClO₂, NaClO, CH₃CN *l.)* KOH, THF *m.)* EDC, HOBt, DMF, NEt₃, β-alanine benzyl ester TsOH, 0° C to RT *n.)* (−)-15, Ghosez's reagent, DCM, 0° C, then (+)-20, AgCN, benzene, reflux

o.) 4-(aminomethyl)piperidine, DCM, then pH 5.5 buffer *p.)* EDC, HOBt, CH₃CN, NEt₃, (−)-4.34, 0° C to RT *q.)* Pd/C, MeOH, H₂

Scheme 5.3.5. *Synthesis of isomeric analog (+)-4.37.*
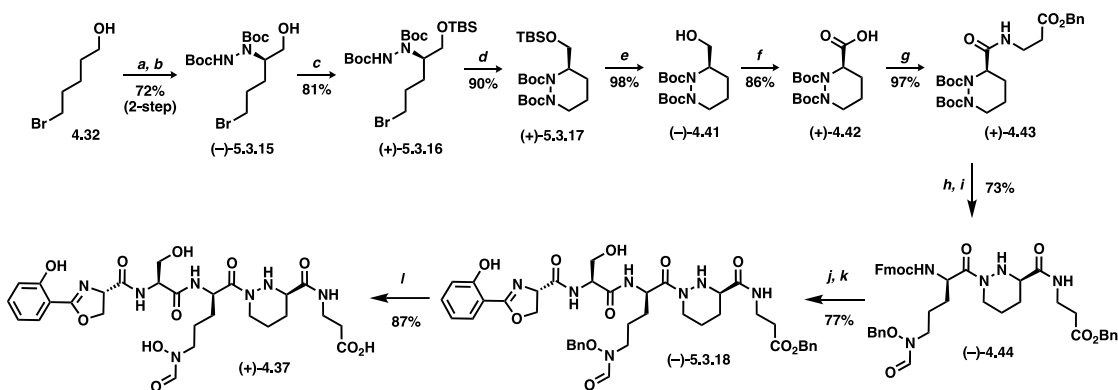
a.) PCC, DCM b.) Di-tert-butyl azodicarboxylate, L-proline, CH₃CN, 0° C, then NaBH₄, EtOH c.) TBSCl, imidazole, DMF d.) NaH, DMF, 0° C e.) TBAF, THF, 0° C f.) TEMPO, NaClO₂, NaClO, CH₃CN 0° C to RT g.) EDC, HOBt, DMF, NEt₃, β-alanine benzyl ester TsOH, 0° C to RT h.) TFA, DCM i.) EDC, HOBt, CH₃CN, NEt₃, (−)-12, 0° C to RT j.) 4-(aminomethyl)piperidine, DCM, then pH 5.5 buffer k.) EDC, HOBt, CH₃CN, NEt₃, Hydrogenation Product of (−)-18 (see Supporting Scheme 2), 0° C to RT l.) Pd/C, MeOH, H₂

Scheme 5.3.6. *Synthesis of isomeric analog (+)-4.38.*

a.) K₂CO₃, BnBr, DMF b.) Fmoc-β-ala, Ghosez's reagent, DCM, 0° C, then (+)-21, AgCN, benzene, reflux c.) 4-(aminomethyl)piperidine, DCM, then pH 5.5 buffer d.) EDC, HOBt, CH₃CN, NEt₃, (−)-12, 0° C to RT e.) EDC, HOBt, CH₃CN, NEt₃, Hydrogenation Product of (−)-18 (see Supporting Scheme 2) 0° C to RT f.) Pd/C, MeOH, H₂

5.3.2. Chemistry

5.3.2.1. General Methods

NMR spectra were recorded using the following spectrometers: Varian INOVA500, Varian INOVA400, VNMR400, and Bruker Ascend 600. All NMR spectra were recorded under ambient temperature. Chemical shifts are quoted in ppm relative to solvents used (^{1}H: δ = 7.26 and ^{13}C: δ = 77.16 for residual CHCl₃, ^{1}H: δ = 3.49, 1.09 and ^{13}C: δ = 50.41 for residual CH₃OH, ^{1}H: δ = 1.56 for residual H₂O. The abbreviations used to describe splitting are as follows: s (singlet), d (doublet), t (triplet), q (quartet), m (multiplet), dd (doublet of doublets), dt (doublet of triplets), etc.

Accurate mass spectra were recorded on a Thermo LTQ-FTMS using either APCI or ESI techniques. Infrared spectra were obtained using a Thermoscientific Nicolet with an attenuated total reflectance (ATR) with a Germanium crystal. Samples were tested neat or in chloroform. Peaks are reported in cm^{-1} and described as either weak (w), strong (s), or broad (b).

Specific rotations were obtained with 1 dm path length using a Perkin Elmer Model 341 Polarimeter with a Na/Hal lamp set to 598 nm. Samples were dissolved in either chloroform or water depending on the solubility restrictions of some compounds. In all cases, the polarimeter was zeroed to the solvent first. Measurements were taken over several minutes and then adjusted based on concentration.

Non-aqueous reactions were performed under an atmosphere of argon in flame-dried glassware with HPLC-grade solvents dried by passage through alumnina. Amine bases were freshly distilled over CaH$_2$ prior to use. Brine refers to a saturated aqueous solution of sodium chloride. Purification via flash chromatography refers to usage of Biotage Isolera One Automated column. Reactions monitored via thin-layer chromatography (TLC) using EMD Millipore® TLC silica gel glass plates with various stains specified in each procedure. Reactions monitored by LCMS were injected into an Agilent Technologies 1220 Infinity HPLC Liquid Chromatograph connected to an Advion Expression Compact Mass Spectrometer. Solvents used were HPLC grade water and acetonitrile each spiked with 0.1% formic acid.

### 5.3.2.2. Procedures and Characterization
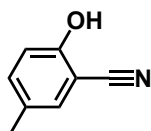
4.16

4.16: To a flask containing commercially available 2-hydroxy-5-methylbenzaldehyde (2.013 g, 14.791 mmol) and formic acid (40 mL) was added hydroxylamine hydrochloride (1.337 g, 19.228 mmol) followed by sodium formate (1.308 g, 19.228 mmol). The reaction was heated to 100 °C and stirred for 5 hours. The reaction was then diluted with ice water and neutralized with saturated aqueous bicarbonate. Aqueous was

extracted three times with diethyl ether then dried over sodium sulfate and concentrated via rotary evaporation. The crude residue was purified by flash chromatography (gradient of 0->15% ethyl acetate in hexanes) to yield pure **4.16** in 72% yield (1.418 g, 10.654 mmol).

1H NMR (400 MHz, cdcl3): δ 7.29 – 7.25 (m, 1H), 7.24 (d, J = 2.4 Hz, 1H), 6.87 (d, J = 8.3 Hz, 1H), 5.99 (s, 1H), 2.27 (s, 3H).

13C NMR (126 MHz, cdcl3): δ 156.55, 135.66, 132.58, 130.51, 116.57, 116.52, 99.02, 20.12.
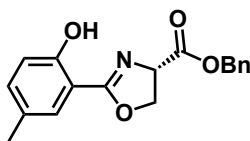
(+)-4.17

(+)-4.17: To a flask containing **4.16** (1.402 g, 10.533 mmol) and methanol (5.1 mL) was slowly added acetyl chloride (6.0 mL), resulting in the evolution of heat. The reaction was stirred at room temperature overnight, during which a precipitate was formed. Precipitate was collected and the crude methyl imidate was taken on without further purification.

To a flask containing L-serine benzyl ester hydrochloride (1.769 g, 7.634 mmol) was added a solution of the crude residue in 1,2-dichloroethane (140 mL). Triethylamine (1.1 mL) was added and the reaction was stirred for 24 hours. Insoluble salts were filtered off and filtrate was washed with bicarbonate. Organic layer was dried over sodium sulfate and concentrated via rotary evaporation. The crude residue was purified by flash chromatography (gradient of 0->30% ethyl acetate in hexanes) to yield pure **(+)-4.17** in 53% yield (1.155 g, 3.710 mmol).

1H NMR (400 MHz, cdcl3): δ 11.47 (s, 1H), 7.46 (dt, J = 2.4, 0.6 Hz, 1H), 7.43 – 7.30 (m, 5H), 7.24 – 7.17 (m, 1H), 6.92 (d, J = 8.4 Hz, 1H), 5.28 – 5.18 (m, 2H), 5.01 (dd, J = 10.4, 7.5 Hz, 1H), 4.67 (dd, J = 8.8, 7.5 Hz, 1H), 4.61 – 4.52 (m, 1H), 2.28 (s, 3H).

13C NMR (126 MHz, cdcl3): δ 170.44, 167.77, 157.98, 135.33, 135.08, 128.81, 128.66, 128.40, 128.33, 128.07, 116.85, 109.75, 77.41, 77.16, 76.91, 68.91, 67.59, 67.53, 20.48.

IR (neat): 697, 746, 1185, 1640, 1726, 2921, 3038.

[α]^{25}$_D$: +7.6 ° (10 mg/mL in chloroform)

HRMS: [C$_{18}$H$_{18}$NO$_4$]$^+$ calcd. 312.12303, found 312.12272.

(−)-4.19
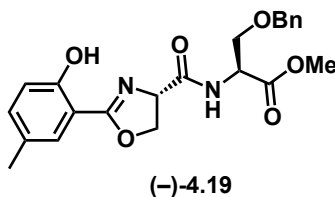
(−)-4.19: To a flask containing **(+)-4.17** (0.096 g, 0.308 mmol) and ethyl acetate (25 mL) was added 10% palladium on activated charcoal (10 wt % of starting material, 0.031 g). The flask was purged, backfilled with hydrogen gas, and stirred at room temperature until consumption of starting material was observed by TLC. The mixture was passed through a Whatman filter and concentrated by rotary evaporation to afford **4.18**. The crude acid was taken on without further purification.

To a flask containing EDC (0.177 g, 0.924 mmol), HOBt (0.141 g, 0.924 mmol), and O-Benzyl-L-serine Methyl Ester Hydrochloride (0.083 g, 0.339 mmol) at 0 °C was added a solution of crude residue in dimethylformamide (10 mL). Triethylamine (0.5 mL) was added slowly, and pH was confirmed to be basic before stirring from 0 °C to room temperature for 16 hours. The reaction was diluted in saturated sodium bicarbonate and the aqueous layer was extracted three times with ethyl acetate. The combined organic layers were washed with brine, dried over anhydrous sodium sulfate, and concentrated by rotary evaporation. The crude residue was purified by flash chromatography to yield pure **(−)-4.19** in 68% yield (0.087 g, 0.211 mmol).

1H NMR (500 MHz, cdcl3): δ 11.21 (s, 1H), 7.51 (dd, J = 1.7, 0.7 Hz, 1H), 7.39 – 7.12 (m, 8H), 6.97 (d, J = 8.4 Hz, 1H), 4.99 (dd, J = 10.9, 8.0 Hz, 1H), 4.72 (dt, J = 8.3, 3.4 Hz, 1H), 4.67 – 4.56 (m, 2H), 4.52 – 4.42 (m, 2H), 3.86 (dd, J = 9.5, 3.4 Hz, 1H), 3.77 (s, 3H), 3.61 (dd, J = 9.5, 3.4 Hz, 1H), 2.31 (s, 3H).

13C NMR (126 MHz, cdcl3): δ 170.75, 170.23, 167.95, 157.87, 137.31, 135.32, 128.60, 128.48, 128.41, 128.32, 127.93, 127.85, 127.78, 116.92, 109.67, 73.21, 69.51, 68.85, 68.08, 52.81, 52.54, 20.48.

IR (neat): 1218, 1646, 1740, 2920, 3062, 3274.

**[α]^{25}$_D$:** -8.5 ° (10 mg/mL in chloroform)

(−)-4.21
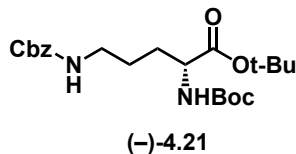
(−)-4.21: To a flask containing commercially available N_α-Boc-N_δ-Cbz-D-Ornithine (1.082 g, 2.95 mmol) and dichloromethane (16 mL) was added *O-tert*-Butyl-*N,N'*-diisopropylisourea (3.55 g, 14.77 mmol) followed by *tert*-butanol (16 mL). The reaction was heated to 50 °C and stirred for 24 hours at which point solvent was removed by rotary evaporation. The crude residue was purified by flash chromatography (gradient of 0->100% ethyl acetate in hexanes) to yield pure **(−)-4.21** as a pale oil in quantitative yield (1.24 g, 2.94 mmol). Characterization data matched those previously reported.[11]

^{1}H NMR (500 MHz, CDCl$_3$): δ 7.40 – 7.27 (m, 5H), 5.08 (s, 2H), 4.92 (s, 1H), 4.16 (q, *J* = 7.3 Hz, 1H), 3.21 (q, *J* = 6.5 Hz, 2H), 1.84 – 1.76 (m, 1H), 1.67 – 1.49 (m, 3H), 1.45 (s, 9H), 1.43 (s, 9H).

^{13}C NMR (126 MHz, CDCl$_3$): δ 171.79, 156.51, 155.54, 136.73, 128.64, 128.21, 110.14, 82.17, 79.87, 66.75, 53.67, 40.75, 30.44, 28.46, 28.13, 25.89.

IR (neat): 1695 (s), 2930 (w), 2980 (w), 3353 (b)

[α]^{25}$_D$: -0.8 ° (10 mg/mL in chloroform)

(−)-4.22
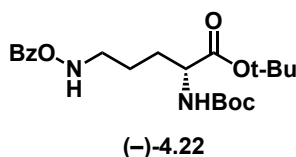
(−)-4.22: To a flask containing **(−)-4.21** (9.05 g, 21.45 mmol) and ethyl acetate (200 mL) was added 10% palladium on activated charcoal (10 wt. % of starting material, 0.9 g). The flask was purged, backfilled with hydrogen gas, and stirred at room temperature until consumption of starting material was observed by TLC. The reaction mixture was filtered through celite and solvent was removed by rotary evaporation. The crude amine was taken on without further purification.

To a flask containing 75% benzoyl peroxide (13.85 g, 42.9 mmol) and cesium carbonate (20.95 g, 64.35 mmol) was added dichloromethane (20 mL). The suspension was stirred for two hours at which time a solution of the crude material in 10 mL dichloromethane and added. The reaction was stirred for 20 hours, at which point the mixture was filtered through celite and the solvent was removed by rotary evaporation. The crude residue was purified by flash chromatography (gradient of 0->100% ethyl acetate in hexanes) to yield pure **(–)-4.22** as a pale oil in 74% yield (6.48 g, 15.87 mmol). Characterization data matched those previously reported.[12]

^{1}H NMR (600 MHz, CDCl$_3$): δ 7.99 (d, *J* = 7.8 Hz, 2H), 7.56 (t, *J* = 7.4 Hz, 1H), 7.43 (t, *J* = 7.1 Hz, 2H), 5.13 (d, *J* = 8.3 Hz, 1H), 4.19 (q, *J* = 7.5, 6.6 Hz, 1H), 3.15 (h, *J* = 5.6, 5.0 Hz, 2H), 1.90 (dq, *J* = 14.9, 9.0, 8.1 Hz, 1H), 1.77 – 1.62 (m, 3H), 1.43 (s, 9H), 1.41 (s, 9H).

^{13}C NMR (151 MHz, CDCl$_3$): δ 171.74, 166.85, 155.41, 133.37, 129.34, 128.52, 128.29, 81.98, 79.67, 53.70, 52.03, 30.50, 28.31, 27.98, 23.18.

IR (neat): 1716 (s), 2977 (w), 3367 (b)

[α]$^{25}_D$: -12 ° (10 mg/mL in chloroform)

(–)-4.23
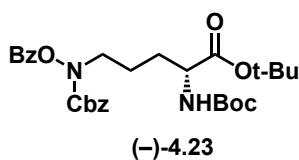
(–)-4.23: To a flask containing **(–)-4.22** (0.272 g, 0.666 mmol) 10% aqueous acetic acid (6.8 mL). Benzyl chloroformate (0.19 mL, 1.332 mmol) was dissolved in 1,4-dioxane (9 mL) and added to flask. The reaction was stirred at room temperature overnight. The reaction was quenched with aqueous bicarbonate and aqueous layer was extracted three times with dichloromethane. Combined organics were washed with water then brine. The crude residue was purified by flash chromatography (gradient of 0->15% ethyl acetate in hexanes) to yield pure **(–)-4.23** in 97% yield (0.350 g, 0.645 mmol).

1H NMR (500 MHz, cdcl3): δ 8.01 (dd, J = 8.4, 1.4 Hz, 2H), 7.57 (d, J = 7.5 Hz, 1H), 7.42 (dd, J = 8.3, 7.5 Hz, 2H), 7.26 (s, 5H), 5.15 (s, 2H), 5.07 (d, J = 8.4 Hz, 1H), 4.13 (d, J = 6.7 Hz, 1H), 3.75 (d, J = 4.8 Hz, 2H), 2.11 (s, 2H), 1.86 (s, 1H), 1.75 – 1.59 (m, 3H), 1.37 (d, J = 5.9 Hz, 18H).

13C NMR (126 MHz, cdcl3): δ 171.60, 164.50, 155.55, 155.37, 135.66, 134.02, 129.96, 128.64, 128.47, 128.45, 128.18, 127.78, 127.44, 127.22, 126.89, 82.99, 81.88, 79.56, 68.18, 68.16, 68.14, 65.13, 53.64, 50.44, 30.09, 29.66, 29.07, 28.28, 27.93, 23.23, 13.65.

IR (neat): 1149, 1710, 1775, 2934, 2975, 3375.

**[α]^{25}$_D$:** -1.5 ° (10 mg/mL in chloroform)

HRMS: [C$_{29}$H$_{38}$N$_2$O$_8$Na]$^+$ calcd. 565.25204, found 565.25134.

4.24
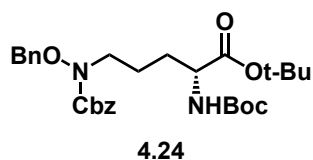
4.24: To a flask containing potassium carbonate (0.135 g, 0.980 mmol) was added **(–)-4.23** (0.266 g, 0.490 mmol) dissolved in methanol (11 mL) under Argon. Cloudy solution was stirred until starting material consumed by TLC (~45 minutes). Benzyl bromide (0.17 mL, 1.471 mmol) was added, and the reaction was stirred until solution became clear (2.5 hours). Solution was concentrated via rotary evaporation then quenched with aqueous bicarbonate. Ethyl acetate was added and washed with water then brine. Organic was dried over sodium sulfate then concentrated via rotary evaporation. The crude residue was purified by flash chromatography (gradient of 0->10% ethyl acetate in hexanes) to yield pure **4.24** in 81% yield (0.211g, 0.399 mmol).

1H NMR (400 MHz, cdcl3): δ 7.42 – 7.28 (m, 10H), 5.20 (s, 2H), 5.01 (d, J = 8.2 Hz, 1H), 4.84 (d, J = 1.0 Hz, 2H), 4.17 (t, J = 6.9 Hz, 1H), 3.48 (t, J = 6.7 Hz, 2H), 1.77 (d, J = 12.9 Hz, 1H), 1.72 – 1.52 (m, 4H), 1.43 (s, 9H), 1.42 (s, 9H).

13C NMR (151 MHz, CDCl$_3$): δ 171.83, 157.32, 155.49, 136.21, 135.40, 129.54, 128.76, 128.71, 128.59, 128.40, 128.26, 82.07, 79.79, 67.89, 53.77, 49.52, 30.26, 29.84, 28.47, 28.10, 23.05.

(–)-4.25
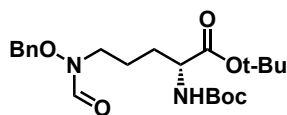
(–)-4.25: To a flask containing EDC (5.75 g, 30.1 mmol) and dichloromethane (25 mL) at 0 °C was added formic acid (1.137 mL, 30.1 mmol) and the mixture was stirred for 15 minutes. **(–)-4.22** (4.15 g, 10.1 mmol) was dissolved in dichloromethane (25 mL) and added to the reaction mixture. The reaction was stirred for one hour at 0 °C and one hour at room temperature. The reaction was cooled to 0 °C and an additional portion of EDC (1.90 g, 10.1 mmol) and formic acid (0.379 mL, 10.1 mmol) were added. The reaction was stirred at 0 °C for 15 minutes and room temperature for 3 hours. The reaction was quenched with water and the aqueous layer was extracted three times with dichloromethane. The combined organic layers were washed with brine, dried over anhydrous sodium sulfate, and concentrated under rotary evaporation. The crude amide was taken on without further purification.

To a solution of the crude material dissolved in methanol at 0 °C was added benzyl bromide (3.60 mL, 30.1 mmol) and diisopropylethylamine (3.50 mL, 20.1 mmol). The reaction was stirred at 0 °C to room temperature for 12 hours, at which time solvent was removed by rotary evaporation. The residue was partitioned between water and ethyl acetate and the aqueous layer was extracted three times with ethyl acetate. The combined organic layers were washed with brine, dried over anhydrous sodium sulfate, and concentrated under rotary evaporation. The crude residue was purified by flash chromatography (gradient of 0->100% ethyl acetate in hexanes) to yield pure **(–)-4.25** as a pale oil in 85% yield (3.62 g, 8.51 mmol). Characterization data matched those previously reported.[12]

¹H NMR (600 MHz, CDCl₃): δ 8.18 (s, 1H), 7.44 – 7.29 (m, 5H), 5.07 (d, *J* = 8.2 Hz, 1H), 4.81 (s, 2H), 4.16 (s, 1H), 3.58 (s, 2H), 1.82 – 1.75 (m, 1H), 1.74 – 1.62 (m, 2H), 1.62 – 1.54 (m, 1H), 1.42 (s, 18H).

¹³C NMR (151 MHz, CDCl₃): δ 171.57, 163.13, 155.40, 134.28, 129.46, 129.15, 128.78, 82.04, 79.71, 77.75, 53.51, 43.76, 30.17, 28.32, 27.96, 25.68, 22.76.

IR (neat): 1684 (s), 1713 (s), 2336 (w), 2935 (w), 2977 (w), 3333 (b)

[α]^{25}$_D$: -20 ° (10 mg/mL in chloroform)
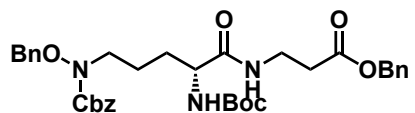
4.26

4.26: To a flask containing **4.24** (0.210 g, 0.397 mmol) and dichloromethane (1.5 mL) was added trifluoroacetic acid (1.5 mL). The reaction was stirred in open air for 4 hours, at which point the solvent was removed by rotary evaporation. The crude residue was re-dissolved in dichloromethane and concentrated five times followed by diethyl ether twice to remove excess trifluoroacetic acid. Removal of *tert*-butyl groups was confirmed by ^{1}H NMR and the crude product was taken on without further purification.
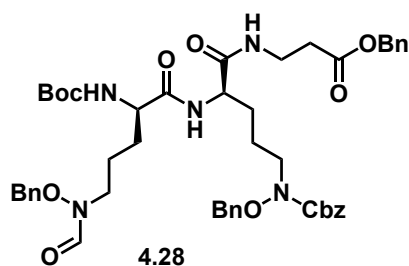
Crude product was dissolved in THF (15 mL). 10% aqueous Na_2CO_3 (15 mL) was added followed by di-tert-butyl dicarbonate (1.1 equiv, 0.095 g, 0.437 mmol). The reaction was stirred overnight at room temperature. The reaction was concentrated to aqueous via rotary evaporation, and then diluted with water. Solution was acidified to pH = 3 using 1M HCl, then extracted three times with ethyl acetate. Combined organic layers were dried over Na_2SO_4 and concentrated using rotary evaporation to afford **4.11**. Presence of the *tert*-butyl group was confirmed by ^{1}H NMR and the crude product was taken on without further purification.

To a flask containing EDC (0.228 g, 1.192 mmol), HOBt (0.182 g, 1.192 mmol) and β-alanine benzyl ester tosylate salt (0.209 g, 0.596 mmol) at 0 °C was added a solution of **4.11** in dimethylformamide (20 mL). Triethylamine (9 mL) was added slowly and pH was confirmed to be basic before stirring at 0 °C to room temperature for 16 hours. The reaction was quenched by dilution in saturated sodium bicarbonate and the aqueous layer was extracted three times with ethyl acetate. The combined organic layers were washed with

brine, dried over anhydrous sodium sulfate, and concentrated by rotary evaporation. The crude residue was purified by flash chromatography (gradient of 0->100% ethyl acetate in hexanes) to yield pure **4.26** in 64% yield (0.161 g, 0.254 mmol).

^{1}H NMR (500 MHz, CDCl₃): δ 7.43 – 7.27 (m, 14H), 6.60 (t, J = 6.1 Hz, 1H), 5.22 (s, 2H), 5.11 (s, 3H), 4.84 (s, 2H), 4.09 (s, 1H), 3.61 (s, 1H), 3.46 (d, J = 6.2 Hz, 3H), 2.53 (t, J = 6.3 Hz, 2H), 1.99 (s, 1H), 1.76 – 1.45 (m, 5H), 1.42 (s, 10H).

^{13}C NMR (126 MHz, CDCl3): δ 171.97, 171.95, 157.25, 155.63, 136.05, 135.65, 135.15, 129.45, 129.37, 128.69, 128.61, 128.57, 128.56, 128.49, 128.43, 128.36, 128.29, 128.26, 128.10, 128.07, 128.06, 79.86, 77.32, 77.19, 77.17, 77.15, 77.07, 76.81, 67.82, 67.80, 67.77, 66.53, 66.51, 66.49, 53.50, 48.66, 34.93, 33.97, 30.13, 28.31, 27.96, 23.19.

4.28

4.28: To a flask containing **(–)-4.25** (0.042 g, 0.099 mmol) and dichloromethane (0.5 mL) was added trifluoroacetic acid (0.5 mL). The reaction was stirred in open air for 5 hours, at which point the solvent was removed by rotary evaporation. The crude residue was re-dissolved in dichloromethane and concentrated five times followed by diethyl ether twice to remove excess trifluoroacetic acid. Removal of *tert*-butyl groups was confirmed by ^{1}H NMR and the crude product was taken on without further purification.

Crude product was dissolved in THF (5 mL). 10% aqueous Na₂CO₃ (5 mL) was added followed by di-tert-butyl dicarbonate (1.1 equiv, 0.024 g, 0.109 mmol). The reaction was stirred overnight at room temperature. The reaction was concentrated to aqueous via rotary evaporation, and then diluted with water. Solution was acidified to pH = 3 using 1M HCl, then extracted three times with ethyl acetate. Combined organic layers

were dried over Na_2SO_4 and concentrated using rotary evaporation to afford **4.12**. Presence of the *tert*-butyl group was confirmed by ^{1}H NMR and the crude product was taken on without further purification.

To a flask containing **4.26** (0.079 g, 0.125 mmol) and dichloromethane (0.5 mL) was added trifluoroacetic acid (0.5 mL). The reaction was stirred in open air for 5 hours, at which point the solvent was removed by rotary evaporation. The crude residue was re-dissolved in dichloromethane and concentrated five times followed by diethyl ether twice to remove excess trifluoroacetic acid to afford crude **4.27**. Removal of *tert*-butyl groups was confirmed by ^{1}H NMR and the crude product was taken on without further purification.

4.27 was dissolved in DMF (5 mL) and added to a flask containing EDC (0.057 g, 0.298 mmol), HOBt (0.046 g, 0.298 mmol) and **4.12** at 0 °C. Triethylamine (3 mL) was added slowly and pH was confirmed to be basic before stirring at room temperature overnight. The reaction was quenched by dilution in saturated sodium bicarbonate and the aqueous layer was extracted three times with ethyl acetate. The combined organic layers were washed with brine, dried over anhydrous sodium sulfate, and concentrated by rotary evaporation. The crude residue was purified by flash chromatography (gradient of 0->100% ethyl acetate spiked with 5% methanol in hexanes) to yield pure **4.28** in 63% yield (0.055 g, 0.062 mmol).

^{1}H NMR (400 MHz, CDCl$_3$): δ 8.20 (s, 1H), 7.43 – 7.27 (m, 17H), 6.81 (s, 1H), 6.61 (s, 1H), 5.21 (s, 3H), 5.09 (s, 2H), 4.83 (s, 4H), 4.37 (s, 1H), 4.24 (s, 1H), 3.90 (s, 1H), 3.62 (d, J = 11.0 Hz, 1H), 3.53 – 3.36 (m, 4H), 2.50 (t, J = 6.3 Hz, 2H), 1.70 (s, 5H), 1.61 – 1.47 (m, 4H), 1.42 (s, 9H).

^{13}C NMR (151 MHz, CDCl3): δ 172.26, 171.96, 171.34, 163.74, 157.30, 155.91, 136.01, 135.63, 135.02, 134.11, 129.57, 129.54, 129.27, 128.87, 128.77, 128.63, 128.56, 128.38, 128.34, 128.32, 128.08, 128.06, 80.01, 77.66, 77.17, 67.87, 66.52, 52.91, 52.17, 48.30, 42.90, 35.09, 34.95, 33.90, 30.21, 29.74, 29.42, 28.31, 28.30, 23.21, 23.04.

IR (neat): 1170, 1674, 2916, 3312.

**HRMS:** $[C_{48}H_{60}N_5O_{11}]^+$ calcd. 882.42838, found 882.42814.
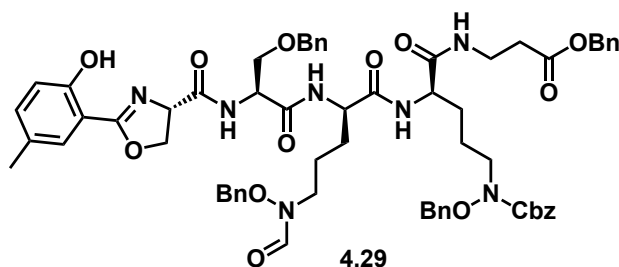
4.29: To a flask containing (–)-**4.19** (0.013 g, 0.0315 mmol) and THF (0.5 mL) was added LiOH (0.002 g, 0.065 mmol) dissolved in water (0.5 mL). Reaction was stirred at room temperature for several hours until consumption of (–)-**4.19** was observed by TLC. Solution was acidified to pH = 3 using 1 M HCl then extracted three times with ethyl acetate. Combined organics were washed with brine then dried over Na_2SO_4 and concentrated using rotary evaporation to afford crude **4.13**. Removal of methyl ester was confirmed by ^{1}H NMR and the crude product was taken on without further purification.

To a flask containing **4.28** (0.043 g, 0.049 mmol) and dichloromethane (0.5 mL) was added trifluoroacetic acid (0.5 mL). The reaction was stirred in open air for 5 hours, at which point the solvent was removed by rotary evaporation. The crude residue was re-dissolved in dichloromethane and concentrated five times followed by diethyl ether twice to remove excess trifluoroacetic acid. Removal of *tert*-butyl group was confirmed by ^{1}H NMR and the crude product was taken on without further purification.

Crude product was dissolved in DMF (1.5 mL) and added to a flask containing EDC (0.018 g, 0.094 mmol), HOBt (0.014 g, 0.094 mmol) and **4.13** at 0 °C. Triethylamine (1 mL) was added slowly and pH was confirmed to be basic before stirring at room temperature overnight. The reaction was quenched by dilution in saturated sodium bicarbonate and the aqueous layer was extracted three times with ethyl acetate. The combined organic layers were washed with brine, dried over anhydrous sodium sulfate, and concentrated by rotary evaporation. The crude residue was purified by flash chromatography (gradient of 0->100% ethyl acetate in hexanes then 0->15% methanol in ethyl acetate). Product was further purified using HPLC (60->100% acetonitrile in water over 15 minutes) to yield pure **4.29** in 56% yield (0.025 g, 0.0176 mmol).

¹H NMR (400 MHz, CDCl₃): δ 11.10 (s, 1H), 8.42 (s, 1H), 8.21 (s, 1H), 8.15 (s, 1H), 7.59 (d, J = 7.2 Hz, 1H), 7.56 – 7.50 (m, 5H), 7.49 – 7.40 (m, 5H), 7.39 – 7.33 (m, 16H), 7.33 – 7.27 (m, 22H), 7.24 (dd, J = 8.2, 2.4 Hz, 4H), 7.21 (s, 6H), 7.20 – 7.16 (m, 2H), 7.11 (t, J = 7.4 Hz, 2H), 6.94 (d, J = 8.4 Hz, 2H), 6.75 (s, 1H), 5.19 (s, 3H), 5.09 (s, 3H), 4.87 (t, J = 9.4 Hz, 2H), 4.82 (s, 4H), 4.78 – 4.71 (m, 2H), 4.52 (d, J = 9.1 Hz, 7H), 4.42 (d, J = 12.5 Hz, 4H), 4.36 (t, J = 8.8 Hz, 2H), 4.02 (s, 3H), 3.80 – 3.73 (m, 2H), 3.74 – 3.64 (m, 1H), 3.64 – 3.50 (m, 4H), 3.45 (t, J = 5.4 Hz, 6H), 2.30 (s, 5H), 1.91 – 1.75 (m, 6H), 1.73 – 1.51 (m, 11H).

¹³C NMR (126 MHz, CDCl₃): δ 171.77, 171.44, 167.78, 163.36, 157.75, 157.24, 136.01, 135.76, 135.19, 135.09, 130.23, 129.48, 129.44, 129.11, 129.02, 128.81, 128.67, 128.55, 128.52, 128.50, 128.48, 128.32, 128.24, 128.22, 128.20, 128.16, 127.97, 127.96, 127.84, 127.47, 125.17, 120.02, 116.81, 109.60, 77.21, 77.15, 77.01, 76.76, 73.42, 69.18, 67.92, 67.80, 66.42, 53.62, 52.78, 35.14, 33.98, 29.68, 29.48, 28.67, 23.60, 20.37.

5.3.1
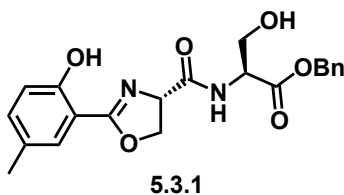
5.3.1: To a flask containing EDC (0.670 g, 3.498 mmol), HOBt (0.536 g, 3.498 mmol), and L-serine benzyl ester hydrochloride (0.405 g, 1.749 mmol) at 0 °C was added a solution of **4.18** in dimethylformamide (38 mL). Triethylamine (2 mL) was added slowly and pH was confirmed to be basic before stirring at room temperature overnight. The reaction was concentrated to aqueous and then diluted with saturated sodium bicarbonate. Aqueous layer was extracted three times with ethyl acetate. The combined organic layers were washed with brine, dried over anhydrous sodium sulfate, and concentrated by rotary evaporation. The crude residue was purified by flash chromatography (gradient of 0->50% ethyl acetate in hexanes) to yield pure **5.3.1** in 35% yield (0.163 g, 0.409 mmol).

1H NMR (400 MHz, cdcl3): δ 7.47 (d, J = 2.4 Hz, 1H), 7.36 (s, 5H), 7.22 (dd, J = 8.4, 2.3 Hz, 1H), 6.93 (t, J = 8.6 Hz, 1H), 5.24 (s, 2H), 4.97 (dd, J = 10.5, 8.5 Hz, 1H), 4.72 – 4.59 (m, 3H), 4.05 – 3.86 (m, 2H), 2.28 (s, 3H).

HRMS: $[C_{21}H_{23}N_2O_6]^+$ calcd. 399.15506, found 399.15442.

4.31
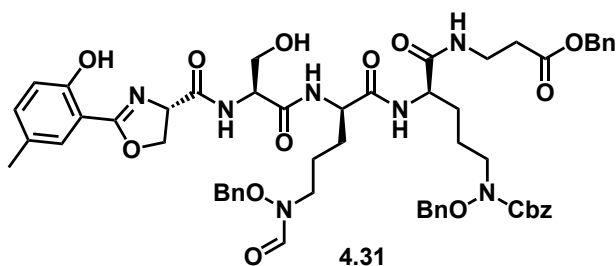
4.31: To a flask containing **5.3.1** (0.081 g, 0.203 mmol) and ethyl acetate (30 mL) was added 10% palladium on activated charcoal (20 wt. % of starting material, 0.020 g). The flask was purged, backfilled with hydrogen gas, and stirred at room temperature until consumption of starting material was observed by TLC. The mixture was passed through a Whatman filter and concentrated by rotary evaporation to afford **4.30**. Removal of the benzyl ester was confirmed by ^{1}H NMR and the crude acid was taken on without further purification.

To a flask containing **4.28** (0.141 g, 0.160 mmol) and dichloromethane (3 mL) was added trifluoroacetic acid (3 mL). The reaction was stirred in open air for 5 hours, at which point the solvent was removed by rotary evaporation. The crude residue was re-dissolved in dichloromethane and concentrated five times followed by diethyl ether twice to remove excess trifluoroacetic acid. Removal of *tert*-butyl group was confirmed by ^{1}H NMR and the crude product was taken on without further purification.

Crude product was dissolved in DMF (5 mL) and added to a flask containing EDC (0.046 g, 0.240 mmol), HOBt (0.037 g, 0.240 mmol) and **4.30** at 0 °C. Triethylamine (2 mL) was added slowly and pH was confirmed to be basic before stirring at room temperature overnight. The reaction was quenched by dilution

in saturated sodium bicarbonate and the aqueous layer was extracted three times with ethyl acetate. The combined organic layers were washed with brine, dried over anhydrous sodium sulfate, and concentrated by rotary evaporation. The crude residue was purified by flash chromatography (gradient of 0->100% ethyl acetate in hexanes then 0->15% methanol in ethyl acetate). Product was further purified using HPLC (60->95% acetonitrile in water over 15 minutes) to yield pure **4.31** in 27% yield (0.023 g, 0.021 mmol).

¹H NMR (600 MHz, CDCl₃): δ 8.14 (s, 1H), 7.77 (d, J = 7.0 Hz, 1H), 7.49 (s, 1H), 7.46 (d, J = 2.3 Hz, 1H), 7.40 – 7.27 (m, 19H), 7.23 – 7.15 (m, 2H), 6.89 (d, J = 8.4 Hz, 1H), 6.78 (s, 1H), 5.19 (d, J = 1.9 Hz, 2H), 5.09 (s, 2H), 4.87 (t, J = 9.7 Hz, 1H), 4.84 – 4.78 (m, 4H), 4.59 (t, J = 8.4 Hz, 1H), 4.52 (t, J = 10.0 Hz, 1H), 4.46 – 4.35 (m, 3H), 4.01 (d, J = 11.2 Hz, 1H), 3.69 (d, J = 10.2 Hz, 1H), 3.61 (s, 3H), 3.48 – 3.37 (m, 4H), 2.57 – 2.49 (m, 2H), 2.28 (s, 3H), 1.91 (s, 2H), 1.78 (s, 3H), 1.74 – 1.67 (m, 2H), 1.67 – 1.51 (m, 6H).

HRMS: $[C_{57}H_{64}N_7O_{14}]^+$ calcd. 1070.45167, found 1070.4513
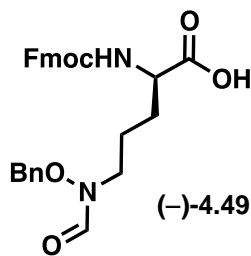
(–)-**4.49:** To a flask containing (–)-**4.25** (2.64 g, 6.26 mmol) and dichloromethane (4 mL) was added trifluoroacetic acid (4 mL). The reaction was stirred in open air for 3 hours, at which point the solvent was removed by rotary evaporation. The crude residue was re-dissolved in dichloromethane and concentrated five times to remove excess trifluoroacetic acid. The crude amino acid was taken on without further purification.

To a flask containing the crude material dissolved in tetrahydrofuran (9 mL) and water (9 mL) was added Fmoc-OSu (2.15 g, 6.37 mmol) and sodium bicarbonate (3.06 g, 36.43 mmol). The pH was confirmed to

be basic and the reaction was stirred for 16 hours, at which time organic solvent was removed by rotary evaporation. The remaining aqueous solution was diluted with water, adjusted to pH 2 by addition of 2M HCl, and extracted three times with ethyl acetate. The combined organic layers were dried over anhydrous sodium sulfate and concentrated by rotary evaporation. The crude residue was purified by flash chromatography (isocratic 94:3:3 dichloromethane/methanol/acetic acid). Fractions containing product were concentrated by rotary evaporation, re-dissolved in pentane and concentrated ten times to remove excess acetic acid. The residue was then partitioned between ethyl acetate and water to remove trace residual acetic acid and the aqueous layer was extracted three times with ethyl acetate at a pH of 2 (maintained by addition of 2M HCl throughout extraction). The combined organic layers were washed with brine, dried over anhydrous sodium sulfate, and concentrated by rotary evaporation to yield pure (**–**)-**4.49** as an amorphous off-white solid in 87% yield (2.65 g, 5.43 mmol). Characterization data matched those previously reported.[12]

^{1}H NMR (400 MHz, CDCl$_3$): δ 8.16 (s, 1H), 7.73 (d, J = 7.5 Hz, 2H), 7.57 (t, J = 6.6 Hz, 2H), 7.41 – 7.22 (m, 9H), 5.61 (d, J = 8.1 Hz, 1H), 4.78 (s, 3H), 4.37 (qd, J = 7.2, 5.1, 3.1 Hz, 2H), 4.18 (t, J = 7.2 Hz, 1H), 3.60 (d, J = 22.5 Hz, 2H), 1.88 (s, 1H), 1.69 (s, 3H).

^{13}C NMR (151 MHz, CDCl$_3$): δ 171.34, 163.22, 155.99, 143.94, 143.82, 141.34, 133.21, 129.49, 129.20, 128.84, 128.81, 127.75, 127.11, 125.15, 120.02, 82.42, 67.00, 53.98, 47.21, 43.68, 29.96, 28.04, 28.00, 22.74.

IR (neat): 1677 (s), 1721 (s), 2976 (w), 3323 (b)

[α]^{25}$_D$: -10 ° (10 mg/mL in chloroform)

(**–**)-**5.3.2**
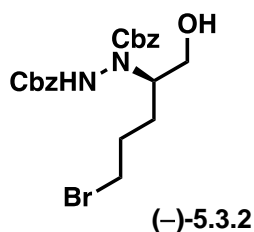
(**–**)-**5.3.2:** To a flask containing PCC (26.0 g, 120.6 mmol) and silica gel (20 g) in dichloromethane (250 mL) was added a solution of commercially available 5-bromo-pentanol (10 g, 59.9 mmol) in

dichloromethane (50 mL) at a rate of 1mL/minute. The reaction was stirred for 1 hour and then filtered through celite and concentrated by rotary evaporation. The residue was redissolved in dichloromethane, passed through a silica plug, and concentrated by rotary evaporation. The crude aldehyde was taken on without further purification.

To a flask containing the crude material in acetonitrile (110 mL) was brought to 0 °C and dibenzyl azodicarboxylate (11.78 g, 39.53 mmol) and L-proline (0.454 g, 3.95 mmol) were added as solids. The reaction was stirred at 0 °C for 16 hours, at which point sodium borohydride (1.18 g, 31.2 mmol) and ethanol (48 mL) were added and the reaction was stirred for 40 minutes. The reaction was quenched with 10% citric acid and solvent was removed under rotary evaporation. The residue was partitioned between ethyl acetate and brine and the aqueous layer was extracted three times with ethyl acetate. The combined organic layers were dried over anhydrous sodium sulfate and concentrated under rotary evaporation. The crude residue was purified by flash chromatography (gradient of 0->100% ethyl acetate in hexanes) to yield pure **(–)-5.3.2** as a white solid in 67% yield (12.31 g, 26.48 mmol). Characterization data matched those previously reported.[13]

^{1}H-NMR (600 MHz, CDCl$_3$): δ 7.39 –7.22 (m, 10H), 5.29 – 5.07 (m, 4H), 4.50 (s, 1H), 4.24 (s, 1H), 3.55 – 3.48 (br. s, 1H), 3.48 – 3.33 (m, 2H), 3.29 (s, 1H), 1.91 – 1.79 (br. s, 1H), 1.80 – 1.67 (br. s, 1H), 1.51 – 1.41 (br. s, 1H), 1.41 – 1.30 (m, 1H).

^{13}C NMR (151 MHz, CDCl$_3$): δ 159.18, 156.99, 156.18, 135.72, 135.59, 135.07, 128.70, 128.66, 128.56, 128.46, 128.30, 128.06, 127.77, 77.30, 77.09, 76.88, 68.73, 68.60, 68.37, 62.03, 60.29, 59.05, 33.57, 33.05, 29.08, 29.00, 26.33, 26.15.

IR (neat): 1712 (s), 2960 (w), 3033 (s), 3274 (b)

**$[\alpha]^{25}_D$:** -5.4 ° (10 mg/mL in chloroform)

(+)-5.3.3
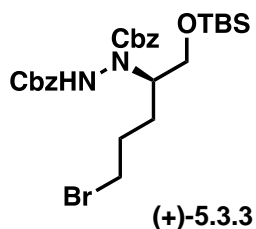
(+)-5.3.3: To a flask containing **(–)-5.3.2** (7.34 g, 15.8 mmol) and imidazole (11 g, 161.5 mmol) in dimethylformamide (50 mL) was added TBSCl (5.51 g, 36.5 mmol). The reaction was stirred for 16 hours, at which point the reaction was quenched with brine and the aqueous layer was extracted three times with ethyl acetate. The combined organic layers were dried over anhydrous sodium sulfate and concentrated under rotary evaporation. The crude residue was purified by flash chromatography (gradient of 0->100% ethyl acetate in hexanes) to yield pure **(+)-5.3.3** as a white solid in 90% yield (8.22 g, 14.22 mmol). Characterization data matched those previously reported.[13]

^{1}H NMR (600 MHz, CDCl$_3$): δ 7.44 – 7.28 (m, 10H), 6.46 (s, 1H), 5.27 – 5.07 (m, 4H), 4.39 – 4.10 (m, 1H), 3.72 – 3.03 (m, 4H), 2.28 – 1.23 (m, 4H), 0.88 – 0.85 (s, 9H), 0.06 (m, 6H).

^{13}C NMR (151 MHz, CDCl$_3$): δ 156.41, 135.97, 135.67, 135.33, 128.61, 128.50, 128.41, 128.34, 128.19, 128.10, 127.92, 127.72, 77.27, 77.06, 76.85, 68.41, 67.99, 67.67, 62.96, 62.37, 59.60, 58.40, 58.28, 45.28, 44.83, 34.69, 34.41, 33.76, 31.61, 28.99, 26.92, 26.74, 25.75, 25.48, 25.30, 22.67, 20.73, 18.03, 14.15, -5.45, -5.53.

IR (neat): 1713 (s), 2856 (w), 2926 (w), 2953 (w), 3284 (b)

[α]^{25}$_D$: +15 ° (10 mg/mL in chloroform)

(+)-5.3.4
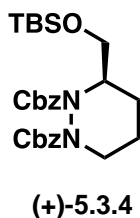
(+)-5.3.4: To a flask containing sodium hydride (0.70 g, 17.516 mmol, 60% in oil) and dimethylformamide (25 mL) at 0 °C was slowly added a solution of **(+)-5.3.3** (5.06 g, 8.76 mmol) in DMF (5 mL). The reaction was stirred at 0 °C for 50 minutes, at which time it was quenched by dilution into 10% citric acid and the
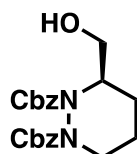
aqueous layer was extracted three times with ethyl acetate. The combined organic layers were washed with brine, dried over anhydrous sodium sulfate, and concentrated by rotary evaporation. The crude residue was purified by flash chromatography (gradient of 0->100% ethyl acetate in hexanes) to yield pure (+)-**5.3.4** as a white solid in 90% yield (3.93 g, 7.89 mmol). Characterization data matched those previously reported.[13]

¹H NMR (mixture of rotamers) (600 MHz, CDCl₃): δ 7.41 – 7.21 (m, 10H), 5.29 – 4.92 (m, 4H), 4.45 – 4.22 (m, 1H), 4.19 + 4.06 (m, 1H), 3.86 + 3.72 (dd x 2, J = 10.1, 5.2 Hz, 1H), 3.62 + 3.51 (t x 2, J = 10.0 Hz, 1H), 3.23 – 2.95 (m, 1H), 1.93 – 1.79 (m, 2H), 1.76 – 1.66 (m, 1H), 1.55 – 1.46 (m, 1H), 0.89 (s x 2, 9H), 0.09 – 0.04 (s x 2, 6H).

¹³C NMR (151 MHz, CDCl₃): δ 155.55, 155.40, 154.95, 136.27, 136.09, 128.55, 128.50, 128.47, 128.19, 128.07, 127.93, 127.81, 127.66, 127.50, 77.26, 77.05, 76.83, 67.76, 67.60, 60.83, 54.32, 45.90, 45.38, 44.98, 44.48, 25.85, 25.81, 22.36, 19.32, 18.88, 18.17, -5.37, -5.44, -5.48, -5.54.

IR (neat): 1709 (s), 2361 (w), 2856 (w), 2953 (w)

[α]²⁵_D: +19.3 ° (10 mg/mL in chloroform)


(–)-5.3.5

(–)-5.3.5: To a flask containing (+)-**5.3.4** (3.89 g, 7.81 mmol) and tetrahydrofuran (40 mL) at 0 °C was added slowly a 1M solution of TBAF in THF (9.43 mL, 9.43 mmol). The reaction was stirred for 50 minutes at which time it was quenched by dilution into brine and extracted three times with ethyl acetate. The combined organic layers were washed with brine, dried over anhydrous sodium sulfate, and concentrated by rotary evaporation. The crude residue was purified by flash chromatography (gradient of 0->100% ethyl acetate in hexanes) to yield pure (–)-**5.3.5** as an amorphous solid in quantitative yield (3.0 g, 7.81 mmol). Characterization data matched those previously reported.[13]

¹H NMR (600 MHz, CDCl₃): δ 7.39 – 7.31 (m, 10H), 5.30 – 5.07 (m, 4H), 4.52 (d, *J* = 53.6 Hz, 1H), 4.24 – 4.05 (m, 1H), 3.66 (dt, J = 60.9, 11.0 Hz, 1H), 3.56 – 3.39 (m, 1H), 3.27 – 3.01 (m, 1H), 2.09 (d, J = 7.8 Hz, 1H), 1.83 – 1.68 (m, 2H), 1.58 – 1.47 (m, 2H).

¹³C NMR (151 MHz, CDCl₃): δ 156.80, 156.21, 155.74, 154.88, 136.15, 135.84, 135.71, 135.37, 128.71, 128.66, 128.59, 128.54, 128.46, 128.28, 128.20, 128.05, 127.83, 127.56, 77.28, 77.07, 76.86, 68.52, 68.42, 68.17, 67.99, 60.55, 59.96, 56.19, 54.97, 45.82, 45.41, 23.09, 22.55, 19.71, 19.38.

IR (neat): 1705 (s), 2947 (w), 3477 (b)

**[α]²⁵_D:** -7.2 ° (10 mg/mL in chloroform)

(+)-5.3.6
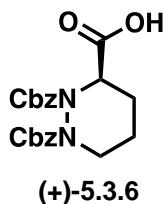
(+)-5.3.6: To a solution of **(–)-5.3.5** (3.0 g, 7.81 mmol) in acetonitrile (40 mL) was added TEMPO (0.193 g, 1.23 mmol) and sodium chlorite (1.42 g, 15.7 mmol) as solids and 1M pH 6.4 phosphate buffer (40 mL). Sodium hypochlorite was diluted in water to 1.6 M and added (1 mL, 1.6 mmol), at which point a purple color was observed, and the reaction was stirred for 4 hours. The reaction was quenched with 1M sodium hydroxide (20 mL) followed by 1M sodium sulfite. The reaction was adjusted to pH 3 by addition of 1M sodium hydrogen sulfate and the aqueous layer was extracted three times with ethyl acetate. The combined organic layers were washed with brine, dried over anhydrous sodium sulfate, and concentrated by rotary evaporation. The crude residue was purified by flash chromatography (gradient of 0->100% ethyl acetate in hexanes) to yield pure **(+)-5.3.6** as pale oil in 83% yield (2.57 g, 6.52 mmol). Characterization data matched those previously reported.[13]

¹H NMR (mixture of rotamers) (600 MHz, CDCl₃): δ 7.46 – 7.21 (m, 10H), 5.32 – 5.02 (m, 4H), 4.23 – 4.04 (m, 1H), 3.17 – 2.89 (m, 2H), 2.29 – 2.24 (m, 1H), 1.94 (dddd, *J* = 14.2, 10.6, 6.5, 4.1 Hz, 1H), 1.87 – 1.69 (m, 1H), 1.66 – 1.58 (m, 1H).

¹³C NMR (151 MHz, CDCl₃): δ 171.17, 170.68, 135.38, 135.15, 134.94, 128.74, 128.70, 128.67, 128.57, 128.36, 128.24, 128.16, 128.00, 77.26, 77.05, 76.84, 69.44, 69.22, 69.01, 68.52, 44.90, 43.44, 23.95, 23.78, 20.41, 20.06.

IR (neat): 1721 (s), 2334 (w), 2361 (w), 2954 (w), 3033 (w)

**[α]²⁵_D:** +30.5 ° (10 mg/mL in chloroform)
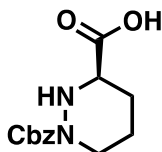
(+)-4.33

(+)-4.33: To a flask containing **(+)-5.3.6** (2.57 g, 6.52 mmol) in THF (50 mL) was added freshly pulverized potassium hydroxide (1.82 g, 32.48 mmol). The reaction was stirred for 12 hours, after which time a gel like consistency was observed. The reaction was partitioned between saturated sodium bicarbonate and hexanes and the aqueous layer was washed twice with hexanes. The aqueous layer was then acidified to pH 4 with concentrated hydrochloric acid and extracted three times with ethyl acetate, maintaining pH throughout extraction. The combined organic layers were concentrated by rotary evaporation and the residue was recrystallized in dichloromethane to yield **(+)-4.33** as an off-white solid in 91% semi-pure yield (1.56 g, 5.93 mmol). Although the material was resistant to further purification, characterization data qualitatively matched those previously reported.[14]

¹H NMR (600 MHz, DMSO-*d*₆): 7.40 – 7.29 (m, 5H), 5.13 – 5.05 (m, 2H), 3.82 (d, *J* = 13.2 Hz, 1H), 3.36 (dd, *J* = 9.7, 3.1 Hz, 1H), 3.07 (s, 1H), 1.90 (dq, *J* = 8.9, 4.4, 3.9 Hz, 1H), 1.69 (m, 1H), 1.54 (m, 2H).

¹³C NMR (151 MHz, DMSO-*d*₆): δ 173.15, 155.23, 137.45, 128.84, 128.68, 128.49, 128.27, 128.03, 127.08, 126.87, 66.71, 58.37, 40.41, 40.28, 40.14, 40.00, 39.86, 39.72, 39.58, 27.58, 23.41.

IR (neat): 1721 (s), 2948 (w)

[α]²⁵_D: +33 ° (10 mg/mL in methanol)
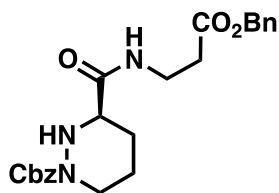
(+)-4.39

(+)-4.39: To a flask containing EDC (2.36 g, 12.37 mmol), HOBt (1.94 g, 12.37 mmol) and β-alanine benzyl ester tosylate salt (4.34 g, 12.37 mmol) at 0 °C was added a solution of **(+)-4.33** (1.08 g, 4.12 mmol) in dimethylformamide (20 mL). Triethylamine (2.2 mL, 15.8 mmol) was added slowly and pH was confirmed to be basic before stirring at 0 °C to room temperature for 12 hours. The reaction was quenched by dilution in saturated sodium bicarbonate and the aqueous layer was extracted three times with ethyl acetate. The combined organic layers were washed with brine, dried over anhydrous sodium sulfate, and concentrated by rotary evaporation. The crude residue was purified by flash chromatography (gradient of 0->100% ethyl acetate spiked with 5% methanol in hexanes) to yield pure **(+)-4.39** as pale oil in 77% yield (1.38 g, 3.18 mmol). Enantiomeric excess, as determined by chiral HPLC, was measured to be greater than 97%.

^{1}H NMR (600 MHz, CDCl$_3$): δ 7.41 – 7.30 (m, 10H), 5.17 (s, 2H), 5.14 (s, 2H), 3.93 (d, J = 13.3 Hz, 1H), 3.50 (d, J = 19.6 Hz, 2H), 3.17 (br. s, 1H), 2.50 (br. s, 2H), 2.33 – 2.25 (m, 1H), 1.73 – 1.53 (m, 3H).
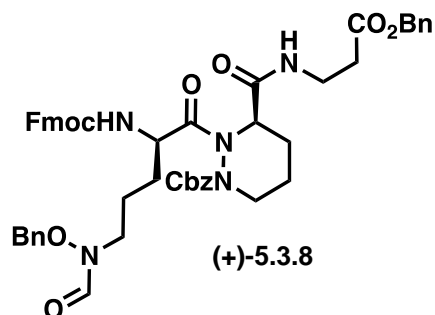
^{13}C NMR (151 MHz, CDCl3): δ 171.59, 170.65, 136.26, 135.85, 128.61, 128.56, 128.35, 128.32, 128.27, 67.76, 66.56, 66.40, 57.96, 34.97, 34.09, 25.39, 21.65.

IR (neat): 1668 (s), 1701 (s), 1733 (s), 2946 (w), 3274 (b)

[α]^{25}$_D$: +25 ° (10 mg/mL in chloroform)

HRMS: [C$_{23}$H$_{27}$N$_3$O$_5$]$^+$ calcd. 426.20290, found 426.20122

(+)-5.3.8: To a flask containing (–)-**4.49** (1.47 g, 3.01 mmol) and dichloromethane (5 mL) at 0 °C was added dropwise Ghosez's reagent (0.56 mL, 4.21 mmol). The reaction was stirred at 0 °C for 45 minutes, at which point it was transferred to a flask containing (+)-**4.39** (0.425 g, 1.00 mmol), silver cyanide (0.135 g, 1.00 mmol), and benzene (10 mL). The reaction was brought to 80 °C and stirred at reflux for 50 minutes. The reaction was allowed to cool to room temperature and quenched by dilution in saturated sodium bicarbonate. The aqueous layer was extracted three times with ethyl acetate. The combined organic layers were washed with brine, dried over anhydrous sodium sulfate, and concentrated by rotary evaporation. The crude residue was purified by flash chromatography (gradient of 0->100% ethyl acetate in hexanes) to yield pure (+)-**5.3.8** as a white solid in 80% yield (0.717 g, 0.80 mmol).

^{1}H NMR (600 MHz, CDCl$_3$): δ 8.22 (s, 1H), 7.78 (d, J = 7.5 Hz, 2H), 7.68 (s, 1H), 7.58 (d, J = 7.5 Hz, 2H), 7.42 (t, J = 7.4 Hz, 2H), 7.38 – 7.30 (m, 12H), 5.36 (br. s, 1H), 5.19 (s, 2H), 5.11 (s, 2H), 5.08 (m, 1H) 4.95 (s, 1H), 4.81 (br. s, 2H), 4.49 (br. s, 1H), 4.40 (d, J = 6.9 Hz, 2H), 4.22 (t, J = 7.1 Hz, 1H), 4.14 (d, J = 12.7 Hz, 1H), 3.57 – 3.49 (m, 1H), 3.44 – 3.35 (m, 1H), 2.50 (s, 2H), 2.20 (m, 1H), 1.93 (s, 1H), 1.81 (s, 1H), 1.69 (s, 2H), 1.60 (s, 2H), 1.53 (s, 1H).

^{13}C NMR (151 MHz, CDCl$_3$): δ 171.39, 168.91, 163.19, 156.75, 156.15, 143.69, 141.35, 141.33, 135.86, 135.36, 129.48, 128.71, 128.62, 128.58, 128.24, 128.18, 127.95, 127.78, 127.09, 125.09, 120.04, 77.75, 77.24, 77.03, 76.81, 69.06, 67.06, 66.33, 56.00, 47.09, 46.69, 35.19, 33.91, 28.74, 23.54, 20.09.

IR (neat): 1674 (s), 1717 (s), 2949 (w), 3034 (w), 3319 (b)

[α]^{25}$_D$: +12.7 ° (10 mg/mL in chloroform)

HRMS: [C$_{51}$H$_{54}$N$_5$O$_{10}$]$^+$ calcd. 896.38652, found 896.38527

(+)-5.3.9
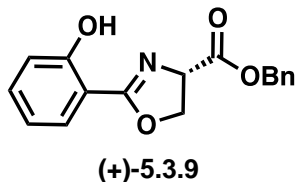
(+)-5.3.9: To a flask containing commercially available 2-hydroxybenzonitrile (5.0 g, 41.9 mmol) and methanol (83 mL) was slowly added acetyl chloride (95 mL), resulting in the evolution of heat. The reaction was stirred for 48 hours at which point an orange precipitate was observed. The reaction was brought to 0 °C and adjusted to pH 7 with saturated sodium bicarbonate. The aqueous layer was extracted three times with ethyl acetate and the combined organic layers were washed with water and brine, dried over anhydrous sodium sulfate, and concentrated by rotary evaporation. The crude methyl imidate was taken on without further purification.

To a flask containing L-serine benzyl ester hydrochloride (8.01 g, 34.5 mmol) was added a solution of the crude residue in 1,2-dichloroethane (80 mL). The reaction was brought to 83 °C and stirred at reflux for 12 hours, at which point the reaction was allowed to cool to room temperature and concentrated under rotary evaporation. The residue was partitioned between 5% citric acid and ethyl acetate, and the aqueous layer was extracted three times with ethyl acetate. The combined organic layers were washed with brine, dried over anhydrous sodium sulfate, and concentrated by rotary evaporation. The crude residue was purified by flash chromatography (gradient of 0->100% ethyl acetate in hexanes) to yield pure **(+)-5.3.9** as a pale yellow solid in 58% yield (7.22 g, 24.3 mmol).
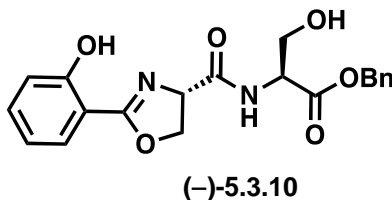
^{1}H NMR (600 MHz, CDCl$_3$): δ 11.55 (s, 1H), 7.54 (d, *J* = 7.8 Hz, 1H), 7.33 – 7.18 (m, 6H), 6.89 (d, *J* = 8.3 Hz, 1H), 6.75 (t, *J* = 7.6 Hz, 1H), 5.15 – 5.07 (m, 3H), 4.89 (ddd, *J* = 9.9, 7.7, 1.5 Hz, 1H), 4.55 (t, *J* = 8.1 Hz, 1H), 4.45 (t, *J* = 9.6 Hz, 1H).

^{13}C NMR (151 MHz, CDCl$_3$): δ 170.31, 167.65, 160.01, 135.20, 134.06, 128.73, 128.59, 128.41, 128.32, 118.83, 116.98, 110.09, 68.85, 67.52, 67.38.

IR (neat): 1614 (s), 1637 (s), 1741 (s), 2957 (w), 3031 (w)

[α]^{25}$_D$: +76 ° (10 mg/mL in chloroform)

HRMS: [C$_{17}$H$_{16}$NO$_4$]$^+$ calcd. 298.10738, found 298.10746

(–)-5.3.10

(–)-5.3.10: To a flask containing **(+)-5.3.9** (0.278 g, 0.935 mmol) and methanol (5 mL) was added 10% palladium on activated charcoal (10 wt % of starting material, 0.028 g). The flask was purged, backfilled with hydrogen gas, and stirred at room temperature until consumption of starting material was observed by TLC. The mixture was passed through a Whatman filter and concentrated by rotary evaporation. The crude acid was taken on without further purification.

To a flask containing EDC (0.536 g, 2.81 mmol), HOBt (0.441 g, 2.81 mmol), and L-serine benzyl ester hydrochloride (0.433 g, 1.87 mmol) at 0 °C was added a solution of crude residue in dimethylformamide (6 mL). Triethylamine (1.0 mL, 7.19 mmol) was added slowly and pH was confirmed to be basic before stirring from 0 °C to room temperature for 16 hours. The reaction was diluted in saturated sodium bicarbonate and the aqueous layer was extracted three times with ethyl acetate. The combined organic layers were washed with brine, dried over anhydrous sodium sulfate, and concentrated by rotary evaporation. The crude residue was purified by flash chromatography (gradient of 0->100% ethyl acetate in hexanes) to yield pure **(–)-5.3.10** as a fluffy white solid in 65% yield (0.234 g, 0.61 mmol).

^{1}H NMR (600 MHz, CDCl$_3$): δ 11.37 (br. s, 1H), 7.70 (dd, *J* = 7.9, 1.7 Hz, 1H), 7.47 – 7.42 (t, *J* = 7.9, 1H), 7.42 – 7.33 (m, 4H), 7.31 (d, *J* = 7.4 Hz, 1H), 7.05 (dd, *J* = 8.3, 1.1 Hz, 1H), 6.93 (ddd, *J* = 8.2, 7.2, 1.1 Hz, 1H), 5.30 – 5.22 (m, 2H), 5.00 (dd, *J* = 10.9, 8.2 Hz, 1H), 4.74 – 4.69 (m, 1H), 4.71 – 4.67 (m, 1H), 4.66 (dd, *J* = 8.9, 8.3 Hz, 1H), 4.03 (dd, *J* = 11.3, 4.1 Hz, 1H), 3.94 (dd, *J* = 11.3, 3.4 Hz, 1H).

^{13}C NMR (151 MHz, CDCl$_3$): δ 171.26, 169.67, 169.65, 168.02, 159.77, 135.04, 134.38, 128.72, 128.61, 128.57, 128.25, 119.17, 117.04, 109.99, 69.51, 68.05, 68.03, 67.70, 63.11, 54.89, 54.81.

IR (neat): 1614 (w), 1638 (s), 1740 (s), 2362 (w), 2954 (w), 3357 (b)

$[\alpha]^{25}_D$: -19 ° (10 mg/mL in chloroform)

HRMS: $[C_{20}H_{21}N_2O_6]^+$ calcd. 385.13941, found 385.13841
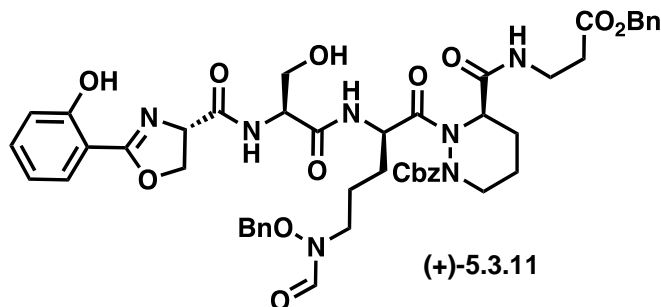
(+)-5.3.11

(+)-5.3.11: To a flask containing **(+)-5.3.8** (0.028 g, 0.03124 mmol) and dichloromethane (0.9 mL) was added 4-(aminomethyl)piperidine (0.1 mL). The reaction was stirred in open air for 30 minutes, diluted in dichloromethane and washed five times with pH 5.5 phosphate buffer and once with brine. The organic layer was dried over anhydrous sodium sulfate and concentrated under rotary evaporation. The crude amine was taken on without further purification.

To a flask containing **(−)-5.3.10** (0.008 g, 0.0208 mmol) and methanol (3 mL) was added 10% palladium on activated charcoal (20 wt. % of starting material, 0.002 g). The flask was purged, backfilled with hydrogen gas, and stirred at room temperature until consumption of starting material was observed by TLC. The mixture was passed through a Whatman filter and concentrated by rotary evaporation to afford **4.34**. The crude acid was taken on without further purification.

To a flask containing EDC (0.012 g, 0.0623 mmol) and HOBt (0.010 g, 0.0623 mmol) at 0 °C was added a solution of crude **4.34** in acetonitrile (3 mL) followed by a solution of crude amine residue in acetonitrile (3 mL). A solution of triethylamine (0.0086 mL, 0.0623 mmol) in acetonitrile (0.1 mL) was added and the pH was confirmed to be basic before stirring from 0 °C to room temperature for 16 hours. The reaction was diluted in saturated sodium bicarbonate and the aqueous layer was extracted three times with ethyl acetate.

The combined organic layers were washed with brine, dried over anhydrous sodium sulfate, and concentrated by rotary evaporation. The crude residue was purified by two rounds of flash chromatography (1st: gradient of 0->100% ethyl acetate spiked with 2% methanol in hexanes. 2nd: 0->10% methanol in dichloromethane) to yield pure (+)-**5.3.11** as colorless oil in 94% yield (0.0187 g, 0.0197 mmol).

^{1}H NMR (600 MHz, CDCl$_3$): δ 11.32 (br. s, 1H), 8.19 (s, 1H), 7.69 (dd, J = 7.9, 1.7 Hz, 1H), 7.46 – 7.41 (t, J = 7.9, 1H), 7.35 (q, J = 9.7, 8.0 Hz, 16H), 7.02 (dd, J = 8.4, 1.1 Hz, 1H), 6.94 – 6.88 (m, 1H), 5.24 – 5.17 (m, 2H), 5.13 (s, 2H), 5.14 – 5.07 (m, 1H), 4.95 (t, J = 9.5 Hz, 1H), 4.81 (s, 2H), 4.68 (s, 1H), 4.66 – 4.59 (m, 2H), 4.47 (s, 1H), 4.17 (d, J = 13.9 Hz, 1H), 3.97 (d, J = 11.4 Hz, 1H), 3.70 – 3.58 (m, 3H), 3.53 (m, 1H), 3.49 – 3.39 (m, 2H), 2.51 (dt, J = 8.6, 4.2 Hz, 2H), 2.17 (d, J = 8.4 Hz, 1H), 1.92 (s, 1H), 1.87 – 1.71 (m, 3H), 1.71 – 1.52 (m, 3H).

^{13}C NMR (151 MHz, CDCl$_3$): δ 176.12, 171.46, 171.30, 170.89, 169.07, 167.76, 163.53, 159.82, 156.92, 135.83, 135.37, 134.25, 134.02, 129.48, 129.28, 128.85, 128.73, 128.64, 128.58, 128.52, 128.26, 128.16, 127.99, 119.05, 117.02, 110.05, 77.79, 69.40, 69.02, 68.10, 66.34, 62.80, 56.40, 54.59, 53.44, 49.93, 46.54, 43.81, 35.18, 33.92, 31.93, 29.71, 29.37, 27.02, 23.54, 23.43, 22.70, 20.01, 14.13.

IR (neat): 1663 (s), 1733 (w), 2930 (w), 3315 (b)

[α]^{25}$_D$: +28 ° (10 mg/mL in chloroform)

HRMS: [C$_{49}$H$_{56}$N$_7$O$_{13}$]$^+$ calcd. 950.39306, found 950.38990

(+)-**4.1**
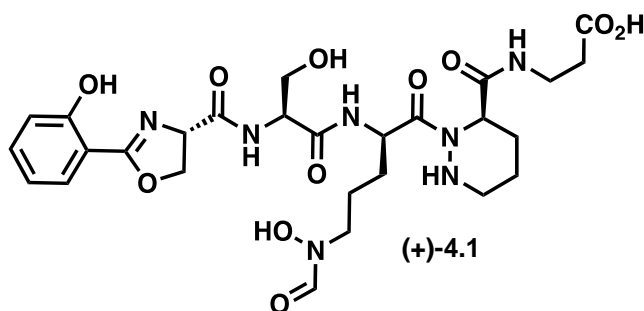
(+)-4.1: To a flask containing (+)-**5.3.11** (0.0139 g, 0.0147 mmol) and methanol (6 mL) was added 10% palladium on activated charcoal (80 wt % of starting material, 0.0111 g). The flask was purged, backfilled with hydrogen gas, and stirred at room temperature until consumption of starting material and partially

deprotected intermediates was observed by LCMS. The mixture was passed through a Whatman filter, concentrated by rotary evaporation, and purified by preperatory HPLC (gradient of 5->95% methanol in water over 20 minutes, 0.1% formic acid, t_R = 15.2 min). Fractions containing product were concentrated by lyophilization to yield pure (+)-**4.1** as a fluffy white powder in 80% yield (0.00749 g, 0.0118 mmol).

¹H NMR (600 MHz, CD₃OD): δ 8.47 (s, 1H), 8.30, (s, 1H) 7.95 (s, 1H), 7.70 (dd, *J* = 7.9, 1.7 Hz, 1H), 7.42 (t, *J* = 7.9 Hz, 1H), 6.97 (d, *J* = 8.3 Hz, 1H), 6.90 (t, *J* = 7.6 Hz, 1H), 5.35 (dd, *J* = 8.9, 4.3 Hz, 1H), 5.08 (dd, *J* = 10.5, 8.0 Hz, 1H), 5.02 (d, *J* = 5.5 Hz, 1H), 4.68 (td, *J* = 10.6, 9.6, 2.7 Hz, 1H), 4.62 (t, *J* = 8.3 Hz, 1H), 4.52 (q, *J* = 5.3 Hz, 1H), 3.85 (dd, *J* = 11.1, 5.1 Hz, 1H), 3.81 (dd, *J* = 11.1, 5.1 Hz, 1H), 3.55 (m, 2H), 3.54 – 3.43 (m, 2H), 3.03 (t, *J* = 12.5 Hz, 1H), 2.88 (q, *J* = 12.2, 11.7 Hz, 1H), 2.44 (t, *J* = *J* = 6.6 Hz, 2H), 2.14 (m, 1H), 1.96 – 1.84 (m, 3H), 1.83 – 1.78 (m, 1H), 1.74 – 1.68 (m, 1H), 1.67 – 1.60 (m, 2H), 1.58 – 1.55 (m, 1H).

¹³C NMR (151 MHz, CD₃OD): δ 175.44, 175.26, 173.27, 172.97, 171.92, 168.90, 168.78, 164.13, 161.02, 159.72, 135.09, 129.53, 120.02, 117.71, 111.49, 70.69, 69.42, 64.75, 63.05, 63.01, 56.72, 52.74, 51.12, 50.49, 50.41, 49.43, 49.28, 49.14, 49.00, 48.86, 48.72, 48.57, 47.93, 47.23, 40.43, 36.82, 35.57, 35.50, 29.78, 29.32, 27.30, 27.20, 25.25, 23.91, 23.80, 22.11.

Full assignments listed in **Table 5.3.2**.

IR (neat): 1640 (s), 1657 (s), 2937 (w), 3295 (b)

[α]²⁵ᴅ: +30 ° (10 mg/mL in methanol)

HRMS: [$C_{27}H_{36}N_7O_{11}$]⁻ calcd. 634.24783, found 634.24783

(+)-5.3.2
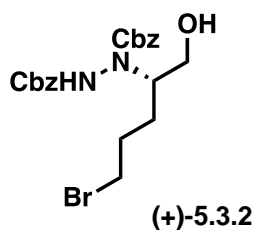
(+)-5.3.2: Synthesized from commercially available 5-bromo-pentanol (1.78 g, 10.69 mmol) and proportional amounts (by molar equivalents) of all reagents/solvents following the same procedure as **(–)-**

5.3.2 with the use of D-proline in place of L-proline. Isolated as white solid in 74% yield (1.5297 g, 3.30 mmol).

¹H-NMR (600 MHz, CDCl₃): δ 7.40 –7.18 (m, 10H), 5.28 – 5.07 (m, 4H), 4.51 – 4.18 (m, 1H), 3.55 – 3.48 (br. s, 1H), 3.48 – 3.33 (m, 2H), 3.29 (s, 1H), 1.91 – 1.79 (br. s, 1H), 1.80 – 1.67 (br. s, 1H), 1.51 – 1.41 (br. s, 1H), 1.41 – 1.30 (br. s, 1H).

¹³C NMR (151 MHz, CDCl₃): δ 156.99, 156.17, 135.71, 135.59, 135.06, 128.70, 128.66, 128.56, 128.46, 128.33, 128.29, 128.06, 127.78, 77.30, 77.09, 76.87, 68.73, 68.61, 68.37, 62.03, 60.29, 33.57, 33.04, 29.09, 29.01, 26.32, 26.14.

IR (neat): 1711 (s), 2960 (w), 3033 (s), 3280 (b)

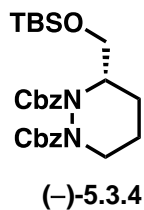**[α]²⁵_D:** +5.7 ° (10 mg/mL in chloroform)
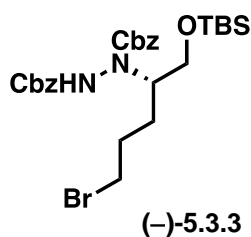
(–)-5.3.3: Synthesized from **(+)-5.3.2** (1.386 g, 2.98 mmol) and proportional amounts (by molar equivalents) of all reagents/solvents following the same procedure as **(+)-5.3.3**. Isolated as white solid in 82% yield (1.41 g, 2.43 mmol).

¹H NMR (600 MHz, CDCl₃): δ 7.44 – 7.28 (m, 10H), 6.46 (s, 1H), 5.27 – 5.07 (m, 4H), 4.39 – 4.10 (m, 1H), 3.72 – 3.03 (m, 4H), 2.28 – 1.23 (m, 4H), 0.88 – 0.85 (s, 9H), 0.06 (m, 6H).

¹³C NMR (151 MHz, CDCl₃): δ 156.41, 135.97, 135.67, 135.33, 128.61, 128.50, 128.41, 128.34, 128.19, 128.10, 127.92, 127.72, 77.27, 77.06, 76.85, 68.41, 67.99, 67.67, 62.96, 62.37, 59.60, 58.40, 58.28, 45.28, 44.83, 34.69, 34.41, 33.76, 31.61, 28.99, 26.92, 26.74, 25.75, 25.48, 25.30, 22.67, 20.73, 18.03, 14.15, -5.45, -5.53.

IR (neat): 1712 (s), 1755 (s), 2856 (w), 2928 (w), 2963 (w), 3285 (b)
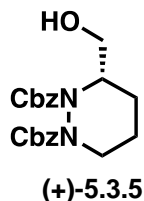
[α]²⁵_D: -14.4 ° (10 mg/mL in chloroform)

TBSO

CbzN
CbzN

(–)-5.3.4

(–)-5.3.4: Synthesized from **(–)-5.3.3** (1.36 g, 2.359 mmol) and proportional amounts (by molar equivalents) of all reagents/solvents following the same procedure as **(+)-5.3.4**. Isolated as white solid in 96% yield (1.12 g, 2.25 mmol).

^{1}H NMR (mixture of rotamers) (600 MHz, CDCl$_3$): δ 7.41 – 7.21 (m, 10H), 5.29 – 4.92 (m, 4H), 4.45 – 4.22 (m, 1H), 4.19 + 4.06 (m, 1H), 3.86 + 3.72 (dd x 2, J = 10.1, 5.2 Hz, 1H), 3.62 + 3.51 (t x 2, J = 10.0 Hz, 1H), 3.23 – 2.95 (m, 1H), 1.93 – 1.79 (m, 2H), 1.76 – 1.66 (m, 1H), 1.55 – 1.46 (m, 1H), 0.89 (s x 2, 9H), 0.09 – 0.04 (s x 2, 6H).

^{13}C NMR (151 MHz, CDCl$_3$): δ 155.54, 155.40, 154.95, 136.27, 136.09, 128.55, 128.50, 128.46, 128.19, 128.07, 127.93, 127.81, 127.66, 127.50, 77.24, 77.03, 76.82, 67.76, 67.60, 60.82, 54.32, 45.90, 45.38, 44.98, 44.48, 25.85, 25.81, 22.35, 19.31, 18.88, 18.16, -5.38, -5.45, -5.48, -5.55.

IR (neat): 1707 (s), 2856 (w), 2929 (w)

[α]^{25}$_D$: -19.6 ° (10 mg/mL in chloroform)

HO

CbzN
CbzN

(+)-5.3.5

(+)-5.3.5: Synthesized from **(–)-5.3.4** (1.10 g, 2.21 mmol) and proportional amounts (by molar equivalents) of all reagents/solvents following the same procedure as **(–)-5.3.5**. Isolated as amorphous solid in 97% yield (0.829 g, 2.16 mmol).

^{1}H NMR (600 MHz, CDCl$_3$): δ 7.39 – 7.31 (m, 10H), 5.30 – 5.07 (m, 4H), 4.52 (d, J = 53.6 Hz, 1H), 4.24 – 4.05 (m, 1H), 3.66 (dt, J = 60.9, 11.0 Hz, 1H), 3.56 – 3.39 (m, 1H), 3.27 – 3.01 (m, 1H), 2.09 (d, J = 7.8 Hz, 1H), 1.83 – 1.68 (m, 2H), 1.58 – 1.47 (m, 2H).

¹³C NMR (151 MHz, CDCl₃): δ 156.80, 156.21, 155.74, 154.88, 136.15, 135.84, 135.71, 135.37, 128.71, 128.66, 128.59, 128.54, 128.46, 128.28, 128.20, 128.05, 127.83, 127.56, 77.28, 77.07, 76.86, 68.52, 68.42, 68.17, 67.99, 60.55, 59.96, 56.19, 54.97, 45.82, 45.41, 23.09, 22.55, 19.71, 19.38.

IR (neat): 1704 (s), 2361 (s), 2948 (w), 3491 (b)

[α]²⁵_D: +7.5 ° (10 mg/mL in chloroform)
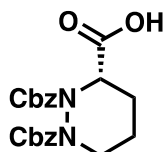
(–)-5.3.6

(–)-5.3.6: Synthesized from **(+)-5.3.5** (0.7807 g, 2.03 mmol) and proportional amounts (by molar equivalents) of all reagents/solvents following the same procedure as **(+)-5.3.6**. Isolated as pale oil in 82% yield (0.657 g, 1.67 mmol).

¹H NMR (mixture of rotamers) (600 MHz, CDCl₃): δ 7.46 – 7.21 (m, 10H), 5.32 – 5.02 (m, 4H), 4.23 – 4.04 (m, 1H), 3.17 – 2.89 (m, 2H), 2.29 – 2.24 (m, 1H), 1.94 (dddd, *J* = 14.2, 10.6, 6.5, 4.1 Hz, 1H), 1.87 – 1.69 (m, 1H), 1.66 – 1.58 (m, 1H).

¹³C NMR (151 MHz, CDCl₃): δ 171.17, 170.68, 135.38, 135.15, 134.94, 128.74, 128.70, 128.67, 128.57, 128.36, 128.24, 128.16, 128.00, 77.26, 77.05, 76.84, 69.44, 69.22, 69.01, 68.52, 44.90, 43.44, 23.95, 23.78, 20.41, 20.06.

IR (neat): 1707 (s), 2954 (w)

[α]²⁵_D: -30.4 ° (10 mg/mL in chloroform)
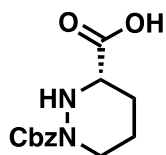
(–)-4.33

(–)-4.33: Synthesized from **(–)-5.3.6** (0.529 g, 1.33 mmol) and proportional amounts (by molar equivalents) of all reagents/solvents following the same procedure as **(+)-4.33**. Isolated as an off white solid in 94%

semi-pure yield (0.33 g, 1.25 mmol). Although the material was resistant to further purification, characterization data qualitatively matched those previously reported.

¹H NMR (600 MHz, DMSO-d_6): 7.40 – 7.29 (m, 5H), 5.13 – 5.05 (m, 2H), 3.82 (d, J = 13.2 Hz, 1H), 3.36 (dd, J = 9.7, 3.1 Hz, 1H), 3.07 (s, 1H), 1.90 (dq, J = 8.9, 4.4, 3.9 Hz, 1H), 1.69 (m, 1H), 1.54 (m, 2H).

¹³C NMR (151 MHz, DMSO-d_6): δ 173.15, 155.23, 137.45, 128.84, 128.68, 128.49, 128.27, 128.03, 127.08, 126.87, 66.71, 58.37, 40.41, 40.28, 40.14, 40.00, 39.86, 39.72, 39.58, 27.58, 23.41.

IR (neat): 1731 (s), 2951 (w)

[α]^{25}$_D$: -31 ° (10 mg/mL in methanol)

(–)-4.39
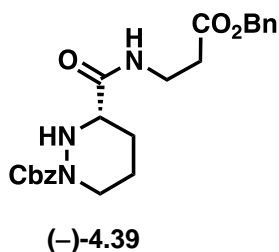
(–)-4.39: Synthesized from **(–)-4.33** (0.323 g, 1.224 mmol) and proportional amounts (by molar equivalents) of all reagents/solvents following the same procedure as **(+)-4.39**. Isolated as a pale oil in 61% yield (0.320 g, 0.7529 mmol). Enantiomeric excess, as determined by chiral HPLC, was measured to be greater than 95%.
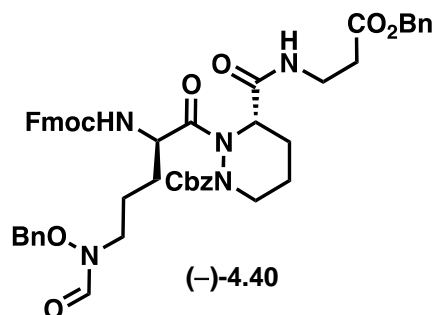
¹H NMR (600 MHz, CDCl₃): δ 7.41 – 7.30 (m, 10H), 5.17 (s, 2H), 5.14 (s, 2H), 3.93 (d, J = 13.3 Hz, 1H), 3.50 (d, J = 19.6 Hz, 2H), 3.17 (br. s, 1H), 2.50 (br. s, 2H), 2.33 – 2.25 (m, 1H), 1.73 – 1.53 (m, 3H).

¹³C NMR (151 MHz, CDCl3): δ 171.59, 170.65, 136.26, 135.85, 128.61, 128.56, 128.35, 128.32, 128.27, 67.76, 66.56, 66.40, 57.96, 34.97, 34.09, 25.39, 21.65.

IR (neat): 1669 (s), 1704 (s), 1734 (s), 2853 (w), 2921 (w)

[α]^{25}$_D$: +25 ° (10 mg/mL in chloroform)

HRMS: $[C_{23}H_{27}N_3O_5]^+$ calcd. 426.20290, found 426.20122

(–)-4.40

(–)-4.40: Synthesized from **(–)-4.39** (0.0967 g, 0.228 mmol), **(–)-4.49** (0.333 g, 0.683 mmol), and proportional amounts (by molar equivalents) of all reagents/solvents following the same procedure as **(+)-5.3.8**. Isolated as a white foam in 90% yield (0.183 g, 0.205 mmol).

^{1}H NMR (600 MHz, CDCl$_3$): δ 8.20 (s, 1H), 7.76 (d, J = 7.5 Hz, 2H), 7.58 (dd, J = 19.1, 7.5 Hz, 2H), 7.40 (t, J = 7.2 Hz, 2H), 7.37 – 7.28 (m, 12H), 5.67 (s, 1H), 5.15 (m, 2H), 5.07 (s, 2H), 4.96 (br. s, 1H), 4.79 (br. s, 2H), 4.38 (s, 1H), 4.31 (s, 1H), 4.19 (m, 2H), 3.66 (s, 1H), 3.51 (s, 2H), 3.33 (m, 1H) 3.04 (m, 1H), 2.45 (m, 2H), 2.22 (m, 1H), 1.72 (m, 3H) 1.66 (s, 3H), 1.46 (m, 1H).

^{13}C NMR (151 MHz, CDCl$_3$): δ 171.50, 163.01, 155.66, 143.73, 141.34, 141.29, 135.81, 129.52, 128.82, 128.68, 128.54, 128.28, 127.73, 127.08, 125.19, 119.99, 77.23, 77.02, 76.81, 69.41, 67.02, 66.36, 50.70, 47.17, 43.31, 33.72, 22.22, 20.18.

IR (neat): 1673 (s), 1726 (s), 2947 (w), 3323 (w)

[α]$^{25}_D$: -12.9 ° (10 mg/mL in chloroform)

HRMS: [C$_{51}$H$_{54}$N$_5$O$_{10}$]$^+$ calcd. 896.38652, found 896.38713
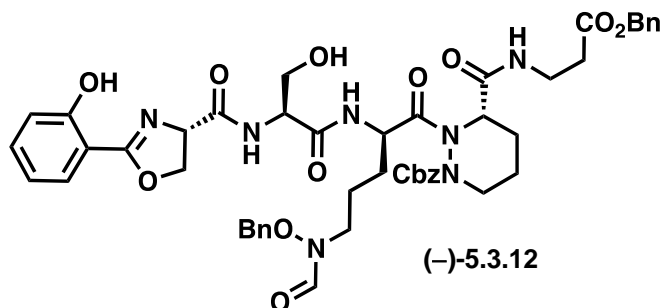
(–)-5.3.12

(–)-5.3.12: Synthesized from **(–)-4.40** (0.100 g, 0.112 mmol) and **(–)-5.3.10** (0.0429 g, 0.112 mmol) and proportional amounts (by molar equivalents) of all reagents/solvents following the same procedure as **(+)-5.3.11**. Isolated as a white foam in 62% yield (0.0662 g, 0.0698 mmol).

^{1}H NMR (600 MHz, CDCl$_3$): δ 11.34 (s, 1H), 8.17 (s, 1H), 7.67 (dd, J = 7.9, 1.7 Hz, 1H), 7.59 (s, 1H), 7.43 – 7.27 (m, 16H), 7.11 (s, 1H), 6.98 (d, J = 8.4 Hz, 1H), 6.91 – 6.85 (t, J = 7.9, 1H), 5.19 (m, 1H), 5.12 (s, 3H), 5.04 (s, 1H), 4.95 (t, J = 9.6 Hz, 1H), 4.89 – 4.76 (m, 2H), 4.71 – 4.58 (m, 2H), 4.53 (s, 1H), 4.15 (d, J = 31.0 Hz, 1H), 3.72 – 3.58 (m, 2H), 3.57 – 3.37 (m, 3H), 3.37 – 3.07 (m, 1H), 2.53 (s, 2H), 2.05 (s, 1), 1.94 – 1.78 (m, 1H), 1.78 – 1.55 (s, 6H), 1.54 – 1.43 (m, 1H).

^{13}C NMR (151 MHz, CDCl$_3$): δ 172.25, 171.30, 169.78, 168.62, 163.10, 159.88, 157.10, 135.75, 134.88, 129.54, 129.25, 128.84, 128.72, 128.54, 128.22, 128.15, 119.03, 117.06, 109.96, 77.24, 77.03, 76.82, 69.63, 69.31, 67.98, 66.56, 62.63, 54.65, 47.99, 47.12, 43.29, 35.07, 33.80, 29.23, 23.29, 22.42, 19.90.

IR (neat): 1665 (s), 1729 (s), 2946 (w), 3325 (w)

[α]^{25}$_D$: -4.6 ° (10 mg/mL in chloroform)

**HRMS:** [C$_{49}$H$_{56}$N$_7$O$_{13}$]$^+$ calcd. 950.39306, found 950.39372

(–)-4.35
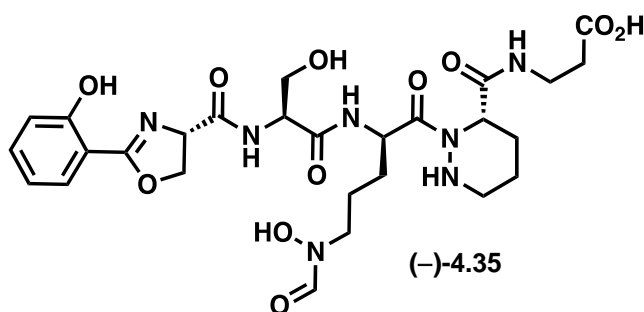
(–)-4.35: Synthesized from **(–)-5.3.12** (0.020 g, 0.02107 mmol) and proportional amounts (by molar equivalents) of all reagents/solvents following the same procedure as **(+)-4.1**. Isolated as a white solid in 86% yield (0.0115 g, 0.01811 mmol).

Full NMR assignments listed in **Supplementary Table 5.3.3**.

IR (neat): 1657 (s), 2935 (w), 3269 (b)

[α]²⁵_D: -3.4° (10 mg/mL in methanol)

**HRMS:** $[C_{27}H_{36}N_7O_{11}]^-$ calcd. 634.24783, found 634.24871

(+)-**4.22**
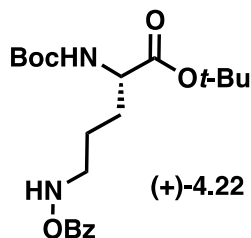
(+)-**4.22:** To a flask containing 75% benzoyl peroxide (0.497 g, 1.539 mmol) and cesium carbonate (0.752 g, 2.309 mmol) was added dichloromethane (7.5 mL). The suspension was stirred for two hours at which time a solution of N^{α}-Boc-L-ornithine *tert*-butyl ester hydrochloride (0.250 g, 0.769 mmol) in 3 mL dichloromethane was added. The reaction was stirred for overnight. 7.5 mL of water was added and stirred for 5 minutes. Aqueous layer was extracted three times with dichloromethane. Combined organics were washed with brine, dried over sodium sulfate, and concentrated via rotary evaporation. The crude residue was purified by flash chromatography (gradient of 0->50% ethyl acetate in hexanes) to yield pure (+)-**4.22** in 65% yield (0.204 g, 0.500 mmol).

¹H NMR (600 MHz, CDCl₃): δ 8.01 (d, J = 7.5 Hz, 0H), 7.90 (s, 0H), 7.58 (t, J = 7.4 Hz, 0H), 7.45 (t, J = 7.7 Hz, 0H), 5.09 (d, J = 8.3 Hz, 0H), 4.21 (d, J = 7.4 Hz, 0H), 3.21 − 3.11 (m, 0H), 1.97 − 1.89 (m, 0H), 1.79 − 1.66 (m, 0H), 1.45 (s, 1H), 1.43 (s, 1H).

¹³C NMR (151 MHz, CDCl₃): δ 171.72, 166.88, 155.39, 133.38, 129.68, 129.36, 128.53, 128.35, 83.14, 82.00, 79.69, 53.69, 52.08, 30.56, 29.22, 28.33, 28.29, 28.00, 23.19, 13.68.

IR (neat): 1150, 1710, 2970, 3226, 3321.


(+)-**4.25**
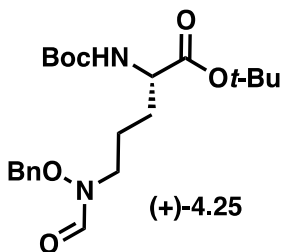
(+)-4.25: To a flask containing EDC (0.269 g, 1.403 mmol) and dichloromethane (1.5 mL) at 0 °C was added formic acid (0.05 mL, 1.403 mmol) and the mixture was stirred for 15 minutes. **(+)-4.22** (0.191 g, 0.467 mmol) was dissolved in dichloromethane (1 mL) and added to the reaction mixture. The reaction was stirred for one hour at 0 °C and one hour at room temperature. The reaction was cooled to 0 °C and an additional portion of EDC (0.090 g, 0.467 mmol) and formic acid (0.02 mL, 0.467 mmol) were added. The reaction was stirred at 0 °C for 15 minutes and room temperature for 3 hours. The reaction was quenched with water and the aqueous layer was extracted three times with dichloromethane. The combined organic layers were washed with brine, dried over anhydrous sodium sulfate, and concentrated under rotary evaporation. The crude amide was taken on without further purification.

To a solution of the crude material dissolved in methanol (10 mL) was added benzyl bromide (0.17 mL, 1.403 mmol) and diisopropylethylamine (0.16 mL, 0.935 mmol). The reaction was stirred at room temperature overnight, at which time solvent was removed by rotary evaporation. The residue was dissolved in ethyl acetate (10 mL) and stirred for 30 minutes. A white precipitate formed, which was filtered off. Filtrate was further diluted with ethyl acetate and washed twice with water then twice with brine. The organic layer was dried over anhydrous sodium sulfate and concentrated under rotary evaporation. The crude residue was purified by flash chromatography (gradient of 0->30% ethyl acetate in hexanes) to yield pure **(+)-4.25** in 80% yield (0.158 g, 0.374 mmol).

^{1}H NMR (600 MHz, CDCl$_3$): δ 8.07 (d, J = 150.2 Hz, 1H), 7.36 (d, J = 12.7 Hz, 4H), 5.06 (d, J = 8.7 Hz, 1H), 4.82 (s, 2H), 4.18 (s, 1H), 3.59 (s, 3H), 1.80 (s, 1H), 1.68 (d, J = 10.6 Hz, 1H), 1.60 (s, 1H).

^{13}C NMR (151 MHz, CDCl$_3$): δ 171.57, 163.14, 155.40, 134.28, 129.46, 129.16, 128.79, 82.06, 79.73, 77.77, 53.52, 43.77, 30.22, 28.33, 27.98, 22.77.

IR (neat): 1150, 1365, 1677, 1709, 2975, 3357.
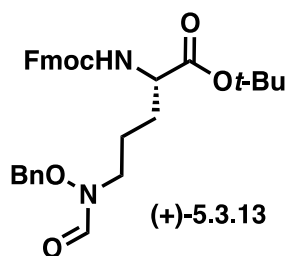
(+)-5.3.13: To a flask containing **(+)-4.25** (0.140 g, 0.331 mmol) at 0 °C was added 4M HCl in dioxane (6.6 mL) and the mixture was stirred for 30 minutes. Mixture was concentrated via rotary evaporation without heat and azeotroped twice with diethyl ether. Cleavage of Boc was confirmed via proton NMR. Crude product was redissolved in dry THF (1 mL) and 1 mL of water was added. Fmoc-OSu (0.123 g, 0.364 mmol) and sodium bicarbonate (0.167 g, 0.014 mmol) were added, and additional sodium bicarbonate was added until pH > 7. Reaction was stirred overnight and then concentrated to aqueous via rotary evaporation. Ethyl acetate and water were added, and solution was neutralized with 1M HCl. Aqueous was extracted with ethyl acetate. Combined organics were washed with brine, dried over sodium sulfate, and concentrated via rotary evaporation. The crude residue was purified by flash chromatography. Additional purification via HPLC yielded pure **(+)-5.3.13** in 31% yield (0.056 g, 0.103 mmol).

¹H NMR (600 MHz, CDCl₃): δ 8.22 (s, 1H), 7.76 (d, J = 7.5 Hz, 2H), 7.60 (d, J = 7.5 Hz, 3H), 7.42 – 7.28 (m, 8H), 5.42 (d, J = 11.4 Hz, 1H), 5.29 (s, 2H), 4.81 (s, 2H), 4.38 (d, J = 7.4 Hz, 2H), 4.28 (s, 1H), 4.22 (t, J = 7.1 Hz, 1H), 3.76 (q, J = 5.2 Hz, 2H), 3.67 – 3.59 (m, 2H), 1.86 (s, 1H), 1.70 (d, J = 37.2 Hz, 4H), 1.45 (s, 13H).

¹³C NMR (151 MHz, CDCl₃): δ 171.27, 163.17, 155.92, 143.92, 143.81, 141.33, 134.25, 129.47, 129.19, 128.80, 127.73, 127.09, 125.13, 120.01, 119.99, 82.43, 77.78, 72.31, 71.14, 66.99, 61.72, 53.94, 53.45, 47.19, 43.66, 42.90, 29.99, 29.71, 28.34, 27.99, 22.71, 14.14.
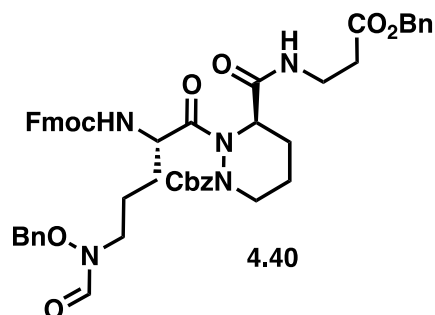
4.40: To a vial containing **(+)-5.3.13** (0.056 g, 0.103 mmol) dissolved in dichloromethane (1.5 mL) was added trifluoroacetic acid (1.5 mL). The mixture was stirred for three hours then concentrated by rotary evaporation and azeotroped three times with toluene. Concentrate was redissolved in equal parts dichloromethane and water. 1M HCl was added until pH = 2-3. Aqueous was extracted three times with dichloromethane then dried over sodium sulfate and concentrated via rotary evaporation. The residue was taken on without further purification after removal of *t*-Bu was confirmed via proton NMR.

To a flask containing crude product and dichloromethane (1.5 mL) at 0 °C was added dropwise Ghosez's reagent (19 μL, 0.144 mmol). The reaction was stirred at 0 °C for 1 hour, at which point it was transferred to a flask containing **(+)-4.39** (0.014 g, 0.034 mmol), silver cyanide (0.005 g, 0.034 mmol), and benzene (3 mL). The reaction was brought to 80 °C and stirred at reflux for 2 hours. The reaction was allowed to cool to room temperature and quenched by dilution in saturated sodium bicarbonate. The aqueous layer was extracted three times with ethyl acetate. The combined organic layers were washed with brine, dried over anhydrous sodium sulfate, and concentrated by rotary evaporation. The crude residue was purified by flash chromatography (gradient of 0->100% ethyl acetate in hexanes then 0->10% methanol in ethyl acetate). Additional purification via HPLC (gradient of 50-95% acetonitrile in water) to yield pure **4.40** in 18% yield (0.017 g, 0.019 mmol).

¹H NMR (400 MHz, CDCl₃): δ 8.20, 7.77, 7.75, 7.61, 7.60, 7.58, 7.56, 7.53, 7.52, 7.42, 7.41, 7.40, 7.39, 7.38, 7.35, 7.35, 7.32, 7.31, 5.69, 5.15, 5.07, 4.79, 4.38, 4.31, 4.19, 3.66, 3.52, 3.34, 3.06, 2.45, 2.22, 1.67, 1.56, 1.54, 1.46.

¹³C NMR (151 MHz, CDCl₃): δ 171.53, 168.51, 155.67, 143.74, 141.34, 141.30, 135.79, 129.56, 129.28, 128.83, 128.69, 128.56, 128.31, 127.74, 127.09, 125.20, 120.03, 119.99, 77.26, 69.44, 67.02, 66.38, 50.68, 47.16, 33.71, 29.73.
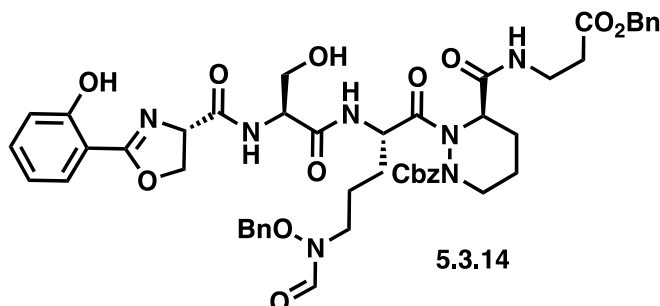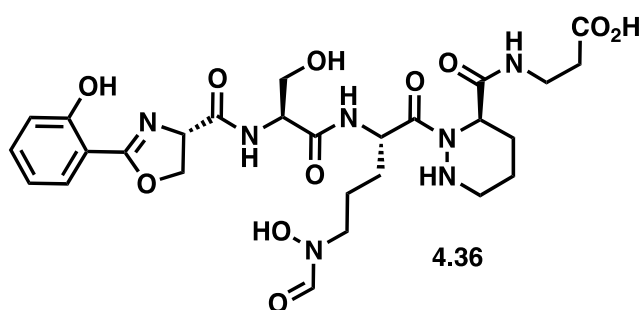

5.3.14

5.3.14: To a flask containing (–)-**5.3.10** (0.005 g, 0.013 mmol) and methanol (2 mL) was added 10% palladium on activated charcoal (20 wt % of starting material, 0.001 g). The flask was purged, backfilled with hydrogen gas, and stirred at room temperature until consumption of starting material was observed by TLC. The mixture was passed through a Whatman filter and concentrated by rotary evaporation to afford (–)-**4.34**. The crude acid was taken on without further purification.

To a flask containing **4.40** (0.016 g, 0.0.018 mmol) and dichloromethane (0.5 mL) was added 4-(aminomethyl)piperidine (0.06 mL). The reaction was stirred in open air for 1 hour, diluted in dichloromethane and washed five times with pH 5.5 phosphate buffer and once with brine. The organic layer was dried over anhydrous sodium sulfate and concentrated under rotary evaporation. The crude amine was taken on without further purification.

To a flask containing EDC (0.007 g, 0.039 mmol) and HOBt (0.005 g, 0.039 mmol) at 0 °C was added a solution of crude acid in acetonitrile (2 mL). Crude amine was dissolved in acetonitrile (2 mL) and added to the flask. Triethylamine was dissolved in acetonitrile and added to the reaction until pH > 7 was achieved. Warmed to room temperature for and stirred overnight. The reaction was quenched with saturated sodium bicarbonate and the aqueous layer was extracted three times with ethyl acetate. The combined organic layers

were washed with brine, dried over anhydrous sodium sulfate, and concentrated by rotary evaporation. The crude residue was purified by flash chromatography (gradient of 0->10% methanol in dichloromethane). Further purification via small silica plug (50% ethyl acetate in hexanes followed by 10% methanol in dichloromethane to elute product) yielded pure **5.3.14** in 35% yield (0.004 g, 0.004 mmol).

¹H NMR (400 MHz, CDCl₃): δ 7.75 (d, J = 7.5 Hz, 2H), 7.68 (dd, J = 7.9, 1.6 Hz, 3H), 7.49 (d, J = 7.2 Hz, 1H), 7.45 – 7.27 (m, 14H), 7.02 (dd, J = 8.4, 1.2 Hz, 1H), 6.93 – 6.84 (m, 2H), 5.11 (q, J = 7.0 Hz, 2H), 4.99 (dd, J = 10.9, 8.2 Hz, 1H), 4.69 (dd, J = 10.8, 8.9 Hz, 1H), 4.64 (d, J = 8.4 Hz, 1H), 4.44 (s, 1H), 4.11 (t, J = 9.1 Hz, 1H), 3.65 (dd, J = 11.4, 5.4 Hz, 1H), 3.27 – 3.10 (m, 3H), 2.39 (d, J = 48.7 Hz, 1H), 2.21 (d, J = 7.6 Hz, 1H), 1.74 (s, 3H), 1.25 (s, 7H), 0.94 – 0.81 (m, 2H).

4.36: To a flask containing **5.3.14** (0.004 g, 0.004 mmol) and methanol (2.5 mL) was added 10% palladium on activated charcoal (80 wt % of starting material, 0.003 g). The flask was purged, backfilled with hydrogen gas, and stirred at room temperature until consumption of starting material was observed by LCMS. The mixture was passed through a Whatman filter and concentrated by rotary evaporation. Crude acid was purified by HPLC (40 -> 95% methanol in water) to afford pure **4.36** in 52% yield (0.0015 g, 0.002 mmol).

¹H NMR (600 MHz, CDCl₃): δ 7.82 (d, J = 7.5 Hz, 1H), 7.69 (d, J = 7.8 Hz, 1H), 7.40 (t, J = 7.4 Hz, 1H), 7.33 (t, J = 7.3 Hz, 1H), 6.93 (d, J = 34.8 Hz, 1H), 5.07 (s, 0H), 4.67 (d, J = 9.9 Hz, 0H), 4.60 (s, 1H), 4.40 (d, J = 7.7 Hz, 1H), 4.24 (s, 1H), 3.84 (s, 1H), 3.77 (s, 1H), 3.66 (d, J = 15.4 Hz, 1H), 3.18 (d, J = 6.7 Hz,

1H), 2.48 (s, 1H), 2.13 (d, J = 10.9 Hz, 1H), 1.94 (s, 1H), 1.82 (s, 1H), 1.60 (s, 1H), 1.43 (s, 1H), 1.42 –
1.35 (m, 3H).
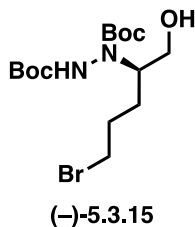
(–)-5.3.15

(–)-5.3.15: To a flask containing PCC (2.76 g, 12.8 mmol) and silica gel (10 g) in dichloromethane (50 mL)
was added a solution of commercially available 5-bromo-pentanol (1.78 g, 10.7 mmol) in dichloromethane
(15 mL) at a rate of 0.5 mL/minute. The reaction was stirred for 2 hour and then filtered through celite and
concentrated by rotary evaporation. The residue was redissolved in dichloromethane, passed through a silica
plug, and concentrated by rotary evaporation. The crude aldehyde was taken on without further purification.

A flask containing the crude material in acetonitrile (32 mL) was brought to 0 °C and di-*tert*-butyl
azodicarboxylate (1.026 g, 4.46 mmol) and L-proline (0.051 g, 0.443 mmol) were added as solids. The
reaction was stirred at 0 °C for 16 hours, at which point sodium borohydride (0.168 g, 4.44 mmol) and
ethanol (13 mL) were added and the reaction was stirred for 40 minutes. The reaction was quenched with
10% citric acid and solvent was removed under rotary evaporation. The residue was partitioned between
ethyl acetate and brine and the aqueous layer was extracted three times with ethyl acetate. The combined
organic layers were dried over anhydrous sodium sulfate and concentrated under rotary evaporation. The
crude residue was purified by flash chromatography (gradient of 0->100% ethyl acetate in hexanes) to yield
pure (–)-S10 as a white solid in 72% yield (1.28 g, 3.21 mmol). Characterization data matched those
previously reported.[13]

¹H-NMR (600 MHz, CDCl₃): 1H NMR (600 MHz, Chloroform-d) δ 6.32 (s, 1H), 4.39 (s, 1H), 4.23 – 4.19
(m, 1H), 3.54 – 3.34 (m, 4H), 1.85 (m, 2H), 1.48 + 1.45 (s x 2, 18H).

^{13}C NMR (151 MHz, CDCl$_3$): δ 158.53, 157.97, 155.86, 155.23, 82.60, 82.45, 82.28, 81.57, 77.28, 77.07, 76.86, 62.23, 62.09, 57.58, 33.64, 32.97, 29.22, 29.13, 28.20, 28.13, 28.10, 28.07, 26.52, 26.28.

IR (neat): 1709 (s), 2978 (s), 3225 (w)

[α]^{25}$_D$: -10.3° (10 mg/mL in chloroform)

HRMS: [C$_{15}$H$_{29}$O$_5$N$_2$^{79}Br^{23}Na]$^+$ calcd. 419.11521, found 419.1149
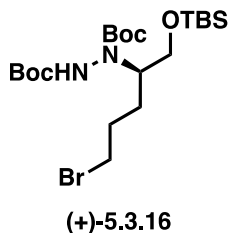
(+)-5.3.16

(+)-5.3.16: Synthesized from (−)-**5.3.15** (1.1 g, 2.75 mmol) and proportional amounts (by molar equivalents) of all reagents/solvents following the same procedure as (+)-**5.3.3**. Isolated as white solid in 81% yield (1.134 g, 2.23 mmol).

^{1}H NMR (600 MHz, CDCl$_3$): δ 6.04 (s, 1H), 4.19 (s, 1H), 4.07 – 3.97 (m, 1H), 3.61 – 3.50 (m, 3H), 3.52 – 3.45 (m, 2H), 3.40 (dt, J = 9.8, 6.5 Hz, 1H), 2.28 – 1.72 (m, 3H), 1.44 (s, 18H), 0.86 (s, 9H), 0.02 (s, 6H).

^{13}C NMR (151 MHz, CDCl$_3$): δ 155.52, 81.44, 80.90, 77.26, 77.05, 76.83, 63.13, 62.44, 59.10, 57.01, 44.98, 34.75, 33.78, 32.41, 32.00, 31.56, 29.00, 28.26, 28.18, 28.13, 27.12, 26.76, 25.93, 25.80, 18.05, 14.09, -5.32, -5.40, -5.48, -5.54.

IR (neat): 1705 (s), 1750 (s), 2929 (s), 2956 (s), 3270 (w)

[α]^{25}$_D$: +6.3 ° (10 mg/mL in chloroform)

HRMS: [C$_{21}$H$_{43}$O$_5$N$_2$^{79}Br^{23}Na^{28}Si]$^+$ calcd. 533.20168, found 533.20206
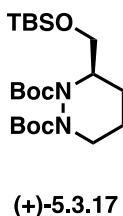
(+)-5.3.17

(+)-5.3.17 Synthesized from **(+)-5.3.16** (1.08 g, 2.12 mmol) and proportional amounts (by molar equivalents) of all reagents/solvents following the same procedure as **(+)-5.3.4**. Isolated as white solid in 90% yield (0.823 g, 1.91 mmol).

^{1}H NMR (600 MHz, CDCl$_3$): δ 4.31 (s, 1H), 4.07 (dq, J = 12.7, 4.7, 4.1 Hz, 1H), 3.95 – 3.79 (m, 1H), 3.74 (dd, J = 9.8, 5.1 Hz, 1H), 3.56 (t, J = 10.2 Hz, 1H), 3.04 – 2.84 (m, 1H), 1.88 – 1.74 (m, 2H), 1.69 – 1.59 (m, 1H) 1.52 – 1.38 (m, 18H), 0.88 (s, 9H), 0.05 (s, 6H).

^{13}C NMR (151 MHz, CDCl$_3$): δ 154.60, 154.47, 80.71, 80.36, 77.23, 77.02, 76.81, 60.67, 53.29, 43.47, 43.22, 28.34, 28.31, 28.28, 28.23, 25.86, 22.30, 18.94, 18.27, -5.31, -5.35, -5.50.

IR (neat): 1701 (s), 2857 (s), 2930 (s)

[α]$^{25}_D$: +20.6 ° (10 mg/mL in chloroform)

HRMS: [C$_{21}$H$_{43}$O$_5$N$_2$^{28}Si]$^+$ calcd. 431.29358, found 431.29347
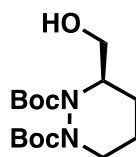
(–)-4.41

(–)-4.41: Synthesized from **(+)-5.3.17** (0.802 g, 1.865 mmol) and proportional amounts (by molar equivalents) of all reagents/solvents following the same procedure as **(–)-5.3.5**. Isolated as amorphous solid in 98% yield (0.577 g, 1.83 mmol).
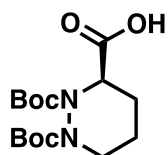
^{1}H NMR (mixture of rotamers) (600 MHz, CDCl$_3$): δ 4.49 – 4.27 (m, 1H), 4.11 – 4.05 (m, 1/2H), 3.95 (m, 1/2H), 3.73 + 3.58 (t x 2, J = 11.1 Hz, 1H), 3.46 (br. s, 1H), 3.05 + 2.91 (br. s x 2, 1H), 2.43 (s, 1H), 1.80 – 1.63 (m, 2H), 1.48 (s, 18H).

^{13}C NMR (151 MHz, CDCl$_3$): δ 155.52, 153.99, 81.77, 77.25, 77.04, 76.83, 60.52, 60.09, 55.91, 53.67, 45.33, 42.75, 28.23, 22.57, 19.76, 19.46.

IR (neat): 1700 (s), 2934 (s), 2976 (s), 3473 (w)

[α]$^{25}_D$: -3.5 ° (10 mg/mL in chloroform)

HRMS: [C$_{15}$H$_{28}$O$_5$N$_2$^{23}Na]$^+$ calcd. 339.18904, found 339.18859

(+)-4.42

(+)-4.42: Synthesized from **(–)-4.41** (0.548 g, 1.73 mmol) and proportional amounts (by molar equivalents) of all reagents/solvents following the same procedure as **(+)-5.3.6**. Isolated as pale oil in 86% yield (0.488 g, 1.48 mmol).

^{1}H NMR (mixture of rotamers) (600 MHz, CDCl$_3$): δ 5.03 – 4.65 (m, 1H), 4.06 + 3.92 (dt x 2, J = 12.8, 4.5 Hz, 1H), 3.28 – 2.79 (m, 1H), 2.32 – 2.01 (m, 1H), 1.91 (s, 1H), 1.83 – 1.64 (m, 1H), 1.50 + 1.46 (s x 2, 18H).

^{13}C NMR (151 MHz, CDCl$_3$): δ 171.17, 170.68, 135.38, 135.15, 134.94, 128.74, 128.70, 128.67, 128.57, 128.36, 128.24, 128.16, 128.00, 77.26, 77.05, 76.84, 69.44, 69.22, 69.01, 68.52, 44.90, 43.44, 23.95, 23.78, 20.41, 20.06.

IR (neat): 1650 (s), 2970 (s), 2930 (s)

$[\alpha]^{25}_D$: +27.6 ° (10 mg/mL in chloroform)

HRMS: [C$_{15}$H$_{27}$O$_6$N$_2$]$^+$ calcd. 331.18636, found 331.1862
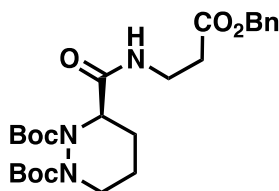
(+)-4.43

(+)-4.43: To a flask containing EDC (0.801 g, 4.191 mmol), HOBt (0.658 g, 4.191 mmol), and β-alanine benzyl ester tosylate salt (1.47 g, 4.191 mmol) at 0 °C was added a solution of **(+)-4.42** (0.461g, 1.397 mmol) in DMF (15 mL). Triethylamine (0.8245 mL, 5.937 mmol) was added and the pH was confirmed to be basic before stirring from 0 °C to room temperature for 16 hours. The reaction was diluted in saturated sodium bicarbonate and the aqueous layer was extracted three times with ethyl acetate. The combined organic layers were washed with brine, dried over anhydrous sodium sulfate, and concentrated by rotary

evaporation. The crude residue was purified by flash chromatography (gradient of 0->100% ethyl acetate in hexanes) to yield pure (+)-**4.43** as pale oil in 97% yield (0.6679 g, 1.36 mmol).

^{1}H NMR (mixture of rotamers) (600 MHz, CDCl$_3$): δ 7.53 – 7.32 (m, 5H), 5.14 (s, 2H), 4.86 (br. s, 1H), 4.05 – 3.82 (m, 1H), 3.71 – 3.60 (m, 1H), 3.51 (br. s, 1H), 3.09 – 2.77 (m, 1H), 2.71 – 2.55 (m, 2H), 2.31 (br. s, 1H), 1.80 – 1.71 (m, 1H), 1.70 – 1.62 (m, 2H), 1.56 – 1.48 (m, 18H).

^{13}C NMR (151 MHz, CDCl$_3$): δ 171.19, 170.09, 135.91, 135.74, 128.57, 128.53, 128.27, 128.22, 128.21, 128.17, 82.83, 81.97, 77.24, 77.03, 76.82, 66.44, 66.33, 35.43, 35.23, 34.32, 34.20, 28.41, 28.24, 28.14, 20.64, 20.35.

IR (neat): 1678 (s), 1709 (s), 1736 (s), 2976 (s), 3323 (w)

[α]^{25}$_D$: +14.8 ° (10 mg/mL in chloroform)

HRMS: [C$_{25}$H$_{38}$O$_7$N$_3$]$^+$ calcd. 492.27043, found 492.27018

(–)-**4.44**
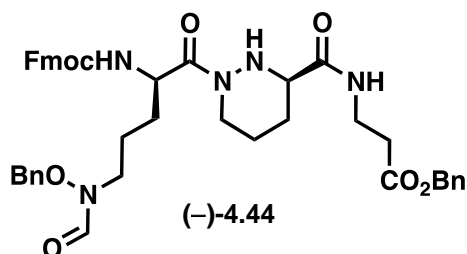
(–)-**4.44:** To a vial containing (+)-**4.43** (0.2689 g, 0.5476 mmol) dissolved in dichloromethane (3 mL) was added trifluoroacetic acid (3 mL). The mixture was stirred for two hours and concentrated by rotary evaporation. The residue was dissolved in toluene and concentrated again (repeat 5x). The residue was taken on without further purification.

To a flask containing EDC (0.251 g, 1.314 mmol), and HOBt (0.206 g, 1.314 mmol) at 0 °C was added a solution of (–)-**4.49** (0.213 g, 0.43811 mmol) in acetonitrile (3 mL), followed by a solution of crude residue from the previous step in acetonitrile (3 mL). Triethylamine (0.31 mL, 2.19 mmol) was added slowly and pH was confirmed to be basic before stirring from 0 °C to room temperature for 16 hours. The reaction was diluted in saturated sodium bicarbonate and the aqueous layer was extracted three times with ethyl acetate.

181

The combined organic layers were washed with brine, dried over anhydrous sodium sulfate, and concentrated by rotary evaporation. The crude residue was purified by flash chromatography (gradient of 0->100% ethyl acetate s in hexanes) to yield pure **(–)-4.44** as a white foam in 73% yield (0.234 g, 0.319 mmol).

^{1}H NMR (600 MHz, CDCl$_3$): δ 8.20 (s, 1H), 7.87 (s, 1H), 7.75 (d, J = 7.6 Hz, 2H), 7.59 (d, J = 7.5 Hz, 2H), 7.43 – 7.28 (m, 14H), 7.19 (br. s, 1H) 5.90 (d, J = 7.0 Hz, 1H), 5.62 – 5.50 (m, 1H), 5.21 – 5.08 (m, 2), 5.04 – 4.90 (s, 1H), 4.86 – 4.75 (m, 1H), 4.44 – 4.29 (m, 3H), 4.19 (t, J = 7.1 Hz, 1H), 3.80 – 3.57 (m, 2H), 3.49 (dq, J = 13.4, 6.4 Hz, 2H), 3.35 – 3.19 (m, 1H), 3.18 – 3.00 (m, 1H), 2.85 – 2.48 (m, 2H), 1.87 – 1.05 (m, 8H).

^{13}C NMR (151 MHz, CDCl$_3$): δ 171.52, 170.80, 159.11, 144.06, 143.87, 141.33, 135.95, 134.05, 129.89, 129.34, 128.75, 128.57, 128.28, 127.67, 127.03, 125.16, 119.98, 119.96, 77.23, 77.02, 76.81, 66.69, 66.38, 60.08, 50.95, 47.83, 47.27, 42.09, 35.10, 34.07, 28.04, 22.62, 20.66.

IR (neat): 1660 (s), 1723 (s), 2942 (w), 3322 (w)

[α]$^{25}_D$: -11.6 ° (10 mg/mL in chloroform)

HRMS: [C$_{43}$H$_{47}$O$_8$N$_5$^{23}Na]$^+$ calcd. 784.33168, found 784.33162
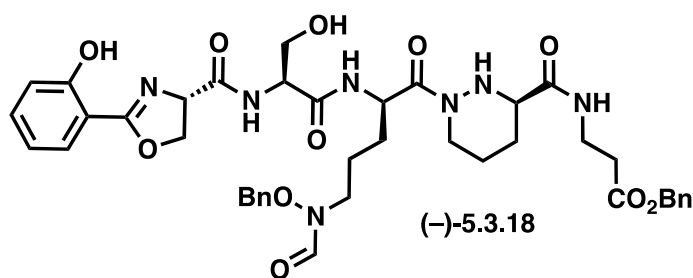
(–)-5.3.18

(–)-5.3.18: Synthesized from **(–)-4.44** (0.082 g, 0.112 mmol), **(–)-5.3.10** (0.0431 g, 0.112 mmol), and proportional amounts (by molar equivalents) of all reagents/solvents following the same procedure as **(+)-5.3.11**. Isolated as a white foam in 77% yield (0.0631 g, 0.0774 mmol).

¹H NMR (600 MHz, CDCl₃): δ 8.16 (s, 1H), 7.86 (s, 1H), 7.67 (dd, J = 7.9, 1.7 Hz, 2H), 7.57 – 7.28 (m, 16H), 7.01 (d, J = 8.4 Hz, 2H), 6.89 (td, J = 7.6, 1.1 Hz, 2H), 5.28 (s, 1H), 5.21 – 5.06 (m, 3H), 5.04 – 4.97 (m, 1H),4.97 – 4.90 (m, 1H) 4.81 (d, J = 10.1 Hz, 2H), 4.67 (d, J = 9.2 Hz, 2H), 4.52 – 4.13 (m, 1H), 4.40 – 4.16 (d, J = 13.3 Hz, 1H), 4.01 (dd, J = 23.5, 11.2 Hz, 2H), 3.90 – 3.75 (m, 1H), 3.68 (s, 2H), 3.63 – 3.46 (m, 3H), 3.35 – 3.22 (m, 1H), 3.19 – 3.09 (m, 1H) 2.73 – 2.61 (m, 2H), 2.60 – 2.50 (m, 1H), 1.94 – 1.46 (m, 8H).

¹³C NMR (151 MHz, CDCl₃): δ 171.61, 170.82, 169.20, 167.92, 163.29, 159.88, 159.13, 135.91, 134.49, 134.04, 129.88, 129.53, 129.32, 128.86, 128.74, 128.61, 128.57, 128.40, 128.27, 119.10, 117.08, 109.83, 77.24, 77.03, 76.81, 76.34, 69.53, 66.54, 66.40, 62.53, 60.04, 54.58, 50.07, 49.70, 47.72, 43.61, 42.17, 35.11, 34.05, 28.85, 27.96, 27.22, 20.82.

IR (neat): 1640 (s), 2941 (w), 3305 (w)

[α]²⁵_D: -5.4 ° (10 mg/mL in chloroform)

HRMS: [C₄₁H₅₀O₁₁N₇]⁺ calcd. 816.3563, found 816.35636

(+)-4.37
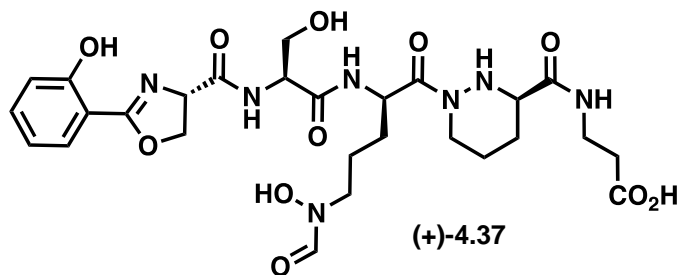
(+)-4.37: Synthesized from **(–)-5.3.18** (0.020 g, 0.02454 mmol) and proportional amounts (by molar equivalents) of all reagents/solvents following the same procedure as **(+)-4.1**. Isolated as a white solid in 87% yield (0.0136 g, 0.02142 mmol).

¹H NMR (600 MHz, CD₃OD): δ 8.32 (s, 1H), 8.24 (s, 1H), 7.91 (s, 1H), 7.65 (dd, J = 7.9, 1.7 Hz, 1H), 7.38 (ddd, J = 8.6, 7.2, 1.7 Hz, 1H), 6.93 (dd, J = 8.4, 1.1 Hz, 1H), 6.86 (t, J = 7.5 Hz, 1H), 5.31 – 5.23 (m, 1H), 5.04 (dd, J = 10.5, 7.9 Hz, 1H), 4.64 (t, J = 8.2 Hz, 1H), 4.57 (t, J = 8.2 Hz, 1H), 4.44 (q, J = 5.2 Hz, 1H), 4.24 – 4.12 (m, 1H), 3.84 – 3.74 (m, 2H), 3.64 – 3.56 (m, 1H), 3.54 – 3.50 (m, 1H), 3.50 – 3.41 (m,

3H), 3.40 – 3.35 (m, 1H), 2.85 (d, J = 9.6 Hz, 1H), 2.51 (t, J = 6.5 Hz, 2H), 1.96 (d, J = 13.4 Hz, 1H), 1.87 – 1.80 (m, 1H), 1.75 – 1.66 (m, 3H), 1.63 – 1.55 (m, 3H).

^{13}C NMR (151 MHz, CD$_3$OD): δ 172.47, 171.90, 170.37, 167.37, 162.66, 159.62, 133.70, 128.13, 118.62, 116.32, 110.07, 69.28, 67.98, 61.63, 61.57, 59.73, 59.70, 55.45, 55.42, 53.40, 49.56, 48.45, 48.03, 47.89, 47.75, 47.61, 47.46, 47.32, 47.18, 45.82, 41.46, 35.12, 33.65, 29.34, 28.36, 28.05, 27.00, 26.78, 22.67, 22.33.

Full assignments listed in **Table 5.3.4**.

IR (neat): 1657 (s), 2930 (w), 3279 (b)

[α]^{25}$_D$: +15° (10 mg/mL in methanol)

HRMS: [C$_{27}$H$_{36}$N$_7$O$_{11}$]$^-$ calcd. 634.24783, found 634.24962
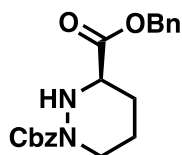
(+)-4.46

(+)-4.46: To a flask containing a solution of **(+)-4.45** (0.357 g, 1.35 mmol) dissolved in DMF (12 mL) was added K$_2$CO$_3$ (0.279 g, 2.02 mmol) followed by benzyl bromide (0.290 g, 1.69 mmol). The reaction was allowed to stir for 12 hours, diluted in saturated sodium bicarbonate, and extracted three times with ethyl acetate. The combined organic layers were washed with brine, dried over anhydrous Na$_2$SO$_4$, and concentrated by rotary evaporation. The crude residue was purified by flash chromatography (gradient of 0->100% ethyl acetate s in hexanes) to yield pure **(+)-4.46** as a pale oil in 77% yield (0.368 g, 1.04 mmol).
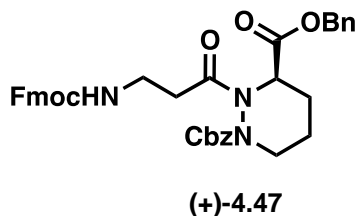
^{1}H NMR (600 MHz, CDCl$_3$): δ 7.39 – 7.32 (m, 10H), 5.20 – 5.12 (m, 4H), 3.99 (d, J = 12.7 Hz, 1H), 3.59 (dd, J = 10.2, 3.2 Hz, 1H), 3.13 (d, J = 14.4 Hz, 1H), 2.08 (dt, J = 12.5, 3.8 Hz, 1H), 1.78 – 1.68 (m, 2H), 1.64 – 1.53 (m, 1H).

^{13}C NMR (151 MHz, CDCl$_3$): δ 170.87, 155.29, 136.43, 135.33, 128.64, 128.53, 128.46, 128.34, 128.15, 127.98, 77.24, 77.03, 76.82, 67.61, 66.82, 58.36, 44.79, 27.45, 23.38.

IR (neat): 1695, (s), 1736 (s), 2946 (w)

[α]^{25}$_D$: +24° (10 mg/mL in chloroform)

HRMS: [C$_{20}$H$_{23}$O$_4$N$_2$]$^+$ calcd. 355.16523, found 355.16508

(+)-4.47

(+)-4.47: Synthesized from commercially available Fmoc-β-alanine (0.646 g, 2.07 mmol), **(+)-4.46** (0.245 g, 0.692 mmol), and proportional amounts (by molar equivalents) of all reagents/solvents following the same procedure as **(+)-5.3.8**. Isolated as a pale oil in 93% yield (0.420 g, 0.649 mmol).

^{1}H NMR (600 MHz, CDCl$_3$): δ 7.76 (d, J = 7.5 Hz, 2H), 7.58 (d, J = 5.8 Hz, 2H), 7.45 – 7.20 (m, 14H), 5.41 (d, J = 5.2 Hz, 2H), 5.26 – 5.14 (m, 1H), 5.08 (d, J = 12.2 Hz, 1H), 4.95 (s, 1H), 4.34 (d, J = 7.4 Hz, 3H), 4.19 (t, J = 7.0 Hz, 1H), 3.43 (s, 2H), 3.06 – 2.84 (m, 1H), 2.55 (br. s, 2H), 2.11 – 2.02 (m, 2H), 1.87 – 1.76 (m, 1H).

^{13}C NMR (151 MHz, CDCl$_3$): δ 169.33, 156.34, 143.99, 141.32, 135.61, 128.75, 128.73, 128.61, 128.58, 128.40, 128.35, 128.26, 128.14, 127.68, 127.04, 125.14, 125.10, 119.98, 77.24, 77.03, 76.82, 68.38, 66.71, 47.23, 36.39, 32.40, 24.92, 19.26.

IR (neat): 1677 (s), 1720 (s), 2960 (w), 3363 (w)

[α]^{25}$_D$: +26.4° (10 mg/mL in chloroform)

HRMS: [C$_{38}$H$_{38}$O$_7$N$_3$]$^+$ calcd. 648.27043, found 648.27064

(+)-4.48
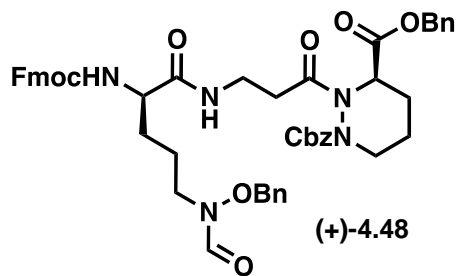
(+)-4.48: To a flask containing **(+)-4.47** (0.301 g, 0.0.464 mmol) and dichloromethane (3 mL) was added 4-(aminomethyl)piperidine (0.35 mL). The reaction was stirred in open air for 1.5 hours, diluted in dichloromethane and washed five times with pH 5.5 phosphate buffer and once with brine. The organic layer was dried over anhydrous sodium sulfate and concentrated under rotary evaporation. The crude amine was taken on without further purification.

To a flask containing EDC (0.119 g, 0.624 mmol) and HOBt (0.098 g, 0.624 mmol) at 0 °C was added a solution of **(–)-4.49** (0.113 g, 0.232 mmol) in acetonitrile (3 mL) followed by a solution of crude amine residue in acetonitrile (3 mL). Triethylamine (0.1 mL, 0.772 mmol) in was added slowly and the pH was confirmed to be basic before stirring from °C to room temperature for 16 hours. The reaction was diluted in saturated sodium bicarbonate and the aqueous layer was extracted three times with ethyl acetate. The combined organic layers were washed with brine, dried over anhydrous sodium sulfate, and concentrated by rotary evaporation. The crude residue was purified by flash chromatography (gradient of 0->100% ethyl acetate in hexanes) to yield pure **(+)-4.48** as white foam in 78% yield (0.161 g, 0.180 mmol).

^{1}H NMR (600 MHz, CDCl$_3$): δ 8.20 (s, 1H), 7.75 (d, J = 7.5 Hz, 2H), 7.59 (t, J = 8.1 Hz, 2H), 7.44 – 7.24 (m, 19H), 6.68 (s, 1H), 5.55 (s, 1H), 5.35 (d, J = 6.0 Hz, 1H), 5.17 (br. s, 1H), 5.06 (br. s, 1H), 4.93 (br. s, 1H), 4.81 (d, J = 9.5 Hz, 2H), 4.36 (d, J = 7.0 Hz, 2H), 4.24 (s, 1H), 4.20 (t, J = 7.2 Hz, 1H), 3.84 (br. s, 1H), 3.63 – 3.16 (m, 3H) 2.91 (br. s, 1H), 2.48 (m, 2H), 1.99 (d, J = 13.3 Hz, 1H), 1.82 – 1.45 (m, 7H).

^{13}C NMR (151 MHz, CDCl$_3$): δ 171.36, 169.32, 163.51, 143.74, 141.31, 141.30, 135.63, 135.41, 134.16, 129.54, 129.52, 129.25, 128.84, 128.74, 128.60, 128.57, 128.40, 128.36, 128.29, 128.25, 128.17, 127.73, 127.13, 127.10, 125.14, 119.99, 77.24, 77.03, 76.82, 68.39, 67.05, 53.61, 50.95, 47.17, 43.08, 34.90, 31.73, 30.54, 24.90, 22.96, 19.22.

IR (neat): 1673 (s), 1721 (s), 2943 (w), 3323 (w)

$[\alpha]^{25}_D$: +18.2° (10 mg/mL in chloroform)

HRMS: $[C_{51}H_{54}O_{10}N_5]^+$ calcd. 896.38652, found 896.38736
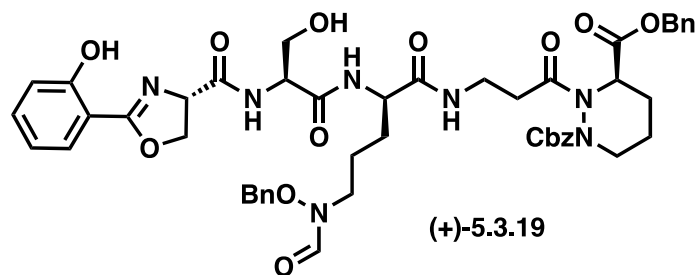
(+)-5.3.19

(+)-5.3.19: Synthesized from **(+)-4.48** (0.100 g, 0.112 mmol), **(−)-5.3.10** (0.0429 g, 0.112 mmol), and proportional amounts (by molar equivalents) of all reagents/solvents following the same procedure as **(+)-5.3.11**. Isolated as a white foam in 73% yield (0.0776 g, 0.0818 mmol).

^{1}H NMR (600 MHz, CDCl$_3$): δ 8.13 (s, 1H), 7.67 (dd, J = 7.9, 1.8 Hz, 1H), 7.42 – 7.28 (m, 16H), 7.23 (s, 1H), 7.00 – 6.95 (m, 1H), 6.90 (t, J = 7.5 Hz, 1H), 5.36 (br. s, 1H), 5.19 (d, J = 12.1 Hz, 1H), 5.12 – 5.02 (m, 1H) 4.94 (q, J = 7.5, 5.2 Hz, 2H), 4.81 (s, 2H), 4.64 – 4.59 (m, 1H), 4.53 (t, J = 10.1 Hz, 1H), 4.44 (s, 1H), 4.24 (br. s, 1H), 4.07 (d, J = 10.1 Hz, 1H), 3.69 – 3.53 (m, 3H), 3.47 (d, J = 13.1 Hz, 1H), 3.38 – 3.20 (m, 1H), 3.16 – 2.88 (m, 1H), 2.70 – 2.27 (m, 2H), 2.08 – 1.89 (m, 2H), 1.82 – 1.66 (m, 4H), 1.57 (dq, J = 12.5, 3.6, 3.2 Hz, 2H).

^{13}C NMR (151 MHz, CDCl$_3$): δ 171.34, 170.93, 167.59, 163.68, 159.74, 155.46, 135.15, 134.27, 134.11, 129.53, 129.24, 128.83, 128.75, 128.62, 128.59, 128.56, 128.42, 128.25, 119.10, 116.91, 110.07, 77.24, 77.03, 76.82, 69.34, 68.02, 67.34, 62.68, 43.69, 34.91, 31.54, 27.70, 23.84.

IR (neat): 1640 (s), 1734 (s), 2935 (w), 3315 (w)

[α]^{25}$_D$: +17.4 ° (10 mg/mL in chloroform)

HRMS: $[C_{49}H_{56}O_{13}N_7]^+$ calcd. 950.39306, found 950.39377

(+)-4.38
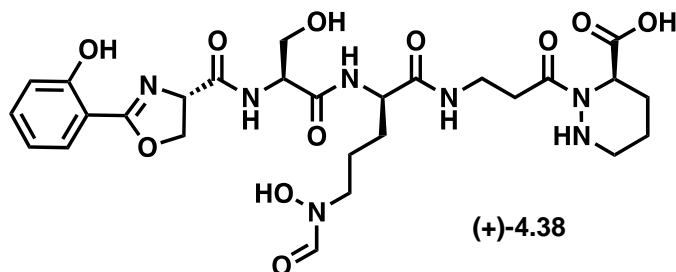
(+)-4.38: Synthesized from **(+)-5.3.19** (0.020 g, 0.02107 mmol) and proportional amounts (by molar equivalents) of all reagents/solvents following the same procedure as **(+)-4.1**. Isolated as a white solid in 78% yield (0.0104 g, 0.01638 mmol).

^{1}H NMR (600 MHz, CD$_3$OD): δ 8.29 (s, 1H), 7.95 (s, 1H), 7.70 (dd, J = 7.9, 1.7 Hz, 1H), 7.42 (ddd, J = 8.8, 7.3, 1.7 Hz, 1H), 6.97 (dd, J = 8.4, 1.1 Hz, 1H), 6.90 (t, J = 7.8 Hz, 1H), 5.15 – 5.05 (m, 2H), 4.72 – 4.60 (m, 2H), 4.45 – 4.33 (m, 2H), 3.85 (qd, J = 11.1, 5.2 Hz, 2H), 3.58 (td, J = 6.4, 2.5 Hz, 1H), 3.54 – 3.50 (m, 1H), 3.46 (dt, J = 7.0, 3.7 Hz, 2H), 2.97 (d, J = 13.8 Hz, 1H), 2.93 – 2.84 (m, 1H), 2.75 (ddt, J = 14.1, 8.3, 4.1 Hz, 2H), 2.26 (d, J = 13.5 Hz, 1H), 1.96 – 1.87 (m, 1H), 1.83 (dt, J = 13.4, 5.7 Hz, 1H), 1.66 (tt, J = 13.5, 6.1 Hz, 3H), 1.59 – 1.48 (m, 2H).

^{13}C NMR (151 MHz, CD$_3$OD): δ 174.05, 171.99, 171.26, 167.28, 162.73, 159.58, 158.17, 133.69, 128.13, 118.65, 116.31, 110.09, 69.24, 67.91, 61.39, 56.00, 53.22, 52.93, 51.94, 49.34, 48.04, 47.89, 47.75, 47.61, 47.47, 47.33, 47.18, 45.69, 35.62, 31.91, 28.26, 27.96, 25.47, 23.21, 22.73, 21.61.

Full assignments listed in **Supplementary Table 5.3.5**.

IR (neat): 1658 (s), 2926 (w), 3281 (b)

[α]$^{25}_D$: +3.4° (10 mg/mL in methanol)

HRMS: [C$_{27}$H$_{38}$N$_7$O$_{11}$]$^+$ calcd. 636.26238, found 634.24783

5.2.3. Biology

To test the ability of compounds to inhibit growth the growth of *Acinetobacter baumannii* ATCC 17978, a -80 °C glycerol stock was used to inoculate 5 mL sterile cation adjusted Mueller Hinton II broth (hereafter MHII) and the culture was shaken aerobically overnight (37 °C, 200 RPM). The next day, 200 μL of overnight culture was used to inoculate 5 mL of fresh MHII and the regrowth culture was shaken aerobically (37 °C, 200 RPM) until in exponential phase (~4-5 hours). Sterile water was used to dilute fresh MHII to 10% by volume and 100 μL of 10%-MHII was added to each well of a 96-well plate. Each compound was dissolved to 10 mM in DMSO, and this stock was further diluted into 10%-MHII to give

800 μM of each compound (equal volume of pure DMSO was used as a control). To the first column was

added 100 μL of compound stock, which was then serially diluted eight columns down the plate to give

nine concentrations of each compound, discarding 100 μL from the final column. The regrowth culture was

diluted into 10%-MHII to an $OD_{600} = 0.004$ and 100 μL of this inoculum was added to each well of the

plate except for the final column, to which 100 μL/well of blank 10%-MHII was added as a control. At this

point, each plate contained 1.) nine inoculated columns of serially diluted compound (or DMSO control) at

nine concentrations from 200-0.78 μM, 2.) one column of inoculated media to measure basal growth levels,

and 3.) one column of sterile media to measure background signal. Plates were then grown aerobically at

37 °C without shaking for 20 hours and OD_{600} readings were recorded as an average of three independent

measurements. The background absorbance of blank media (OD = 0.032) was subtracted from each

measurement to give the final values depicted.

5.4. References

(1)   Kaliappan, K. P.; Ravikumar, V. Angucyclinone Antibiotics: Total Syntheses of YM-181741, (+)-Ochromycinone, (+)-Rubiginone B2, (-)-Tetrangomycin, and MM-47755. *J. Org. Chem.* **2007**, *72* (16), 6116–6126. https://doi.org/10.1021/jo070709p.
(2)   Kerhervé, J.; Botuha, C.; Dubois, J. New Asymmetric Synthesis of Protein Farnesyltransferase Inhibitors via Palladium-Catalyzed Cross-Coupling Reactions of 2-Iodo-Imidazoles. *Org. Biomol. Chem.* **2009**. https://doi.org/10.1039/b902601k.
(3)   Hon, Y. S.; Hsieh, C. H.; Liu, Y. W. Dibromomethane as One-Carbon Source in Organic Synthesis: Total Synthesis of (±)- and (-)-Methylenolactocin. *Tetrahedron* **2005**. https://doi.org/10.1016/j.tet.2005.01.057.
(4)   Keohane, C. E.; Steele, A. D.; Fetzer, C.; Khowsathit, J.; Van Tyne, D.; Moynié, L.; Gilmore, M. S.; Karanicolas, J.; Sieber, S. A.; Wuest, W. M. Promysalin Elicits Species-Selective Inhibition of Pseudomonas Aeruginosa by Targeting Succinate Dehydrogenase. *J. Am. Chem. Soc.* **2018**, *140* (5), 1774–1782. https://doi.org/10.1021/jacs.7b11212.
(5)   Ruprecht, J.; Yankovskaya, V.; Maklashina, E.; Iwata, S.; Cecchini, G. Structure of Escherichia Coli Succinate: Quinone Oxidoreductase with an Occupied and Empty Quinone-Binding Site. *J. Biol. Chem.* **2009**. https://doi.org/10.1074/jbc.M109.010058.
(6)   Leaver-Fay, A.; Tyka, M.; Lewis, S. M.; Lange, O. F.; Thompson, J.; Jacak, R.; Kaufman, K.; Renfrew, P. D.; Smith, C. A.; Sheffler, W.; Davis, I. W.; Cooper, S.; Treuille, A.; Mandell, D. J.; Richter, F.; Ban, Y. E. A.; Fleishman, S. J.; Corn, J. E.; Kim, D. E.; Lyskov, S.; Berrondo, M.; Mentzer, S.; Popović, Z.; Havranek, J. J.; Karanicolas, J.; Das, R.; Meiler, J.; Kortemme, T.; Gray, J. J.; Kuhlman, B.; Baker, D.; Bradley, P. Rosetta3: An Object-Oriented Software Suite for the Simulation and Design of Macromolecules. In *Methods in Enzymology*; 2011. https://doi.org/10.1016/B978-0-12-381270-4.00019-6.

(7)   Hawkins, P. C. D.; Skillman, A. G.; Warren, G. L.; Ellingson, B. A.; Stahl, M. T. Conformer Generation with OMEGA: Algorithm and Validation Using High Quality Structures from the Protein Databank and Cambridge Structural Database. *J. Chem. Inf. Model.* **2010**. https://doi.org/10.1021/ci100031x.

(8)   Hawkins, P. C. D.; Nicholls, A. Conformer Generation with OMEGA: Learning from the Data Set and the Analysis of Failures. *J. Chem. Inf. Model.* **2012**. https://doi.org/10.1021/ci300314k.

(9)   Steele, A. D.; Keohane, C. E.; Knouse, K. W.; Rossiter, S. E.; Williams, S. J.; Wuest, W. M. Diverted Total Synthesis of Promysalin Analogs Demonstrates That an Iron-Binding Motif Is Responsible for Its Narrow-Spectrum Antibacterial Activity. *J. Am. Chem. Soc.* **2016**, *138* (18), 5833–5836. https://doi.org/10.1021/jacs.6b03373.

(10)   Preparation of 2-pyridinylguanidines as urokinase inhibitors. Reference Detail | CAS SciFinder[n] https://scifinder-n.cas.org/searchDetail/reference/6254550daaa21311b5c3d3cd/referenceDetails (accessed Apr 11, 2022).

(11)   Yokokawa, F.; Sugiyama, H.; Shioiri, T.; Katagiri, N.; Oda, O.; Ogawa, H. An Expeditious Synthesis of Pentosidine, an Advanced Glycation End Product. *Tetrahedron* **2001**, *57* (22), 4759–4766. https://doi.org/10.1016/S0040-4020(01)00399-4.

(12)   Mashiach, R.; Meijler, M. M. Total Synthesis of Pyoverdin D. *Org. Lett.* **2013**, *15* (7), 1702–1705. https://doi.org/10.1021/ol400490s.

(13)   Henmi, Y.; Makino, K.; Yoshitomi, Y.; Hara, O.; Hamada, Y. Highly Efficient Synthesis of (R)- and (S)-Piperazic Acids Using Proline-Catalyzed Asymmetric α-Hydrazination. *Tetrahedron Asymmetry* **2004**, *15* (21), 3477–3481. https://doi.org/10.1016/j.tetasy.2004.09.025.

(14)   Chen, Y.; Lu, Y.; Zou, Q.; Chen, H.; Ma, D. A Scalable Process to the Key Intermediate of Cilazapril, (S) - 1- Benzyloxycarbonylhexahydropyridazine-3-Carboxylic Acid, Through a Novel Cascade Course. **2013**, 1209–1213. https://doi.org/10.1021/op400155u.